PFC/RR-85-9

DOE/ET-51013-150
UC20D

Economic Evaluation of Fissile Fuel Production Using Resistive Magnet Tokamaks

James C. Doyle, Jr.*

June 1985

Plasma Fusion Center
Massachusetts Institute of Technology
Cambridge, Massachusetts 02139 USA

*present address: Los Alamos National Laboratory
Los Alamos, NM 87545

ECONOMIC EVALUATION OF FISSILE FUEL PRODUCTION USING RESISTIVE MAGNET TOKAMAKS

by

JAMES COLEMAN DOYLE, JR.

B.S., University of Tulsa
1974
M.S., University of Missouri - Columbia
1980

Submitted to the Department of
Nuclear Engineering
in Partial Fulfillment of the
Requirements for the Degree of

DOCTOR OF SCIENCE
at the
MASSACHUSETTS INSTITUTE OF TECHNOLOGY
MAY 1985

Signature of Author
Department of Nuclear Engineering, May 15, 1985

Certified by
Daniel R. Cohn
Thesis Supervisor

Certified by
Lawrence M. Lidsky
Thesis Supervisor

Accepted by
Allan F. Henry
Chairman, Departmental Graduate Committee

ECONOMIC EVALUATION OF FISSILE FUEL PRODUCTION USING RESISTIVE MAGNET TOKAMAKS

by

JAMES COLEMAN DOYLE, JR.

Submitted to the Department of Nuclear Engineering
on May 15, 1985 in Partial Fulfillment of the
Requirements for the Degree of Doctor of Science

ABSTRACT

The application of resistive magnet tokamaks to fissile fuel production has been studied. Resistive magnet offer potential advantages over superconducting magnets in terms of robustness, less technology development required and possibility of demountable joints.

Optimization studies within conservatively specified constraints for a compact machine result in a major radius of 3.81 m. and 618 MW fusion power and a blanket space envelope of 0.35 m. inboard and 0.75 m. outboard. This machine is called the Resistive magnet Tokamak Fusion Breeder (RTFB).

The blanket studies are based on a configuration composed of two zones. The first zone (11 cm. thick) consists of uranium metal plates, clad in steel and cooled by liquid lithium. The second zone (24-64 cm. thick) contains a thorium bearing molten salt as the heat transfer and breeding medium. With self-sustaining tritium production, the net fissile production is 1734 kg/yr ^{239}Pu and 2056 kg/yr ^{233}U . The maximum blanket power is 5830 MWth and average net electric power is 1247 MWe. Pressure drops in the liquid lithium cooling system for the multiplier region are shown to be within acceptable limits for both insulated and uninsulated ducts.

A computer code was developed to estimate the cost of the resistive magnet tokamak breeder. This code scales from STARFIRE values where appropriate and calculates costs of other systems directly. The estimated cost of the RTFB is \$3.01B in 1984\$. The cost of electricity on the same basis as STARFIRE is 42.4 mills/kWhre vs. 44.9 mills/kWhre for STARFIRE (this does not include the fuel value or fuel cycle costs for the RTFB).

The breakeven cost of U_3O_8 is 150\$/lb when compared to a PWR on the once through uranium fuel cycle with no inflation and escalation. On the same basis, the breakeven cost for superconducting tokamak and tandem mirror fusion breeders is 160\$/lb and 175\$/lb. Thus, the RTFB appears to be competitive in breakeven U_3O_8 cost with superconducting magnet fusion breeders and offers the potential advantages of resistive magnet technology.

Thesis Supervisor: Dr. Daniel R. Cohn
Title: Senior Scientist, Plasma Fusion Center

Thesis Supervisor: Dr. Lawrence M. Lidsky
Title: Professor of Nuclear Engineering

ACKNOWLEDGMENTS

I would like to thank my advisers, Dr. Dan Cohn and Professor Larry Lidsky, for their guidance and assistance over the course of this thesis, as well as their role in my education at M.I.T. Additionally, Dr. Leslie Bromberg provided his keen insight, not only in fusion, but in human nature. The assistance of Rene LeClaire in learning the intricacies of the STRESS code and providing the parameters for the fission-suppressed design was appreciated.

I would also like to thank Dr. Ralph Moir and Dr. J. D. Lee of LLNL and Dr. Dave Berwald of TRW for their assistance with questions regarding fusion breeder work at LLNL and TRW, as well as commenting on my work. The summer at LLNL working with Ralph and J. D., during my fellowship practicuum, was enlightening, informative and very worthwhile. I'm sure we all look forward to a resurgence in interest in fusion breeders.

My family has been a continuing source of support and encouragement. I would especially like to acknowledge my mother and father, whose unwavering faith and support has meant more than they know. Thanks, Mom and Dad.

Finally, I would like to thank Ruth. Her continuing support, encouragement and faith have seen me through the rough spots and through to the end of this work.

This work was performed under appointment to the Magnetic Fusion Energy Technology Fellowship Program which is administered for the U. S. Department of Energy by Oak Ridge Associated Universities.

TABLE OF CONTENTS

LIST OF FIGURES

Page

Chapter 4.

Chapter 5.

LIST OF TABLES

Page

Chapter 2.

Chapter 3.

Appendix C.

1. INTRODUCTION

1.1 Foreword

A potential application of fusion is in the production of fissile fuel for subsequent use in fission reactors. The production of fissile fuel might allow consideration of fusion machines of relatively low performance to be economically attractive. This economic attractiveness could come from either increased electricity production in the fusion machine allowed by energy-multiplying blankets or the value of the fissile fuel produced by the fusion breeder. Thus, a fusion machine of poor or marginal performance could become attractive. Fusion machines of the required performance may become available prior to machines attractive for pure fusion electricity production. Thus, the fusion breeder could represent an early application of fusion which might allow further development and refinement of attractive pure fusion machines.

Several fusion configurations have been previously evaluated as fusion breeders by others. These include the tokamak [1.1-1.4] and the tandem and standard mirror [1.5-1.8] using superconducting magnets. The Riggatron, which is an extremely compact resistive magnet tokamak, was also considered for fissile fuel production [1.9]. This study is the first to consider a moderate-size, modest performance resistive magnet tokamak, using Bitter plate toroidal field magnets, for fissile fuel production. This machine will be called the Resistive magnet Tokamak Fusion Breeder (RTFB).

1.2 The Resistive Magnet Tokamak

The type of resistive magnet tokamak considered in this study uses Bitter-plate type magnet construction. This type of magnet construction is shown in Fig. 1.1. Interleaved plates of copper and stainless steel in the outboard leg of the toroidal field coil give high structural strength with lower resistive power losses than discrete coils. Stainless steel plates bridge the gaps in the copper plates for structural strength. The gaps are provided to maintain each copper plate as an individual turn. The semi-monolithic construction in the outboard leg requires less structure than individual coil construction to counteract overturning moment forces generated by interaction of the poloidal field and toroidal field, as well as allowing increased access to the blanket region for limited maintenance. In traditional concept of the Bitter plate construction, as exemplified by ALCATOR A and ALCATOR C, the outboard leg of the toroidal field coil is a continuous structure of copper and stainless steel with penetrations for ports. The semi-monolithic construction modifies this construction by using continuous plates which are tapered on the inside and a constant thickness on the outboard side. Thus, the plates form a continuous structure on the inboard side and discrete coils, with space between the coils, on the outboard side. This space between coils may allow some access to the blanket region for maintenance. The semi-monolithic construction also offers the attractive possibility of demountable toroidal field coils in the outboard region, which can greatly simplify maintenance [1.10,1.11].

The inboard leg is composed of copper plates only, with appropriate cooling channels. This allows the current density to be relatively low to minimize resistive power losses. Use of copper only in the throat of the magnet requires that stresses be kept relatively low.

Bitter plate type resistive magnets offer advantages relative to superconducting magnets for fusion applications. These advantages include:

- More compact - less shielding. Superconducting toroidal field coils typically require massive shields to limit the nuclear heat deposition in the magnet and minimize refrigeration requirements. Resistive toroidal fields coils typically require less shielding or no shielding, other than the shielding provided by the breeding blanket, since the limiting parameter is damage to the insulation between turns. The reduced shielding requirement translates into a more compact design for the tokamak.

- Possibility of demountable joints. Designs for joints in superconducting magnets have been proposed, but face the formidable task of providing contact between the many superconducting filaments in a typical superconductor cable. Additionally, the superconducting joint must be in a configuration which allows cooling by liquid helium. Recent studies have developed preliminary designs for demountable joints in Bitter plate type toroidal field coils [1.11]. Demountable joints would allow easier access to components within the toroidal field coils and should simplify maintenance.

- More robust design. Superconducting materials are subject to limitations of temperature, magnetic field and current density. Beyond specific values of each of these parameters (the magnitude of which differs for various superconductors), the superconductor becomes normally conducting. These limitations must be taken into account in magnet design. Resistive magnets have no such inherent limitations, but do have some practical limitations. The

current density must be maintained low enough that the heat generated can be removed. Magnetic field limits are imposed by stress limitations. Temperature restrictions are generally imposed by the need to keep resistive power requirements low.

- Less structure required. For a Bitter plate type magnet, the magnet comprises most of the structure. Minimal additional external structure is required.

- No refrigeration. The necessity of removing heat from the liquid helium at a temperature of 4°K is eliminated. Cooling of the magnet is typically by water flowing in channels or tubes imbedded in the plates. Helium gas for coolant is also a possibility.

The Bitter-plate magnet construction was used in the ALCATOR A and ALCATOR C fusion confinement experiments at MIT [1.12]. ALCATOR A was a very compact machine (major radius=0.54 m., minor radius=0.11 m.) which had a design field of 12 T. on axis. ALCATOR C is a larger machine (major radius=0.64 m., minor radius=0.165 m.) which has a design magnetic field of 14 T. on axis and uses inertial cooling at liquid nitrogen temperatures to minimize electrical power requirements. ALCATOR C is shown in Fig. 1.2.

An ignition test reactor proposed in the Federal Republic of Germany would have used Bitter-plate magnets [1.13]. This machine, known as ZEPHYR, would have used neutral beam heating and compression to achieve ignition. The design of the Bitter-plate toroidal field coils was studied carefully due to the elongation of the bore in the radial direction. ZEPHYR would have used inertial cooling at liquid nitrogen temperatures to minimize resistive power requirements. Unfortunately, funding for ZEPHYR was terminated in the design phase due to extensive budget cuts. A schematic of the proposed ZEPHYR

design is shown in Fig. 1.3.

The series of Long pulse Ignition Test Experiment (LITE) designs typifies the design of the machine used in the present study [1.14,1.15]. These machines are characterized by relatively small major radius and low aspect ratio. Shield thickness is minimum, since the LITE design is for a limited life ignition test machine. Bitter-plate toroidal field coils are used. A typical LITE design is shown in Fig. 1.4.

Resistive magnet tokamaks using Bitter-plate type magnet construction are also being considered as a basis for a fusion reactor design for commercial electricity production [1.16-19]. These machines are typically larger than the machines considered in this study. An example of the Resistive magnet Commercial Tokamak Reactor (RCTR) is shown in Fig. 1.5.

The Riggatron is a very compact resistive magnet tokamak which relies on ohmic heating for ignition [1.9]. Thus, no space is available inside the toroidal field coils for blanket or shield. The fusion neutron energy spectrum and intensity is degraded before reaching the breeding region, which is located outside the coils. Additionally, the coils must be replaced frequently since no shielding is provided.

The RTFB is a moderate size resistive magnet tokamak using Bitter plate magnet construction. A comparison of the size of the RTFB and STARFIRE, a commercial fusion reactor design, is shown in Fig. 1.6.

The present study considers only the deuterium-tritium (D-T) fusion fuel cycle. The D-T reaction produces neutrons with an energy of 14 MeV which are useful in neutron-multiplying reactions which can enhance fissile fuel production. Additionally, the D-T fuel cycle has the least stringent requirements, in

terms of required temperature, to attain a self-sustaining fusion reaction. Thus, consistent with the time frame of this study, the D-T fuel cycle was selected.

The D-D fuel cycle may also be attractive for fusion breeders due to the absence of the requirement for tritium breeding. This would allow more of the fusion neutrons to be used for breeding of fissile material, although the lower average energy of the neutron spectrum would result in less breeding than the D-T spectrum. Additionally, the use of energy multiplying breeder blankets could benefit potential D-D reactors by multiplying the fusion energy to achieve higher net electric production. However, the consideration of the D-D fuel cycle was beyond the scope of the present study.

1.3 The Fusion Breeder

The fusion breeder is similar in many aspects to a pure fusion machine. Differences in the nuclear island are primarily in the blanket. In a pure fusion machine, the blanket is designed to recover the energy of the 14 MeV neutrons produced in the fusion reaction and breed sufficient tritium to sustain its own requirements. In the fusion breeder, the blanket has the additional function of producing fissile material. In producing this fissile material, the blanket may also multiply the energy of the fusion neutrons through exoergic reactions, primarily fission.

Tritium occurs only in very small quantities in nature and must be produced in a fusion reactor. Tritium is produced by neutron capture in lithium in the fusion breeder blanket. This reaction occurs in both naturally occurring isotopes of lithium, ^{6}Li and ^{7}Li. The reactions for breeding of fusile material from lithium are shown in Fig. 1.7. The ^{6}Li tritium production cross section is highest at thermal energies. ^{7}Li tritium production occurs at higher neutron

energies and results in the production of a neutron. Thus, tritium production in ^{7}Li does not result in the loss of a neutron. Small amounts of tritium may also be produced from other materials in the blanket, but the quantities are small relative to that produced by neutron capture in lithium.

Fissile material is produced by neutron capture in fertile material. The fissile materials of interest are ^{233}U and ^{239}Pu. These fissile materials are produced by neutron capture in ^{232}Th and ^{238}U as shown in Fig. 1.8.

For the machines considered most extensively in this study, some form of energy multiplication is necessary for net electric production. Energy multiplication is accomplished through fissions in the fertile materials in the blanket. The number of fissions which occur is dependent on the concentration of fertile material, the type of fertile material, the blanket composition and the neutron energy spectrum. For maximum energy multiplication through fission of fertile materials, the concentration of fertile material should be relatively high; it should be a major blanket component. The fission cross section should be relatively high in the energy range which dominates the neutron energy spectrum. The blanket should contain a minimum amount of structural material to minimize parasitic captures of neutrons and scattering which degrades the neutron energy spectrum. The neutron energy spectrum should be of as high energy as possible since the (n,xn) and fast fission cross sections, as well as ν(the number of neutrons per fission), increase with neutron energy. Thus, the fertile material should be as close to the plasma as possible.

Machines of higher performance in terms of fusion power relative to resistive power requirements may be able to operate in the fission-suppressed mode. In this mode, fissioning of the fertile and bred fissile material is minimized and thus, the energy multiplication is minimized. The minimization of the blanket energy multiplication results in a larger amount of fissile fuel produced per unit

of blanket thermal energy. Thus, for the same gross blanket thermal power, a fission-suppressed design can support more client reactors than a fast fission design. However, the fission suppressed design requires a higher performance system (from a fusion standpoint) than the fast fission system to attain the same gross blanket thermal power for similar sized machines. Thus, the emphasis in the present study is on more compact machines of modest performance which rely upon blanket energy multiplication for net electric output.

A number of design studies have been done for various types of fusion breeder reactors [1.1-1.9]. Each of these concepts has disadvantages. The RTFB design attempts to avoid these disadvantages by using the unique advantages of the semi-monolithic Bitter plate magnet construction to the fullest extent. A brief discussion of each class of previous fusion breeder design studies follows.

Superconducting tokamaks have already been considered for fusion breeder application [1.1-1.4]. These machines are typically much larger than the RTFB due to the shielding required to limit nuclear heat deposition in the superconducting magnets. Designs have been developed for both fast fission and fission-suppressed blankets. A representative design is shown in Fig. 1.9.

Numerous studies have been done using superconducting tandem mirror fusion reactors as the basis for fusion breeders [1.5-1.7]. These machines are quite large, with a central cell length of ~200 m. In addition the end coil sets have become very large and complex. The most recent design is shown in Fig. 1.10.

The Riggatron was also evaluated as a fusion breeder [1.9]. The breeding performance is decreased by the necessity of placing the blanket outside the toroidal field coils due the extremely compact configuration. The fusion neutron spectrum is degraded in energy such that fast fission blankets are less

effective. Additionally, the technology constraints required to be overcome to achieve ohmic ignition, as assumed in the Riggatron development program, are formidable.

Thus, the superconducting magnet tokamak and tandem mirror reactors considered for fissile fuel production are both very large and, consequently, expensive. At the other extreme, the Riggatron is very compact, but suffers from poor breeding performance due to the necessary physical location of the breeding blanket.

In contrast, the RTFB is a modest performance tokamak with compact size. The modest performance should translate into increased reliability and confidence in the physics for the basis of the design. The compact size should allow lower cost for the nuclear island, which is a major cost component of typical fusion reactor designs. Thus, the RTFB should represent a design that is more reliable and less expensive than previous fusion breeder designs.

1.4 Potential Client Reactor Systems

The complete evaluation of the RTFB requires, in addition to a design for the RTFB, the following elements: definition of the time frame of the study, selection of a standard for comparison and selection of a client reactor system. This section addresses each of these elements in turn.

The conceptual time frame selected for this study is beginning of construction of the RTFB on January 1, 1984 and initial commercial operation on January 1, 1990. The construction period of six years is not intended to be indicative of the actual construction period, but was selected to be consistent

with STARFIRE [1.20]. The start date is the date of the most recent information available from the Handy Whitman index [1.21], which was used to adjust all input costing information to a consistent basis, at the time the economic evaluation was initiated.

In the time frame for the initial commercial operation of the RTFB of January 1, 1990, a choice must be made for a standard for comparison of the electricity cost from the system of the RTFB and its client reactors. The dominant nuclear technology for generation of electricity in the United States in the time frame of interest is the Light Water Reactor (LWR). Thus, the LWR was selected as the standard for comparison of electricity costs. Two type of LWRs are currently in widespread commercial use – the Boiling Water Reactor (BWR) and the Pressurized Water Reactor (PWR). Due to the dominance in numbers of the PWR in commercial operation, the PWR was selected as the basis for comparison to the RTFB-client reactor system.

Current LWR operation uses the once-through uranium fuel cycle. In this cycle, uranium is mined and processed into the form of U_3O_8, also known as yellowcake. The yellowcake is converted into UF_6, a form suitable for enrichment. In the enrichment process, the atom fraction of ^{235}U in the mixture of ^{235}U and ^{238}U is increased from ~ 0.7 a/o to ~ 3 a/o. The enriched UF_6 is then converted into UO_2 powder which is pressed and sintered into pellets. These pellets are placed into Zircaloy tubes. The Zircaloy tubes are bundled into fuel assemblies. These fresh fuel assemblies are placed into the reactor core, with one third of the core typically replaced at a time. Thus, the residence time of a fuel assembly is three years. The fuel assemblies which are removed from the core are placed in a spent fuel storage facility where they may be safely stored prior to permanent disposition. This is the end of the fuel cycle in all current US nuclear power plants. The once-through uranium fuel cycle was thus selected as the fuel cycle for the LWR comparison.

The spent fuel assemblies contain significant amounts of fissile uranium and plutonium. Earlier visions of the nuclear power industry foresaw "closing" the back end of the nuclear fuel cycle by reprocessing of the spent fuel to recover useful products and discard the radioactive waste produced in the fission process. With current low uranium prices and high projected costs of reprocessing spent fuel, coupled with the lack of a reprocessing industry in the United States, reprocessing does not now appear economically attractive. However, for the purposes of this study, a mature reprocessing industry is assumed to exist, and the effect of higher uranium prices is explored.

In evaluating the fusion breeder, consideration must also be given to the system of client fission reactors which will burn the fissile fuel produced. Potential candidate client reactor systems cover a broad range of feasibility and state of development. Many advanced converter reactor (ACR) systems have been proposed which allow more efficient utilization of uranium and thorium than the current once-through LWR. These systems rely upon reactor systems which have not been constructed and would not be available in the time frame of this study. Accordingly, ACRs are not considered as client reactors in the present work. It is noted, however, that the increased uranium prices which are explored in this study may also make ACRs more attractive due to the more efficient use of uranium.

The client reactor selected for this study is the PWR, since the PWR is expected to be the dominant nuclear technology in the time frame of this study. Two fuel cycles were selected for the client reactors. One fuel cycle is based on ^{233}U with recycle. The second fuel cycle is based on ^{239}Pu with recycle. These two fuel cycles were selected since the blanket of the RTFB produces both ^{233}U and ^{239}Pu . ^{239}Pu is produced in the uranium metal in the multiplier region which also multiplies the energy of the fusion neutrons through fast fission reactions. ^{233}U is produced through captures in the Th in

the molten salt. Thus, the client reactor system is composed of PWRs operating on two different fuel cycles, both with reprocessing and recycle of the spent fuel. Make-up fuel is provided by the RTFB.

Another potential source of fissile fuel is the fast breeder reactor (FBR). In a FBR system, excess fuel is produced at a net rate sufficient to provide make-up fuel for one client LWR from three FBRs. Thus, the system is mostly FBRs. This could add to siting difficulties. The economics of the system could also be affected, since it could be affected by the uncertainties added by the FBR technology, which could dominate the system. In contrast, the fusion breeder system would consist of one fusion breeder supplying fuel to a larger number of client reactors. Thus, the system economics would be dominated by the client reactors.

Additional technologies which have been proposed for production of fissile fuel include electronuclear breeding [1.22] and extraction of uranium from seawater [1.23]. In electronuclear breeding, a particle accelerator is used to accelerate protons which are then directed to a target which contains a fertile material. Collisions of the protons and fertile material result in a large number of neutrons. These neutrons are then captured in the surrounding fertile material and produce fissile material. Energy is produced by the slowing down of the protons, the evaporation of target nuclei and fission of fertile material and the bred fissile material. This energy is recovered from the target and used to produce electricity, which is recycled to the accelerator.

Uranium may be extracted from seawater by processing large quantities of seawater through ion exchange beds, where the uranium (along with other elements) is collected. The uranium which is concentrated on the beds is then removed. This process is projected to be relatively expensive, with a projected realistic price range of 250-350 \$/lb U_3O_8 [1.24]. A more recent opinion expresses

optimism that a price of 150 $/lb may be achievable [1.25]. An implicit goal is to achieve prices of 200 $/lb by the year 2000 [1.26]. Extraction of uranium from seawater has the practical effect of placing an upper bound on the price of uranium extracted from the ground which would be expected to rise as the lower recovery cost deposits are depleted. In accordance with the above discussion, the upper limit on uranium prices considered in the present study is 200 $/lb U_3O_8 in 1990$.

1.5 Summary

The ALCATOR A and ALCATOR C experiments at MIT have established the application of resistive magnets of Bitter-plate construction for toroidal field coils in tokamaks. The design studies related to ZEPHYR provided further information on the characteristics of Bitter-plate type magnets in larger machines. The recent series of LITE and RCTR studies are investigating the application of Bitter-plate type magnets to ignition test experiments and commercial fusion reactors. Resistive magnets appear to offer significant advantages over superconducting magnets in terms of robustness and compactness of design along with the attractive possibility of demountable joints to increase access for maintenance.

Fusion breeders have been investigated as potential applications of superconducting magnet tokamak and tandem mirror reactors. Additionally, the Riggatron was considered for fissile fuel production. These studies have shown that fissile fuel production can be achieved with fusion machines, but at higher prices than may be currently acceptable. However, if uranium prices rise in the future, these machines could produce fissile fuel which is cost competitive with mined uranium.

The conceptual time frame of this study is January 1, 1984 for the beginning of construction of the RTFB and initial commercial operation on January 1, 1990. In this time frame, the PWR on the once-through uranium fuel cycle is selected as the basis for comparison of electricity costs from the RTFB-client reactor system. Similarly, the PWR on the ^{233}U and ^{239}Pu fuel cycles with recycle is selected as the client reactor system.

Other potential sources of fissile fuel include fast breeder fission reactors, accelerator breeders and uranium from seawater. Due to the lower number of client reactors supported by each FBR, the FBR-client reactor system characteristics would be dominated by the FBR. In contrast, the RTFB would supply make-up fuel to a larger number of client reactors. Thus, the RTFB-client reactor system characteristics would be dominated by the client reactors.

Uranium from seawater is currently projected to have a wide range of costs. The goal for uranium from seawater, and hence, the upper limit for uranium prices considered in the present study, is 200 \$ /lb U_3O_8. Hence, uranium from seawater is be considered to place an upper bound on the price of mined uranium with which the fusion breeder must compete.

References

[1.1] Moir, R. W., et al., "Feasibility Study of a Fission-Suppressed Tokamak Fusion Breeder," Lawrence Livermore National Laboratory Report UCID-20154, (December 1984).

[1.2] Jassby, D. L., et al., "Fast-Fission Tokamak Breeder Reactors," *Proceedings of the Sixth Topical Meeting on the Technology of Fusion Energy*, San Francisco, CA (1985), to be published in *Fusion Technology*.

[1.3] Westinghouse Electric Corporation, "Conceptual Design of a Commercial Tokamak Hybrid Reactor (CTHR) Final Report," WFPS: TME-80-012, (December 1980).

[1.4] Westinghouse Electric Corporation, "Design Study of a Fusion-Driven Tokamak Hybrid Reactor for Fissile Fuel Production." Electric Power Research Institute Report ER-1083, Volume 1 and 2, (May 1979).

[1.5] Berwald, D.H., et al.,"Fission-Suppressed Hybrid Reactor – The Fusion Breeder," Lawrence Livermore National Laboratory Report UCID-19638, (December 1982).

[1.6] Lee, J.D., et.al., "Feasibility Study of a Fission-Suppressed Tandem-Mirror Hybrid Reactor," Lawrence Livermore National Laboratory Report UCID-19327, (April 1982).

[1.7] Moir, R.W. et.al., "Tandem Mirror Hybrid Reactor Design Study Final Report," Lawrence Livermore National Laboratory Report UCID-18808, (September 1980).

[1.8] Bender, D. J., et al., "Reference Design for the Standard Mirror Hybrid Reactor," Lawrence Livermore National Laboratory Report UCRL-52478, (May 1978).

[1.9] INESCO, Inc., "Presentation to the Riggatron Review Group," U. S. Department of Energy, Germantown, MD (July 16, 1979).

[1.10] Jassby, D. L., Jacobsen, R. A., Kalnavarns, J., Masson, L. S. and Sekot, J. P., "Resistive Demountable Toroidal Field Coils for Tokamak Reactors," Princeton Plasma Physics Laboratory Report 1809 (July 1981)

[1.11] Yang, T. F., LeClaire, R. J., Bobrov, E. S., Bromberg, L., Cohn, D. R. and Williams, J. E. C., "A Demountable Copper TF Coil System for Ignition Test Experiments and Commercial Reactors," *Proceedings of the Sixth Topical Meeting on the Technology of Fusion Energy*, San Francisco, CA (1985), to be published in *Fusion Technology*.

[1.12] Weggel, C., Hamburger, W., Montgomery, B., and Pierce, N., "The Alcator C Magnetic Coil System," in Engineering Problems of Fusion Research

(Proc. 7th Symposium, Knoxville, TN, 1977).

[1.13] Williams, J. E. C., et al., "Conceptual Design of a Bitter Magnet Toroidal Field System for the ZEPHYR Ignition Test Reactor," Massachusetts Institute of Technology Plasma Fusion Center Report PFC/RR-81-24, (May 1981).

[1.14] Bromberg, L., Cohn, D. R., Williams, J. E. C., Yang, T. and Jassby, D. L., "Engineering Aspects of LITE (Long Pulse Ignition Test Experiment) Devices," in *Proceedings of the Tenth Symposium on Fusion Engineering*, Philadelphia, PA, (December 1983).

[1.15] Bromberg, L.,Cohn, D. R., Williams, J. E. C. and Jassby, D. L., "A Long Pulse Ignited Test Experiment (LITE)." *Nuclear Technology/Fusion*, Vol. 4, 1013 (1983).

[1.16] LeClaire, R. J., Potok, R. E., Bromberg, L., Cohn, D. R., Meyer, J. E. and Yang, T. F., "Systems Studies of Commercial Tokamak Reactors with Resistive Magnets," *Proceedings of the Sixth Topical Meeting on the Technology of Fusion Energy*, San Francisco, CA (1985), to be published in *Fusion Technology*.

[1.17] Bromberg, L., " Design Options for Commercial Reactors with Resistive Magnets." *Proceedings of the Sixth Topical Meeting on the Technology of Fusion Energy*, San Francisco, CA (1985), to be published in *Fusion Technology*.

[1.18] Bromberg, L., Cohn, D. R., and Jassby, D. L., "Commercial Tokamak Reactors with Resistive Magnets", *Fusion Technology*, **6** 597 (1984).

[1.19] Bromberg, L., Cohn, D.R., Williams, J.E.C., Becker, H., LeClaire, R., and Yang, T., "Tokamaks with High Performance Resistive Magnets: Advanced Test Reactors and Prospects for Commercial Applications," *Proceedings of the 9th Symposium on Engineering Problems of Fusion Research*, Chicago, IL (1981).

[1.20] Baker, C. C., et al., "STARFIRE – A Commercial Tokamak Fusion Power Plant Study," Argonne National Laboratory Report ANL/FPP-80-1, (September 1980).

[1.21] *The Handy Whitman Index of Public Utility Construction Costs*, Whitman, Requardt and Associates, Bulletin No. 119, To January 1, 1984, Baltimore, MD.

[1.22] Steinberg, M., et al., "Linear Accelerator-Breeder: A Preliminary Analysis and Proposal," Brookhaven National Laboratory Report BNL-50592, (November 1976).

[1.23] Driscoll, M. J., and Best, F. R., "System Studies on the Extraction of Uranium From Seawater," Massachusetts Institute of Technology Report MITNE-248 (November 1981).

[1.24] Kellner, A. and Bitte, J. "Cost Studies on the Extraction of Uranium from Seawater Based on a Diffusion-Fluidized Bed Arrangement," in *Progress Toward the Recovery of Uranium From Seawater*. Driscoll, M. J. and Best, F. R. (Eds.), Massachusetts Institute of Technology Nuclear Engineering Department Report MITNE-256 (December 1982).

[1.25] Kennedy, D., "Ocean Uranium: Limitless Energy?," *Technology Review*, Vol. 87, No. 7, (October 1984).

[1.26] Driscoll, M. J., personal communication, Massachusetts Institute of Technology.

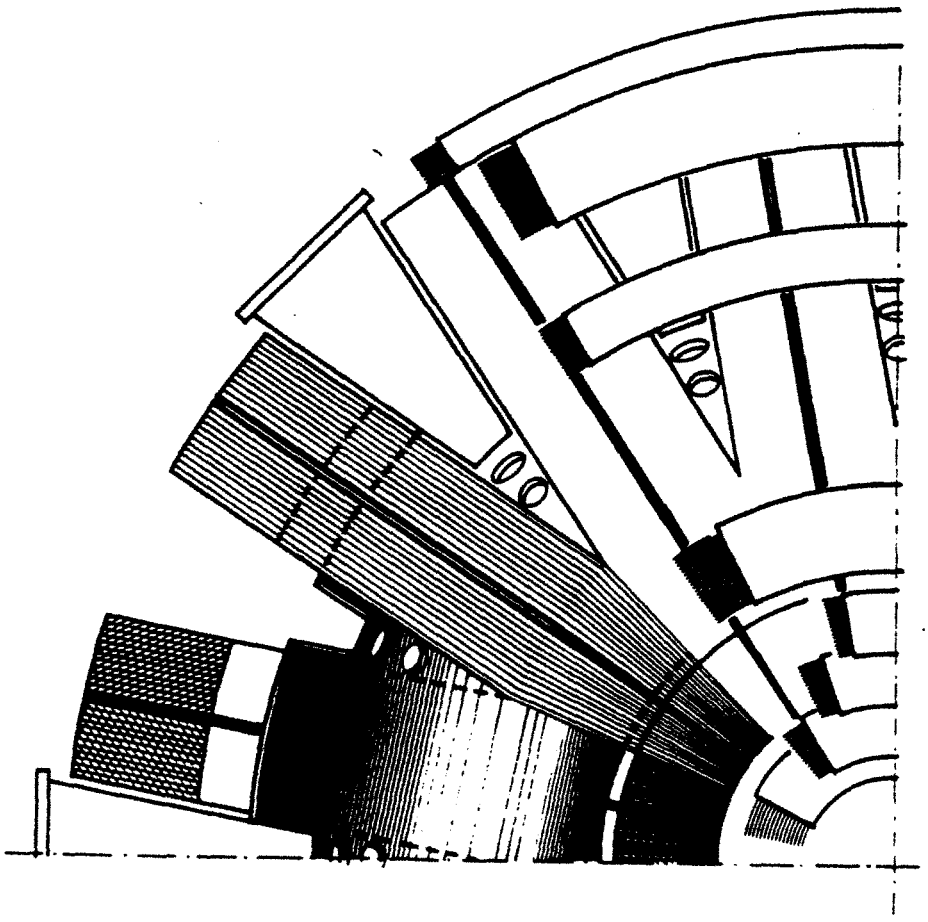

Figure 1.1 Semi-Monolithic Bitter Plate Magnet Construction

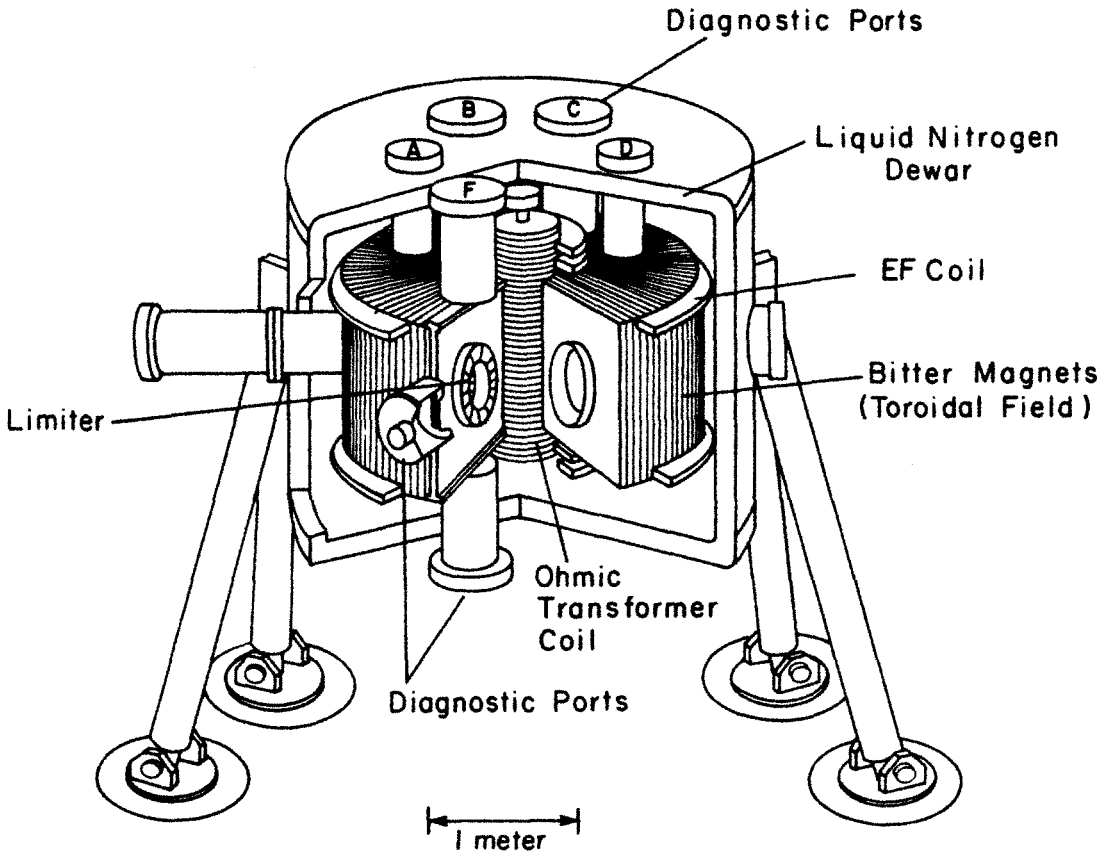

Figure 1.2 ALCATOR C Experiment

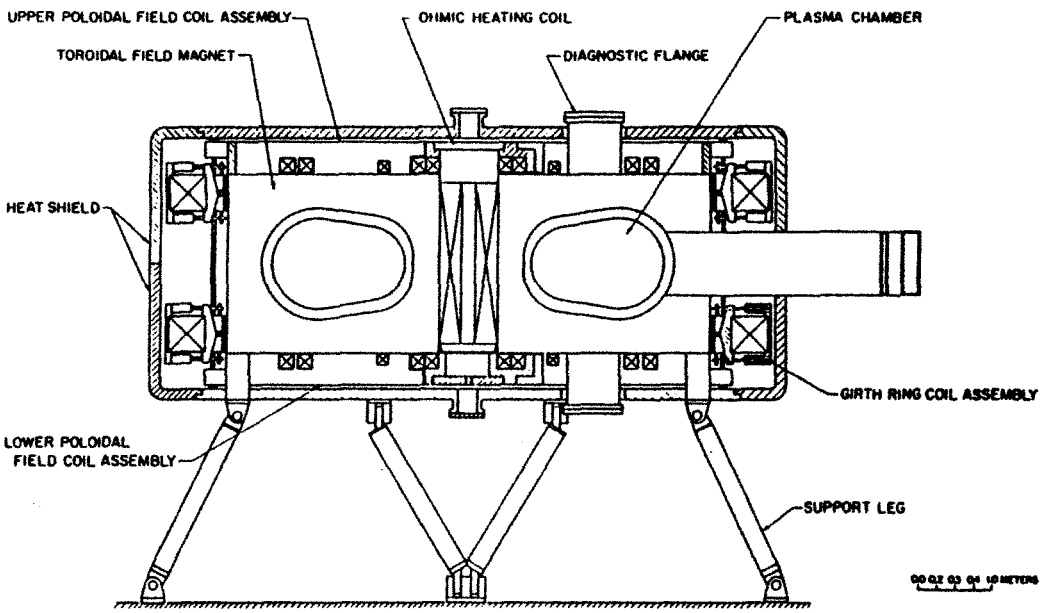

Figure 1.3 ZEPHYR Ignition Test Experiment

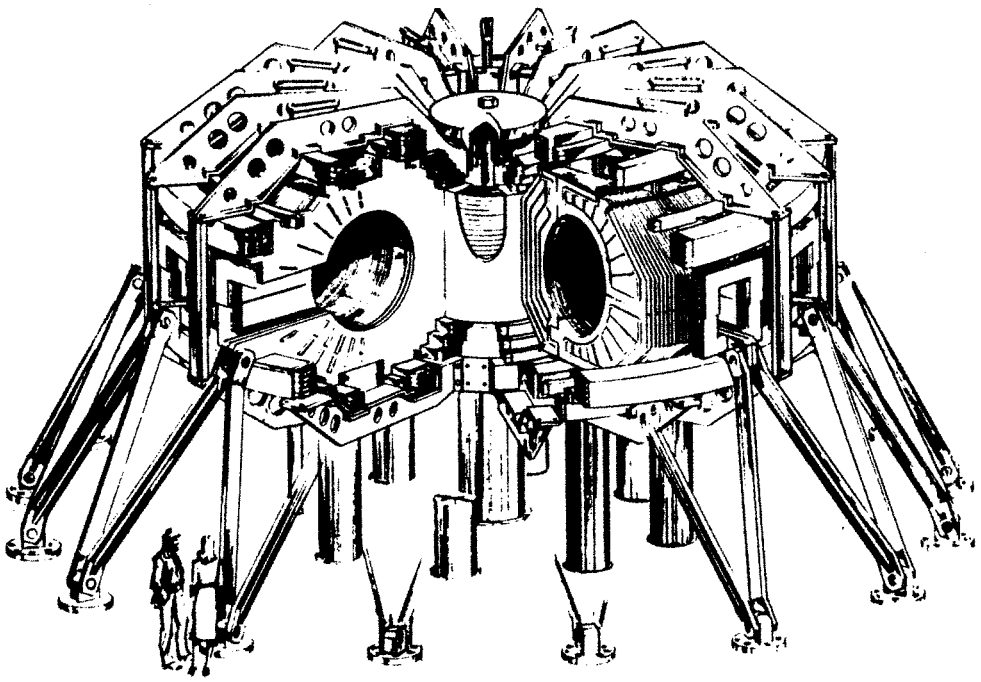

Figure 1.4 LITE Ignition Test Experiment

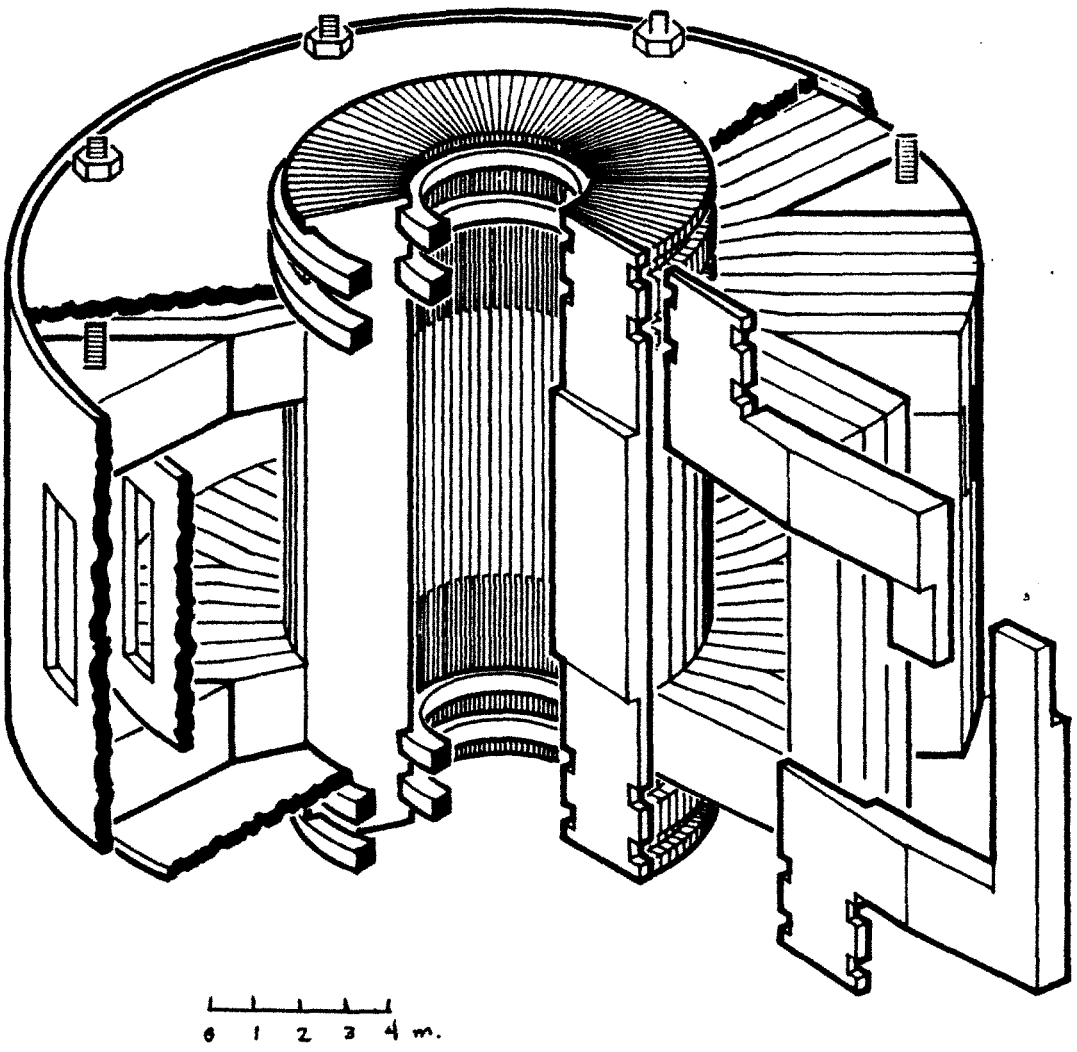

Figure 1.5 Resistive Commercial Tokamak Reactor

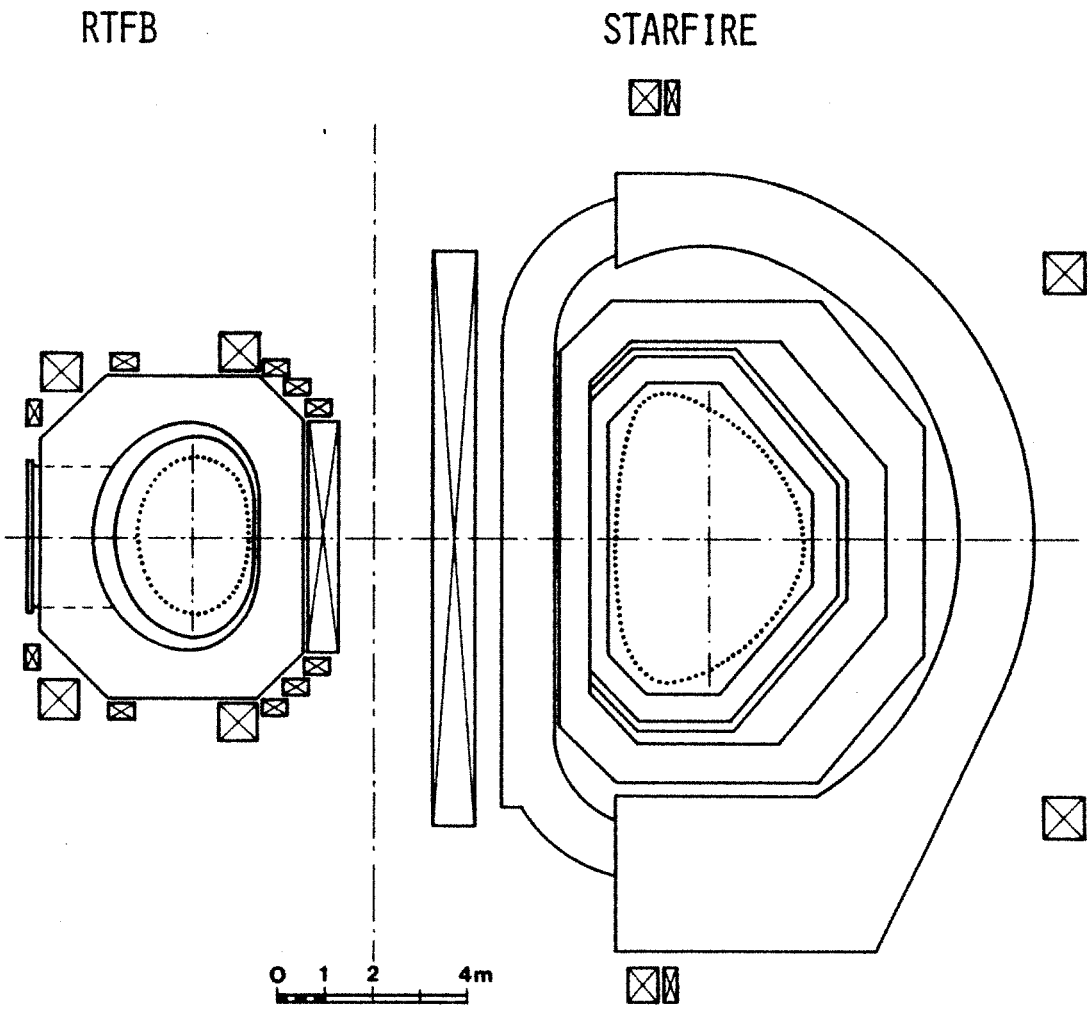

Figure 1.6 Resistive Magnet Tokamak Fusion Breeder Comparison With STARFIRE

$$^{6}Li + n \longrightarrow T + {}^{4}He + 4.8\ MeV$$

$$^{7}Li + n \longrightarrow T + {}^{4}He + n - 2.47\ MeV$$

Figure 1.7 Fusile Breeding Reactions

$$^{232}Th - n \longrightarrow {}^{233}Th \xrightarrow{22.2\ min.} {}^{233}Pa \xrightarrow{27\ d.} {}^{233}U$$

$$^{238}U - n \longrightarrow {}^{239}U \xrightarrow{23.5\ min.} {}^{239}Np \xrightarrow{2.35\ d.} {}^{239}Pu$$

Figure 1.8 Fissile Breeding Reactions

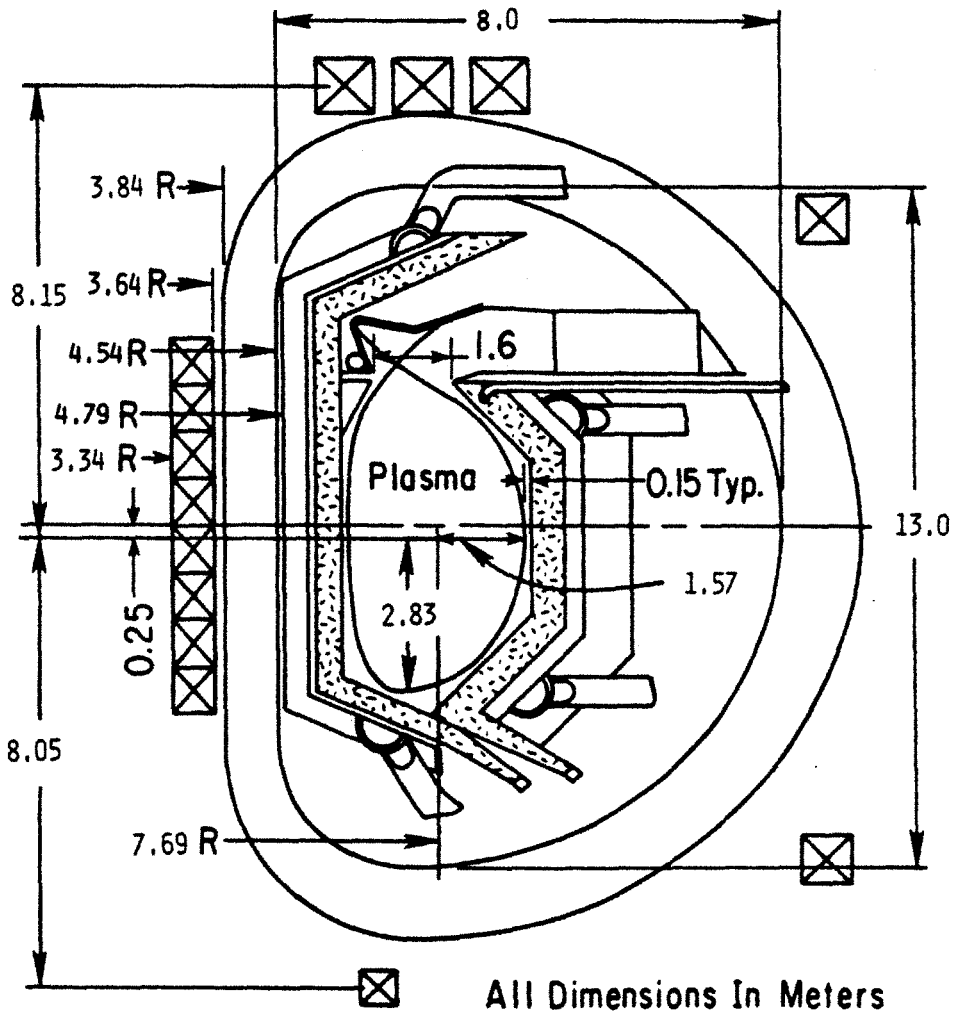

Figure 1.9 Superconducting Magnet Tokamak Fusion Breeder

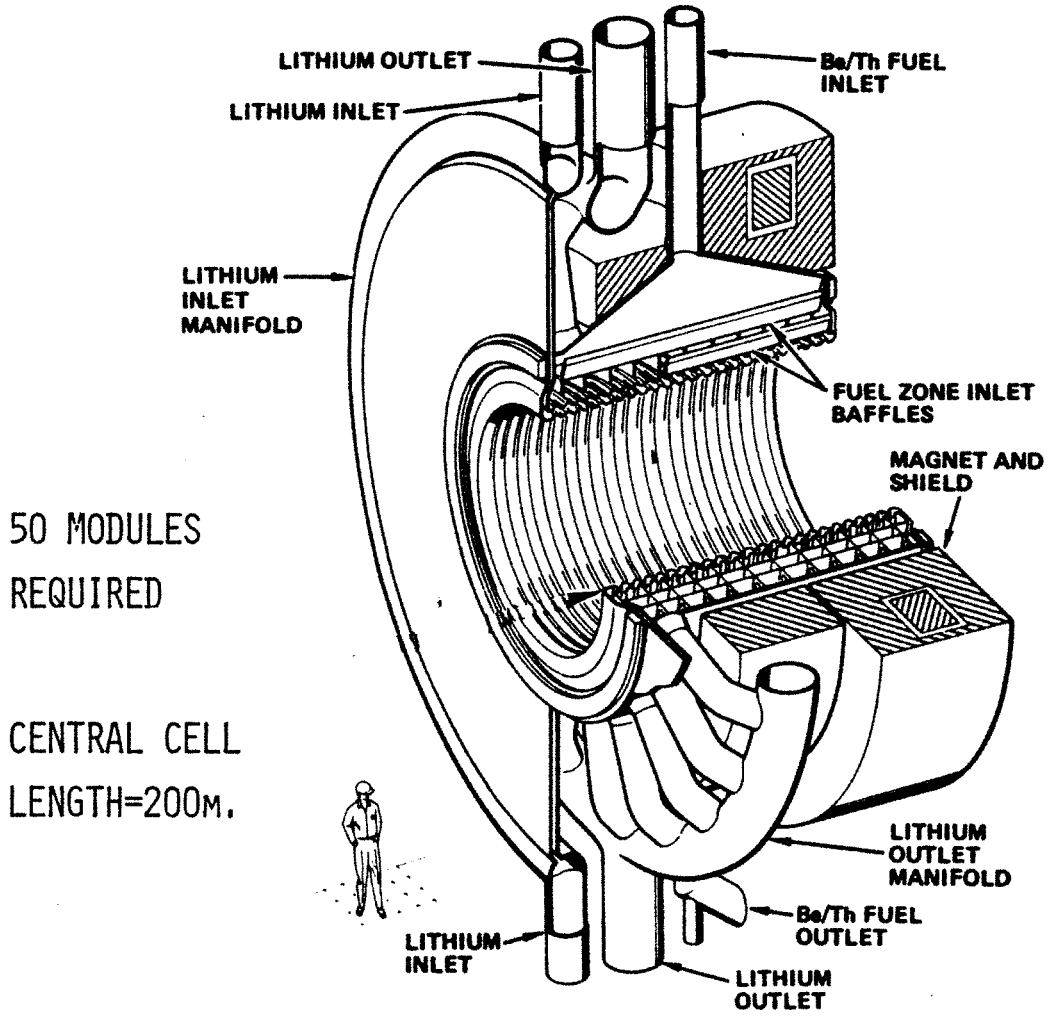

Figure 1.10 Superconducting Magnet Tandem Mirror Fusion Breeder

2. PARAMETRIC ANALYSIS

2.1 Introduction

Selection of a reference design for the resistive magnet fusion breeder requires a scan of the option space available, subject to constraints imposed from various considerations. These considerations may be established to take advantage of the unique characteristics of the resistive magnet tokamak. This chapter discusses the computer code used in the parametric studies of the RTFB, the STRESS code. Establishment of the selected design constraints is then considered, followed by parametric variations using the STRESS code. From the parametric scans of the option space, a single reference design is selected for further study. The chapter is then summarized.

2.2 The STRESS Code

A computer code for parametric analysis of resistive magnet tokamaks has previously been developed within the Reactor Studies Group at the MIT Plasma Fusion Center [2.1]. This code, known as STRESS, is written in the algebraic manipulation language MACSYMA and runs on the MC PDP-10 at the MIT Laboratory for Computer Science. STRESS uses simple relationships, scaling laws and numerical fits to more complicated analytic techniques to quickly scan parameter space. Thus, self-consistent designs can be quickly generated for a large number of cases to locate attractive regimes of operation.

STRESS was used in the present work to parametrically examine potential designs for resistive magnet tokamaks for fusion breeder application. The STRESS code was originally developed in the MIT Plasma Fusion Center Reactor Studies Group for use in the design of the ZEPHYR (Zund Experiment

PHYsiken Reactor) ignition test experiment at the Max Planck Institute für Plasma Physik, Garching, Federal Republic of Germany [2.1]. ZEPHYR was a tokamak ignition test reactor which would have used toroidal field magnets based on the Bitter plate principle. Ignition would have been achieved through adiabatic compression and neutral beam heating. Thus, the toroidal field coils would have required an extended horizontal bore to allow space for compression. The designs on which the principles for the ZEPHYR magnets were based, Alcator A and Alcator C, have round bores. Hence, the ZEPHYR toroidal field coils were studied extensively.

These studies required many parametric iterations to examine potential designs. Therefore, a parametric computer code was written to simplify the iteration of designs. This code contains analytic expressions for simplified geometries and numerical fits to more complex analyses. Various parameters can be fixed and/or allowed to vary in a self-consistent manner. Important parameters for the present study are shown in Table 2.1. A description of each of these parameters follows.

The neutron wall load, P_n (MW/m^2), determines the first wall area necessary for a fixed fusion power level. The neutron wall load is also important to first wall lifetime, which can impact the economics of the machine. Additionally, higher neutron wall loads are accompanied by higher heat loads which can cause more problems with cooling and stress considerations in the first wall [2.2].

The major radius, R, and minor radius, a, determine the envelope in which the plasma resides. These two parameters, along with the elongation, determine the volume of the plasma. The volume of the plasma, along with the power constant, determines the fusion power of the machine.

Another important parameter is the plasma β. The plasma β is defined as

$$\beta = \frac{\sum nkT}{B^2/2\mu_0} \tag{2.1}$$

where the summation is over all species in the plasma, n is the density of each species and T is the temperature of each species. Boltzman's constant is denoted by k. The magnetic field strength is B and μ_0 is the permeability of free space. In words, β is defined as:

$$\beta = \frac{\text{particle pressure}}{\text{magnet field pressure}} \tag{2.2}$$

and is a measure of the power density in the plasma for a given magnetic field.

Plasma elongation affects the β which can be reached. In general, the higher elongations allow reaching higher β. However, the higher elongations come at the expense of more stringent requirements on the poloidal field coil systems. Additionally, the elongation affects the height, and thus the mass, of the toroidal field coils.

The outer radius of the ohmic heating coil determines the space envelope inside the toroidal field coil, and thus, the minimum inside dimension of the toroidal field coil. The outer radius of the ohmic heating coil, along with the inner radius and the pulse length requirement, determines the stress levels in the ohmic heating coil. Thus, longer pulse length machines generally require larger ohmic heating coils which make the entire machine larger. The burn time for all machines in this study is 100 seconds. The performance of the ohmic heating coils could be increased within the same space envelope to give longer burn times or the coil could be moved into a position within the toroidal field

coil to give longer pulse lengths. Therefore, options exist for extending the burn time beyond the present value.

The stress limit in the throat of the toroidal field coil determines the thickness of the throat of the coil. The stresses are calculated from the vertical force and moment due to the magnetic field. The magnetic field is determined from the major and minor radii. the neutron wall load, the power constant, the elongation and the β scaling parameter. These relationships are then iterated on until the throat stress reaches the input limit. Stress limits in the throat are typically low (for example, the vertical force intensity is limited to 103 MPa), since the throat is of all copper construction in order to minimize resistive power losses. No stainless steel is used in the throat for structural strength.

Although not an input parameter. the STRESS code calculates the resistive power requirements of the toroidal field coil. This is usually a relatively large power requirement which results in a large recirculating power. The simplified model in STRESS does not calculate accurate values of the toroidal field magnet power requirements. but is useful for quick parametric scans. The power requirements of the toroidal field magnet will be calculated separately for the reference design. Additionally, the power requirement for the equilibrium field coil system will be calculated separately.

The inboard and outboard plasma-magnet distances determine the space available for the first wall/scrape off region and breeding blankets or shielding. These dimensions should be small enough that the machine is not unnecessarily large, but large enough to achieve the required parameter, such as, adequate breeding or shielding.

The power constant contains all the information about plasma densities and temperature, averaged over profiles. It is related to the average power

density within the plasma region.

The β scaling parameter, C_β, is the constant in the expression in which the achievable β scales inversely with aspect ratio

$$\beta = \frac{C_\beta}{A} \tag{2.3}$$

where A is the aspect ratio (plasma major radius divided by plasma minor radius).

The above parameters are generally set by the user of the STRESS code and parametrically varied. STRESS calculates other quantities of interest. The important calculated quantities include the ohmic heating coil resistive power and stress, the toroidal field coil resistive power, the equilibrium field coil resistive power, the fusion power, the performance index and the margin to ignition.

2.3 Design Constraints

In order to restrict the parameter space to manageable proportions, a number of constraints were imposed. These constraints were based on previous experience and preliminary parametric studies. These constraints were established to ensure that the final reference design is conservative, but not unduly so. The general constraints are summarized in Table 2.2. A discussion of each of these constraints follows.

The major radius was limited to 4 m. to keep the RTFB as compact as possible. This was done to take maximum advantage of the capabilities of the resistive toroidal field magnets.

The toroidal field coil throat stress was limited to 15 ksi in order to have the throat be conservatively stressed, but not be unduly conservative. This stress level corresponds to that usable with all copper construction in the throat and is the vertically acting stress in the throat of the TF coil. No stainless steel will be needed for structural strength.

The plasma elongation was set at 1.6. since this will allow reaching average β of about 6% for the aspect ratios initially envisioned. It was thought that this β was realistically achievable.

The inboard blanket-shield thickness was to be as thick as necessary to shield the insulation in the throat of the toroidal field coil so that reasonable magnet lifetimes could be attained. Minimizing this thickness would allow the machine to be as compact as possible, consistent with insulation shielding requirements.

2.4 Parametric Variations

This section describes several of the parametric variations performed using the STRESS code. The following discussion is a distillation of the many studies done. The parameters considered important are the major radius, the neutron wall load, fusion power, stress in the ohmic heating and toroidal field coils, the plasma-magnet distance, plasma β and mass of the toroidal field coil.

2.4.1 Neutron Wall Load

Parametric variation of the neutron wall load is shown in Table 2.3 for average neutron wall loads of 1.0, 2.0 and 4.0 MW/m^2 and minor radii of 0.70, 0.90, 1.10 and 1.30 m. The engineering Q (fusion power/TF power) is shown in Fig. 2.1 and the toroidal field coil mass utilization (TF mass/fusion power) is shown in Fig. 2.2. The following general trends may be observed.

As the neutron wall load increases with fixed minor radius, the engineering Q, fusion power, TF power, TF mass utilization and the toroidal magnet field also increase. However, as the minor radius increases, for fixed neutron wall load, the toroidal magnetic field decreases. This decrease in the toroidal magnet field is due to the constraint of fixed wall load and fixed stress in the throat of the TF coil. The decrease in the magnetic field will be important to lithium pressure drop calculations, to be considered in the next chapter, since the pressure drop scales with B^2. An increase in the minor radius, with fixed neutron wall load, also results in an increase in the major radius and the fusion power, as well as increases in the engineering Q and the TF mass utilization. However, the increase in engineering Q and mass utilization with increasing minor radius are not as large as the corresponding increases with wall load.

2.4.2 Blanket Envelope

Parametric variation of the blanket envelope is shown in Table 2.4 for plasma-magnet distances of 0.50, 0.70 and 0.90 m. These parametrics are for uniform distance around the entire plasma. The first wall/scrape off region and blanket-shield assembly must fit into this space envelope. An allowance of 0.15 m. is used for the first wall/scrape off region. This leaves blanket-shield spaces of 0.35, 0.55 and 0.75 m.

As the blanket envelope is increased, for fixed minor radius, the fusion power increases due to the increased size of the machine. The toroidal field coil power requirement also increases more rapidly than fusion power so that the engineering Q and mass utilization decrease, as seen in Fig. 2.4 and Fig. 2.5. However, these decreases are relatively minor.

2.4.3 Plasma β

Parametric variation of the plasma β scaling parameter (C_β) is shown in Table 2.5. It is seen that as C_β increases, the plasma β increases. However, the plasma β also increases as the minor radius increases since the aspect ratio decreases. However, the cause of these two changes is different. The change in C_β is an assumed variation for parametrics, while the change in β is due to the change in aspect ratio with minor radius.

The variation of the engineering Q and the toroidal field coil mass utilization for various C_β is shown in Fig. 2.6 and Fig. 2.7. The change in these figures of merit is relatively small with C_β.

2.5 Selection of the Reference Design

From the above parametrics, a reference case was selected for further study. The reference design was limited to a major radius of less than 4 m. to take advantage of the compact designs possible with resistive magnets. The neutron wall load of 2.0 MW/m^2 was selected to give a relatively long first wall lifetime, in comparison to the 4.0 MW/m^2 neutron wall load. Additionally, for the energy multiplication of the blankets considered (~8) and the projected thermal power of the blanket for a typical large plant at beginning of cycle (4000-5000 MWth), the 1.0 MW/m^2 neutron wall load cases would have given a total blanket power

lower than the typical range and the 4.0 MW/m^2 neutron wall load case would have given a higher blanket power than the typical range, except for the a=0.70 m. case. However, this case was not considered due to the lower engineering Q and TF mass utilization than the reference case which was selected. The higher wall loads would also have increased the heat load to the first wall, and thus, increased the cooling requirements, although the cooling requirements of the first wall were not evaluated.

The plasma-magnet distance of 0.50 m. inboard was selected since neutronic calculations showed that this was the minimum thickness necessary to provide shielding to limit radiation at the toroidal field coils to levels which would allow the magnets to last the life of the plant. The upper and lower plasma-magnet distances were set at 0.90 m. to both protect the magnets in these regions without shielding other than the blanket and allow adequate thickness of the molten salt to reduce the neutron leakage into the magnet. Thus, the molten salt breeding captures would be as large as possible.

Thus, the reference design is based on nominal parameters and optimized for maximum engineering Q and TF mass utilization within the constraints of a major radius of less than 4 m. and neutron wall load of 2.0 MW/m^2. The fusion power level is adequate to give a blanket thermal power in the 4000-5000 MWth range with the energy-multiplying blankets which are considered.

At this point, a more accurate calculation was performed to determine the resistive power losses in the toroidal field coil. The results of this calculation are shown in Table 2.7 for the base STRESS configuration and cases in which the upper and lower plasma-magnet distances were increased to 0.90 m. and the thickness of the outboard leg of the toroidal field coil was varied. The case with the thicker upper and lower blanket was adopted as the reference case for all following analyses since this gives more breeding and insures that

magnet shielding will be limited only by the shielding effectiveness of the inboard blanket.

This information is be used in the parametric costing to evaluate the effects of varying the outboard magnet thickness, and thus the mass of the toroidal field coil, accounting for the change in resistive power requirements. This evaluation shows that the 0.75 m. outboard leg thickness gives a minimum cost of electricity.

Additionally, a calculation was done to estimate the resistive power requirement of the equilibrium field magnet system. This calculation gives an equilibrium field magnet system power requirement of 170 MWe.

2.6 Summary

The STRESS code has been previously developed in the Reactor Studies Group at the MIT Plasma Fusion Center. The STRESS code uses analytic expressions, scaling rules and fits to more complex analytic techniques to model resistive magnet tokamaks. The STRESS code was used to parametrically examine potential designs for the RTFB.

Major parametric scans were done varying neutron wall load, blanket envelope and the plasma β scaling parameter. Constraints were placed on the design to take advantage of the unique attributes of the resistive magnet tokamak. The major radius of the plasma was limited to less than 4 m. The neutron wall load was selected to be 2.0 MW/m^2 which gives a fusion power that will keep the total blanket power in the 4000-5000 MWth range. The stress in the throat of the toroidal field coil was fixed at 103 MPa. to insure conservative stress levels in the throat of the magnet. The thickness of the outboard leg of the toroidal

field coil was set at 0.75 m., since costing calculations, presented in Chapter 4, show this thickness to give the lowest cost of capacity.

These constraints resulted in a machine with a major radius of 3.81 m. and a minor radius of 1.3 m. The fusion power is 618 MW and the toroidal field coil power requirement is 260 MWe. The equilibrium field magnet power requirement is 170 MWe. The space envelope for the blanket is 0.35 m. inboard and 0.75 m. outboard and upper and lower. This includes a 0.15 m. allowance for first wall/scrape off.

References

2.1 Williams, J. E. C., et al., "Conceptual Design of a Bitter Magnet Toroidal Field System for the ZEPHYR Ignition Test Reactor," Massachusetts Institute of Technology Plasma Fusion Center Report PFC/RR-81-24, (May 1981).

2.2 LeClaire, R. J., "Methods of First Wall Structural Analysis With Applications to the Long Pulse Commercial Tokamak Reactor Design," Eng. Thesis, Dept. of Nucl. Engr., M. I. T., (May 1984).

TABLE 2.1

Important Parameters in the STRESS Code

Neutron Wall Load
Major Radius
Minor Radius
Plasma Elongation
Outer Radius of Ohmic Heating Coil
TF Coil Throat Stress
TF Coil Resistive Power
Inboard Plasma-Magnet Distance
Outboard Plasma-Magnet Distance
Power Constant
Critical β

TABLE 2.2

Preliminary Design Constraints

Major Radius	$\leq$ 4m.
Throat Stress	$\leq$ 15ksi.
Plasma Elongation	$\sim$ 1.6
Inboard Blanket-Shield Thickness	Minimum

TABLE 2.3

Neutron Wall Load Variation

	Minor Radius (m)			
	0.70	**0.90**	**1.10**	**1.30**
P_n = 1.0 MW/m^2				
Major Radius (m)	3.13	3.28	3.45	3.64
sp ect Ratio	4.47	3.64	3.14	2.80
OH Stress (MPa)	8.87	14.8	23.1	34.2
OH Power (MW/e)	7.6	14.5	25.7	42.6
TF Power (MW/e)	174	166	163	164
TF Mass (Gg)	2.19	2.66	3.23	3.90
B_{TF} (T)	5.6	4.7	4.2	3.8
Fusion Power (MW/th)	137	184	237	296
P_n = 2.0 MW/m^2				
Major Radius (m)	3.37	3.47	3.62	3.81
Aspect Ratio	4.81	3.86	3.29	2.93
OH Stress (MPa)	14.0	22.9	35.3	51.9
OH Power (MW/e)	12.7	23.5	40.8	66.9
TF Power (MW/e)	219	201	194	193
TF Mass (Gg)	2.57	3.04	3.66	4.36
B_{TF} (T)	6.9	5.8	5.1	4.6
Fusion Power (MW/th)	294	390	498	618
P_n = 4.0 MW/m^2				
Major Radius (m)	3.79	3.79	3.90	4.06
Aspect Ratio	5.41	4.21	3.55	3.12
OH Stress (MPa)	23.9	37.3	56.2	81.5
OH Power (MW/e)	23.2	40.5	68.1	109
TF Power (MW/e)	299	261	245	238
TF Mass (Gg)	3.29	3.69	4.29	5.07
B_{TF} (T)	8.7	7.2	6.3	5.7
Fusion Power (MW/th)	663	852	1070	1320

Elongation=1.6, $\delta_{f,t}$=0.50 m., δ_i=0.90 m., C_β=0.16
Power Constant=0.864. TF Stress=103 MPa. OH Radius=1.5 m.

TABLE 2.4

Blanket Envelope Variation

	Minor Radius (m)			
	0.70	**0.90**	**1.10**	**1.30**
δ=0.50 m.				
Major Radius (m)	3.29	3.42	3.59	3.77
Aspect Ratio	4.70	3.80	3.26	2.90
OH Stress (MPa)	13.6	22.3	34.6	51.2
OH Power (MWe)	11.9	22.4	39.2	64.8
TF Power (MWe)	218	203	197	197
TF Mass (Gg)	2.11	2.51	3.10	3.74
B_{TF} (T)	6.8	5.8	5.1	4.6
Fusion Power (MWth)	288	384	492	613
δ=0.70 m.				
Major Radius (m)	3.73	3.80	3.93	4.10
Aspect Ratio	5.33	4.22	3.57	3.15
OH Stress (MPa)	16.5	26.4	40.2	58.6
OH Power (MWe)	16.6	29.8	50.4	81.0
TF Power (MWe)	265	238	226	222
TF Mass (Gg)	2.98	3.42	3.99	4.75
B_{TF} (T)	7.3	6.1	5.3	4.8
Fusion Power (MWth)	326	427	540	666
δ=0.90 m.				
Major Radius (m)	4.24	4.22	4.31	4.46
Aspect Ratio	6.05	4.69	3.92	3.43
OH Stress (MPa)	20.1	31.2	46.6	66.9
OH Power (MWe)	23.0	39.2	64.2	100
TF Power (MWe)	326	280	260	250
TF Mass (Gg)	4.19	4.56	5.19	5.97
B_{TF} (T)	7.8	6.4	5.6	5.0
Fusion Power (MWth)	371	474	592	723

Elongation=1.6, C_β=0.16, P_n=2.0 MW/m^2
Power Constant=0.864, TF Stress=103 MPa, OH Radius=1.5 m.

TABLE 2.5

Plasma β Variation

	Minor Radius (m)			
	0.70	**0.90**	**1.10**	**1.30**
C_β =0.12				
Major Radius (m)	3.70	3.72	3.85	4.01
Aspect Ratio	5.29	4.13	3.50	3.08
$\langle\beta\rangle$	0.023	0.029	0.034	0.039
OH Stress (MPa)	19.3	30.3	45.9	66.7
OH Power (MWe)	18.5	32.6	55.1	88.9
TF Power (MWe)	281	248	234	229
TF Mass (Gg)	3.16	3.55	4.16	4.87
B_{TF} (T)	8.4	7.0	6.1	5.5
Fusion Power (MWth)	323	418	528	651
C_β =0.16				
Major Radius (m)	3.37	3.47	3.62	3.81
Aspect Ratio	4.81	3.86	3.29	2.93
$\langle\beta\rangle$	0.033	0.041	0.049	0.055
OH Stress (MPa)	14.0	22.9	35.3	51.9
OH Power (MWe)	12.7	23.5	40.8	66.9
TF Power (MWe)	219	201	194	193
TF Mass (Gg)	2.57	3.04	3.66	4.36
B_{TF} (T)	6.9	5.8	5.1	4.6
Fusion Power (MWth)	294	390	498	618
C_β =0.20				
Major Radius (m)	3.20	3.33	3.50	3.69
Aspect Ratio	4.57	3.70	3.18	2.84
$\langle\beta\rangle$	0.043	0.054	0.063	0.070
OH Stress (MPa)	11.3	18.8	29.3	43.4
OH Power (MWe)	9.9	18.8	33.0	54.6
TF Power (MWe)	188	176	173	173
TF Mass (Gg)	2.31	2.77	3.36	4.04
B_{TF} (T)	6.0	5.1	4.5	4.1
Fusion Power (MWth)	280	376	481	600

Elongation=1.6, $\delta_{f,t}$=0.50 m., δ_i=0.90 m., P_n=2.0 MW/m^2
Power Constant=0.864, TF Stress=103 MPa. OH Radius=1.5 m.

TABLE 2.6

Resistive Magnet Tokamak Fusion Breeder Reference Design

Plasma Parameters	
Major Radius of Plasma (m)	3.81
Minor Radius of Plasma (m)	1.30
Aspect Ratio	2.93
$\langle\beta\rangle$	0.055
Plasma Elongation	1.6
Performance × Elongation	3.8
Margin to Ignition × Elongation	2.9
Average Electron Density (m^{-3})	1.0+20
Average Electron Temperature (keV)	20
Plasma Current (amps)	9.3+6
Magnet Field at the Plasma Axis (T)	4.6
Inboard Magnet-Plasma Distance (m)	0.50
Outboard Magnet-Plasma Distance (m)	0.90
Upper and Lower Magnet-Plasma Distance (m)	0.90
Plasma Scrape-Off/First Wall Region (m)	0.15
Volume of Plasma (m^3)	203.36
Fusion Power (MWth)	618
Magnet Parameters	
Toroidal Field Magnet Height (m)	7.17
Toroidal Field Magnet Inner Radius (m)	1.50
Toroidal Field Magnet Outer Radius (m)	6.76
Volume of Toroidal Field Magnet (m^3)	379
Mass of Toroidal Field Magnet (Gg)	3.0
Toroidal Field Magnet Power (MWe)	260
Toroidal Field Magnet Stress (MPa)	103
Ohmic Heating Magnet Inner Radius (m)	0.75
Ohmic Heating Magnet Outer Radius (m)	1.50
Volume of Ohmic Heating Magnet (m^3)	22.05
Mass of Ohmic Heating Magnet (Gg)	0.2
Ohmic Heating Magnet Stress (MPa)	51.9
Ohmic Heating Magnet Power (MWe)	66.9
Equilibrium Field Magnet Power (MWe)	170

TABLE 2.7

Toroidal Field Coil Resistive Power Requirements

Outboard TF Coil Thickness	Resistive Power (MWe)
Base Case	
1.50 m.	215
δ_t = 0.9m.	
0.50 m.	282
0.75 m.	260
1.00 m.	247
1.50 m.	232

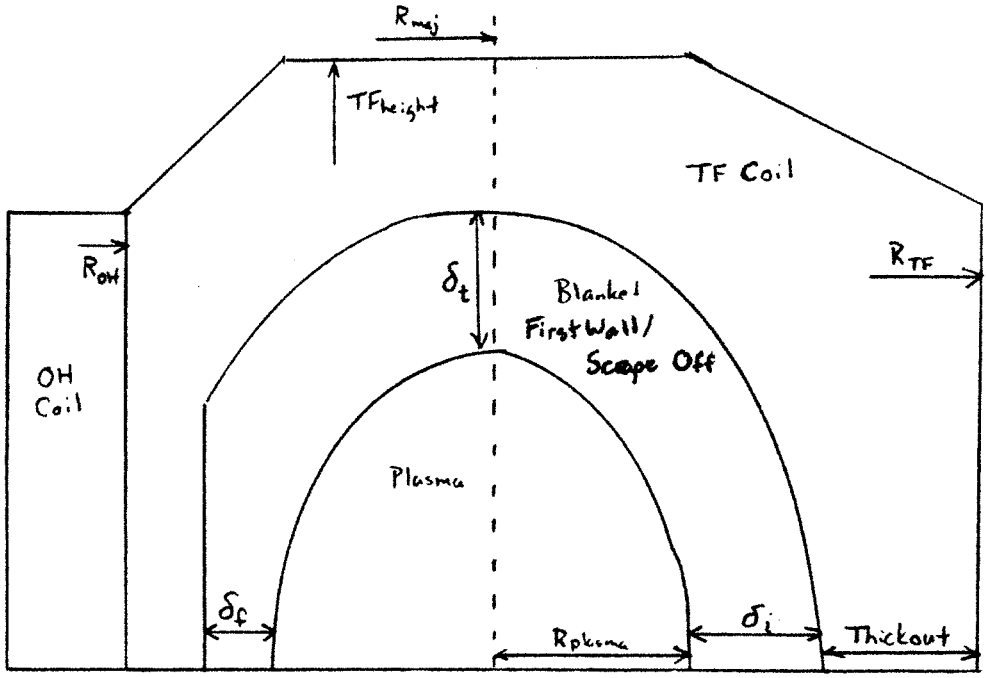

Figure 2.1 Schematic of STRESS Code Representation

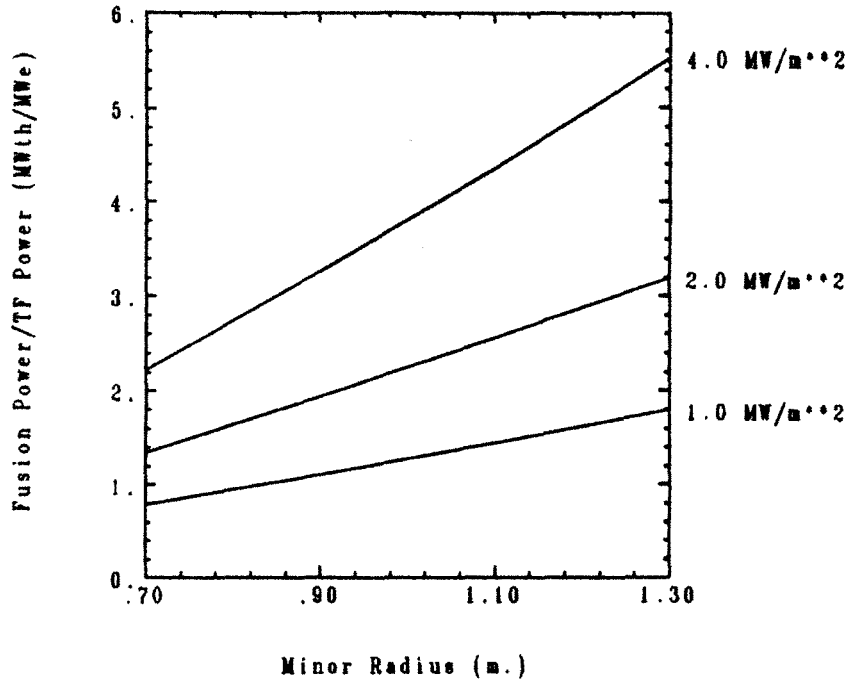

Figure 2.2 Fusion Power/TF Power for Various Neutron Wall Loads

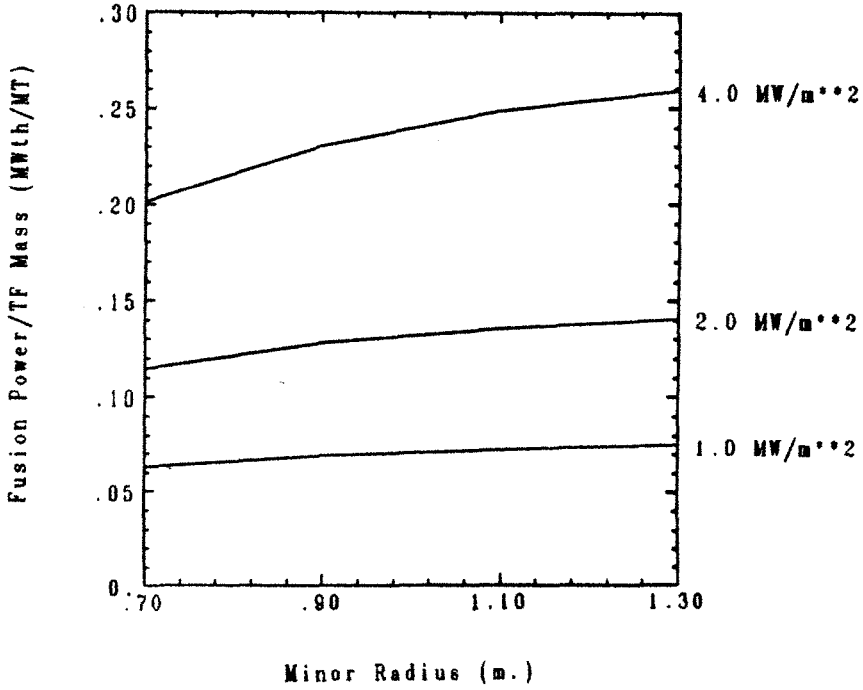

Figure 2.3 Fusion Power/TF Mass for Various Neutron Wall Loads

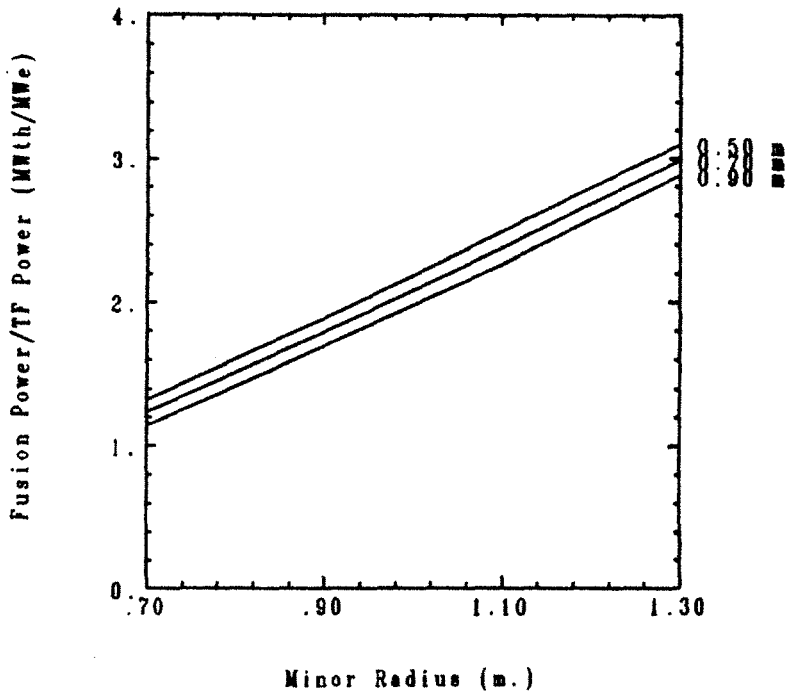

Figure 2.4 Fusion Power/TF Power for Various Blanket Envelopes

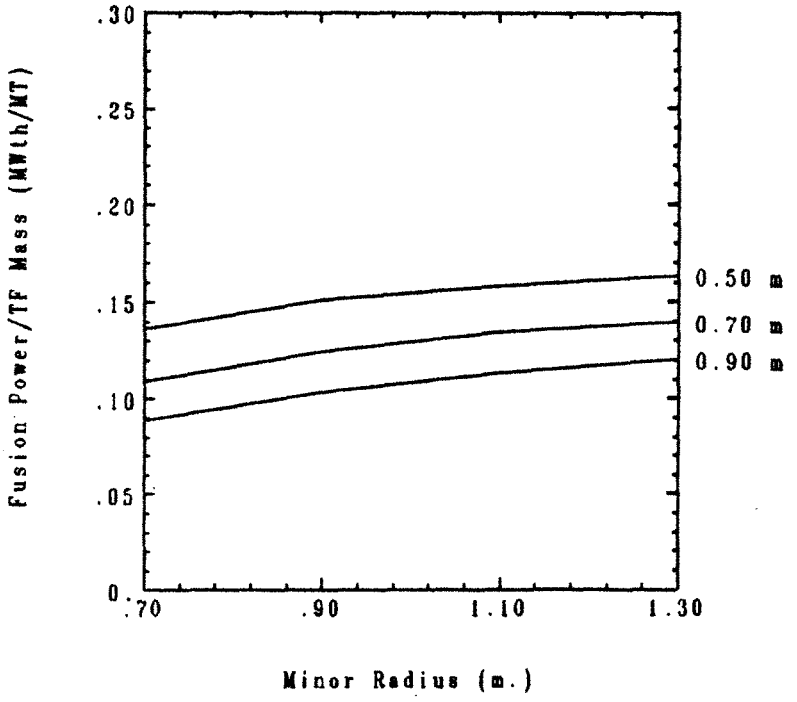

Figure 2.5 Fusion Power/TF Mass for Various Blanket Envelopes

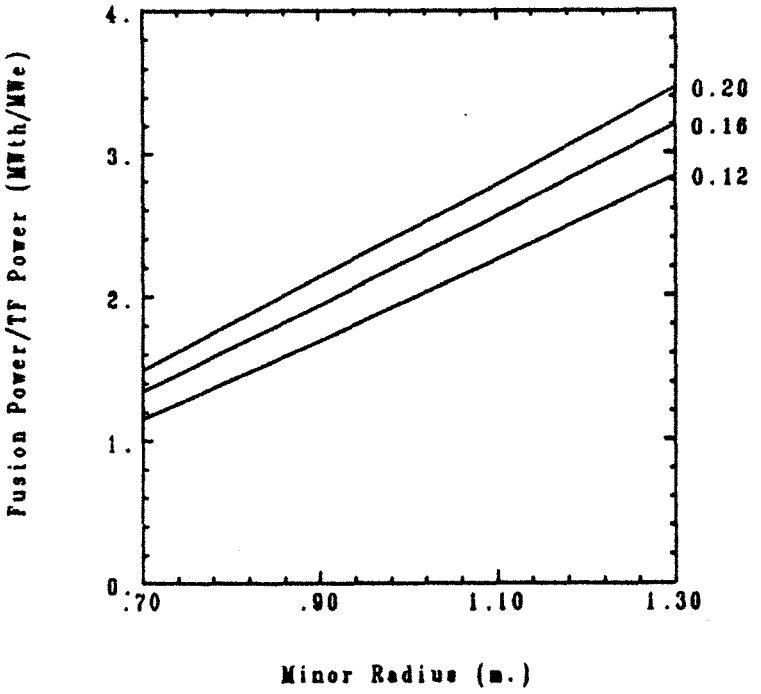

Figure 2.6 Fusion Power/TF Power for Various C_β

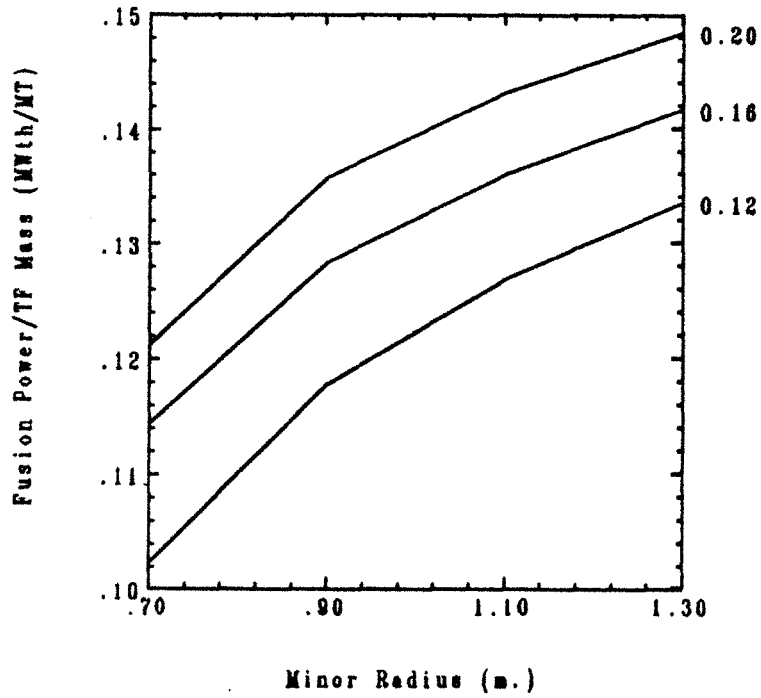

Figure 2.7 Fusion Power/TF Mass for Various C_β

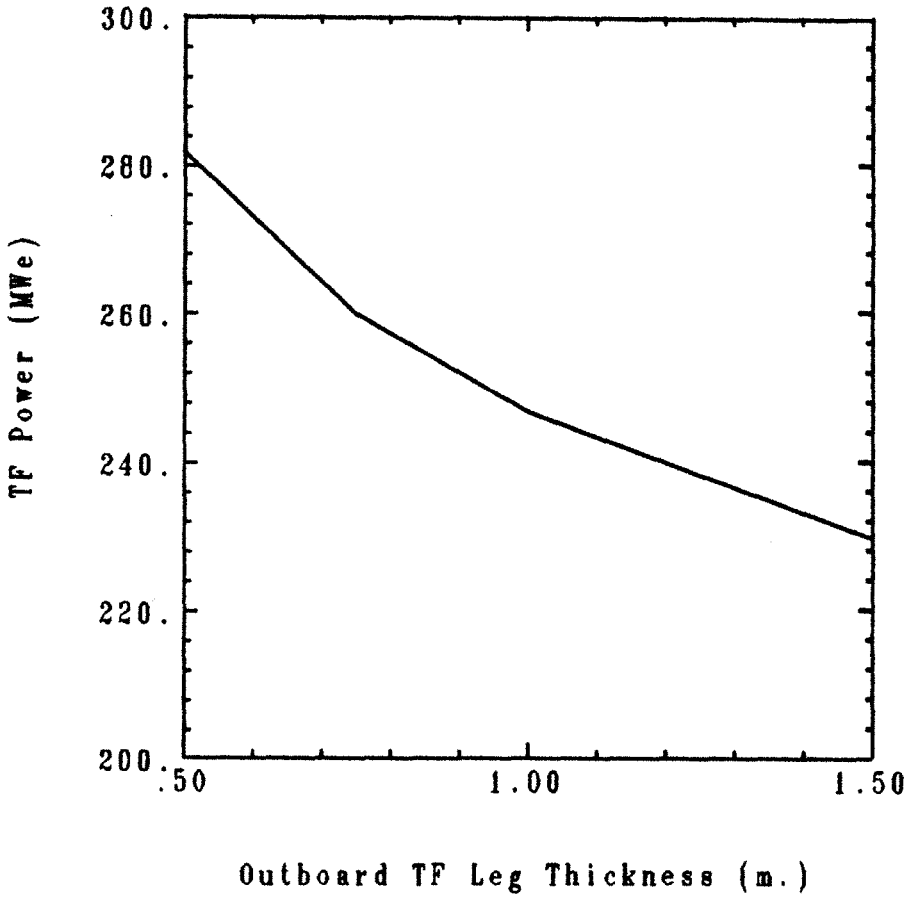

Figure 2.8 TF Power for Varying Outboard Leg Thickness

3. BLANKET ANALYSIS

3.1 Introduction

The reference design selected in the previous chapter included a space envelope for a blanket assembly. This chapter considers the blanket which will be placed in this space.

The blanket in a conventional fusion reactor serves the function of recovering the energy of the neutrons produced by the fusion reaction at a high enough temperature so that efficient conversion of this energy into electricity is possible. Additionally, the blanket must produce sufficient tritium to sustain the fusion reaction, accounting for losses of tritium within the system and during processing. The fusion breeder blanket has the additional function of producing fissile fuel for use in client fission reactors.

The chapter begins with a discussion of the nuclear data and codes used in the nuclear analysis. A description of the blanket configuration is presented, followed by the results of the one- and three-dimensional breeding and power calculations. An analysis of the lithium coolant flow is next presented, with the development of a design for the lithium flow ducts and an evaluation of the pressure drop and pumping power. An analysis of the uranium multiplier plate thickness is next performed, to insure that adequate heat transfer can be obtained to maintain the uranium multiplier well below the melting point of uranium. Finally, the chapter is summarized.

3.2 Nuclear Data and Codes

All of the nuclear analyses done for the RTFB were performed on the National Magnetic Fusion Energy Computer Center machines. These machines are a CDC-7600, a CRAY-1 and a CRAY-1S.

Two nuclear design code systems were used in the analysis of the RTFB blanket. The one-dimensional discrete ordinates code ONEDANT was used for investigation of the thickness and composition of the various zones in the blanket [3.1]. The three-dimensional Monte Carlo code MCNP was used for analyses which determined the breeding and power of the reference blanket design [3.2]. The various ONEDANT parametrics were used to adjust the three-dimensional MCNP values to investigate the effects of variations in the reference blanket design.

ONEDNT is a one-dimensional, diffusion accelerated neutral particle transport code developed at Los Alamos National Laboratory. ONEDANT solves the linear Boltzman transport equation using the method of discrete ordinates. In this approximation, the scattering integral is divided into discrete directions. Particles are then allow to scatter only in these directions. Anisotropic scattering is allowed through Legendre polynomial expansion of the angular scattering cross section. Thus, the magnitude of the scattering cross section in each of the discrete directions can vary.

ONEDANT uses multigroup data for neutron and photon transport. This data is supplied as a separate file, known as the cross section input library. The nuclear data used in this analysis was extracted from the file MATXS5 which existed on the NMFECC system [3.3]. MATXS5 is a coupled 30 x 12 neutron-gamma transport cross section file which was collapsed from ENDF/B-

V pointwise data. The ENDF/B-V pointwise data contain energy-cross section pairs which can be linearly or logarithmically interpolated. Additionally, resonance information is provided for some nuclei. The amount of information varies between isotopes, but the file is very large. The neutron energy spectrum used for weighting is the standard LANL 30 group spectrum consisting of a 14 MeV fusion peak, a fission spectrum, a 1/E spectrum and a Maxwellian thermal spectrum. A flat gamma weighting spectrum is used. MATXS5 contains a very large number of isotopes and cross sections for each isotope. The TRANSX code is used to extract a subset of the isotopes and cross sections in MATXS5 and make a library of the isotopes and reaction rates of interest for input to ONEDANT [3.4]. Additionally, the order of scatter approximation can be selected as well as the transport correction.

MCNP is a three-dimensional Monte Carlo neutral particle transport code also developed at Los Alamos National Laboratory. MCNP solves the linear Boltzman transport equation using the Monte Carlo method. In this method, particles are followed with the sequence of interactions governed by selection from distributions using a random series of numbers. A sufficient number of particles is followed until the accumulated quantities of interest have an uncertainty that is acceptably small.

Several nuclear data options exist in MCNP. Continuous energy cross sections based on ENDF/B-V are available. These cross sections are given on a linear-linear neutron energy-cross section grid. The number of cross section-energy pairs is sufficient to match the ENDF/B-V data to within a specified percent, usually 0.1%. Resonances are incorporated and Doppler-broadened to a specified temperature. Additionally, a discrete cross section set in which all cross sections have been collapsed into a 240 group structure is provided. This set is particularly useful in reducing the storage requirements for nuclear data where the energy resolution of the continuous energy treatment is not necessary.

ONEDANT is useful for performing parametric studies since the run time is relatively short, compared to MCNP. However, the limitation of one dimensional variation in the model can introduce problems in the modeling of realistic geometries. Additionally, the multigroup energy approximation used in ONEDANT can inappropriately represent nuclear cross sections, particularly in the case of isotopes which have resonance regions, such as uranium and thorium. On the positive side, ONEDANT can give pointwise values relatively economically compared to MCNP.

MCNP is useful to provide a check of the ONEDANT multigroup treatment of nuclear data by simulating the one-dimensional geometry. The MCNP geometry can model ONEDANT geometry exactly and thus reduce the differences to the cross section treatment (30 group in ONEDANT and 240 group and continuous energy in MCNP) and the MCNP uncertainties. The comparisons are based on region averaged values, such as breeding reactions and energy deposition.

3.3 Blanket Configuration

The basic blanket design used in this analysis is shown in Fig. 3.1. The blanket design is based on earlier work by Cook [3.5]. The breeding region of the blanket consists of two zones. The first zone is composed of uranium metal, clad in steel and cooled by liquid lithium. The second zone is cooled by a thorium-bearing molten salt, which also acts as a breeding medium. The dimensions of the regions in the one-dimensional model are given in Table 3.1. The composition of each of these zones is shown in Table 3.2. The atom number densities for the various materials are given in Table 3.3.

The first wall is modelled as steel 0.5 cm. thick in all neutronics analyses. No detailed analysis was done for the first wall.

Uranium metal is used in the front zone of the blanket to multiply the energy of the fusion neutrons. Since the reference design selected for the RTFB is a low performance fusion machine, energy multiplication is necessary to raise the power supplied to the turbine so that a net electric output may be achieved. Energy multiplication using uranium is more effective than with thorium since the fast fission cross section for ^{238}U is higher than for ^{232}Th. Additionally, the value of ν (neutrons produced per fission) is higher for ^{238}U than for ^{232}Th for the incident neutron energies of interest. Use of uranium in the front zone results in the production of plutonium, which may be used in client reactors.

Uranium could be used in several forms. Uranium oxide is used in LWRs since it has a relatively high melting point. Uranium carbide could be used since the lack of water coolant would allay the concern of production of flammable hydrocarbons during an accident. Uranium nitride is also a possible form. Of these three ceramics, uranium oxide has by far the largest experience base. However, it is currently projected that the reprocessing of oxide fuel using aqueous techniques will be relatively expensive [3.6]. Pyrochemical reprocessing of uranium metal is projected to be less costly, primarily due to the compactness of the equipment required, relative to aqueous reprocessing [3.7]. Since the RTFB may require reprocessing of significant amounts of material from the multiplier region to both recover the bred material and limit the energy generation in the region, uranium metal was chosen as the multiplying material. It should be noted that pyrochemical processing may also be applied to fuel in the oxide form with an additional step to reduce the oxide to metal.

3.4 One-Dimensional Nuclear Analysis

This section describes the one-dimensional neutronic analyses done for the RTFB. These analyses include breeding, energy multiplication and shielding of insulation in the toroidal field magnet. The nomenclature used is as follows: ^{6}T and ^{7}T denote tritium breeding from ^{6}Li and ^{7}Li , respectively. T, the total tritium breeding, is the sum of ^{6}T and ^{7}T. ^{233}F indicates captures in thorium which results in the production of ^{233}U . ^{239}F denotes captures in ^{238}U which result in the production of ^{239}Pu . F, the total fissile breeding, is the sum of ^{233}F and ^{239}F. All breeding values are per fusion neutron. The region integrated heating values are eV/sec/fusion neutron per cm. of height of the plasma.

3.4.1 One-Dimensional Breeding Analysis

A ONEDANT analysis was done to estimate breeding and energy multiplication in the reference RTFB blanket. The results of this analysis are shown in Table 3.4. A measure of the breeding performance is the total fissile and tritium breeding, T + F, which is 2.89 for the reference case. Although the tritium breeding does not appear to be sufficient (T=0.97), it will later be demonstrated that adequate tritium breeding can be attained, at the expense of ^{233}U production.

It may also be seen from Table 3.4 that considerable energy multiplication of the fusion neutrons occurs. This is due primarily to fissions in the multiplier region. Not only do these fissions multiply the energy of the neutron, but each fission results in the release of ~3 neutrons, some of which are of sufficient energy to cause further fast fissions. Thus, the net breeding ratio, T + F, can be significantly greater than 1. Other blankets have achieved high values of T + F, ranging from 1.6 to 3.7 for systems that breed ^{239}Pu [3.8].

A number of parametric studies were also done to investigate the effects of varying the thickness and composition of the various zones. A comparison of the reference configuration with a case in which the inboard molten salt zone was replaced with stainless steel is shown in Table 3.5. Although the tritium and ^{239}Pu breeding increase slightly, the total T + F decreases due to the loss of ^{233}U breeding in the inboard molten salt region.

The effect on breeding of varying the materials in the inboard blanket is shown in Table 3.6. The inboard molten salt and multiplier regions are replaced by stainless steel, lead and tungsten. It can be seen that the blanket power decreases significantly due to the loss of the energy multiplication of the inboard uranium region. However, although the total value of T + F decreases by as much as 27%, breeding in the outboard region increases by as much as 12%.

When stainless steel replaces the inboard multiplier and molten salt region, breeding in the outboard region changes. In the outboard region, tritium production increases by 2% and ^{239}Pu production increases by 5%, while ^{233}U production decreases by 1%.

When lead replaces the inboard multiplier and molten salt region, the total T + F for the outboard blanket increases by 12% . This is due to the neutron multiplication which occurs in the lead in the inboard region through the (n,2n) reaction.

When tungsten replaces the inboard multiplier and molten salt region, the total T + F in the outboard region decreases by 2%. The total breeding is also lower than the case with stainless steel by 4%, indicating that stainless steel is a better reflector of neutrons than tungsten.

The effect of changing the outboard multiplier configuration can be seen

in Table 3.7. These cases are for the inboard multiplier and molten salt replaced by lead. If the outboard multiplier thickness is increased from 11 cm. to 16 cm., displacing 5 cm. of molten salt, the total T + F increases by only 6%. However, tritium breeding increases by 23%. ^{239}Pu breeding increases by 21% while ^{233}U breeding decreases by 30% . The power also increases by 11% . This case will be used in the system economic evaluation section to determine the cost or value of increasing the multiplier thickness, which will increase the blanket thermal power and total capital cost.

Variation of the inboard blanket thickness is shown in Table 3.8. The inboard molten salt thickness was decreased in increments of 5 cm. from a total blanket thickness of 35 cm. to a total blanket thickness of 15 cm. The effect on breeding is primarily in the loss of ^{233}U production in the inboard molten salt region. It should be noted that some geometry effects may also be seen, since the major radius was decreased as the inboard blanket thickness was decreased. In the breeding values which are mostly affected by the geometry (*i.e.*, ^{239}Pu production), inboard values decrease slightly while outboard values increase slightly, with the total staying relatively constant.

Variation of the molten salt thickness in the outboard blanket has little effect on breeding, as can be seen from Table 3.9. The largest effect is the change of ^{233}U breeding which increases (0.18%) slightly when the molten salt thickness is increased by 10 cm. and decreases slightly (0.54%) when the molten salt thickness is decreased by 10 cm. This indicates that the outboard molten salt thickness could be reduced by 10 cm. without a large penalty in reduced breeding.

The increase in ^{239}Pu concentration in the multiplier with blanket life will result in an increase in the effective multiplication factor, k_{eff}. This factor must be kept less than 1 to insure that the blanket remains subcritical. In order to

insure that the blanket does not reach criticality, k_{eff} will be limited to 0.9.

The calculated value of k_{eff} for the reference blanket configuration with 0.02 a/o ^{239}Pu is 0.43. However, even though this value is significantly less than 0.9, further consideration is necessary since the multiplier geometry may be reconfigured after an accident. Thus, infinite medium calculations were done to determine the infinite medium multiplication factor, k_{∞}. The material used in the infinite medium calculations was uranium metal only with varying a/o of ^{239}Pu . The lithium and steel clad were conservatively not included since they would increase absorptions and reduce the value of k_{∞}. Additionally, the lithium and steel clad might not be retained with the uranium metal after an accident.

The calculated values for k_{∞} are shown in Table 3.10 for ^{239}Pu a/o of 0.01, 0.02 and 0.03. The values of k_{∞} are, respectively, 0.66, 0.82 and 0.95. Thus, the ^{239}Pu a/o will be limited to 0.02, to conservatively keep the value of k_{∞} less than 0.9.

Additionally, the effect of water intrusion into the metal was examined. The calculated values of k_{∞} are shown for varying metal and water fractions in Table 3.11. From Table 3.11, it is seen that the value of k_{∞} for metal with no water is more limiting than the cases in which water is present.

The production of fissile fuel in the blanket of the RTFB will cause a change in the energy multiplication of the blanket. Power levels in the molten salt will not change appreciably due to fissioning of ^{233}U , since the bred ^{233}U is removed in order to keep the power in the molten salt low and avoid "losing" the fuel to neutron capture. However, the power level in the multiplier region will change significantly, since the bred ^{239}Pu stays in the uranium metal until the uranium is removed for reprocessing. The molten salt region undergoes

continuous processing to remove ^{233}U and ^{233}Pa while the multiplier undergoes periodic batch reprocessing.

The effect of the blanket lifetime build-up of ^{239}Pu was simulated by adding 0.01 and 0.02 a/o ^{239}Pu to the multiplier region. This was done for both natural (0.00711 a/o ^{235}U) and depleted uranium (0.0020 a/o ^{235}U) in the multiplier region. The results are shown in Table 3.12 for natural uranium in the multiplier and in Table 3.13 for depleted uranium in the multiplier. Both cases are shown for 0.00, 0.01 and 0.02 a/o ^{239}Pu in the multiplier It may be seen from Tables 3.12 and 3.13 that the blanket power increases significantly as the concentration of ^{239}Pu in the blanket increases. A power increase of approximately 45% occurs from beginning of cycle (BOC) to a plutonium concentration of 0.02 a/o for both the natural and depleted uranium multipliers. Tritium and ^{233}U breeding also increase, due to the increased fissions with ^{239}Pu in the multiplier. The net production rate of ^{239}Pu decreases as the concentration of ^{239}Pu increases. Although the build-up of ^{239}Pu causes increased fissions, and thus increased ^{239}Pu breeding, the captures in ^{239}Pu also increase so that the net production of ^{239}Pu decreases with blanket lifetime. The natural uranium multiplier is used for all further analyses due to the higher attainable power level.

It should be noted that this simplified analysis neglects the effects of fission product production, which would tend to reduce breeding through increased parasitic (non-breeding) captures and the effect of build-up of a mixture of trans-^{239}Pu isotopes, some of which would be parasitic and some of which would be fissile. However, since the discharge burnup of the multiplier is expected to be relatively low, approximately 15000 MWd/MT, these effects would be expected to be mostly offsetting, and are thus neglected.

Comparison to a more detailed analysis for a fissioning blanket supports this contention [3.9]. The analysis for the reference design for the standard

mirror hybrid reactor included an evaluation of the blanket lifetime exposure effects. The net ^{239}Pu breeding was seen to decrease by a factor of 0.88 from BOC to an exposure that corresponds to the 0.02 a/o ^{239}Pu considered above. The corresponding decrease in net ^{239}Pu breeding for the RTFB is a factor of 0.94 from BOC to 0.02 a/o ^{239}Pu . Thus, the ^{239}Pu breeding results are in general agreement. This comparison is only intended to indicate that the RTFB results are reasonable, since the blankets in the standard mirror hybrid reactor and the RTFB are different.

As the exposure of the uranium increases, the parasitic absorptions would be expected to increase and, thus, the production rate of ^{239}Pu would be less than predicted by this simplified analysis.

The total tritium breeding parameter, T, must be equal to one (one tritium atom produced per fusion reaction) in order to replenish the tritium consumed in the plasma. The parameter must in reality be somewhat greater than one to allow for losses in processing and recovery. The value of T for the reference design is 0.97. This is not adequate. However, since the molten salt, in which ^{233}U is being produced along with a small amount of tritium, contains LiF with the Li depleted in ^{6}Li, the enrichment of ^{6}Li can be adjusted to give the value of T desired. This basically involves trading the production of an atom of ^{233}U for an atom of tritium. The effect of replacing the depleted lithium in the molten salt (0.01 a/o ^{6}Li) with natural lithium (0.075 a/o ^{6}Li) can be seen in Table 3.14. The value of T increases by 0.21 to 1.18 as the ^{233}U production decreases by 0.17 to 0.68. The total fissile breeding, F, decreases by 0.21 indicating that some of the neutrons that were previously reflected from the molten salt back into the multiplier and captured in ^{238}U are now being captured in ^{6}Li . Therefore, the tritium breeding parameter can be increased up to a value of 1.18, at the penalty of a reduced ^{233}U breeding rate. Thus, the tritium breeding will be increased to a value of 1.05 in the economic analyses

and the ^{233}U breeding decreased accordingly. Note that this discussion is for BOC tritium breeding. The tritium breeding increases with multiplier exposure. The average tritium breeding is maintained at 1.05.

3.4.2 Insulation Damage Analysis

Several ONEDANT studies were done to estimate the radiation dose to the insulation in the toroidal field coil. The thinnest blanket region is on the inboard side of the plasma. Thus, the plasma side of the inboard leg of the toroidal field is the location where insulation dose rate would be expected to be the highest.

The inboard leg of the toroidal field coil contains only copper, water and insulation. No stainless steel is used for structural strength, as in the outboard leg. The insulation is placed between individual plates to keep single turn voltages low and effectively make each plate a single turn winding. The insulation is in compression and does not serve a dielectric function due to the low voltages; it serves primarily to physically separate the plates and provide vertical restraint to prevent the plates from moving relative to each other.

It should be noted that the ONEDANT calculations are for regions which are homogenized. The atom densities of individual materials are averaged over the large zones. Thus, the heterogeneity of the interleaved plates and associated insulation, along with the cooling channels, is not preserved. However, the predicted insulation dose rates should be reliable, since no strong thermal absorbers are present. A particular concern would be the presence of boron in the insulation, which could result in enhanced energy deposition in the insulation near water-filled cooling channels due to the high thermal cross section of ^{10}B which results in the emission of an α particle.

Recent studies have indicated that integral insulation doses of 1.4+12 rads may be acceptable from the standpoint of insulation integrity [3.10]. This value will be used in determining magnet lifetimes, assuming that insulation degradation is the limiting factor.

Insulation dose rate variation with tungsten replacing the inboard multiplier and molten salt region in varying thickness is shown in Table 3.15. The dose rates shown are for full power operation. Even the 34 cm. tungsten thickness would give a toroidal field magnet lifetime of 5.5 years at 75% capacity factor. Thus, additional material combinations for magnet shielding were examined.

The insulation dose rates for these materials are shown in Table 3.16. The magnet lifetime is seen to vary from 0.9 years to 26.3 years. The longest magnet lifetime (lowest insulation dose rate) is given by the composite shield. This shield consists of tungsten, steel, titanium hydride, boron carbide and water (0.55, 0.15, 0.15, 0.10 and 0.05 v/o). The shield of tungsten and water does almost as well, with an insulation lifetime of 19.9 years. The two shields of tungsten and uranium at less than theoretical density give short magnet lifetimes. These shields could be considered as representative of helium cooled designs. The addition of hydrogen, possibly in the form of titanium hydride, could improve the performance of these two shields. This is seen in the cases in which 0.1 v/o water is used.

Thus, the shield which will be used is the composite shield, which gives the longest magnet lifetimes. This shield will displace a section of the multiplier and molten salt, and thus, reduce the blanket power and breeding. These effects are evaluated in the following section.

3.4.3 Comparison with Monte Carlo Calculations

As was previously noted, the ONEDANT calculations are based on multigroup cross sections which are averaged over various energy intervals. In fertile materials, such as ^{238}U and ^{232}Th , large variations in cross section may occur in energy ranges small compared to the width of the multigroup treatment. In resonance regions, these effects may become important to predicting absorption rates, since significant energy self-shielding may occur. This effect may be accounted for in the multigroup treatment by averaging the pointwise cross sections over the multigroup intervals using a neutron flux spectrum representative of the region. This is usually an iterative procedure. Alternatively, a calculation can be done using a method which uses a more realistic representation of neutron cross sections to check the multigroup method. Since the ONEDANT cross sections were not corrected for energy self shielding, this was necessary. The comparison calculation was done with the Monte Carlo code MCNP, which uses nuclear data represented by a set of energy, cross section pairs which are interpolated to the neutron energy. The number of these energy, cross section pairs is sufficient that the MCNP data reproduce the ENDF data, within a small percentage, usually 0.1%.

An MCNP model was used which matches the ONEDANT reference blanket geometry model exactly. Thus, the differences in the two calculations could be attributed to the differences in cross sections and cross section treatment in the two codes. It should be noted that the MCNP calculations are also for homogenized regions, and thus, do not account for spatial self-shielding effects, which are related to energy self-shielding effects.

The comparison between ONEDANT and MCNP one-dimensional breeding calculations is shown in Table 3.17. MCNP predicts fewer captures in ^{232}Th

(1.3% less) and ^{238}U (5.4% less) than ONEDANT and more captures in ^{6}Li (0.4% more). Thus, the largest difference is in ^{238}U captures which is an indication of ^{239}Pu production. The total breeding value, T+F, is 2.0% less. Also, the number of fissions decreases by 3.7 % which is important to energy multiplication. This will be investigated more fully in the energy multiplication calculation in the following section.

3.5 Three-Dimensional Nuclear Analysis

ONEDANT geometry is limited to variation in one dimension only. MCNP has a much more general three-dimensional geometry modeling capability. Thus, MCNP can be used to simulate a more realistic configuration.

A section view of the MCNP model used in the three-dimensional analyses is shown in Fig. 3.2. This section is rotated about the centerline of the ohmic heating coil. Note that the model is uniform in the toroidal direction. Additionally, no penetrations are included. However, this model should more accurately predict breeding in the thinner inboard and thicker outboard blanket in addition to including the geometry effect of the nested elliptic torii representing the various regions.

A comparison of the ONEDANT and 3-D MCNP results is shown in Table 3.18. MCNP predicts 4% lower tritium breeding than ONEDANT and 10.7% lower ^{239}Pu breeding. However, the ^{233}U breeding is higher by 9.8% . The total T + F is lower by 2.4% . The fissions also drop by 5.2% which contribute to the decrease in the predicted blanket thermal power from 4986 MWth to 4436 MWth or a decrease of 11%.

The reason for this difference is primarily in the multiplier region. Reduced captures in ^{238}U resulting from the self-shielding effect discussed previously are reflected in both the lower ^{239}Pu breeding and fewer fast fissions. The result of fewer fissions is that not only is the blanket power lower, but fewer neutrons are available to be captured in breeding materials.

Another interesting comparison is between the one-dimensional MCNP and the three-dimensional MCNP. These two calculations use the same cross section sets and treatments and thus the differences can be attributed to geometry. This comparison is shown in Table 3.19. Although the total values of T + F agree well, the individual values differ significantly between one- and three-dimensional treatments. The tritium and ^{239}Pu breeding are lower and the ^{233}U breeding higher in the three-dimensional case. A qualitative explanation of this effect is as follows.

The one-dimensional model represents a slice of an "infinitely" high set of nested cylinders, with no variation in the axial direction, as shown in Fig. 3.3. Since the particles are emitted isotropically within the source region, the "average" length of a particle trajectory through the multiplier region is greater than the thickness of the multiplier region. However, in the three-dimensional model, as also shown in Fig. 3.3, the "average" length of a particle trajectory is more nearly the thickness of the multiplier region. Thus, the number of mean free paths within the region is less, and fewer interactions in the multiplier region are predicted in the three-dimensional model than in the one-dimensional model. This corresponds to lower tritium and ^{239}Pu breeding in the three-dimensional MCNP model.

The total values of breeding are approximately the same because the multiplier and molten salt regions are thick enough that very little leakage occurs. Thus, any neutron that enters these regions or is born through fission is cap-

tured. The fissions are only slightly different since this involves only the neutrons with an energy above ~ 2 MeV, the fast fission threshold.

From the three-dimensional MCNP breeding and energy multiplication calculations, the reference breeding and energy multiplication values for the beginning of cycle were selected. These values are shown in Table 3.20 for the case in which the composite shield is used in the inboard region to shield the toroidal field magnets and a case in which the shield is not used. The case in which no separate shield (other than the blanket itself) is used to shield the toroidal field magnets will be considered in the economic analyses to determine the penalty for use of the shield to extend the toroidal field coil lifetime to the life of the plant. Note that the case with the shield is lower in power and breeding than the case without the shield. This is due to the displacement of a segment of the multiplier and molten salt by the shield.

3.6 Blanket Pressure Drop Calculations

Liquid lithium metal is used for cooling the high power density multiplier region in the resistive magnet fusion breeder. Lithium is attractive as a material for production of tritium to sustain the fusion reaction. However, since lithium is a metal and a good conductor of electricity, its motion in the magnetic fields present in the fusion breeder will induce electromotive forces (emf) in the flowing lithium [3.11]. The induced emf can in turn generate currents in the lithium and adjacent structure. The induced currents can cause pressure gradients far in excess of those experienced in normal flow in the absence of a magnetic field. These pressure gradients must be estimated to determine if pressure drops in the lithium coolant are reasonable and can be contained.

This section summarizes the phenomena involved and the equations necessary to calculate the pressure drop for the fusion breeder. The implementation of the pressure drop equations in the COST code for the fusion breeder geometry is discussed. Analyses for both insulated and uninsulated ducts are presented.

3.6.1 Pressure Drop for Liquid Metals in Magnetic Fields

The flow of liquid metals in magnetic fields is governed by the Navier-Stokes equation with an additional term in the momentum balance which comes from the forces due to induced currents. These currents are induced by the motion of the metal, which is a good electrical conductor, in the magnetic field. Consideration is given only to the pressure drops induced by the magnetic field since, for typical fusion breeder parameters, the normal fluid flow pressure drops are much less. The equations which govern this motion are summarized as follows:

The force acting on a conductor moving in a magnetic field is given by

$$\mathbf{F} = \mathbf{J} \times \mathbf{B}, \tag{3.1}$$

where $\mathbf{J}$ is the current induced in the conductor by the magnetic field $\mathbf{B}$. The force term can also be written as a pressure gradient:

$$\nabla \mathbf{P} = \mathbf{J} \times \mathbf{B}. \tag{3.2}$$

The current induced in the conductor is given by:

$$\mathbf{J} = \sigma \mathbf{V} \times \mathbf{B}, \tag{3.3}$$

where $\mathbf{V}$ is the velocity of the fluid and σ is the conductivity along the path the currents follow. Thus, the pressure gradient is given by:

$$\nabla \mathbf{P} = \sigma \mathbf{V} \times \mathbf{B} \times \mathbf{B}, \tag{3.4}$$

This is the general form which will be further simplified to the fusion breeder geometry. Assuming thin wall circular ducts, the pressure drop simplifies to

$$\frac{dp}{dx} = \sigma V B^2 \frac{c}{1+c} \tag{3.5}$$

where V is the average fluid velocity and the conductivity ratio of the wall to the fluid, c, is

$$c = \frac{\sigma_w t_w}{\sigma a} \tag{3.6}$$

where a is the pipe radius or channel half thickness, t_w is the wall thickness, σ is the fluid conductivity and σ_w is the wall conductivity [3.12]. In the thin wall approximation, $c \ll 1$ and $Ha \cdot c \gg 1$ and the pressure drop is limited by the conductivity of the wall. In the lithium duct $c \approx 5 \times 10^{-4}$ and the Hartman number, which is discussed in the next section, is $Ha \approx 5 \times 10^4$. Thus the conditions for the thin wall regime are satisfied.

For the case of a rectangular duct of rectangular cross section and unequal wall thickness

$$\frac{dp}{dx} = \frac{\sigma B^2 c_1}{4ab\rho} \frac{Q}{1 + \frac{t_1 a}{3t_2 b}} \tag{3.7}$$

where t_1 is the duct thickness normal to the **B** field and t_2 is the duct half thickness parallel to the **B** field [3.14]. The channel half thickness along the **B** field is a and b is the channel half thickness perpendicular to the **B** field. Q is the mass flow rate of the fluid. Note that c_1 is given by

$$c_1 = \frac{\sigma_1 t_1}{\sigma a} \tag{3.8}$$

The duct geometry is shown in Fig. 3.4.

The pressure drop associated with an abrupt change in flow area or field is given by

$$\Delta p = 0.2\sigma V B^2 a\sqrt{c} \tag{3.9}$$

The pressure drop for a bend in the flow channel with one leg parallel to **B** is

$$\Delta p = 0.5\sigma V B^2 a N^{-\frac{1}{3}} \tag{3.10}$$

where N , the Stuart number, also known as the interaction parameter, relates to the ratio of the electromagnetic force to the inertia force and is given by

$$N = \frac{\sigma B_0^2 a}{\rho V} \tag{3.11}$$

Appropriate physical data for lithium and the duct wall material are shown in Table 3.21 and Table 3.22.

The preceding discussion has developed the necessary relationships to calculate pressure drops in the resistive magnet fusion breeder. The following section applies these relationships to the resistive magnet fusion breeder to evaluate pressure drops in the primary coolant system.

3.6.2 Resistive Magnet Fusion Breeder Flow Geometry

Flow of liquid metals in magnetic fields is accompanied by an increased pressure drop due to the magnetic field. This pressure drop increase is greatest when the flow is perpendicular to the magnetic field direction. Thus, blanket designs should have shorter flow paths perpendicular to magnetic fields and longer flow paths aligned with the field to minimize pressure drops.

The general flow path for the resistive magnet fusion breeder lithium coolant circuit is shown in Fig. 3.5 in section view and Fig. 3.6 in plan view. The blanket is divided into toroidal sectors. Each of these toroidal sectors is cooled by flowing lithium which enters through the top of the magnet at one end of the sector, flows along the multiplier region and exits out the top of the magnet. The inlet and outlet regions at each end of a sector consist of a plenum region which is connected to a single pipe.

The plenum region distributes the lithium flow into rectangular ducts, each of which is connected to a poloidal segment of the multiplier region. The plenum region would require an orifice at the inlet to each duct to distribute the flow such that each poloidal segment receives adequate cooling.

The inlet and outlet regions are confined in the radial direction from the inboard side of the inboard multiplier region to the outboard side of the outboard multiplier region, as shown in Fig. 3.5. The toroidal extent of the inlet and outlet regions is twice the channel half thickness, which is allowed to vary in the parametrics which follow. The thickness of the channel wall is also varied to simulate the effect of insulated walls.

3.6.3 Implementation in the COST Code

The above formulations were used in the COST code to calculate the pressure drops in the liquid metal primary coolant circuit and the resultant pumping power. The procedure for this calculation is as follows.

The blanket is first divided into toroidal sectors, since it is unlikely that the entire multiplier region would be cooled by a single coolant circuit. The number of toroidal sectors determines the length of the flow path for removal of heat from the uranium metal.

Each toroidal sector is then divided poloidally into a number of segments. The segments would each be cooled by a separate downcomer and separate toroidal flow path, provided by structure between the poloidal segments. The power in each segment is determined by multiplying the total multiplier power by the fraction of first wall area subtended by each segment and the first wall

heat load by the area of each segment. The mass flow rate of lithium required to remove the heat from each segment is determined by

$$Q_{seg} = \frac{P_{seg}}{c_p \Delta T} \tag{3.13}$$

The temperature rise across each segment is fixed at 150 °C. It is limited by compatibility of the lithium and structural material.

The lithium flow enters the plenum region at the top of the toroidal field coil. Lithium is distributed into each of the downcomers. The lithium then flows down, through the magnet and into the molten salt region, where the toroidal field is encountered. The flow then proceeds through the molten salt and into the end region of the multiplier segment. Lithium then turns and flows parallel to the toroidal field, removing heat from the multiplier region. After exiting the multiplier, the lithium flow turns up and moves out of the magnet to an outlet plenum region and then on to the primary heat exchanger.

The COST code only calculates the pressure drops associated with the magnetic field since these should dominate the primary lithium circuit pressure drops. The pressure drops calculated are for (a) entering the magnetic field, (b) flowing downward through the molten salt region and (c) turning from perpendicular to parallel to the toroidal field. These pressure drops are calculated as follows: (a) Eqn. 3.9, (b) using Eqn. 3.7 and (c) using Eqn. 3.10. These pressure drops are summed and multiplied by 2, to account for inlet and outlet pressure drops. The pumping power is calculated for each poloidal segment by the relationship

$$P_{pump,seg} = \frac{Q\Delta p}{\rho} \tag{3.14}$$

The total pumping power is obtained by summing the pumping power for each poloidal segment, multiplying by the number of toroidal segments and multiplying by 2, to account for the top and bottom of the tokamak.

Additionally, the mass of the downcomers and risers is calculated, since this should be a measure of the relative cost of each configuration.

3.6.4 Parametric Variations

The above formulation was used to parametrically examine the lithium duct configuration. These calculations were done for channel half-thicknesses along the direction of the magnetic field of 5, 10 and 15 cm., for 2, 4 and 8 toroidal segments and 10, 20, 30, 40, 50 and 60 poloidal segments. Additionally, two duct wall thickness were considered: one representing uninsulated ducts, 0.5 cm., and one representing insulated ducts, 0.025 cm. The insulated duct construction would consist of a structural wall of 0.5 cm. thickness coated with a thin layer of insulating material and lined with a thin section of steel of thickness 0.025 cm. [3.14].

The calculation results are summarized in Table 3.23 for an uninsulated and an insulated duct. More parametrics are given in Appendix C. The pumping power values shown are the sum of the pumping power for the differing pressure drops across each poloidal segment. The maximum pumping power column is calculated assuming each poloidal segment experiences the same pressure drop as the maximum due to the orificing to achieve the required lithium flow rates through each poloidal segment. The duct mass is calculated based on the wall

thickness for the uninsulated case and on the basis of a 0.5 cm. structural wall thickness for the insulated case. Note that these structural thicknesses may not be adequate for the calculated pressures.

Although detailed structural evaluations were beyond the scope of this evaluation, a simplified analysis can determine which cases are most reasonable. For the case of a rectangular flat plate clamped along all edges:

$$\sigma_{max} = 0.5q\frac{l^2}{t_1^2} \tag{3.14}$$

where σ_{max} is the maximum stress in the plate which occurs at the center of the long edge, q is the uniform load on the plate, t_1 is the thickness of the plate and l is the width of the plate [3.13]. The factor of 0.5 is for the case in which the width is much less than the length, as for the lithium pumping duct. This can be rearranged to give

$$q = 2\sigma_{max}\frac{l^2}{t_1^2} \tag{3.15}$$

For a σ_{max} of 107 MPa, as an illustrative parameter, and the various values of l which correspond to the number of poloidal segments, the allowable pressure inside the duct for a given duct thickness can be estimated. These values are shown in Table 3.24 for duct thickness of 0.5 cm. and 1.0 cm. Using the data from Table 3.24 for a duct thickness of 0.5 cm. and Table 3.23 for the uninsulated duct, it can be seen that none of the cases demonstrate a pressure drop that is within the limit taken from Table 3.24. However, the case for the duct half-thickness of 15 cm. has a pressure drop of 2.20 MPa. The duct limit for this case is 1.98 MPa.

In view of the uncertainties in the MHD pressure drop calculations, it may be argued that a reduction in the uncertainties may give a pressure drop which results in a usable duct design, even with uninsulated ducts. This is because of the uncertainty in the MHD calculations which is thought to predict pressure drops in excess of those which would be seen in a real configuration. For example, the inlet and turning pressure drops are 67% of the total calculated pressure drop. Each of these pressure drop correlations have a coefficient which is based on experimental configurations. Although the coefficients used are constant, the coefficient for the bend calculation is expected to decrease as c decreases [3.14]. Thus, the calculated pressure drop for the bend would also decrease. This is one example of the uncertainties in the MHD pressure drop calculations. Thus, it is considered that the uninsulated case shown in Table 3.23 for 8 toroidal segments and 60 poloidal segments is an acceptable design.

For the case of insulated ducts, also shown in Table 3.23, smaller ducts can be used with acceptable pressure drops. This would result in less steel structure added in the molten salt region, which would decrease breeding due to increased parasitic captures. This structure was not considered in the neutronics calculations. However, the ducts also add lithium in the molten salt region which will increase tritium production.

It should be noted that the pumping power for all cases in which the pressures are reasonable are within an acceptable range.

If the duct thickness is increased to 1 cm., the pressure drops would approximately double. Minor differences would occur due to the change of flow area decreasing slightly. However, using the simple plate model, the allowable pressure within the duct would increase by a factor of 4. This is in contrast to circular ducts where the allowable pressure scales with the thickness of the wall and the MHD pressure drop scales inversely with the wall thickness, and thus,

increasing the wall thickness does not result in any improvement.

3.7 Uranium Plate Thickness Analysis

The uranium fuel form is conceived as plate fuel with the lithium coolant flow oriented toroidally, as shown in Fig. 3.6. For lithium flow along the toroidal magnetic field, MHD effects can be expected to affect the heat transfer between the fuel and lithium. Specifically, turbulence will be suppressed [3.14]. This section presents an analysis of the uranium plate thickness to demonstrate that a reasonable design can be achieved to keep the uranium metal temperature well below the melting point.

3.7.1 Heat Transfer Correlations for Liquid Metals in MHD Flow

Magnetic fields modify the velocity distributions in liquid metals flowing in closed channels [3.11]. Velocity gradients at the walls are increased due to suppression of turbulence. Thus, the convective heat transfer rate is increased. However, this effect is usually overshadowed by the heat transfer due to molecular conduction, which is high in metals. At moderate values of the Hartman number, which is the square root of the ratio of the electromagnetic force to the viscous force, the heat transfer rate may increase due to the increased velocity gradient at the wall. However, as the field increases further and the Hartman number increases, a "saturation" occurs and increasing the field further does not increase the heat transfer rate. This is the regime in which the RTFB multiplier lithium coolant operates.

The heat transfer correlation used in this work is

$$Nu = 1.62 + \frac{0.005Pe}{1 + 1890(Ha/Pe)^{1.7}} \tag{3.15}$$

This is for flow in a longitudinal magnetic field (**B** field along the direction of flow) [3.11]. The Nusselt number is given by

$$Nu = \frac{ha}{\kappa} \tag{3.16}$$

and the Peclet number is the ratio of inertial forces to heat diffusivity and is given by

$$Pe = \frac{\rho c_p V a}{\kappa} = Re \cdot Pr \tag{3.17}$$

The Prandtl number is the ratio of the rate at which momentum may diffuse through a fluid due to molecular motion (related to the kinematic viscosity, ν) to the rate at which heat may diffuse in the fluid (related to the thermal diffusivity, α) and is given by

$$Pr = \frac{\nu}{\alpha} \tag{3.18}$$

The thermal diffusivity is given as

$$\alpha = \frac{\kappa}{\rho c_p} \tag{3.19}$$

Thus, the Prandtl number is

$$Pr = \frac{c_p \mu}{\kappa} \tag{3.20}$$

The Hartman number is the square root of the ratio of the electromagnetic force to the viscous force and is given by

$$Ha = B_0 a \sqrt{\frac{\sigma}{\rho \nu}} = \sqrt{N \cdot Re} \tag{3.21}$$

The Reynolds number is the ratio of momentum forces to viscous forces and is given by

$$Re = \frac{V a}{\nu} \tag{3.22}$$

The above relationships will be used to calculate the heat transfer coefficient for the RTFB multiplier geometry.

3.7.2 Uranium Plate Analysis

The plate fuel geometry is shown in Fig. 3.7. The equation for the temperature distribution in the fuel and clad is

$$T = T_b + q_w \left[\frac{a^2 - x^2}{2 k_f a} + \frac{\delta_c}{k_c} + \frac{1}{h} \right] \tag{3.23}$$

where T_b is the bulk temperature of the coolant, q_w is the heat transferred to the coolant through the clad, a is the fuel half-thickness, x is the distance from the fuel centerline, k_f is the thermal conductivity of the fuel, δ_c is the thickness of the clad, k_c is the thermal conductivity of the clad and h is the convective heat transfer coefficient in the coolant [3.15]. This model accounts only for the heat deposited in the uranium region, since heat deposition in the clad and coolant is much less. Additionally, it is assumed that the heat generation rate is constant across the uranium region.

A short computer program, HTCAL, was written to quickly examine temperature profiles for various thicknesses of the uranium plates. These calculations were performed for power densities representing peak and average locations within the multiplier region. The magnetic fields throughout the multiplier region are sufficiently high that all turbulence in the lithium is suppressed and heat transfer is by molecular conduction. The Nusselt number was observed to have a uniform value of 1.62 for all cases considered. Pertinent values from the analyses are summarized in Table 3.25.

The constraints considered were the uranium melting point of 1135 °C, the lithium melting point of 180 °C and the maximum interface temperature of the clad and lithium of 550 °C. From the blanket temperature rise of 150 °C, the inlet temperature was set at 340 °C and the outlet temperature was set at 490 °C. From Table 3.25, it is seen that for both the peak and average power density the limiting factor is the clad-lithium interface temperature. A uranium thickness of 1.0 cm. is seen to limit the clad-lithium interface temperature to 540o^C and the maximum temperature in the uranium to $\sim$ 300 °C below the melting temperature.

Thus, a reasonable design for the uranium multiplier has been demonstrated. This system will require removal of heat after shutdown of the plasma

due to the large fission power density. The fixed uranium fuel form necessitates maintaining the heat removal capability of the lithium coolant loop.

This can be demonstrated by a simple calculation. For a uranium metal heat capacity $c_p = 0.16\ kJ/kg \cdot^0 K$, an average multiplier temperature during operation of 750°C, a uranium melting temperature of 1135°C, and a uranium metal mass of 375 MT in the multiplier, the integrated energy for the uranium metal to reach melting temperature is 2.3+4 MJ total or 1200 MJ/m^3 of uranium metal. For the operating average power density of 240 MW/m^3 in the metal, this gives a time to reach melting of 5 seconds in normal operation if all cooling is removed with no heat removal from the uranium. If the plant shuts down immediately, the decay heat from the fission products will continue to provide heat to the multiplier. The time to reach melting for this condition can be obtained from Fig. 4.12 of Reference [3.15], which gives the integrated fission product decay energy for infinite operation (essentially after 1 year of operation). The time to reach melting is approximately 3 minutes.

The time of 3 minutes is used to determine the required capacity of the residual heat removal (RHR) system. From Reference [3.15], it seen that after 3 minutes of shutdown, the power will have decayed to a level of 2.5% of the operating level. Thus, the RHR system is sized at 2.5% of the capacity of the primary coolant system.

It should be noted that this simplified analysis does not consider any heat transfer to the lithium coolant or conduction to the structure or molten salt. Inclusion of these effects would lengthen the time to reach the melting point of uranium. However, the indication from the simplified analysis is that cooling will have to be maintained for the multiplier region after shutdown.

3.8 Summary

This chapter has presented an analysis of the blanket for the RTFB. This blanket produces tritium to sustain the plasma and fissile fuel for use in a client reactor system. Additionally, the energy of the fusion neutrons is recovered and multiplied in the blanket. Consequently, the blanket was analyzed for neutronic performance in terms of breeding and energy multiplication. Additionally, the heat removal from the blanket was evaluated in terms of the pressure drop in the lithium coolant circuit and the uranium multiplier plate thickness. The size of the residual heat removal system was also determined. A summary of each of these analyses follows.

The blanket consists of two zones: a multiplier zone adjacent to the plasma and a molten salt zone following the multiplier. The multiplier zone contains uranium metal clad in steel and cooled by liquid lithium. Fissions in the multiplier zone multiply the energy of the fusion neutrons. These fissions occur primarily in ^{238}U , but as the concentration of ^{239}Pu increases with blanket life, fissions in ^{239}Pu increase and cause the blanket power to increase.

The molten salt zone is continuously processed to remove the bred ^{233}U . Thus, the power level in the molten salt does not change due to an increase in concentration of ^{233}U , but does change due to the increased number of fissions in the multiplier.

Nuclear analyses were performed for the RTFB using the one-dimensional discrete ordinates code ONEDANT and the three-dimensional Monte Carlo code MCNP. The ONEDANT analyses were done to examine the effect of changing the materials in the inboard and outboard regions of the blanket and varying the thickness of the different regions. The ONEDANT calculations for the reference

blanket yield a value of total breeding, T+F, of 2.89 and a blanket thermal power of 4986 MWth. Although the tritium breeding parameter is less than one for the reference configuration (T=0.97), it is shown that the value of T can be increased to 1.18 by using natural Li in the molten salt in place of the depleted Li. This increase in tritium breeding comes at the expense of ^{233}U breeding, which decreases. These values of T are for the ONEDANT BOC analyses.

The effect on breeding of the substitution of stainless steel, tungsten and lead for the inboard blanket region was also studied with ONEDANT. Use of lead in the inboard region results in the highest breeding in the outboard region (T+F=2.41), followed by stainless steel (T+F=2.19) and tungsten (T+F=2.09). However, the blanket power drops by approximately 20% for these three cases due to the displacement of the multiplier by the different materials.

The effect of increasing the thickness of the multiplier region and increasing and decreasing the thickness of the molten salt region on breeding and energy multiplication was also investigated with ONEDANT. It was shown that increasing the multiplier thickness from 11 cm. to 16 cm. increases the total T+F by 6% and the blanket power by 11%. This case will be investigated more completely in Chapter 5 where the change in the amounts of fissile fuel will be considered. The effect on breeding and energy multiplication of increasing and decreasing the outboard molten salt thickness by 10 cm. is small, for example, less than 1% effect on ^{233}U breeding.

Additionally, ONEDANT analyses were done to investigate the effects on blanket power and breeding of the increasing concentration of ^{239}Pu in the multiplier. The limit of ^{239}Pu concentration was established by calculating the infinite medium multiplication factor, k_∞, for the uranium metal with varying concentration of ^{239}Pu . This value was limited to 0.9 to insure that criticality would not be reached, even under accident scenarios. This limit was determined

to be 0.02 a/o ^{239}Pu in the uranium metal. The blanket power increases by a factor of 1.45 as the concentration of ^{239}Pu increases from 0.00 a/o to 0.02 a/o. The tritium and ^{233}U production rates increase with blanket lifetime due to the increased fissions as more ^{239}Pu is present in the blanket. Although the production rate of ^{239}Pu from captures in ^{238}U increases with blanket lifetime, the net production rate of ^{239}Pu decreases due to the increased captures in ^{239}Pu .

It was also shown with ONEDANT that the tritium breeding parameter could be varied over a wide range, with a maximum increase of 20%, by varying the lithium isotopic composition in the molten salt from depleted in ^{6}Li to natural ^{6}Li concentration.

The dose rates to the magnet insulation on the plasma side of the inboard leg of the toroidal field coil was also calculated with ONEDANT. The dose rates with the reference blanket were shown to give a magnet insulation lifetime of 1.1 years. The shield selected to replace the blanket consists of tungsten, steel, titanium hydride, boron carbide and water and gives a magnet insulation lifetime of 26.3 years, which is considered sufficient.

MCNP analyses were done for both one-dimensional and three-dimensional models. The one-dimensional results were compared to the ONEDANT calculation for the reference blanket and showed relatively good agreement in breeding, with a total T+F value from MCNP that is 2% lower than ONEDANT. The three-dimensional MCNP results were used to estimate the beginning of cycle (BOC) values of the breeding parameters and energy multiplication with and without the shield in place. The total breeding from MCNP was 2.4% less than ONEDANT and the blanket power was 11% lower than ONEDANT, for the case without the shield. With the shield in place the BOC breeding values are T=0.85, ^{233}F=0.87, ^{239}F=0.87, T+F=2.59 and the blanket thermal power is

4071 MWth.

The design of the lithium coolant system for the multiplier region was also considered. Pressure drop and pumping power calculations were done considering the MHD induced pressure drops for both uninsulated and insulated ducts of 0.5 cm. thickness. For the uninsulated case, it was shown that a 15 cm. duct half thickness along the magnetic field can give a maximum duct pressure of 2.20 MPa. This duct geometry gives a maximum allowable pressure of 1.98 MPa. However, considering the uncertainties in the pressure drop calculations, this design is considered to be acceptable. For the uninsulated duct, a duct half thickness of 5 cm. gives a maximum pressure drop of 1.35 MPa, which is less than the allowed value of 1.98 MPa. It is also noted that the pumping power for all cases in which the pressure drop is considered acceptable, the pumping power is within a reasonable range (less than 40 MW).

The uranium plate fuel thickness was also evaluated to determine that the multiplier region could be cooled using uranium plates of reasonable thickness. A uranium plate thickness of 1.0 cm. allows maintaining the clad-lithium interface at less than 550°C and the peak uranium temperature ~300°C below the melting point of uranium metal. Additionally, the size of the residual heat removal system was determined to be 2.5% of the primary coolant system capacity to allow removal of the decay heat in the multiplier region after shutdown.

References

[3.1] O'Dell, R. D., Brinkley, F. W. and Marr D. R., "User's Manual for ONEDANT: A Code Package for One-Dimensional, Diffusion-Accelerated, Neutral Particle Transport." Los Alamos National Laboratory Report LA-9184-M, (February 1982).

[3.2] Los Alamos Monte Carlo Group, "MCNP - A General Monte Carlo Code for Neutron and Photon Transport. Version 2D." Los Alamos National Laboratory Report LA-7396-M, Revised (December 1982).

[3.3] Baxman, C. 1. and Young, P. G., "Applied Nuclear Data Research and Development January 1 - March 31, 1977." Los Alamos National Laboratory Report LA-6893-PR, (july 1977).

[3.4] MacFarlane, R. E. and Barrett, R. J., "TRANSX." Los Alamos National Laboratory Document T-2-L-2923, (August 1978).

[3.5] Cook, A. G., "The Feasibility of ^{233}U Breeding in Deuterium-Tritium Fusion Devices," Eng. Thesis, Dept. of Nucl. Eng., M.I.T., (May 1976).

[3.6] U.S. Department of Energy, "Nuclear Proliferation and Civilian Nuclear Power; Report of the Nonproliferation Alternative System Assessment Program." DOE-NE-0001, (June 1980).

[3.7] Berwald, D.H., et al.,"Fission-Suppressed Hybrid Reactor - The Fusion Breeder," Lawrence Livermore National Laboratory Report UCID-19638, (December 1982).

[3.8] Youssef, M.Z. and Conn, R.W., "A Survey of Fusion-Fission System Designs and Nuclear Analyses." UWFDM-308, June, 1979.

[3.9] Bender, D. J., et al., "Reference Design for the Standard Mirror Hybrid Reactor." Lawrence Livermore National Laboratory Report UCRL-52478, (May 1978).

[3.10] Shmunck, R. E. and Becker, H., "Extension of the Irradiation and Testing of SPAULRAD-S for Fusion Magnet Application." *Proceedings of the Sixth Topical Meeting on the Technology of Fusion Energy*, San Francisco, CA (1985), to be published in *Fusion Technology*.

[3.11] Branover, H., *Magnetohydrodynamic Flow in Ducts*, John Wiley & Sons, Inc., (1978).

[3.12] Smith, D. L., et al., "Blanket Comparison and Selection Study - Final Report," Argonne National Laboratory Report ANL/FPP-84-1, (September

1984).

[3.13] Roark, R. J. and Young, W. C., *Formulas for Stress and Strain*. McGraw-Hill Book Company, (1975).

[3.14] Abdou, M. A., et al., "Blanket Comparison and Selection Study," Argonne National Laboratory Report ANL/FPP-83-1, (October 1983).

[3.15] El-Wakil, M. M., *Nuclear Heat Transport*. The American Nuclear Society, (1981).

TABLE 3.1

Zone Dimensions for One-Dimensional Model of Reference Blanket

Zone	Description	Inner Radius (m)	Outer Radius (m)
0	Void	0.000	0.750
1	OH Coil	0.750	1.500
2	TF Coil	1.500	2.010
3	Structure	2.010	2.015
4	Molten Salt	2.015	2.240
5	Second Wall	2.240	2.245
6	Multiplier	2.245	2.355
7	First Wall	2.355	2.360
0	Scrape Off	2.360	2.510
0	Plasma	2.510	5.110
0	Scrape Off	5.110	5.260
8	First Wall	5.260	5.265
9	Multiplier	5.265	5.375
10	Second Wall	5.375	5.380
11	Molten Salt	5.380	6.005
12	Structure	6.005	6.010
13	TF Coil	6.010	7.510

TABLE 3.2

Zone Compositions for One-Dimensional Breeding Calculations For Reference Blanket

Zone	Material	(v/o)
Multiplier	Uranium	0.63
	Lithium (0.70 a/o ^{6}Li)	0.24
	Stainless Steel	0.13
Molten Salt	$LiF - ThF_4 - BeF_2$ (0.71-0.27-0.02 m/o) (0.01 a/o ^{6}Li)	1.0
Structure	Steel	1.00
Inboard TF Coil	Copper	0.94
	Water	0.04
	Insulation	0.01
Outboard TF Coil	Copper	0.40
	Stainless Steel	0.55
	Water	0.04
	Insulation	0.01

TABLE 3.3

Material Number Densities for Breeding Calculations

Material	Element	Number Density
Molten Salt	^{6}Li	1.852-4
	^{7}Li	1.833-2
	^{9}Be	5.216-4
	^{19}F	4.773-2
	^{232}Th	7.042-3
Lithium	^{6}Li	2.871-2
	^{7}Li	1.231-2
Steel	Fe	8.490-2
Stainless Steel	C	1.990-4
	Si	1.360-3
	Ti	4.980-5
	Cr	1.150-2
	Mn	1.650-3
	Fe	5.430-2
	Ni	1.060-2
	Mo	1.290-3
Natural Uranium	^{235}U	3.417-4
	^{238}U	4.773-2
Depleted Uranium	^{235}U	9.614-5
	^{238}U	4.797-2
Copper	Cu	8.290-2
Water	H	6.687-2
	O	3.343-2
Insulation	H	2.902-2
	C	3.809-2
	O	2.616-2
	Si	5.712-3
	Al	4.394-3
	Mg	8.878-4

TABLE 3.4

One-Dimensional Breeding Calculations For Reference Blanket

	Reactions/Fusion Neutron
Inboard	
^{6}T	0.2593
^{7}T	0.0056
^{233}F	0.1814
^{239}F	0.2966
Fissions	0.1417
MS Heating *	1.92+6
Mult. Heating *	3.24+7
Outboard	
^{6}T	0.6831
^{7}T	0.0211
^{233}F	0.6704
^{239}F	0.7697
Fissions	0.4506
MS Heating *	7.08+6
Mult. Heating *	1.01+8
Total	
^{6}T	0.9424
^{7}T	0.0267
$^{6}T + ^{7}T$	0.9691
^{233}F	0.8518
^{239}F	1.0663
$^{233}F + ^{239}F$	1.9181
T+F	2.8872
Fissions	0.5923
MS Heating *	9.00+6
Mult. Heating *	1.33+8
Total Heating *	1.42+8
Thermal Power (MWth)	4986

* eV/fusion neutron

TABLE 3.5

One-Dimensional Breeding Calculations
Inboard Molten Salt Replaced by Stainless Steel

	Reference Case	Inboard MS → SS
Inboard		
^{6}T	0.2593	0.2632
^{7}T	0.0056	0.0023
^{233}F	0.1814	-
^{239}F	0.2966	0.2974
Fissions	0.1417	0.1414
MS Heating*	1.92+6	1.48+6
Mult. Heating*	3.24+7	3.27+7
Outboard		
^{6}T	0.6831	0.6962
^{7}T	0.0211	0.0211
^{233}F	0.6704	0.6783
^{239}F	0.7697	0.7847
Fissions	0.4506	0.4515
MS Heating*	7.08+6	7.12+6
Mult. Heating*	1.01+8	1.01+8
Total		
^{6}T	0.9424	0.9594
^{7}T	0.0267	0.0234
$^{6}T - ^{7}T$	0.9691	0.9828
^{233}F	0.8518	0.6783
^{239}F	1.0663	1.0821
$^{233}F - ^{239}F$	1.9181	1.7604
T-F	2.8872	2.7432
Fissions	0.5923	0.5929
MS Heating*	9.00+6	8.60+6
Mult. Heating*	1.33+8	1.34+8
Total Heating*	1.42+8	1.43+8
Thermal Power (MWth)	4986	5021

* eV/fusion neutron

TABLE 3.6

One-Dimensional Breeding Calculations Varying Inboard Blanket Materials

	Reference Case	MS → SS Mult → SS	MS → Pb Mult → Pb	MS → W Mult → W
Inboard				
^{6}T	0.2593	–	–	–
^{7}T	0.0056	–	–	–
^{233}F	0.1814	–	–	–
^{239}F	0.2966	–	–	–
Fissions	0.1417	–	–	–
MS Heating*	1.92+6	1.77+6	8.00+5	1.43+6
Mult. Heating*	3.24+7	2.95+6	1.68+6	4.38+6
Outboard				
^{6}T	0.6831	0.6951	0.7729	0.6712
^{7}T	0.0211	0.0210	0.0211	0.0207
^{233}F	0.6704	0.6621	0.7218	0.6442
^{239}F	0.7697	0.8068	0.8901	0.7587
Fissions	0.4506	0.4440	0.4584	0.4356
MS Heating*	7.08+6	1.77+6	7.40+6	6.83+6
Mult. Heating*	1.01+8	2.95+6	1.04+8	9.79+7
Total				
^{6}T	0.9424	0.6951	0.7729	0.6712
^{7}T	0.0267	0.0210	0.0211	0.0207
$^{6}T + ^{7}T$	0.9691	0.7161	0.7940	0.6919
^{233}F	0.8518	0.6621	0.7218	0.6442
^{239}F	1.0663	0.8068	0.8901	0.7587
$^{233}F + ^{239}F$	1.9181	1.4689	1.6119	1.4029
T+F	2.8872	2.1850	2.4059	2.0948
Fissions	0.5923	0.4440	0.4584	0.4356
MS Heating*	9.00+6	8.75+6	8.20+6	8.26+6
Mult. Heating*	1.33+8	1.03+8	1.06+8	1.02+8
Total Heating*	1.42+8	1.12+8	1.14+8	1.10+8
Thermal Power (MWth)	4986	3930	4003	3860

* eV/fusion neutron

TABLE 3.7

One-Dimensional Breeding Calculations
Varying Outboard Blanket
Inboard Molten Salt and Multiplier Replaced by Lead

	Comparison Case	OB Mult 11 cm → 16 cm	OB Mult $0.7^6Li \rightarrow 1.0^6Li$
Inboard			
MS Heating*	8.00−5	8.09+5	7.71+5
Mult. Heating*	1.68+6	1.69+6	1.66+6
Outboard			
MS Heating*	7.40+6	4.61+6	7.04+6
Mult. Heating*	1.04+8	1.21+8	1.03+8
Total			
^6T	0.7729	0.9617	0.9563
^7T	0.0211	0.0151	0.0133
$^6T + ^7T$	0.7940	0.9768	0.9696
^{233}F	0.7218	0.5035	0.6627
^{239}F	0.8901	1.0814	0.7730
$^{233}F + ^{239}F$	1.6119	1.5849	1.4357
T+F	2.4059	2.5617	2.4053
Fissions	0.4584	0.5277	0.4516
MS Heating*	8.20+6	5.42+6	7.81+6
Mult. Heating*	1.06+8	1.22+8	1.05+8
Total Heating*	1.14+8	1.27+8	1.13+8
Thermal Power (MWth)	4003	4460	3970

* eV/fusion neutron

TABLE 3.8

One-Dimensional Breeding Calculations
Inboard Blanket Thickness Decreased
Major Radius Decreases

	Reference Case 35 cm	30 cm	25 cm	20 cm	15 cm
Inboard					
^{6}T	0.2593	0.2561	0.2523	0.2471	0.2392
^{7}T	0.0056	0.0053	0.0048	0.0041	0.0030
^{233}F	0.1814	0.1562	0.1214	0.0766	0.0259
^{239}F	0.2966	0.2940	0.2909	0.2860	0.2745
Fissions	0.1417	0.1402	0.1385	0.1366	0.1340
MS Heating*	1.92+6	1.73+6	1.45−6	1.05+6	4.37+5
Mult. Heating*	3.24+7	3.21−7	3.18−7	3.14+7	3.10+7
Outboard					
^{6}T	0.6831	0.6853	0.6877	0.6903	0.6938
^{7}T	0.0211	0.0212	0.0213	0.0214	0.0215
^{233}F	0.6704	0.6728	0.6754	0.6781	0.6816
^{239}F	0.7697	0.7723	0.7750	0.7779	0.7814
Fissions	0.4506	0.4518	0.4532	0.4545	0.4559
MS Heating*	7.08+6	7.10+6	7.13+6	7.17+6	7.20+6
Mult. Heating*	1.01+8	1.01+8	1.02−8	1.02+8	1.02+8
Total					
^{6}T	0.9424	0.9414	0.9400	0.9374	0.9330
^{7}T	0.0267	0.0265	0.0261	0.0255	0.0245
$^{6}T + ^{7}T$	0.9691	0.9679	0.9661	0.9629	0.9575
^{233}F	0.8518	0.8290	0.7968	0.7547	0.7075
^{239}F	1.0663	1.0663	1.0659	1.0639	1.0559
$^{233}F + ^{239}F$	1.9181	1.8953	1.8627	1.8186	1.7634
T−F	2.8872	2.8632	2.8288	2.7815	2.7209
Fissions	0.5923	0.5920	0.5917	0.5911	0.5899
MS Heating*	9.00+6	8.83+6	8.58−6	8.22+6	7.64+6
Mult. Heating*	1.33−8	1.33+8	1.34−8	1.33+8	1.33+8
Total Heating*	1.42+8	1.42+8	1.43−8	1.41+8	1.41+8
Thermal Power (MWth)	4986	5005	5040	4951	4970

* eV/fusion neutron

TABLE 3.9

One-Dimensional Breeding Calculations Varying Outboard Blanket Thickness

	Reference Case	Outboard 75 cm → 65 cm	Outboard 75 cm → 85 cm
Inboard			
^{6}T	0.2593	0.2593	0.2593
^{7}T	0.0056	0.0056	0.0056
^{233}F	0.1814	0.1814	0.1814
^{239}F	0.2966	0.2966	0.2966
Fissions	0.1417	0.1417	0.1417
MS Heating*	1.92+6	1.92−6	1.92+6
Mult. Heating*	3.24+7	3.24−7	3.24+7
Outboard			
^{6}T	0.6811	0.6830	0.6831
^{7}T	0.0211	0.0211	0.0211
^{233}F	0.6704	0.6658	0.6720
^{239}F	0.7697	0.7698	0.7697
Fissions	0.4506	0.4505	0.4506
MS Heating*	7.08+6	7.04−6	7.09+6
Mult. Heating*	1.01+8	1.01−8	1.01+8
Total			
^{6}T	0.9424	0.9423	0.9424
^{7}T	0.0267	0.0267	0.0267
$^{6}T + ^{7}T$	0.9691	0.9690	0.9691
^{233}F	0.8518	0.8472	0.8534
^{239}F	1.0663	1.0664	1.0663
$^{233}F + ^{239}F$	1.9181	1.9136	1.9197
T−F	2.8872	2.8826	2.8888
Fissions	0.5923	0.5922	0.5923
MS Heating*	9.00+6	8.96−6	9.01+6
Mult. Heating*	1.33+8	1.33+8	1.33+8
Total Heating*	1.42+8	1.42−8	1.42+8
Thermal Power (MWth)	4986	4990	4990

* eV/fusion neutron

TABLE 3.10

Calculated Values of k_∞ Uranium Metal With ^{239}Pu

^{239}Pu a/o	k_∞
0.01	0.66
0.02	0.82
0.03	0.95

TABLE 3.11

Calculated Values of k_∞ Water and Uranium Metal With 0.02 a/o ^{239}Pu

Uranium v/o	Water v/o	k_∞
0.9	0.1	0.62
0.2	0.8	0.54
0.1	0.9	0.79
0.01	0.99	0.68

TABLE 3.12

One-Dimensional Breeding Calculations
Natural Uranium in Multiplier
0.00, 0.01, and 0.02 a/o ^{239}Pu

	Natural Uranium 0.00 a/o ^{239}Pu	Natural Uranium 0.01 a/o ^{239}Pu	Natural Uranium 0.02 a/o ^{239}Pu
Inboard			
^{6}T	0.2592	0.2827	0.3104
^{7}T	0.0056	0.0057	0.0058
^{233}F	0.1815	0.1992	0.2204
^{239}F	0.2967	0.3212	0.3504
^{239}Pu abs.	-	0.0307	0.0674
Fissions	0.1417	0.1785	0.2227
MS Heating*	1.92+6	2.09+6	2.29+6
Mult. Heating*	3.24+7	4.00+7	4.90+7
Outboard			
^{6}T	0.6831	0.7399	0.8069
^{7}T	0.0211	0.0214	0.0217
^{233}F	0.6704	0.7279	0.7959
^{239}F	0.7697	0.8286	0.8983
^{239}Pu abs.	-	0.0821	0.1781
Fissions	0.4506	0.5472	0.6613
MS Heating*	7.08+6	7.57+6	8.15+6
Mult. Heating*	1.01+8	1.21+8	1.44+8
Total			
^{6}T	0.9423	1.0226	1.1173
^{7}T	0.0267	0.0271	0.0275
$^{6}T + ^{7}T$	0.9690	1.0497	1.1448
^{233}F	0.8519	0.9271	1.0163
^{239}F	1.0664	1.1498	1.2487
^{239}Pu abs.	-	0.1128	0.2455
$^{239}F_{net}$	1.0664	1.0370	1.0032
$^{233}F - ^{239}F_{net}$	1.9183	1.9641	2.0195
T+F	2.8873	2.9867	3.1643
Fissions	0.5923	0.7257	0.8840
MS Heating*	9.00+6	9.66+6	1.04+7
Mult. Heating*	1.33+8	1.61+8	1.93+8
Total Heating*	1.42+8	1.71+8	2.03+8
Thermal Power (MWth)	4986	6000	7130

* eV/fusion neutron

TABLE 3.13

One-Dimensional Breeding Calculations
Depleted Uranium in Multiplier
0.00, 0.01 and 0.02 a/o ^{239}Pu

	Depleted Uranium 0.00 a/o ^{239}Pu	Depleted Uranium 0.01 a/o ^{239}Pu	Depleted Uranium 0.02 a/o ^{239}Pu
Inboard			
^{6}T	0.2522	0.2744	0.3006
^{7}T	0.0055	0.0056	0.0058
^{233}F	0.1753	0.1922	0.2123
^{239}F	0.2910	0.3145	0.3422
^{239}Pu abs.	–	0.0300	0.0656
Fissions	0.1274	0.1621	0.2034
MS Heating*	1.86+6	2.01+6	2.20+6
Mult. Heating*	2.96+7	3.67+7	4.52+7
Outboard			
^{6}T	0.6658	0.7199	0.7835
^{7}T	0.0210	0.0212	0.0215
^{233}F	0.6506	0.7053	0.7696
^{239}F	0.7567	0.8131	0.8795
^{239}Pu abs.	–	0.0800	0.1738
Fissions	0.4132	0.5046	0.6122
MS Heating*	6.89+6	7.35+6	7.91+6
Mult. Heating*	9.36+7	1.12+8	1.34+8
Total			
^{6}T	0.9180	0.9943	1.0841
^{7}T	0.0265	0.0268	0.0273
$^{6}T - ^{7}T$	0.9445	1.0211	1.1114
^{233}F	0.8259	0.8975	0.9819
^{239}F	1.0477	1.1276	1.2217
^{239}Pu abs.	–	0.1100	0.2394
$^{239}F_{net}$	1.0477	1.0176	0.9823
$^{233}F - ^{239}F_{net}$	1.8736	1.9151	1.9642
T+F	2.8181	2.9362	3.0756
Fissions	0.5406	0.6667	0.8156
MS Heating	8.75+6	9.36+6	1.01+7
Mult. Heating*	1.23+8	1.49+8	1.79+8
Total Heating*	1.32+8	1.58+8	1.89+8
Thermal Power (MWth)	4630	5550	6630

* eV/fusion neutron

TABLE 3.14

One-Dimensional Breeding Calculations
Natural Lithium Composition in Molten Salt

	Reference Case	Natural Li in Molten Salt
Inboard		
^{6}T	0.2593	0.3062
^{7}T	0.0056	0.0054
^{233}F	0.1814	0.1486
^{239}F	0.2966	0.2879
Fissions	0.1417	0.1413
MS Heating*	1.92+6	2.00+6
Mult. Heating*	3.24+7	3.23+7
Outboard		
^{6}T	0.6831	0.8490
^{7}T	0.0211	0.0202
^{233}F	0.6704	0.5288
^{239}F	0.7697	0.7460
Fissions	0.4506	0.4496
MS Heating*	7.08+6	7.22+6
Mult. Heating*	1.01+8	1.01+8
Total		
^{6}T	0.9424	1.1552
^{7}T	0.0267	0.0256
$^{6}T - ^{7}T$	0.9691	1.1808
^{233}F	0.8518	0.6774
^{239}F	1.0663	1.0339
$^{233}F - ^{239}F$	1.9181	1.7113
T+F	2.8872	2.8921
Fissions	0.5923	0.5909
MS Heating*	9.00+6	9.22+6
Mult. Heating*	1.33+8	1.34+8
Total Heating*	1.42+8	1.42+8
Thermal Power (MWth)	4986	4990

* eV/fusion neutron

TABLE 3.15

Insulation Damage Calculation
Energy Deposition and Dose Rate in Insulation
Plasma Side, Inboard Leg of TF Coil
Inboard Blanket Replaced by Varying Tungsten Thickness

	34 cm.	24 cm.	14 cm.	4 cm.
Energy Deposition				
Neutron*	1.45	6.76	29.4	119.4
Gamma*	1.07	4.07	13.4	40.3
Total*	2.52	10.8	42.8	159.7
Dose Rate (rads/yr)				
Total	3.38+11	1.45+12	5.74+12	2.14+13

*eV/sec/cm^3 per n/sec/cm

TABLE 3.16

Energy Deposition and Dose Rate in Insulation
Plasma Side, Inboard Leg of TF Coil

Inboard Blanket	Neutron*	Gamma*	Total*	Total Dose Rate (Rads/Yr)	Magnet Lifetime (Years)
Reference	4.86	7.56	12.42	1.66−12	1.1
34 cm. W	1.45	1.07	2.52	3.38+11	5.5
Composite	0.35	0.18	0.53	7.10+10	26.3
0.9 v/o U	11.62	4.29	15.91	2.13+12	0.9
0.9 v/o W	2.46	1.71	4.17	5.59+11	3.3
0.9 v/o U					
0.1 v/o water	2.54	1.10	3.64	4.88+11	3.8
0.9 v/o W					
0.1 v/o water	0.43	0.27	0.70	9.38+10	19.9

*eV/sec/cm^3 per n/sec/cm

TABLE 3.17

One-Dimensional Breeding Calculations For Reference Blanket Comparison of ONEDANT and MCNP Results

	ONEDANT	MCNP
Inboard		
^{6}T	0.2593	0.2612
^{7}T	0.0056	0.0048
^{233}F	0.1814	0.1759
^{239}F	0.2966	0.2837
Fissions	0.1417	0.1345
Outboard		
^{6}T	0.6831	0.6853
^{7}T	0.0211	0.0203
^{233}F	0.6704	0.6649
^{239}F	0.7697	0.7248
Fissions	0.4506	0.4356
Total		
^{6}T	0.9424	0.9465
^{7}T	0.0267	0.0251
$^{6}T + {}^{7}T$	0.9691	0.9716
^{233}F	0.8518	0.8408
^{239}F	1.0663	1.0085
$^{233}F - {}^{239}F$	1.9181	1.8493
T+F	2.8872	2.8290
Fissions	0.5923	0.5701

TABLE 3.18

Breeding and Power Calculations For Reference Blanket
Comparison of ONEDANT and Three-Dimensional MCNP Results

	ONEDANT	3-D MCNP
Breeding		
^{6}T	0.9424	0.9022
^{7}T	0.0267	0.0293
$^{6}T + ^{7}T$	0.9691	0.9315
^{233}F	0.8518	0.9350
^{239}F	1.0663	0.9525
$^{233}F + ^{239}F$	1.9181	1.8875
T+F	2.8872	2.8190
Fissions	0.5923	0.5615
Power		
Molten Salt*	9.00	9.71
Multiplier*	133	116.7
Total*	142	126.4
Power (MWth)	4986	4436

*MeV/fusion neutron

TABLE 3.19

Breeding Calculations For Reference Blanket
Comparison of One- and Three-Dimensional MCNP Results

	1-D MCNP	3-D MCNP
Breeding		
^{6}T	0.9465	0.9022
^{7}T	0.0251	0.0293
$^{6}T + ^{7}T$	0.9716	0.9315
^{233}F	0.8408	0.9350
^{239}F	1.0085	0.9525
$^{233}F + ^{239}F$	1.8493	1.8875
T+F	2.8290	2.8190
Fissions	0.5701	0.5615

TABLE 3.20

Reference BOC Breeding and Energy Deposition With and Without Shield

	With Shield	Without Shield
Breeding		
T	0.85	0.93
^{233}F	0.87	0.94
^{239}F	0.87	0.95
T–F	2.59	2.82
BOC Energy Deposition		
Molten Salt (MWth)	314	341
Multiplier (MWth)	3757	4095
Total (MWth)	4071	4436

TABLE 3.21

Lithium Physical Properties

Density (kg/m^3)	430
Viscosity ($mPa \cdot sec$)	0.32
Electrical Conductivity $(ohm \cdot m)^{-1}$	3.2+6
Thermal Conductivity ($W/m \cdot {}^{\circ}K$)	49.6
Heat Capacity ($J/kg \cdot {}^{\circ}K$)	4200

TABLE 3.22

HT-9 Physical Properties

Density (kg/m^3)	7980
Electrical Conductivity $(ohm \cdot m)^{-1}$	1.0+6
Thermal Conductivity ($W/m \cdot {}^{\circ}K$)	17.1

TABLE 3.23

Pumping Power and Pressure Drops for Uninsulated and Insulated Ducts

Toroidal Segments	Poloidal Segments	Max. Pumping Power (MW)	Duct Mass (MT)	Maximum Δp (MPa)
a = 0.15 m. t_1 = 0.005m. t_2 = 0.0025m.				
8	10	54.80	22.94	3.09
8	20	48.50	29.78	2.73
8	30	44.62	36.23	2.51
8	40	42.09	42.32	2.37
8	50	40.31	48.06	2.27
8	60	39.01	53.50	2.20
a = 0.05 m. t_1 = 0.00025m. t_2 = 0.000125m.				
8	10	30.57	18.98	1.72
8	20	28.71	21.36	1.62
8	30	27.07	23.60	1.52
8	40	25.77	25.71	1.45
8	50	24.73	27.70	1.39
8	60	23.89	29.57	1.35

TABLE 3.24

Allowable Pressures Within Lithium Ducts

Poloidal Segments	l	q(MPa) t_1 = 0.5cm.	q(MPa) t_1 = 1.0cm.
10	31.2	0.05	0.22
20	15.6	0.22	0.88
30	10.4	0.49	1.98
40	7.8	0.88	3.52
50	6.2	1.37	5.50
60	5.2	1.98	7.91

TABLE 3.25

Uranium Plate Thickness Analysis

	Average Outlet	Average Inlet	Peak Outlet	Peak Inlet
q(MW/m^3)	235	235	422	422
a(cm)	0.60	1.00	0.50	0.70
δ_c(cm)	0.09	0.15	0.08	0.11
δ_{Li}(cm)	0.23	0.38	0.19	0.27
T_b(°C)	490	340	490	340
T_{max}(°C)	748	1056	811	970
T_c(°C)	530	451	540	438

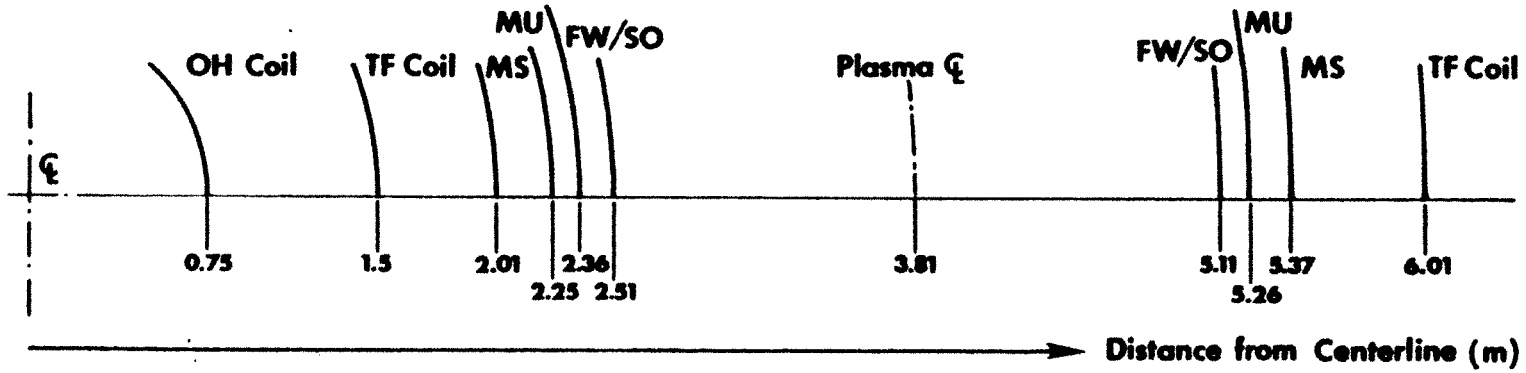

MU=MULTIPLIER
MS=MOLTEN SALT
FW/SO=FIRST WALL/SCRAPE OFF

Figure 3.1 ONEDANT Reference Blanket Model

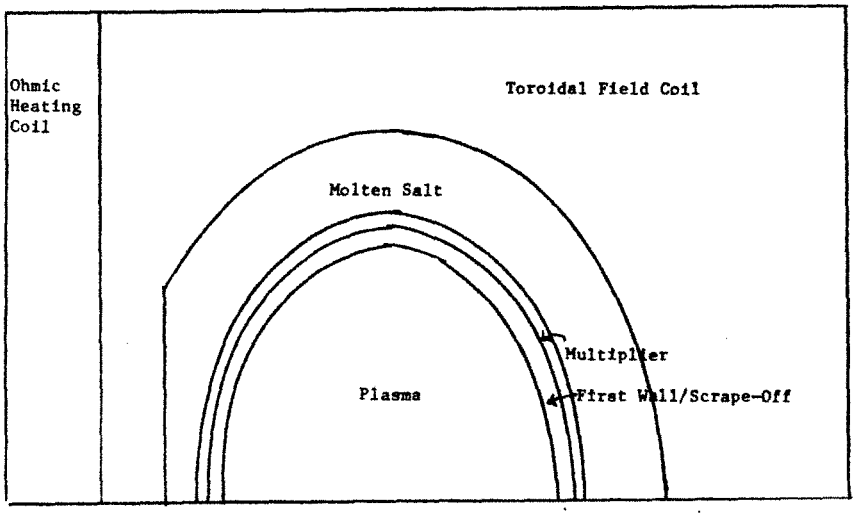

Figure 3.2 MCNP Three-Dimensional Model Section View

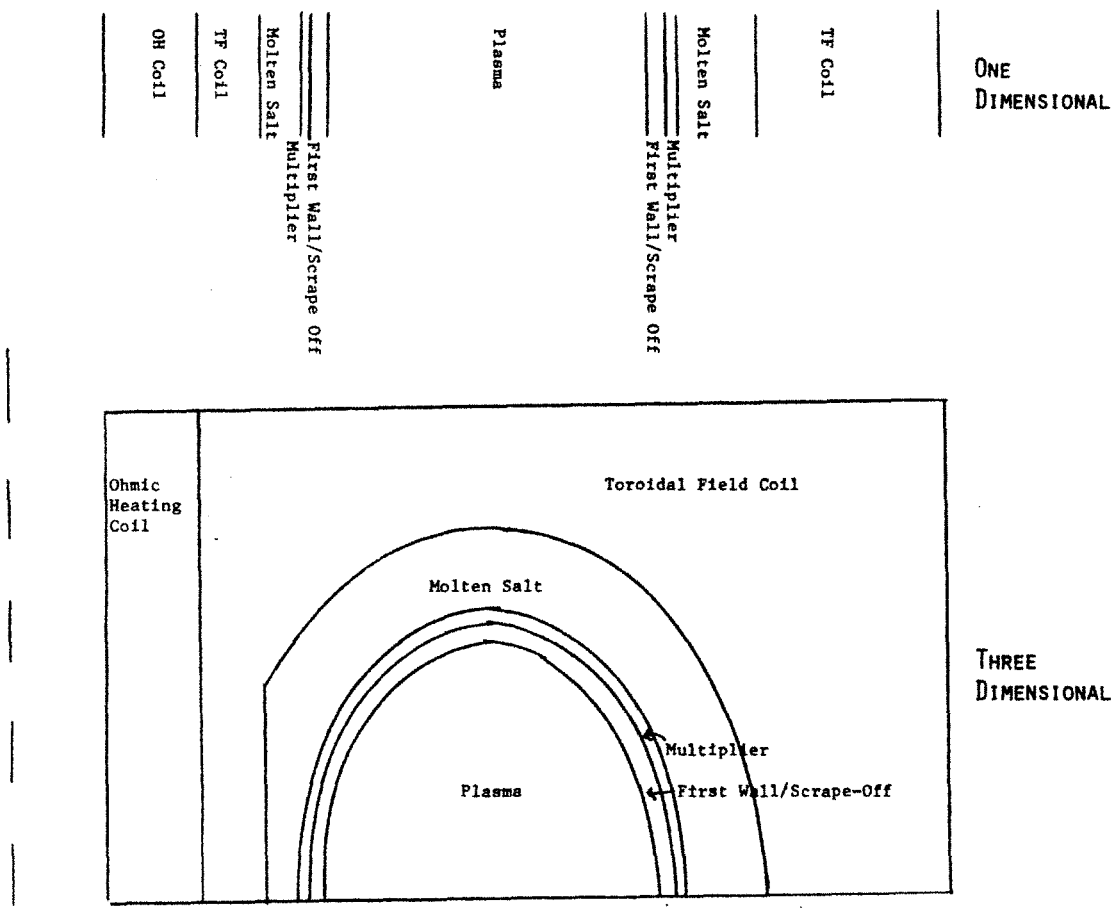

Figure 3.3 Comparison of One- and Three-Dimensional Models

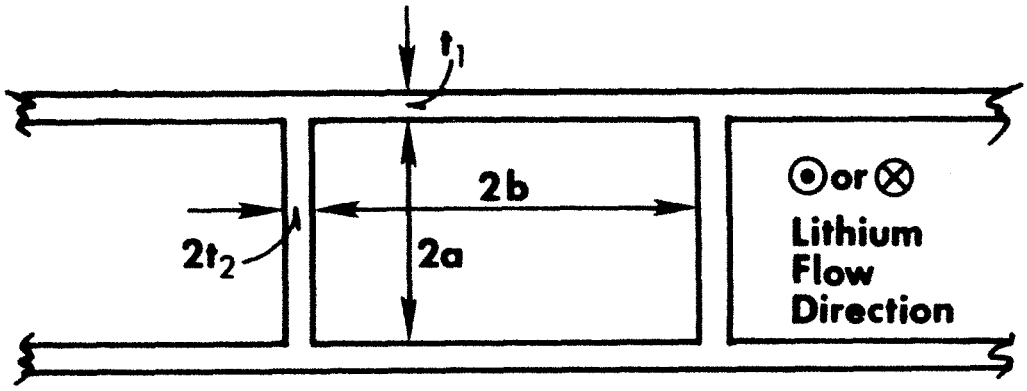

Figure 3.4 Lithium Duct Geometry

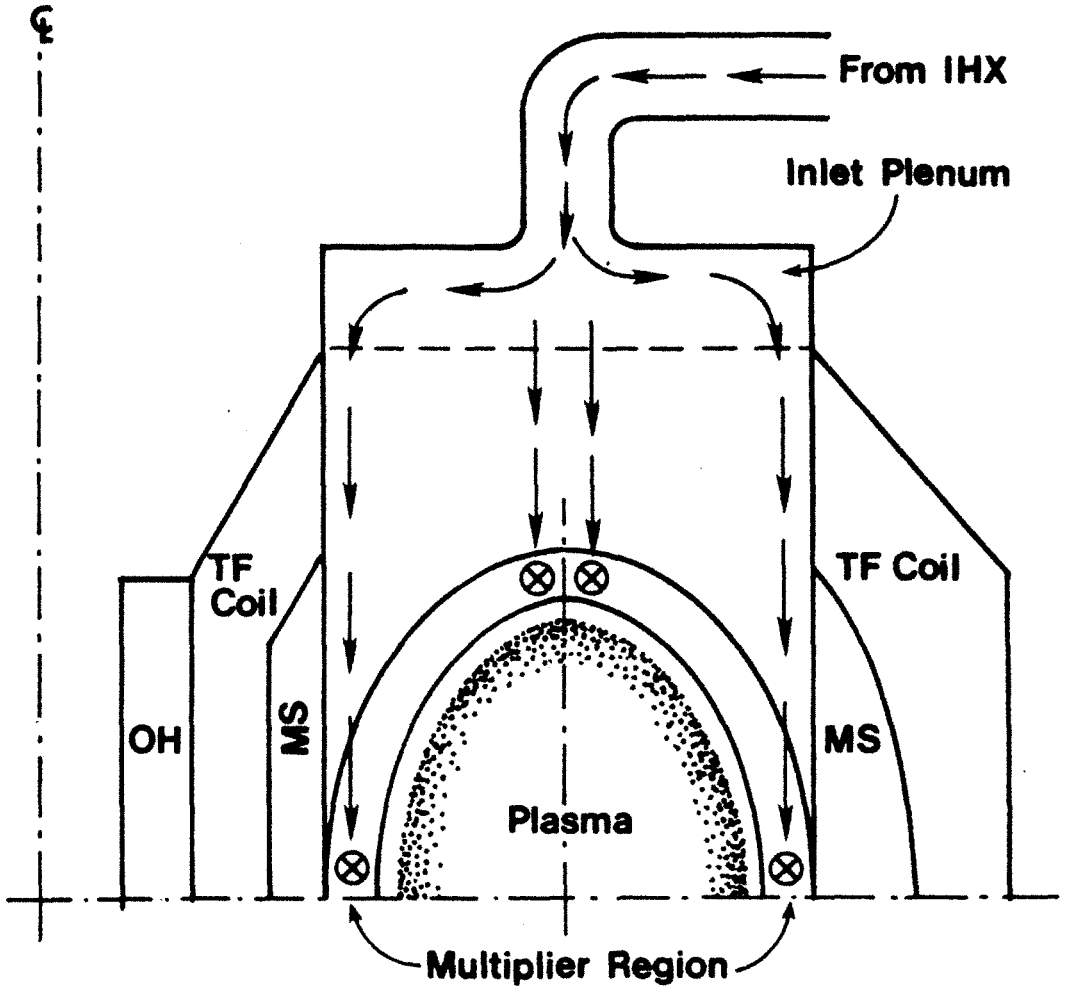

Figure 3.5 Lithium Flow Path - Section View

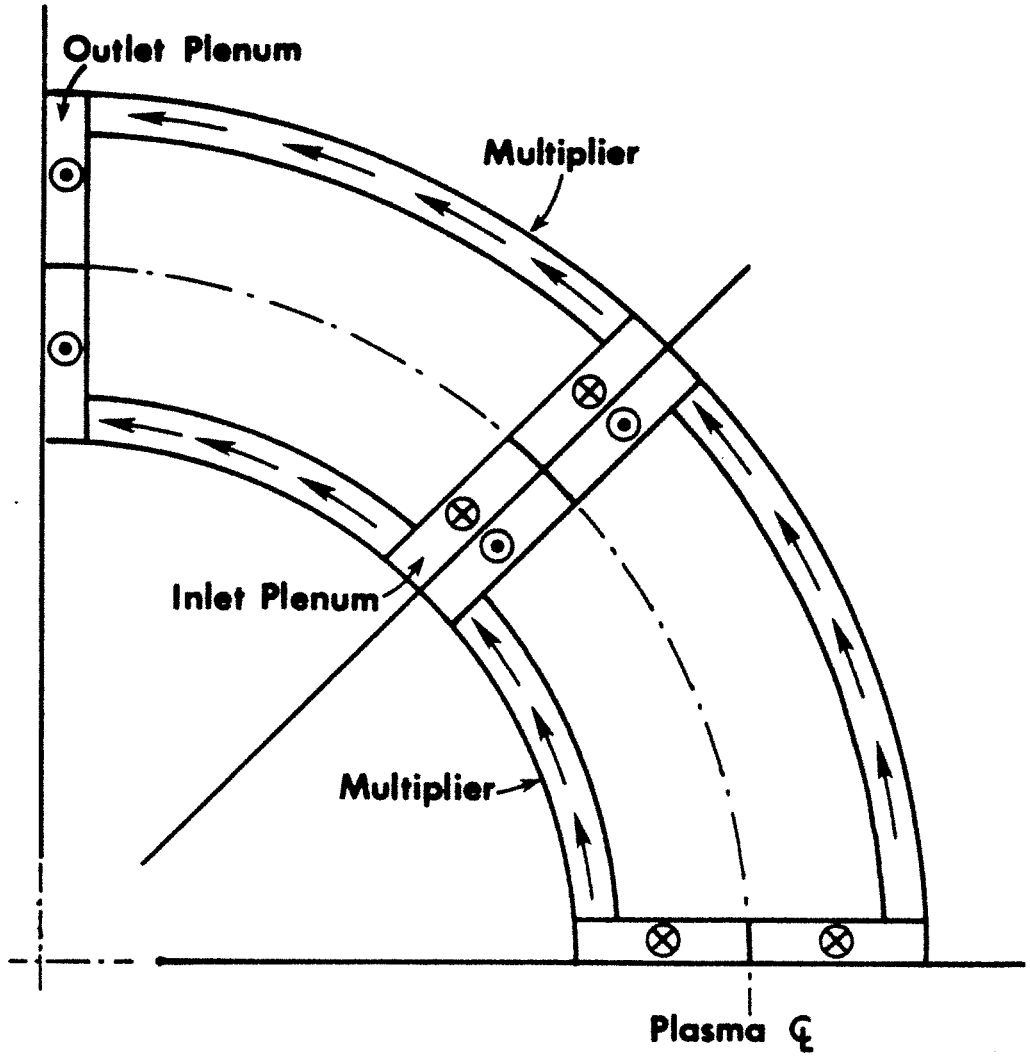

Figure 3.6 Lithium Flow Path - Plan View

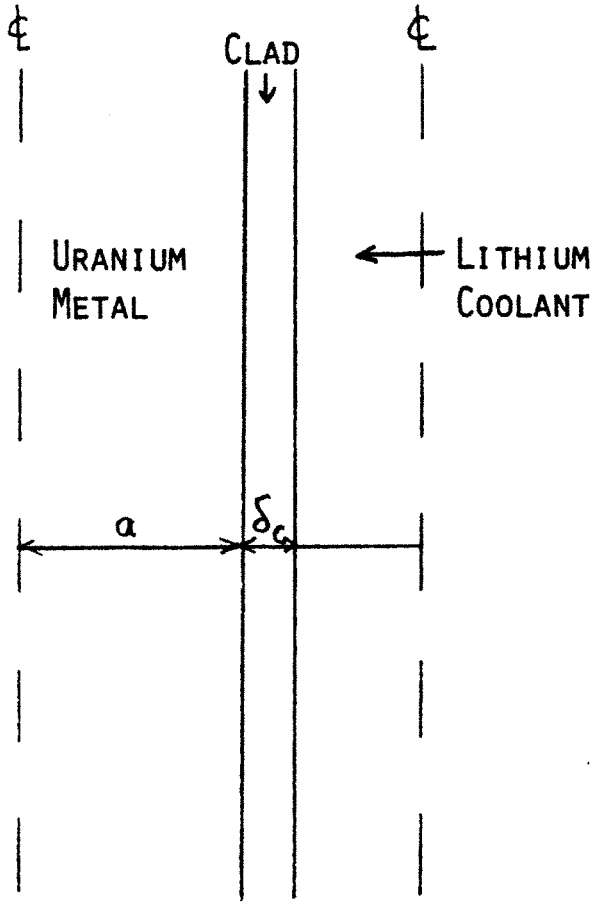

Figure 3.7 Uranium Fuel Plate Model

4. COST ESTIMATE FOR RTFB

4.1 Introduction

An important part of any evaluation of a source of electricity or fissile fuel is the answer to the question "What does it cost?" This chapter addresses the cost of the RTFB. A description of the costing methodology is given. A cost estimate for the reference design of the RTFB is next developed. The sensitivity of this cost estimate to variations in the major parameters is investigated. Finally, the chapter is summarized.

4.2 Costing Methodology

This section discusses the costing methodology used in estimating the cost of the RTFB. The two methods used in estimating cost are described first. Standard cost accounts used for fusion reactor cost estimates are next reviewed. Adjustment of cost to a common basis is then presented.

4.2.1 Cost Scaling and Unit Costing

Two basic methods are generally used for cost estimating. In the first method, known as system scaling costing, comparisons are done on a system or subsystem basis with similar design for which the cost has already been estimated. The cost of the components is then scaled by a parameter, such as the mass or power, to a size or capacity appropriate for the application. These scaled costs are then summed to give the total cost for the new system.

The second method is known as unit costing. The size or capacity of each piece of equipment in a subsystem is determined. The cost of the single piece of equipment is estimated by multiplying by a unit cost, such as $/MWth or $/kg. The total cost of the subsystem is determined by summing the cost of all the individual pieces of equipment in the subsystem. The process proceeds through all subsystems and systems until all equipment has been included. The total estimated cost is then obtained by summing all system costs.

The costing method used in this work is a combination of the two methods. A detailed cost estimate using unit costing was done for the STARFIRE commercial superconducting magnet tokamak reactor design study [4.1]. From this detailed costing, a simplified costing algorithm was developed which uses cost scaling on various systems [4.2]. This STARFIRE costing model was the starting point for the cost estimate for the RTFB.

In the systems in which the RTFB is similar to STARFIRE, the cost of the entire system for the RTFB is scaled from STARFIRE costs by the appropriate parameters. However, there are many systems which are quite different for the RTFB than the corresponding system in STARFIRE. For example, STARFIRE has a solid breeder blanket with water cooling and a massive shield to limit energy deposition in the superconducting toroidal field coils; the RTFB has a liquid tritium breeding blanket with a solid fissile breeding region using both liquid metal and molten salt for cooling with little additional shielding for the resistive toroidal field coils. In these cases, system scaling of the STARFIRE costs is not appropriate. Unit costing is used instead, with the costing basis, *i.e.*$/kg or $/kWth, calculated for specific components or systems.

4.2.2 Cost Accounts

Standard cost accounts have been recommended for fusion reactor cost estimates [4.3]. Use of these standard accounts facilitates comparisons between designs done by different groups. A discussion of the major accounts follows.

Account 20 includes land purchase and relocation of any required services, such as highways and utilities. This account is fixed in cost.

All structures and site facilities are included in Account 21. All buildings on the site (reactor, turbine, electrical equipment and supply, plant auxiliary systems, hot cell, reactor service, service water, fuel handling and storage, control room, on-site AC power supply, administration, site service, cryogenic and inert gas storage and security buildings) as well as the cooling system structures and ventilation stack are included. General improvements and transportation access to the site are also included.

Reactor plant equipment is included in Account 22. This includes the reactor equipment (blanket and first wall, shield, magnets, heating and current drive, primary structure and support, reactor vacuum, power supply, impurity control and plasma breakdown), main heat transfer and transport systems (primary coolant system, intermediate coolant system, limiter cooling system and residual heat removal system), cryogenic cooling system, radioactive waste treatment and disposal, fuel handling and storage systems, other reactor plant equipment (such as maintenance equipment, gas systems etc.) and instrumentation and control. Also in this account is a spare parts and contingency allowance.

Account 23 includes all turbine plant equipment. The turbine-generators, main steam system, heat rejection system, condensing system, feed heating sys-

tem and other turbine plant equipment (auxiliaries, chemical treatment and condensate purification, etc.) as well as instrumentation and control are in this account. Spare parts and contingency allowances are included.

Electric plant equipment is contained in Account 24. This includes switchgear, station service equipment, switchboards, protective equipment, electrical structures and wiring containers, power and control wiring and electrical lighting. A spare parts and contingency allowance is also included.

Account 25 contains miscellaneous plant equipment. This is a catch-all account that includes transportation and lifting equipment, air and water service systems, communications equipment and furnishing and fixtures. Spare parts and contingency allowances are included.

Special materials are included in Account 26. These include initial supply of non-fuel and non-structural materials which are non-standard in the accounting. Examples are special fluids and gases.

Account 27 contains construction facilities, equipment and services. This includes temporary facilities, all construction equipment and construction services (for example, utilities, security, training and testing of labor, site cleanup, etc.).

Engineering and construction management services are in Account 92. Account 93 is for other costs (i.e., taxes and insurance, staff training and startup).

Accounts 94 and 95 are for interest during construction and escalation during construction, the latter for inflated dollar analyses.

4.2.3 Adjustment of Costs to 1984 Dollars

In this study, costs were obtained from many sources. The cost estimates from the various sources were done at different times. Due to the time value of money, as discussed in Chapter 5, each of these costs must be adjusted to the same point in time to be consistent.

The prescribed standard method for adjusting the costs estimated at various points in time to the same point in time is to use indices from the Handy Whitman Index of Public Utility Construction Costs [4.4] and the Department of Commerce publication Survey of Current Business [4.5]. The indices necessary for this analysis are summarized in Table 4.2. In order to convert a cost from Year Y dollars to Year X dollars:

$$\text{Cost in Year X} = \text{Cost in Year Y} \times \frac{\text{Index for Year X}}{\text{Index for Year Y}} \qquad (4.1)$$

Note that the indices are different for different accounts.

The cost information was taken primarily from three sources: The Non-Proliferation Alternative Systems Assessment Study (NASAP) [4.6], the Battelle Pacific Northwest Laboratory report "Fusion Reactor Design Studies - Standard Unit Costs and Cost Scaling Rules" [4.7] and the STARFIRE design study [4.1]. These sources will be referred to as NASAP, PNL and STARFIRE. NASAP costs are in January, 1978 dollars. PNL costs are in July, 1979 dollars. STARFIRE costs are in 1980 dollars (assumed January). The present costs are assumed to be January, 1984 due to the lag in availability of the Handy Whitman data.

4.3 Cost Estimate for Reference Design

This section presents the cost estimate for the RTFB reference design. This is accomplished by first presenting a power balance for the RTFB. Detailed cost accounting is then discussed. Next is presented a cost estimate for the RTFB reference design. Sensitivity of the cost estimate to various assumptions is also investigated.

4.3.1 RTFB Power Balance

A power balance was done for the RTFB to determine the quantities of heat deposition in the various regions of the blanket and first wall. This is used to determine the input power to the turbine. From the turbine power and the thermal to electric conversion efficiency, the gross electric power can be determined. The power requirements within the plant can be subtracted from the gross electric power to give the net electric power. The net electric power is the power that the plant sends to the busbar to sell.

A diagram showing the thermal and electric energy flows within the RTFB plant is shown in Fig. 4.1. This figure is for the reference case at EOC with a BOC blanket thermal power of 3757 MWth and a fuel cycle length of 4 years.

The power balance for the reference RTFB at EOC is shown in Table 4.3, along with a comparison with STARFIRE. Although the RTFB fusion power is lower than STARFIRE by a factor of 5.8. the turbine input power is higher by a factor of 1.45. This is because of the blanket power enhancement in the RTFB. due to fissioning of the fertile materials and the bred ^{239}Pu . The recirculating power in the RTFB is a factor of 2.3 higher than STARFIRE.

The largest power requirement in the RTFB is for the resistive magnets (452 MWe) while in STARFIRE, the largest power requirement is for rf heating and current drive. The net power output of the RTFB is 1552 MWe at EOC and for STARFIRE, 1202 MWe. The average electric output of the RTFB is 1247 MWe. Thus, even though the RTFB has a higher gross electric power than STARFIRE by a factor of 1.45 (2094 MWe vs. 1440 Mwe), the net electric power of the RTFB is higher than STARFIRE by a factor of 1.3 (1552 MWe vs. 1202 MWe) due to the higher recirculating power in the RTFB (542 MWe vs. 238 MWe). Note also that the average net electric power of the RTFB is comparable to the STARFIRE net electric output (1247 MWE vs. 1202 MWe).

4.3.2 Cost Estimate for RTFB

The cost estimate for the RTFB reference design is shown in Table 4.4. Also shown for comparison is cost information for STARFIRE. Note that all costs are in millions of January 1, 1984 dollars. The STARFIRE values have been adjusted to 1984 dollars using the Handy Whitman indices.

The total capital cost of the RTFB is 2% less than the capital cost of STARFIRE. The RTFB is less expensive than STARFIRE by 9% in the structures and site facilities account since the RTFB is more compact than STARFIRE. The RTFB is 14% less expensive than STARFIRE in the reactor plant equipment account. The differences in the reactor plant equipment account are considered in more detail below. The RTFB is more expensive than STARFIRE in the turbine plant equipment account (by 48%) and the electric plant equipment account (by 9%) due to the higher blanket power in the RTFB and the use of two turbines instead of one, as in STARFIRE.

Due to the larger net electric output of the RTFB, the RTFB is less expensive than STARFIRE per unit of net electric output by 6% (2414 $/kWe vs. 2566 $/kWe). This is a useful figure of merit, known as the cost of capacity, since it is the capital cost per unit of electricity for sale and relates closely to the cost of electricity. Note that the cost of capacity of the RTFB of 2414 $/kWe is based on the average net electric output.

Another interesting comparison is the capital cost per unit of gross electricity production. This quantity is 1437 $/kWe for the RTFB and 2142 $/kWe for STARFIRE. Thus, the RTFB is 33% less expensive than STARFIRE per unit of gross electric production.

More detail is shown in Table 4.5 for Account 22, Reactor Plant Equipment since this single account contains ~50% of the total direct cost for both plants. The two major subaccounts are reactor equipment (Account 22.01) and main heat transfer and transport (Account 22.02). In the reactor equipment account, the RTFB is about 45% as expensive as STARFIRE. Major savings of $215M are realized by not needing the massive shield used in STARFIRE to protect the superconducting toroidal field coils. A much more compact and less expensive shield is used only in the inboard side of the RTFB. Savings in other accounts, such as blanket and first wall, primary structure and support, reactor vacuum system and impurity control system, are due to the more compact size of the RTFB. Also the reference design for the RTFB has no heating or current drive. The possibility of adding heating and/or current drive will be addressed later.

The cost of the power supplies for the RTFB is approximately 75% of the cost of the STARFIRE power supplies. The total capacity of the RTFB power supplies is 500 MWe. The total size of the largest STARFIRE power supplies is 435 MWe (293 MVA for toroidal and equilibrium field coils and 142 MWe for current drive power supplies) plus 90 MWe for power supplies for correction

field coils and ECRH gyrotrons. Thus, the total for STARFIRE power supplies is 525 MWe. The cost of these power supplies was estimated at 80 $/kWe in 1980$, which translates into 104 $/kWe in 1984$. The estimated cost of the power supplies for the RTFB was taken to be the same as the STARFIRE power supply cost. Thus, most of the difference in the power supply account is due to the lower capacity of the RTFB power supplies.

The RTFB main heat transfer and transport system (Account 22.02) is a factor of 3.8 more expensive than the STARFIRE system. The cost of the main heat transfer and transport system for the RTFB is primarily in the primary coolant system (66%) and the intermediate coolant system (32%) with a small amount in limiter cooling and residual heat removal (RHR) systems (2%). The primary coolant system of the RTFB uses both liquid lithium, for cooling the multiplier region, and molten salt for cooling and breeding in the outer blanket region. Intermediate sodium loops are required to minimize the possibility of contact of radioactive coolant (liquid lithium and molten salt) from the primary coolant system and water in the main steam system. Since STARFIRE uses pressurized water coolant in the primary coolant system, no intermediate coolant system was used. The RHR system for the RTFB was sized at 2.5% of the cost of the primary coolant system, as discussed in Chapter 3.

The limiter cooling system for the RTFB is presumed to be the same as STARFIRE, namely water cooling. The presence of water cooling circuits (limiter and magnet system) in proximity to lithium cooling circuits (multiplier cooling system) is a concern. The feasibility of limiter cooling with liquid metals in a configuration that does not require lithium flow at high velocities across magnetic field lines is currently under investigation [4.8]. Helium cooling for the limiter may be possible [4.8], and may also be considered for magnet cooling.

The cryogenic cooling system (Account 22.03) is not required for the RTFB

and is deleted. The radioactive waste treatment and disposal system, the reactor plant instrumentation and control system and other reactor plant equipment accounts (Accounts 22.04, 22.07 and 22.06) are assumed to cost the same as the corresponding STARFIRE accounts. The fuel handling and storage cost (Account 22.05) for the RTFB include the cost of the molten salt processing system to recover the tritium and uranium bred in the molten salt region.

The RTFB is more expensive than STARFIRE in the turbine plant equipment account (Account 23) due to the larger thermal input power to the turbine (5864 MWth for RTFB vs. 4033 MWth for STARFIRE) and resultant larger gross electric power (2094 MWe for RTFB vs. 1440 MWe for STARFIRE). The larger gross electric output for the RTFB also results in a higher cost for the electric plant equipment (Account 24).

Miscellaneous plant equipment and special materials for the RTFB (Accounts 25 and 26) are assumed to cost the same as for STARFIRE.

The total direct cost (Account 90) for the RTFB is 10% less than for STARFIRE. Accounts 91, 92 and 93 are estimated based on fractions of the total direct cost (0.10, 0.08 and 0.05 respectively). The interest during construction (Account 94) is estimated as a fraction of the total of Accounts 90, 91, 92, and 93. This fraction is a function of the interest rate, the inflation rate, the construction time and the expenditure pattern during construction. The interest during construction shown for the RTFB uses a fraction of 0.1303, which is the same as STARFIRE [4.1]. Use of this factor assumes that the RTFB has the same expenditure pattern as STARFIRE, the same interest rate (5%/yr) and the same total construction period (6 yr.). Note also that the factor of 0.1303 is for no inflation.

The total direct cost and the indirect costs (Accounts 91 through 94) are

summed to give the total reactor capital cost (Account 99). Note that this is a constant dollar analysis in which the total capital cost is in January 1, 1984$, assumed to be the beginning of construction. The total construction period of 6 years gives the beginning of operation date of January 1, 1990.

From the total capital cost and additional information, the cost of electricity from the RTFB can be estimated. It should be noted that the cost of electricity which follows is estimated on the same basis as STARFIRE for comparison purposes. The costs related to the recovery of the bred fuel from the multiplier are not included and the value of the fissile fuel produced are also not included. These costs and credits are considered in the system economic analysis in a consistent evaluation. The following evaluation is only for comparison with STARFIRE.

The breakdown of the cost of electricity for the RTFB and STARFIRE is shown in Table 4.6. The yearly carrying charges assumed for the RTFB are 10%, the same as in STARFIRE. The capacity factor assumed in the calculations is 75% for both RTFB and STARFIRE. The operation and maintenance cost was assumed to scale with the gross electric output. The scheduled component replacement cost scales with the blanket lifetime. The fuel cost is for deuterium, which is practically negligible in this analysis. The total cost of electricity is 6% less from the RTFB compared to STARFIRE. Note that this comparison does not include the fuel cycle costs related to the reprocessing of the uranium multiplier or the value of the recovered fuel.

4.3.3 Sensitivity of Cost Estimate for RTFB

In the development of the cost analysis, many assumptions were made regarding the cost of various components of systems, and the method by which the cost of these components and systems could be estimated. This section explores the effect on the RTFB capital cost of varying the cost assumptions related to several components and systems.

The toroidal field coil system of the RTFB was estimated to cost \$30/kg in 1980\$ for the reference case cost estimate. Additionally, the thickness of the outboard leg was 1.5 m. The cost of the toroidal field coil system is dependent on the cost of the coils in \$/kg. The mass of the TF coils in the reference case is affected by the thickness of the outboard leg of the coil. As the thickness of the outboard leg is decreased, the mass, and hence the cost, of the TF coil decreases. However, the resistive power requirement of the TF coil increases since the current density in the outer leg increases. This causes the cost of the power supplies to increase and the net electric power output to decrease. These effects must be considered in combination to determine the net effect on the cost of electricity.

The effect on the cost of the toroidal field coils of varying the input unit cost of the toroidal coils in 1980\$ from \$0/kg to \$100/kg is shown in Fig. 4.2 for outer leg thicknesses of 0.5, 0.75, 1.0 and 1.5 m. The cost of the toroidal field coils is seen to vary from 0\$ to 330 M\$ for the 0.5 m. thickness and 0\$ to 580 M\$ for the 1.5 m. thickness as the unit cost increases from \$0/kg to \$100/kg. The TF cost of \$0/kg is not intended to represent an expected cost, but to show a limiting value. The effect of varying the toroidal field magnet unit cost on the total capital cost of the RTFB is shown in Fig. 4.3. The total RTFB capital cost is seen to increase by a factor of 1.2 for the outboard leg thickness of 0.5

m. as the toroidal field magnet unit cost increases from \$0/kg to \$100/kg and by a factor of 1.4 for the outboard leg thickness of 1.5 m., for the same increase in unit cost.

The variation of the cost of capacity with the toroidal field coil unit cost and the outboard leg thickness is shown in Fig. 4.4. From Fig. 4.4, it is seen that each outboard leg thickness can give a lower cost of capacity than all other thicknesses shown over a range of magnet unit cost. Thus, the cost of capacity is lowest for the outboard leg thickness of 1.5 m. for \$0/kg to \$12/kg; for 1.0 m., from \$12/kg to \$28/kg; for 0.75 m., from \$28/kg to \$60/kg; for 0.5 m., from \$60/kg to \$100/kg. Thus, as the toroidal field magnets become more expensive, on a unit cost basis, the decreased mass of the thinner outboard leg more than offsets the increased resistive power requirement of the thinner outboard leg.

The variation of the cost of electricity with the unit cost of the toroidal field coil and the outboard leg thickness is shown in Fig. 4.5. Similar to the cost of capacity, each outboard leg thickness can give a lower cost of electricity than all other thicknesses shown over a range of magnet unit cost. The cost of electricity is lowest for an outboard leg thickness of 1.5 m. for a magnet unit cost from \$0 kg to \$16/kg; for 1.0 m., from \$16 kg to \$30/kg; for 0.75 m., from \$30/kg to \$68/kg; for 0.5 m., from \$68/kg to \$100/kg. Over a range of unit costs from \$20/kg to \$80/kg, very little difference in electricity cost is seen for the 0.5, 0.75 and 1.0 m. outboard leg thicknesses.

For the estimated cost of the toroidal field coil of \$30/kg, the cost of capacity is minimized with a 0.75 m. outboard leg thickness and the cost of electricity is also minimized with an outboard leg thickness of 0.75 m. Thus, the outboard leg thickness will be changed to 0.75 m. in the reference case and the toroidal field power changed accordingly to 260 MWe since this configuration minimizes both the cost of capacity and the cost of electricity in the previous

analysis.

Other cost sensitivities are also of importance. These include the number of turbine-generator sets, the capacity factor, the total capital cost and the recirculating electric power.

The gross electric output of the RTFB is 2094 MWe. This is larger than any single turbine generator unit currently in existence. Thus, consideration will be given to dividing the electrical output between multiple turbine-generator units. This sensitivity will also examine the effect of the capacity factor, since using multiple turbine-generator sets may increase the availability of the RTFB since one turbine-generator unit could stay in operation while the other was being serviced. It is not clear that the capacity factor would increase, so the effect of lower capacity factor will also be considered.

Variation of the cost of Account 23, which contains the turbine plant equipment, the total capital cost and the cost of capacity with the number of turbine-generator sets is shown in Table 4.7. The change in the cost of Account 23 is due to the difference in cost assuming the cost of the unit scales with the square root of the size of the capacity of the unit. Thus, two turbine-generator sets would cost $\sqrt{2}$ times the cost of one unit of twice the capacity. Note that the turbine-generators are only one part of Account 23, so that the total cost of Account 23 does not follow this scaling. Thus, as the number of turbine-generator set increases the total capital cost and the cost of capacity increase, as shown in Table 4.7.

The cost of electricity also increases with the number of turbine-generator sets, as shown in Fig. 4.6. However, as also shown in Fig. 4.6, the capacity factor is also important to the cost of electricity. This is because the RTFB is a very capital intensive plant; most of the cost of electricity is due to the capital

cost of the plant. These costs are fixed and must be paid even when the plant is not operating or operating at reduced capacity. The variable charges, such as fuel, which depend on the level at which the plant operates, are small relative to the capital charges. It should be kept in mind that for the RTFB operating at full power, 1 mill/kWhre translates into $11 M/yr.

As an example of the importance of the capacity factor, for the base case of 0.75 capacity factor, the cost of electricity is 42.4 mills/kWhre; for a decreased capacity factor of 0.65, the cost of electricity is 49.5 mills/kWhre; for an increased capacity factor of 0.85, the cost of electricity is 37.0 mills/kWhre. Thus, an increase of 0.1 in the capacity factor results in a decrease in the cost of electricity by 13%. However, a decrease of 0.1 in the capacity factor results in an increase in the cost of electricity of 17%. The rewards of a higher capacity factor are not so great as the penalties of a lower capacity factor.

Fig. 4.6 can be used to determine the increase in capacity factor necessary to give the same cost of electricity for an increased number of turbine-generator sets. For example, to produce electricity at the same cost as a plant with one turbine-generator set and a capacity factor of 0.75, the plant with two turbine-generators would need a capacity factor of 0.772; the plant with three turbine-generators would need a capacity factor of 0.790. These capacity factors represent increases of 3.0% and 5.3% over the base case capacity factor of 0.75. Alternatively, for the same capacity factor of 0.75, the cost of electricity from the single turbine-generator plant is 41.0 mills/kWhre; for the two turbine-generator plant, 42.4 mills kWhre: for the three turbine-generator plant, 43.4 mills/kwhre. These costs of electricity represent a decrease of 3.4% and an increase of 2.4% over the base case of 2 turbines.

Variation of the cost of electricity with the total capital cost is shown in Fig. 4.7. The cost of electricity is linear with the total capital cost over the range

of capital costs shown because the capital cost dominates the cost of electricity. The cost of electricity is seen to vary from 24 to 78 mills/kWhre as the capital cost varies from a factor of 0.5 times the reference estimate to a factor of 2 times the reference estimate.

The recirculating power is also of importance. If it is necessary to use more of the gross electric production of the RTFB within the plant, less net electric power will be available for sale. Additionally, any use of the power internally may require the provision of additional power supplies which will affect the capital cost of the RTFB. Thus, the sensitivity of various parameters to the recirculating power is evaluated.

Variation of the recirculating power is simulated by changing the toroidal field coil power requirement. Note that this also changes the capital cost since the capacity, and thus the cost, of the power supplies changes with the power requirement. Additionally, the net electric output is changed, which affects the cost of capacity and the cost of electricity.

The decrease in the net electric power with increasing magnet power requirements is shown in Fig. 4.8. Note that in addition to the magnet power requirements, additional recirculating electric power is required for pumping and auxiliaries (72 MWe for 200 MWe magnet power). The additional recirculating power increases by 7 MWe as the magnet power requirement increases from 200 MWe to 1000 MWe due to the increased pumping requirements for magnet cooling. The toroidal field magnet power requirement is varied to simulate the additional recirculating power. The range of 200 MWe to 1000 MWe magnet power requirement is intended to be illustrative only.

As the magnet power requirement increases, the total capital cost also increases due to the increased capacity of the magnet power supplies. This

increase is shown in Fig. 4.9. Since the magnet power supplies are a small fraction of the total capital cost (1.2% for 200 MWe magnet power) The total capital cost only increases by 6% as the magnet power increases by a factor of 5 (from 200 MWe to 1000 MWe).

However, the more important effect can be seen in Fig. 4.10. The cost of capacity rises as the magnet power requirement increases due to the decreased net electric output. For a cost of capacity equal to STARFIRE ($2566/kWe), the magnet power requirement could increase to 485 MWe from the reference case value of 452 MWe.

The cost of electricity as a function of magnet power is shown in Fig. 4.11. The trend in the cost of electricity is very similar to that of the cost of capacity since the cost of electricity is dominated by the capital cost. It may be seen from Fig. 4.11 that, similar to the evaluation for the cost of capacity, the magnet power requirement for the RTFB could rise to 500 MWe from the reference case of 452 MWe and still maintain the cost of electricity the same as STARFIRE (45 mills kWhre).

Thus, if the magnet power requirement is larger than calculated by a factor of 1.07, the RTFB would have the same cost of capacity and cost of electricity as STARFIRE.

The above evaluations are all for the reference case with shield in which the BOC blanket thermal power is 4071 MWth. It was shown in Chapter 3 that the blanket will experience a power swing from BOC to EOC due to the buildup of ^{239}Pu in the multiplier. This power swing must also be taken into account in the cost calculations. The method is as follows.

The blanket power variation model used for the multiplier is

$$P_{mult} = P_{mult,BOC}(1 + 22.6E) \tag{4.2}$$

where E is the atom fraction of ^{239}Pu in the multiplier. The power variation in the molten salt is given by

$$P_{ms} = P_{ms,BOC}(1 - 7.78E) \tag{4.3}$$

The blanket power variation models are derived from the calculations discussed in Chapter 3 for 0.01 and 0.02 a/o ^{239}Pu in the multiplier region.

If the blanket power is maintained constant, the fusion power must steadily decrease as the concentration of ^{239}Pu in the multiplier increases. In this mode of operation, the plant components must be sized for the initial fusion power. Thus, the capital cost of the plant is fixed and the electricity output of the plant is also fixed. As the fusion power decreases, the rate of fissile fuel and tritium production decreases due to the decrease in fusion power. Note that the values of T and F increase due to the increased number of fissions and the resulting increased number of neutrons. For the present analysis, the cost of electricity would not be affected, since the value of the fissile fuel is not taken into account. This case will be discussed in more detail in the system economic analysis.

If the fusion power remains constant, the blanket power will increase due to the increase of ^{239}Pu in the multiplier. Hence, the size of the plant must be such that the heat generated in the blanket at EOC can be removed and converted into electricity.

This mode of operation is modelled in the COST code by setting the blan-

ket power equal to the power at EOC. The EOC power is determined by the RTFB fuel cycle length, which is limited by the ^{239}Pu a/o in the multiplier, as discussed in Chapter 3. This sizes all components for the maximum power output of the blanket. The variation of power from lower power at BOC to maximum power at EOC is simulated by calculating the ratio of the average net electric output to the peak net electric output. The cost of capacity and the cost of electricity can then be calculated based on average net electric output values.

The total capital cost of the plant as a function of the RTFB fuel cycle length is shown in Fig. 4.13. The total capital cost is seen to rise almost linearly from \$2.7B to \$3.0B as the RTFB fuel cycle length increases from 1 to 4 years because the large capital cost items which vary in size with blanket power are generally estimated based on unit costing. An exception to this is the turbine-generator set, which scales with the square root of the thermal input.

Similarly, from Fig. 4.14, it may be seen that the net electric output scales linearly with the RTFB fuel cycle length, increasing from 1100 MWe to 1550 MWe as the fuel cycle length increases from 1 to 4 years. However, as seen in Fig. 4.15, the cost of capacity decreases by 9% as the RTFB fuel cycle length varies from 1 to 4 years. This occurs because as the total capital cost rises by 11%, the net electric output rises by 41% and ratio of the average to peak power decreases from 0.93 to 0.80.

The cost of electricity variation with the RTFB fuel cycle length is shown in Fig. 4.16. The cost of electricity is seen to decrease by 8% as the RTFB fuel cycle length varies from 1 to 4 years.

From these figures, it would appear that the ^{239}Pu a/o, and hence, the blanket power, could be increased even further with resulting lower electricity

costs. However, the value of k_{eff} limits the ^{239}Pu a/o as discussed in Chapter 3. Additionally, the maximum pressure for the lithium pumping calculations is shown in Fig. 4.17. The increase in the maximum pressure drop would be limited by the pressure allowed in the duct, as discussed in Chapter 3. This issue will be explored more fully in the system economics evaluation, where the cost of reprocessing the multiplier is evaluated.

4.4 Summary

This chapter has presented the cost estimating methodology and the cost estimate for the RTFB. The cost was estimated by using two methods: system cost scaling and unit costing. In system cost scaling, the cost is estimated by using a previous cost estimate for a similar system and adjusting the cost for the RTFB by an appropriate factor. In unit costing, the cost of the RTFB item or system is estimated by calculating, for example, the capacity or mass (such as, MWth or kg) and multiplying by the unit cost (for example, \$/MWth or \$/kg). The costs of the various systems are summed to give the cost of each account. The standard accounts for fusion reactor cost estimating have been established to insure uniformity among fusion reactor cost estimates. The accounts are assigned contingency allocations and summed to give the total cost of the reactor. A construction time and expenditure pattern are then assumed to give the interest during construction. The interest, along with construction and management charges, is added to the total direct cost to give the total capital cost.

The costs used in the RTFB cost estimate are taken from many sources which estimated costs at different times. Hence, the costs must all be adjusted to the same point in time. The prescribed method for this adjustment is to use indices from the Handy Whitman Index or the Department of Commerce

Survey of Current Business. Most of the cost information was taken from the Non-Proliferation Alternative Systems Assessment Study, the Battelle Pacific Northwest Laboratory report "Fusion Reactor Design Studies - Standard Unit Costs and Cost Scaling Rules," and the STARFIRE design study.

The RTFB is compared to STARFIRE, which is the basis for the cost estimate. Although the RTFB fusion power is lower than STARFIRE by a factor of 5.8, the input power to the turbine is higher by a factor of 1.45. This is due to the energy multiplication in the RTFB blanket. The recirculating power of the RTFB is a factor of 2.3 higher than in STARFIRE. The net electric output of the RTFB is 1552 MWe at EOC, compared to 1202 MWe for STARFIRE. The average electric output of the RTFB is 1247 MWe.

The RTFB capital is 2% less than the STARFIRE capital cost. Although the RTFB nuclear island is more compact than STARFIRE, the reactor plant equipment account is only 14% less expensive than STARFIRE. This is due to the different cooling system of the RTFB, which uses liquid metal and molten salt. STARFIRE uses water cooling, which eliminates the need for an intermediate coolant loop between the primary cooling system and the main steam system. However, the RTFB does not require the massive shield used in STARFIRE to limit nuclear heat deposition in the superconducting magnets.

It should be noted that the limiter cooling system for the RTFB is assumed to be the same as STARFIRE, namely, water cooling. Other options for cooling the limiter are available if water cooling is considered unacceptable from a safety standpoint.

The cost of electricity for the RTFB was estimated, on the same basis as STARFIRE. Note that this comparison does not include the fuel cycle costs and the value of the fissile fuel produced by the RTFB. The comparison is on the

same basis as the STARFIRE financial assumptions. On this basis, the cost of electricity from the RTFB is 42.4 mills/kWhre and 44.9 mills/kWhre from STARFIRE. These costs are in 1984$.

The sensitivity of the RTFB cost estimate and cost of electricity to various parameters is also investigated. The cost of electricity is seen to be a minimum for each outboard leg thickness over a range of toroidal field coil unit costs. For the estimated toroidal field coil cost of $30/kg, the cost of electricity is minimum for an outboard leg thickness of 0.75 m.

The effect of the number of turbines and availability on the electricity cost is also evaluated. Increasing the number of turbines increases the cost of electricity from the RTFB. Decreasing the capacity factor increases the cost of electricity and increasing the capacity factor decreases the cost of electricity. As an example, the base case capacity factor of 0.75 gives a cost of electricity of 42.4 mills/kWhre; a decreased capacity factor of 0.65 gives a cost of electricity of 49.5 mills/kWhre, an increase of 17%; an increased capacity factor of 0.85 gives a cost of electricity of 37.0 mills/kWhre, a decrease of 13%. Thus, the benefits of an increased capacity factor are not as great as the penalties of a decreased capacity factor.

It is also shown that the RTFB magnet power requirement could rise by a factor of 1.07, from 452 MWe to 500 MWe, and maintain the same cost of electricity as STARFIRE.

The blanket power variation with blanket lifetime is modelled in the COST code by sizing all components based on the EOC power level, which is the highest power, and calculating the cost of all electricity cost components on the basis of the average electric output. The RTFB fuel cycle length is selected to be 4 years, since this length gives the lowest cost of capacity and cost of electricity.

consistent with the limitations on k_{eff} discussed in Chapter 3. Thus, the cost of the reference design of the RTFB is \$3.01B in 1984\$.

References

[4.1] Baker, C. C., et al., "STARFIRE – A Commercial Tokamak Fusion Power Plant Study," Argonne National Laboratory Report ANL/FPP-80-1, (September 1980).

[4.2] Evans, K., "A Tokamak Reactor Cost Model Based on STARFIRE / WILDCAT Costing," Argonne National Laboratory Report ANL/FPP/TM-168, (March 1983).

[4.3] Schulte, S. C., Willke, T. L., Young, J. R., "Fusion Reactor Design Studies – Standard Accounts for Cost Estimates," Pacific Northwest Laboratory Report PNL-2648, (May 1978).

[4.4] *The Handy Whitman Index of Public Utility Construction Costs*, Whitman, Requardt and Associates, Bulletin No. 119. To January 1, 1984, Baltimore, MD.

[4.5] *Survey of Current Business*. United States Department of Commerce, Bureau of Economic Analysis, Washington, D. C., (July 1984).

[4.6] U.S. Department of Energy, "Nuclear Proliferation and Civilian Nuclear Power: Report of the Nonproliferation Alternative System Assessment Program," DOE-NE-0001, (June 1980).

[4.7] Schulte, S. C., et al., "Fusion Reactor Design Studies – Standard Unit Costs and Cost Scaling Rules," Pacific Northwest Laboratory Report PNL-2987, (September 1979).

[4.8] Smith, D. L., et al., "Blanket Comparison and Selection Study – Final Report," Argonne National Laboratory Report ANL/FPP-84-1, (September 1984).

TABLE 4.1

Standard Fusion Reactor Cost Accounts

Account	Description
20	Land Acquisition and Relocation
21	Structure and Site Facilities
22	Reactor Plant Equipment
23	Turbine Plant Equipment
24	Electric Plant Equipment
25	Miscellaneous Plant Equipment
26	Special Materials
90	Total Direct Cost
91	Construction Facilities, Equipment & Services
92	Engineering and Construction Management Services
93	Other Costs
94	Interest During Construction
99	Total Reactor Capital Cost

TABLE 4.2

Summary of Cost Adjustment Indices

	January 1978	July 1979	January 1980	January 1984
Survey of Current Business	178	–	219	261
Handy Whitman Index				
Reactor Plant Equipment	151	173	181	235
Structures and Improvements	–	–	172	212
Turbogenerators	–	–	191	251
Total Distribution Plant	–	–	184	229
Misc. Power Plant Equipment	–	–	184	250

TABLE 4.3

Power Flow Comparison – RTFB and STARFIRE

	RTFB	STARFIRE
Fusion Power	618	3608
Blanket Neutron Power	5209	457
Plasma Heating	0	90
Limiter Heating	35	200
Shield Reject Heat	0	65
Primary	5792	3800
Turbine Input	5864	4033
Gross Electric	2094	1440
Turbine Waste Heat	3771	2593
Turbine Reject Heat	3810	2620
Heating Reject Heat	0	63
BOP Auxiliaries	13	13
Magnets	452	5
Heating	0	153
Cryogenics	0	7
Pumping	37	33
Heat Transport	39	27
Thermal Power	5827	4065
Recirculating Power	542	238
Total Reject Heat	3810	2685
Net Electric	1552	1202
Average/Peak Electric	0.804	-
Average/Peak Thermal	0.849	-

TABLE 4.4

RTFB Cost Comparison With STARFIRE (January 1, 1984 M$)

Account	Items	RTFB	STARFIRE
20	Land Acquisition and Relocation	4.01	4.01
21	Structure and Site Facilities	387.50	427.18
22	Reactor Plant Equipment	1075.52	1257.61
23	Turbine Plant Equipment	484.08	328.11
24	Electric Plant Equipment	158.64	145.96
25	Misc. Plant Equipment	55.39	55.39
26	Special Materials	0.30	0.30
90	Total Direct Cost	2165.43	2218.57
91	Construction Facilities. Equipment & Services	216.54	221.86
92	Engineering & Construction Management Services	173.23	177.49
93	Other Costs	108.27	110.93
94	Interest During Construction	347.05	355.57
99	Total Reactor Capital Cost	3010.53	3084.41
	Cost of Capacity($/kWe ave.)	2414	2566
	Cost of Electricity (mills/kWhre)	42.4	44.9

TABLE 4.5

RTFB Cost Comparison With STARFIRE (1984 M$)
Account 22 – Reactor Plant Equipment

Account	Items	RTFB	STARFIRE
22	Reactor Plant Equipment	1075.52	1257.61
22.01	Reactor Equipment	345.38	765.06
22.01.01	Blanket and First Wall	80.72	106.93
22.01.02	Reactor Shield	32.96	241.58
22.01.03	Magnets	152.76	222.76
22.01.04	Heating and/or Current Drive	0.00	43.48
22.01.05	Primary Structure and Support	21.60	68.47
22.01.06	Reactor Vacuum System	1.64	6.31
22.01.07	Power Supply	53.04	68.68
22.01.08	Impurity Control System	1.82	3.18
22.01.09	ECRH Breakdown	0.84	3.66
22.02	Main Heat Transfer and Transport	345.81	90.68
22.02.01	Primary Coolant System	227.25	81.93
22.02.02	Intermediate Coolant System	110.15	0.00
22.02.03	Limiter Cooling System	3.86	8.04
22.02.04	Residual Heat Removal System	4.55	0.71
22.03	Cryogenic Cooling System	0.00	19.35
22.04	Radioactive Waste Treat. and Disposal	6.23	6.23
22.05	Fuel Handling and Storage	78.37	50.12
22.06	Other Reactor Plant Equipment	56.80	56.80
22.07	Instrumentation and Control	30.39	30.39
22.98	Spare Parts	83.07	86.19
22.99	Contingencies	129.45	152.79

TABLE 4.6

RTFB Cost of Electricity Comparison With STARFIRE

Cost of Electricity by Component (mills/kWhre)	RTFB	STARFIRE
Capital Cost	36.9	39.1
Operation and Maintenance	4.5	3.0
Scheduled Component Replacement	1.1	2.9
Fuel Cost	0.0	0.1
Total Cost of Electricity	42.4	44.9

TABLE 4.7

RTFB Account 23, Total Capital Cost and Cost of Capacity for Number of Turbines

Number of Turbines	Account 23	Total Capital Cost	Cost of Capacity
1	421.56	2896.49	2322
2	484.08	3010.53	2414
3	532.05	3095.92	2482

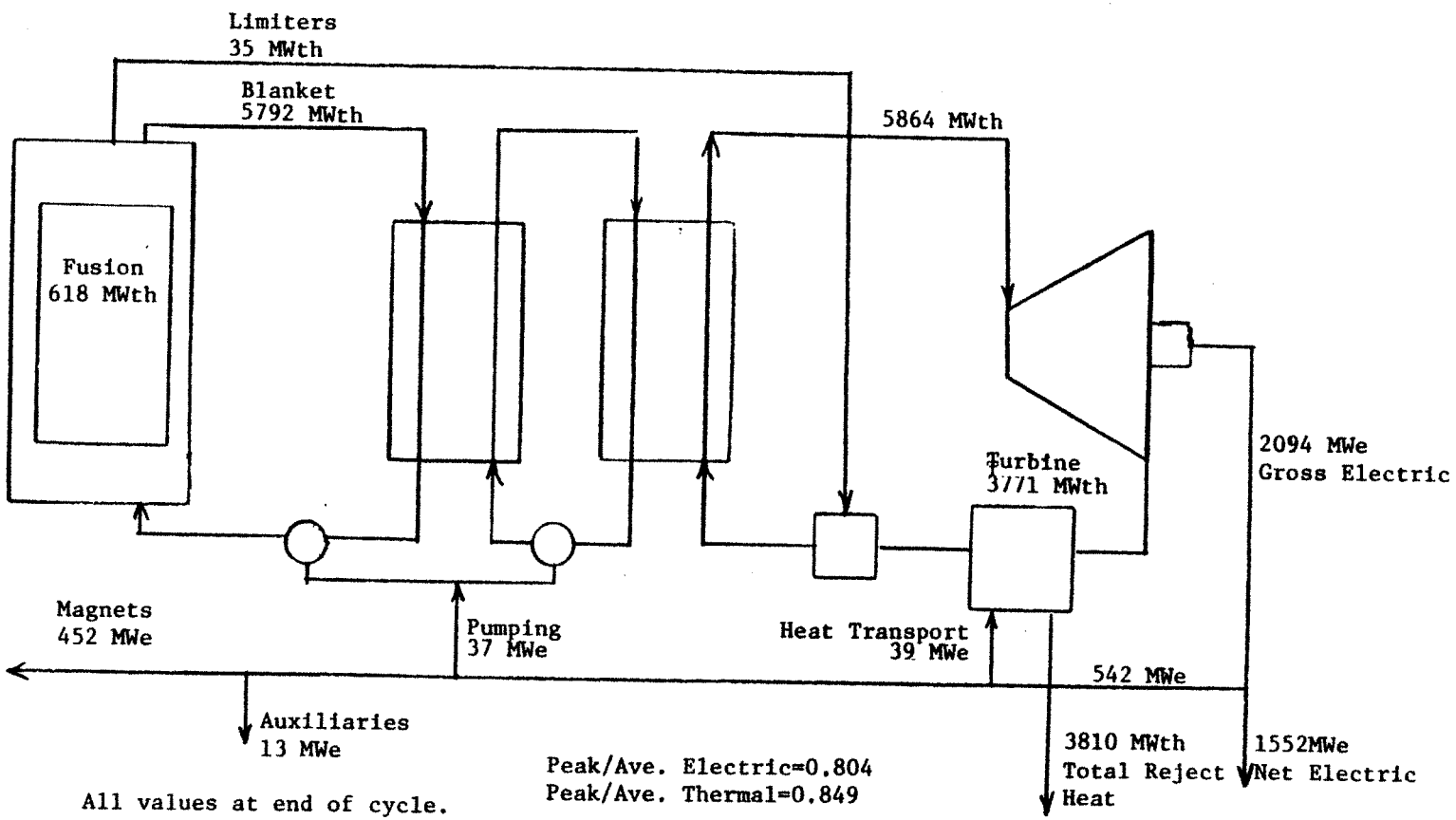

Figure 4.1 RTFB Power Balance Schematic

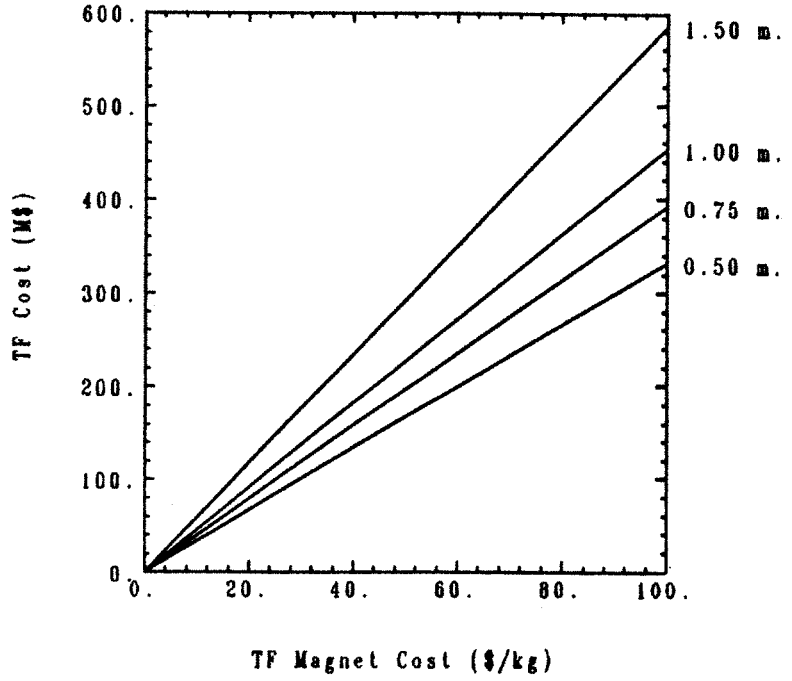

Figure 4.2 TF Magnet Cost for Unit Cost and and Outboard Leg Thickness

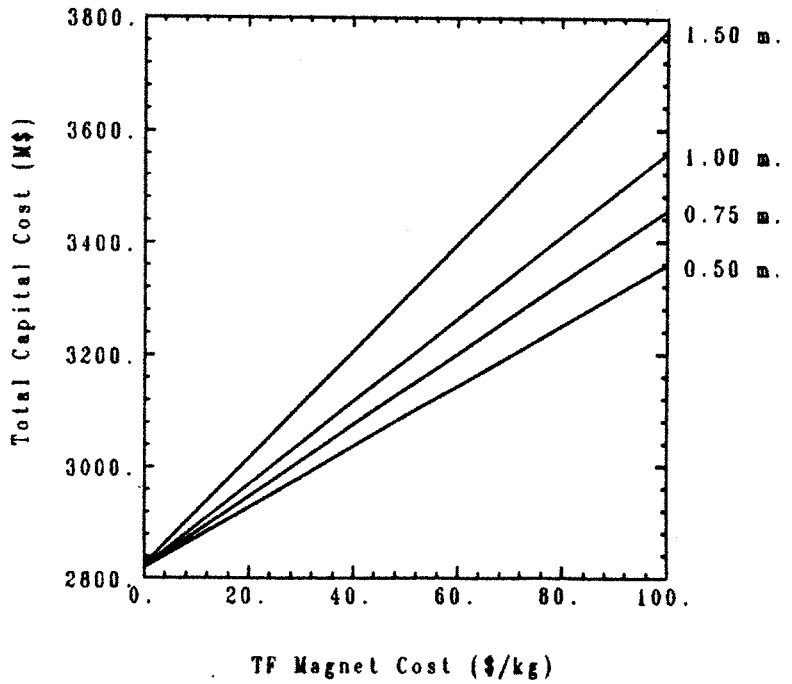

Figure 4.3 Total Capital Cost for TF Magnet Unit Cost and Outboard Leg Thickness

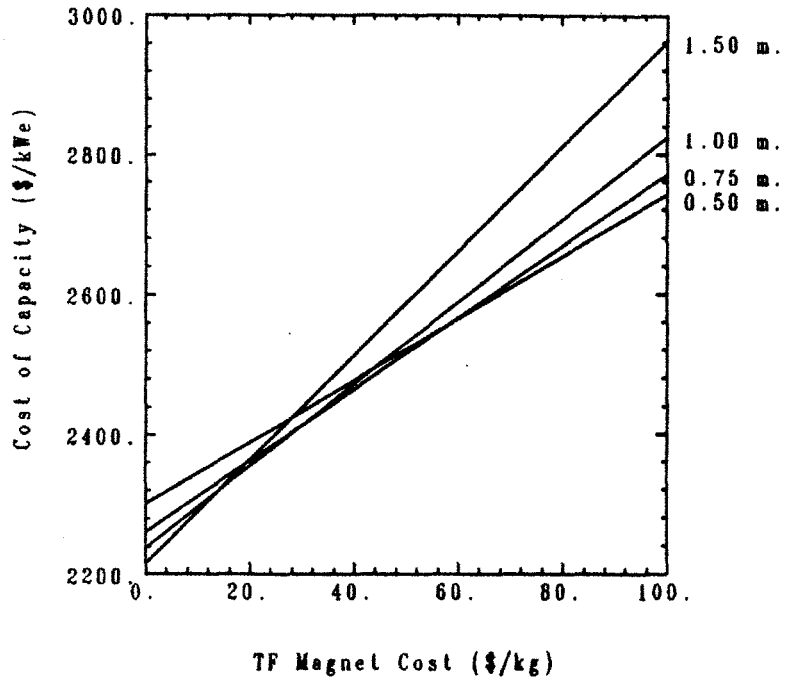

Figure 4.4 Cost of Capacity for TF Magnet Unit Cost and Outboard Leg Thickness

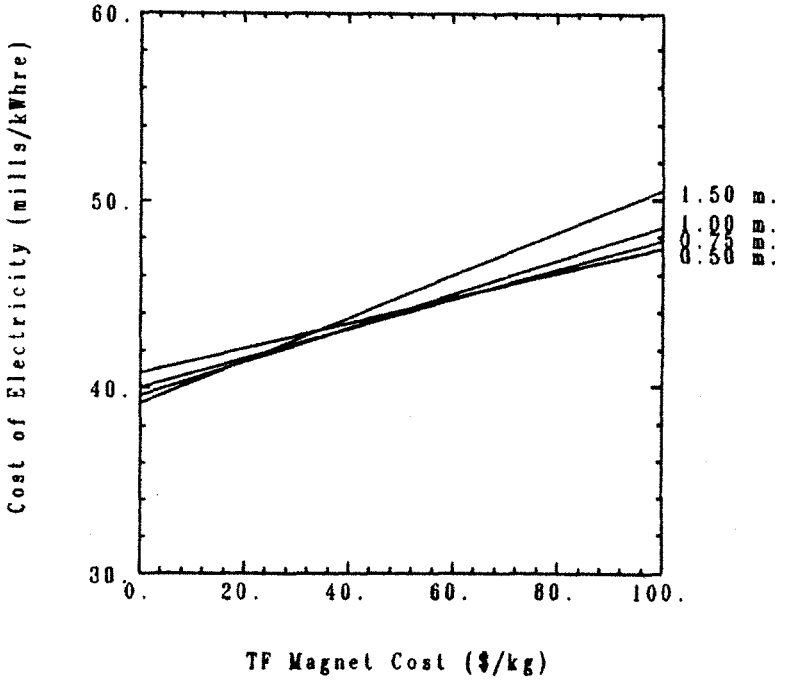

Figure 4.5 Cost of Electricity for TF Magnet Unit Cost and Outboard Leg Thickness

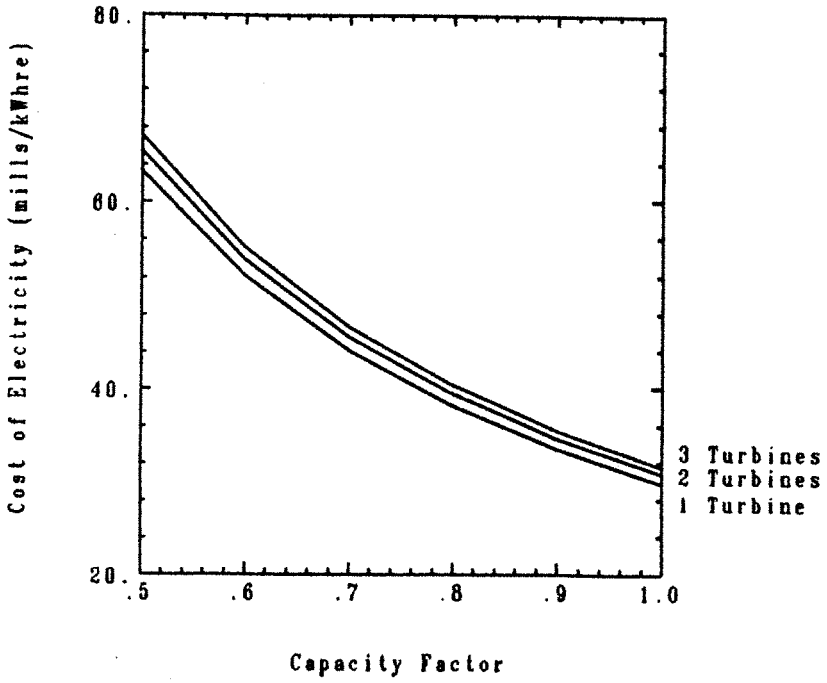

Figure 4.6 Cost of Electricity for Capacity Factor and Number of Turbines

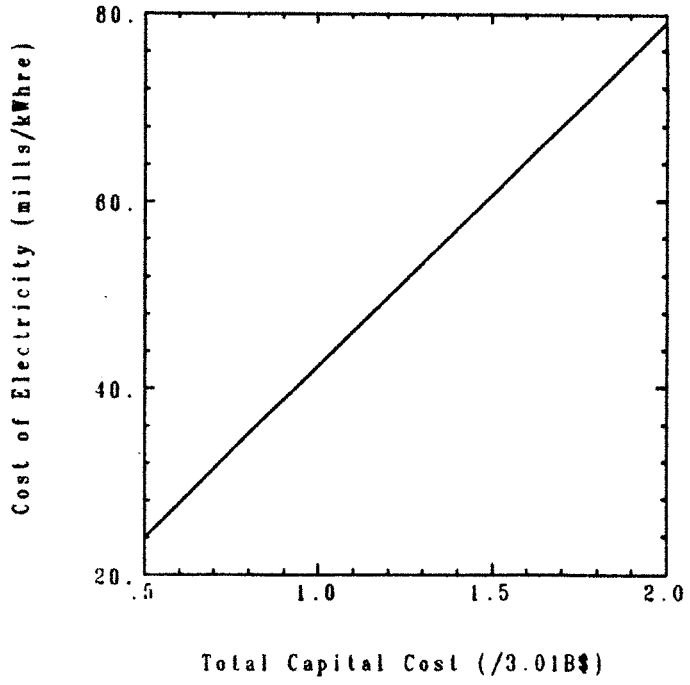

Figure 4.7 Cost of Electricity for Total Capital Cost

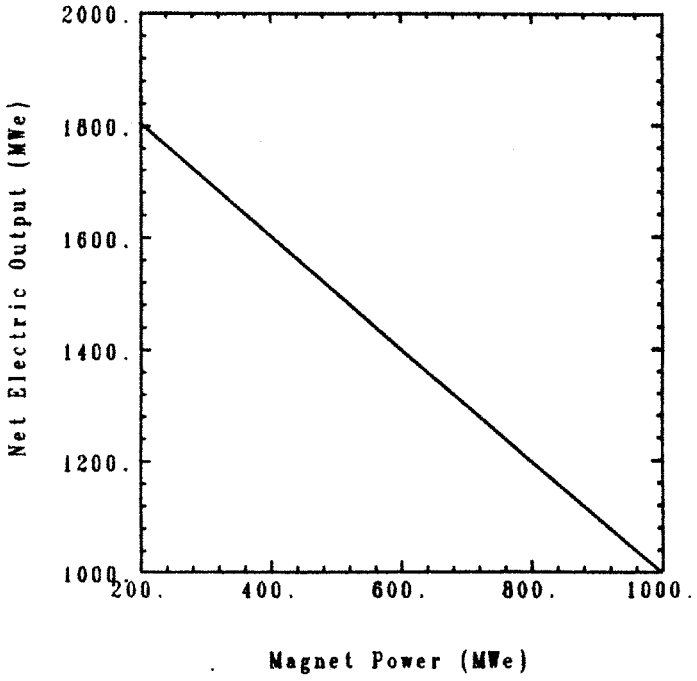

Figure 4.8 Net Electric Output for Magnet Power

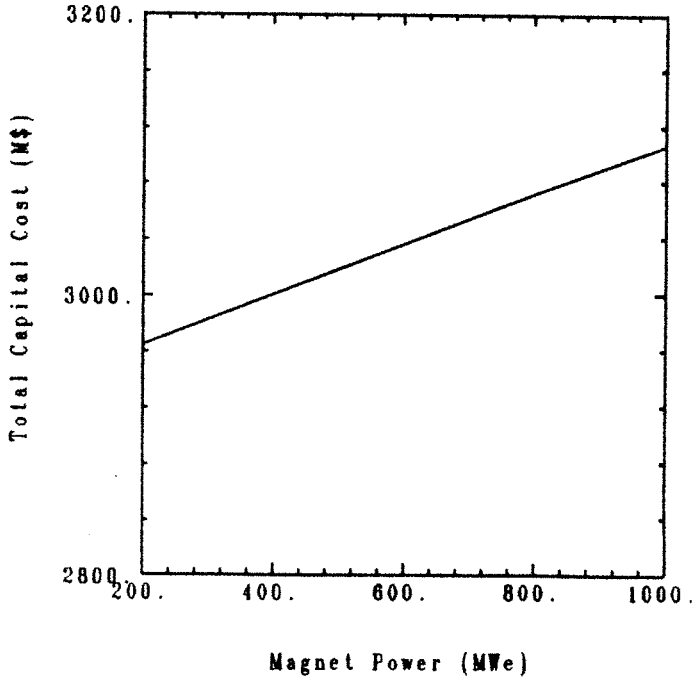

Figure 4.9 Total Capital Cost for Magnet Power

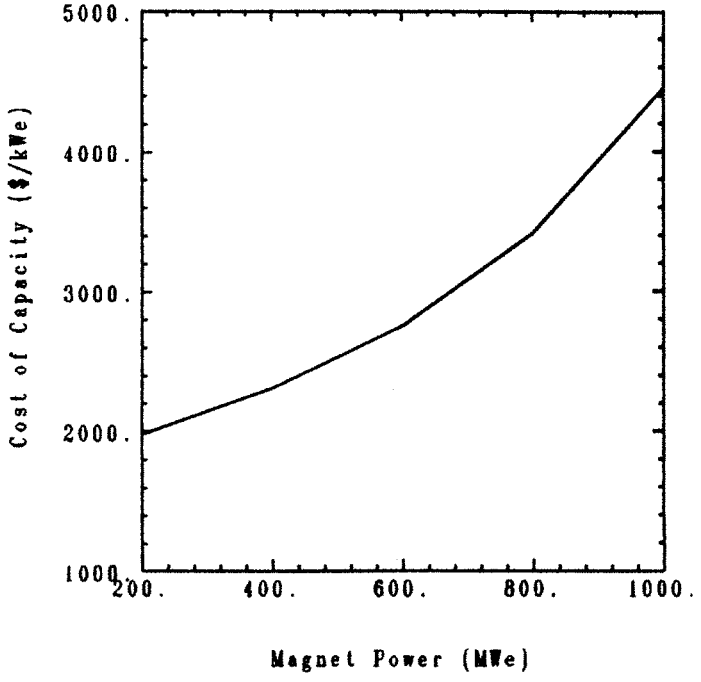

Figure 4.10 Cost of Capacity for Magnet Power

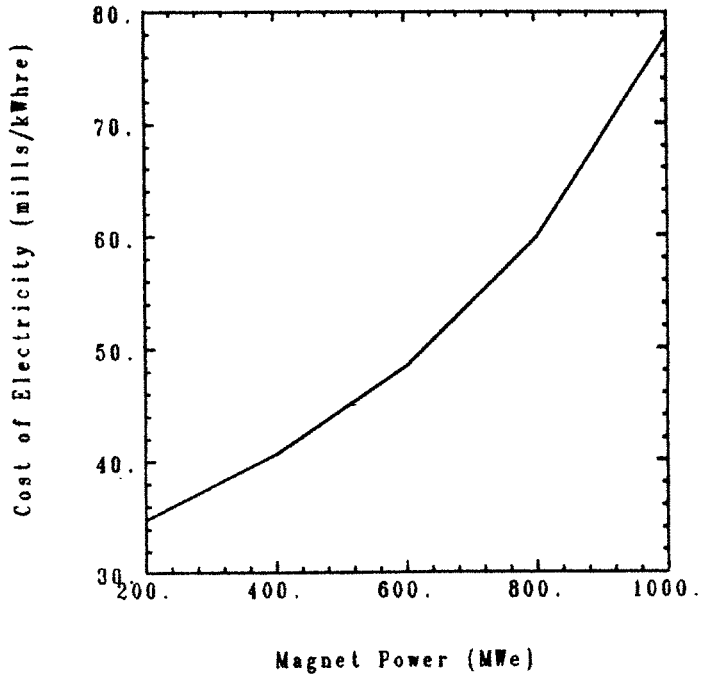

Figure 4.11 Cost of Electricity for Magnet Power

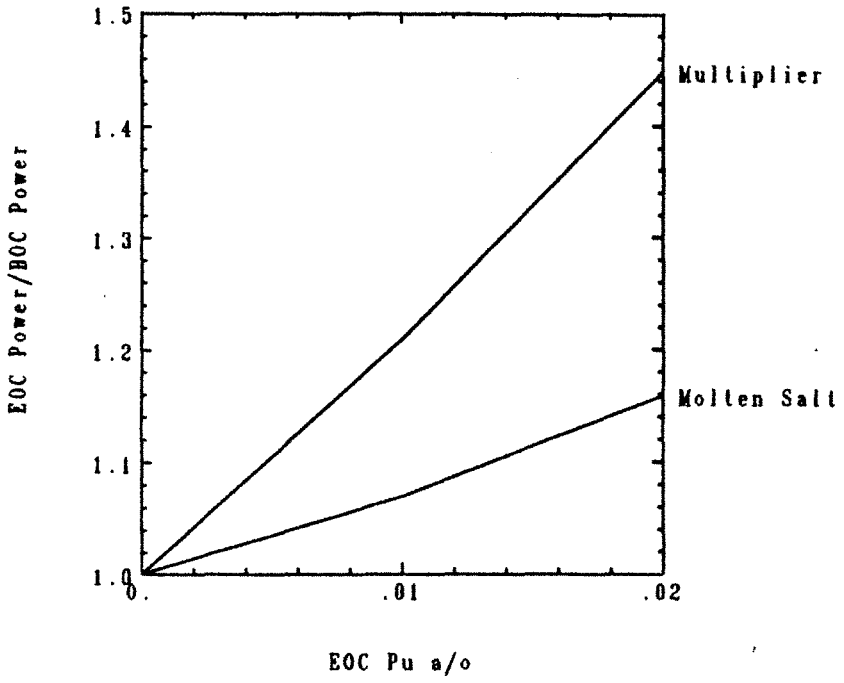

Figure 4.12 Blanket Power Variation for EOC ^{239}Pu a/o

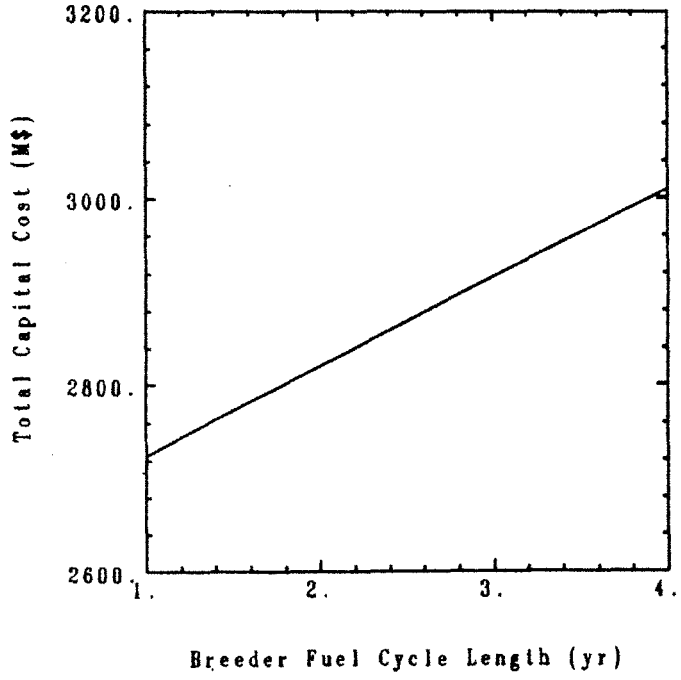

Figure 4.13 Total Capital Cost for RTFB Fuel Cycle Length

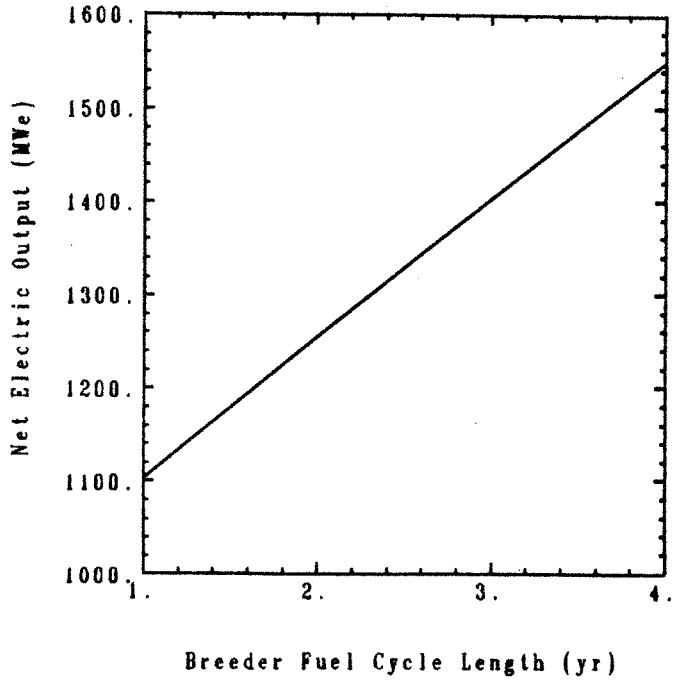

Figure 4.14 Net Electric Output for RTFB Fuel Cycle Length

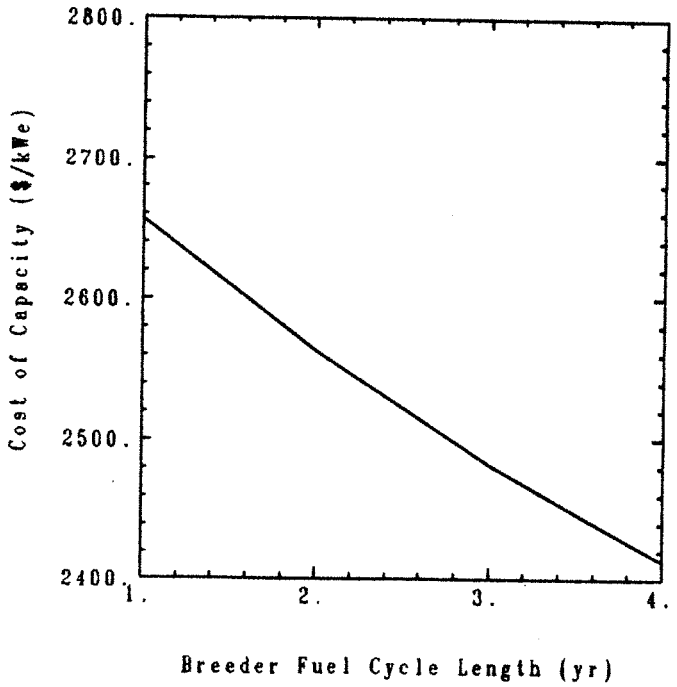

Figure 4.15 Cost of Capacity for RTFB Fuel Cycle Length

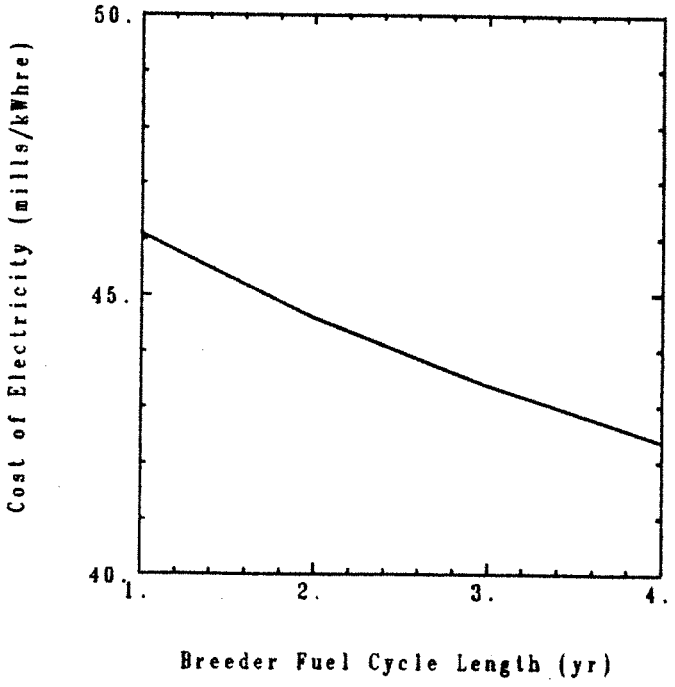

Figure 4.16 Cost of Electricity for RTFB Fuel Cycle Length

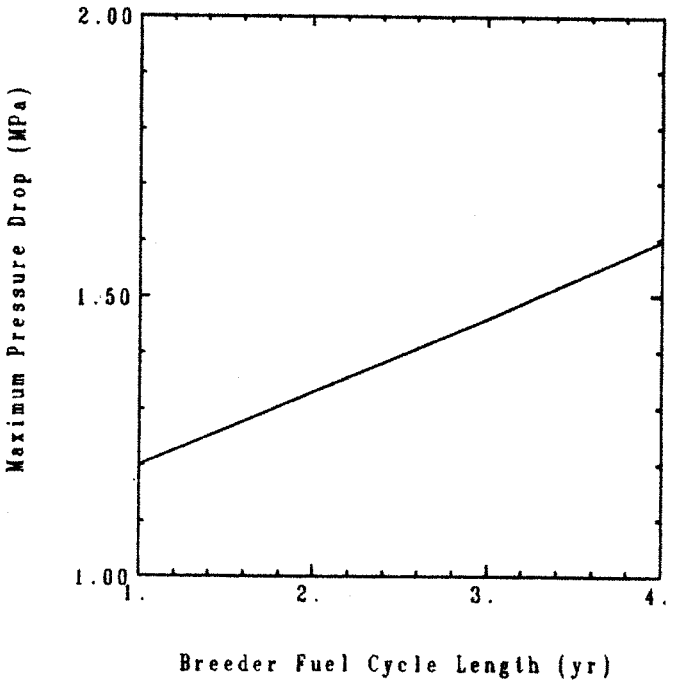

Figure 4.17 Maximum Pressure Drop for RTFB Fuel Cycle Length

5. SYSTEM ECONOMIC ANALYSIS

5.1 Introduction

This chapter presents the economic evaluation of the system of the RTFB and the associated client reactors. The discussion begins with a description of the PWR which is used as the basis for comparison. The once through fuel cycle is the standard against which the RTFB-client reactor system is compared. The client PWR fuel cycle is then discussed. The client PWRs operate on two different fuel cycles: the ^{233}U and the ^{239}Pu fuel cycles. The system economic evaluation methodology is then developed. The system economic evaluation is then performed, including investigation of the sensitivity of the various figures of merit to the many input parameters. Additionally, a comparison to a superconducting tokamak fusion breeder and a superconducting tandem mirror fusion breeder is presented. Finally, the chapter is summarized.

5.2 Once Through and Client PWR Information

The basis for comparison to the RTFB-client reactor system is the PWR on the once-through fuel cycle. The client reactor system consists of PWRs on the ^{239}Pu and ^{233}U fuel cycles. The PWRs are identical for all evaluations, but operate on different fuel cycles. This section describes the characteristics of the PWR and the three (once through, ^{239}Pu , ^{233}U) fuel cycles.

The PWR used for comparison is taken from the NASAP study [5.1]. Unit size, capacity factor, mass flows and timing of mass flows for the PWR on the once through, ^{233}U based and ^{239}Pu based fuel cycles are shown in Table 5.1. The capital, operating and maintenance and fuel cycle unit costs are shown in Table 5.2. All costs are shown for 1978$ (the date of the NASAP estimate),

1984$ (for a comparison basis) and 1990$ (the date of initial operation of the RTFB).

The front end costs for the once through fuel cycle include uranium, enrichment and fabrication. Front end costs for the ^{233}U and ^{239}Pu fuel cycles only include fabrication, since the make up fuel is exchanged within the system. Sufficient ^{232}Th and ^{238}U are available from within the system that make up of these fertile materials is neglected.

The back end costs for the once through system include spent fuel shipping and disposal costs since the fuel is discarded after discharge from the reactor. The back end costs for the ^{233}U and ^{239}Pu fuel cycles include transportation, reprocessing and waste disposal.

5.3 RTFB Fuel Cycle Information

A summary of the RTFB fuel cycle cost information is shown in Table 5.3. The cost of fabrication was taken from NASAP and is for uranium metal breeder blanket assemblies [5.1]. The cost for transportation and waste shipping and disposal was also taken from NASAP. The projected estimated cost of pyrochemical processing was taken from a LLNL report in which the application of pyrochemical reprocessing to fusion breeders was discussed [5.2]. It is noted that the cost of pyrochemical processing is substantially lower than the aqueous processing assumed for the client reactors.

The cost of the uranium multiplier is determined from the cost of U_3O_8 in each analysis, since the purchase cost of the metal would depend on the current price of U_3O_8.

A summary of RTFB performance parameters is given in Table 5.4. The total fissile production is 3790 kg yr.

5.4 System Economic Evaluation Methodology

This section is a discussion of the basic economic principles necessary for an evaluation of the cost of electricity from the RTFB-client reactor system. It begins with the concepts of the time value of money and proceeds to apply this concept to a PWR on the once through fuel cycle and the RTFB-client reactor system.

In the construction of any large project, expenditures are spread over a period of many years. Additionally, the useful life of the project may spread over a (hopefully) much longer period of time. Thus, in order to evaluate the cost of the service provided by the facility, the time value of money must be considered.

The time value of money has three components: basic return on investment, inflation and risk. The basic return on investment is normally called the uninflated interest rate. Inflation is taken to be the general rate of escalation of prices within an economy. Risk is directly related to the perception of the probability of the successful completion and operation of the project, so that the capital borrowed will be repaid. Of these three basic components, only the basic return on investment, or interest, and inflation will be considered. Risk will not be considered.

An additional economic factor is escalation. Escalation is the rate at which the price of a commodity increases in excess of interest and inflation rates. This is usually caused by increasing scarcity of the commodity. As an example, as

the easily mined deposits of uranium are depleted, more expensive (i.e., lower grade) deposits will be developed. These deposits will require a higher price for uranium to recover the increased investment necessary to recover the uranium. This increase may exceed the increase due to inflation by s substantial amount. This was seen to happen with uranium in the early 1970's.

In this analysis, all discounting and cash flows will be assumed to occur at the end of the year. All discount, inflation and escalation rates are discrete annual, and not continuous.

5.4.1 Time Value of Money

The reference time used for present values is the beginning of operation. The present value of an expenditure at some point in the future is given by:

$$P = F\frac{(1+r)^n}{(1+i)^n} \tag{5.1}$$

where:

P = Present value of a future expense
F = Future expense in Year 0 Dollars
r = Annual inflation rate
i = Annual interest rate
n = Time at which the expense occurs

Similarly, for the future value of a present investment:

$$F = P\frac{(1+i)^n}{(1+r)^n} \tag{5.2}$$

Note that in the two previous equations, the annual interest rate includes an allowance for inflation. These two equations will be used to adjust expenditures occurring at different points in time to a common basis, including the effects of inflation.

The capital recovery factor gives the annual payment required to "pay back" an investment over a number of years:

$$A = P\left[\frac{i(1+i)^K}{(1+i)^K - 1}\right] \tag{5.3}$$

where:

A = Annual payment to recover a capital investment
P = Capital investment
K = Number of uniform annual payments

These are the basic concepts needed for the financial analysis.

5.4.2 Cost Components of Electricity Production

This section details the calculation of cost components of electricity production. The calculational method closely follows Reference [5.3], with the addition of inflation. The same method is applied to the fusion breeder with appropriate modifications, which are noted.

The discussion is based on an LWR on the conventional once-through fuel cycle. Appropriate modifications for the client reactor system with recycle and the fusion breeder fuel cycle are also noted.

The effective interest rate is:

$$i = (b \times i_b) + (e \times i_e) \tag{5.4}$$

where:

b = bond fraction

i_b = bond interest rate

e = equity fraction

i_e = equity interest rate

Note also that the interest rate may include an allowance for inflation ($i > r$). Typical utility values are shown in Table 5.4.

The return on a capital investment is:

$$C_u = C\left[\frac{i(1+i)^K}{(1+i)^K - 1}\right] \tag{5.5}$$

This is the annual amount, C_u, that must be charged to recover the capital investment, C, in the plant. K is the lifetime of the plant.

The annual production of electricity is given by

$$\text{E} = \text{Power} \times \text{Capacity Factor} \times 8766 \text{ hr/yr} \tag{5.6}$$

Thus, the levelized capital cost contribution to electricity cost is:

$$L_{cap} = \frac{C_u}{E} \tag{5.7}$$

The fixed charges on a capital investment (i.e., property insurance, property taxes) are given by

$$L_{fc} = \frac{f \times C}{E} \tag{5.8}$$

where f is the fixed charge rate, typically 0.05. These charges are assumed to be unresponsive to inflation since they are based on the capital cost of the plant, which is a sunk cost. Additionally, the fixed costs are nontaxable.

The taxes on the income to recover a capital investment are given by:

$$L_{ctax} = \left(\frac{t}{1-t}\right)\left(\frac{L_{cap} \times E - cdep}{E}\right) - \left(\frac{t}{1-t}\right)\left(\frac{bi_b}{i}\right)\left(\frac{1}{E}\right) \times \left[\frac{i(1+i)^K}{(1+i)^K - 1}\right]\left[C - \frac{KC_u}{(1+i)} + \frac{KiC}{(1+i)}\right] \tag{5.9}$$

where t is the tax rate and straight line depreciation

$$cdep = \frac{C}{K} \tag{5.10}$$

has been assumed. These are taxes that must be paid on the income collected to pay for the capital investment. The taxes are basically the income tax rate times the revenue collected to pay for the plant minus the plant depreciation.

The operating and maintenance costs are given by:

$$L_{om} = \frac{\text{fixed O \& M} + [(\text{variable O \& M}) \times (\text{capacity factor})]}{E} \tag{5.11}$$

Fuel cycle costs will now be considered. The basis for the calculation is a single equilibrium batch. Startup and final fuel batches are considered as equilibrium batches. The reference time to which all transactions are adjusted is the fuel load time.

The direct expenses for the once through and client PWRs are given by:

$$L_b = \frac{F\frac{(1+i)^{td}}{(1+r)^{td}} + B\frac{(1+r)^{td+N}}{(1+i)^{td+N}}}{\frac{E}{N}\left[\frac{(1+r)}{(1+i)} - \frac{(1+r)^2}{(1+i)^2} \cdots - \frac{(1+r)^N}{(1+i)^N}\right]} \tag{5.12}$$

where:

F = Front end costs

ld = Front end lead time

B = Back end costs

lg = Back end lag time

N = Number of batches in fuel cycle

The lead time is the time before fuel load that all front end transactions occur. The lag time is the time after discharge when all back end transactions occur. Discharge occurs in N years after fuel load. It has been assumed that one batch load produces $\frac{1}{Nth}$ of the energy produced in each year of its N years residence in the core.

The direct expenses for the RTFB are given by:

$$L_b = \frac{F\frac{(1+i)^{ld}}{(1+r)^{ld}} + B\frac{(1+r)^{lg+bfcl}}{(1+i)^{lg+bfcl}}}{E\left[\frac{(1+r)}{(1+i)} + \frac{(1+r)^2}{(1+i)^2} \cdots + \frac{(1+r)^{bfcl}}{(1+i)^{bfcl}}\right]} \tag{5.13}$$

where $bfcl$ is the RTFB fuel cycle length. Note that the entire multiplier region is replaced at one time.

The front end costs are given by:

$$F = \text{uranium} - \text{enrichment} + \text{fabrication} \tag{5.14}$$

for the once through PWR and

$$F = \text{fuel} + \text{fabrication} \tag{5.15}$$

for the client PWRs with recycle. For the RTFB, the front end costs are given by:

$$F = \text{uranium} + \text{fabrication.} \tag{5.16}$$

The back end costs are given by:

$$B = \text{spent fuel shipping and disposal} \tag{5.17}$$

for the once through PWR and

$$B = \text{transportation, reprocessing and waste disposal} \tag{5.18}$$

for the client PWRs and the RTFB.

Taxes must be paid on this income. The fuel is considered a depreciating asset for the once through PWR since it has no value after use. The fuel for the client reactors, however, is not depreciated and is considered a capital asset since it is recycled and reused within the system. Hence, a carrying charge will be paid on the value of the fuel. Although the value of the fuel is not depreciated in the RTFB-client reactor system, all expenses related to fabrication and reprocessing are depreciated. The depreciation allowance is directly proportional

to the amount of energy produced by a batch in any year. All direct expenses associated with a batch are depreciated. However, the time value of money can only be considered for expenses occurring before or after operation.

The taxes on a single batch of fuel are given by:

$$L_{btax} = \left(\frac{t}{1-t}\right)\left[L_b - \frac{F(1+i)^{ld} + \frac{B}{(1+i)^{lu}}}{E}\right] \tag{5.15}$$

Note that the front end costs include the value of the fuel for the once through PWR and do not include the value of the fuel for the client reactor system.

The RTFB fuel cycle costs are calculated in the same manner as the PWR fuel cycle costs, except the fuel cycle length for the RTFB may be different than for the once through or ^{233}U and ^{239}Pu systems.

The RTFB-client reactor system electricity cost is determined by averaging the RTFB electricity cost and the client reactor electricity cost (without the fuel charge, since the fuel is only exchanged within the system) over the total electricity generation of the entire system. This gives the system electricity cost without the fissile fuel carrying charges. These charges are determined by calculating the effective fuel cost to each type of client reactor fuel cycle (^{233}U and ^{239}Pu) and using this cost, in conjunction with the make up fuel requirements, to determine the value of each type of fuel within the system. This value, along with the total inventories and carrying charge rate, determines the carrying charges, with an allowance for taxes on the income related to the carrying charges. The carrying charges are then added to the system electricity cost to obtain the total system electricity cost.

Additionally, the cost of fuel from an alternate source to maintain the same total cost of electricity from the client reactors as the once through reactor is determined. This cost of fuel (in \$/gm) is the price of ^{233}U or ^{239}Pu from any source which would keep the total fuel cycle cost the same as the once through fuel cycle costs.

The preceding evaluation allows calculation of the cost components and total cost of electricity for the once through PWR and the RTFB-client reactor system. These expressions were incorporated into the COST code to examine parametrically the system electricity cost and its sensitivity to the many input factors.

The COST code implementation also allows inflated dollar analyses to be levelized over the life of the plant by calculating year by year values for the variable costs and levelizing, using Eqn. 5.3, and discounting these costs to the beginning of operation. Escalation of uranium costs beyond the allowance for inflation is also allowed.

An additional quantity which is calculated only for comparison purposes with other fusion breeder systems is the average present value of the various figures of merit. This is calculated by taking the year by year inflated and escalated values, discounting these year by year values to the beginning of operation and taking the average of all of the present values of each quantity of interest. It is not clear what this figure of merit means in economic terms, but the average present value is calculated here as a basis for comparison because it is commonly used in fusion breeder evaluations.

5.5 System Economic Evaluation and Sensitivities

This section presents the system economic evaluation. This evaluation includes examination of the sensitivities of the total system electricity cost to the many input parameters.

5.5.1 RTFB Fuel Cycle Length

The fuel cycle length of the RTFB is of importance due to the significant fuel cycle costs associated with the purchase of the multiplier and the reprocessing of the multiplier to recover the bred ^{239}Pu . Thus, the fuel cycle costs vary with the fuel cycle length as shown in Fig. 5.1 for uranium costs of 0, 50, 100, 150 and 200 \$/lb U_3O_8. It may be seen from Fig. 5.1 that the fuel cycle costs decrease steadily as the RTFB fuel cycle length increases. This decrease is due to several factors.

The most important factor is the averaging of the expenses associated with the multiplier over a longer period of operation and, hence, reducing the cost per kWhre. Effectively, the cost per year of operation associated with the multiplier is reduced.

As the fuel cycle is extended in length, the end of cycle power increases since the EOC ^{239}Pu concentration increases. Thus, the electric power output is greater for the same fuel cycle costs. The cost of capacity also decreases since the net electric output increases faster than the capital cost. The decrease in the cost of capacity may be seen in Fig. 5.2.

Additionally, the reprocessing and other back end costs are deferred for a longer period of time, which results in a lower cost when referred to the fuel

load time. The RTFB fuel cycle costs are seen to be relatively insensitive to the cost of U_3O_8 with the fuel cycle cost increasing by a factor of 2 as U_3O_8 costs vary from 0 \$/b to 200\$/lb.

Although the ^{239}Pu production decreases slightly, the ^{233}U production increases as the RTFB fuel cycle length is lengthened as shown in Fig. 5.3. Note that this is the net ^{239}Pu production. The result is an increase in total fissile production. This increase in fissile fuel production is reflected in the number of client reactors supported by the RTFB, which is shown in Fig. 5.4. The number of client reactors supported increases from 7.8 for a RTFB fuel cycle length of 1 year to 9.2 for a RTFB fuel cycle length of 4 years. This becomes important in the system electricity cost evaluation since the higher costs of the RTFB are "spread out" over the client reactor system. Note that, although the net ^{239}Pu production decreases, the number of ^{239}Pu fueled client reactors actually increases slightly. This is due to the increase in the number of ^{233}U fueled client reactors, which each discharge 84 kg/yr of ^{239}Pu . This ^{239}Pu is used as make up fuel for the ^{239}Pu fueled client reactors, as well as fuel produced by the RTFB.

The total system electricity cost for the reference case is shown in Fig. 5.5 for RTFB fuel cycle lengths from 1 to 4 years and U_3O_8 prices of 0, 50, 100, 150 and 200 \$/lb. Additionally, electricity costs are shown for the once through PWR for U_3O_8 prices of 0, 50, 100, 150 and 200 \$/lb.

From Fig. 5.5, it may be seen that the system electricity cost decreases as the RTFB fuel cycle length increases. The system electricity cost is seen to decrease by a factor of 1.3 as the RTFB fuel cycle length is extended from 1 year to 4 years. This is due to the decreased RTFB costs, as discussed above, and the increased number of client reactors within the system. Also, the system electricity cost increases as U_3O_8 prices increase. The once through PWR

electricity cost increases as U_3O_8 prices increase, also. Fig. 5.5 can be used to determine the fuel cycle length necessary for the RTFB-client reactor system to produce electricity at a cost equivalent to the once through PWR.

5.5.2 RTFB Capital Cost

A great deal of uncertainty is contained in the RTFB capital cost estimate due to the uncertainty in the technology relative to present technology. Therefore, the effect of an increased and decreased capital cost of the RTFB over the estimated cost was investigated.

The variation in the RTFB cost of capacity with capital cost is shown in Fig. 5.6. From Fig. 5.6, it may be seen that as the RTFB capital cost varies from \$1.5B to \$6B, the cost of capacity increases from \$1200/kWe to \$4800/kWe. It should be noted that these factors of variation in the RTFB capital cost are for illustrative purposes only.

The effect of the increased capital cost of the RTFB on the total system electricity cost for uranium costs from 0 to 200\$/lb U_3O_8 is shown in Fig. 5.7. Additionally, electricity costs for the once through PWR are shown in Fig. 5.7. This information can be used to determine the factor by which the RTFB capital cost could exceed the estimated cost and still remain competitive with electricity from the once through PWR. As an example, for 100\$/lb U_3O_8 the RTFB could cost 0.8 times the estimated cost and competitive with the once through PWR. At a price of 200\$/lb U_3O_8 , the allowable cost of the RTFB is 1.2 times the estimated cost to remain competitive with the once through PWR. It is noted that this analysis assumes no inflation and escalation.

It may also be seen from Fig. 5.7 that the total system electricity cost is relatively insensitive to the range of uranium costs from 0 to 200$/lb U_3O_8 . This is consistent with the data shown in Fig. 5.5 for a breeder fuel cycle length of 4 years. Additionally, it is noted that an increase in the RTFB capital cost of a factor of 2 increases the system electricity cost by a factor of 1.3 and shifts the breakeven U_3O_8 cost to beyond 200$/lb. Decreasing the RTFB capital cost by a factor of 2 reduces the system electricity cost by a factor of 0.85 and shifts the breakeven U_3O_8 cost to 25$/lb. Thus, the system electricity cost is significantly affected by changes in the RTFB capital cost.

This capital cost sensitivity evaluation may also be used to evaluated the effect of any required heating for start up, which would affect the capital cost, but have a small effect on the power balance if used only for start up.

5.5.3 RTFB Fuel Cycle Costs

Another area of uncertainty is the fuel cycle cost of the RTFB. Specifically, the costs related to the fabrication and reprocessing of the uranium multiplier are a significant fraction of the cost of electricity from the RTFB alone. Thus, the effect of both reducing and increasing the fabrication and reprocessing costs are investigated.

The variation of the RTFB fuel cycle costs is shown in Fig. 5.8. From Fig. 5.8, it may be seen that an increase in U_3O_8 cost from 0 to 200$/lb increases the system electricity cost by approximately the same amount (2.5 mills/kWhre or 5%) as doubling the RTFB fuel cycle costs (2 mills/kWhre). This doubling of the fuel cycle costs only includes the fabrication and back end costs of reprocessing, transportation and waste shipping and disposal. The cost of uranium metal in the multiplier varies with the cost of U_3O_8 .

5.5.4 Client Reactor Fuel Cycle Costs

The client reactor fuel cycle costs are also subject to uncertainty since no reprocessing industry currently exists. Additionally, no industry which fabricates fuel which has been reprocessed and recycled exists. Thus, the effect of variation of the client reactor fuel cycle costs as also studied.

For reference, the once-through and client reactor electricity cost components are shown in Table 5.6 for 50$/lb U_3O_8 and no inflation or escalation.

The effect of varying the client reactor fuel cycle costs on the total system electricity cost is shown in Fig. 5.9. The effect on the total system electricity cost of doubling the client reactor fuel cycle costs (an increase of 5.4 mills/kWhre or 10%) is approximately 2.3 times the effect of increasing the U_3O_8 cost from 0 to 200$/lb (an increase of 2.4 mills/kWhre). Doubling the client reactor fuel cycle costs also shifts the breakeven U_3O_8 cost, compared to the once through PWR, from 145$/lb U_3O_8 to in excess of 200$/lb U_3O_8 .

Decreasing the client reactor fuel costs by a factor of 2 results in a decrease in the system electricity cost of 2.8 mills/kWhre. This is approximately the same as the increase in system electricity cost as the cost of U_3O_8 is increased from 0 to 200$/lb. The decrease of a factor of 2 in the client reactor fuel cycle cost also results in a decrease of the break even U_3O_8 cost from 145$/lb to 105$/lb.

5.5.5 RTFB Breeding Performance

The RTFB blanket breeding performance affects the system electricity cost through the number of client reactors supported. The variation of the number of client reactors supported as the RTFB breeding performance is increased and decreased is shown in Fig. 5.10. From Fig. 5.10, it may be seen that decreasing the breeding performance below the reference level results in a large decrease in the total number of client reactors supported. This decrease in the total is due primarily to the smaller number of ^{233}U fueled client reactors. The rapid decrease in the number of ^{233}U fueled client reactors as the breeding performance is degraded is due to the requirement to maintain the tritium breeding at a fixed value of T=1.05. Thus, not only is the value of breeding of ^{233}U decreased due to the application of the factor of reduction, but the ^{233}U breeding is decreased further to maintain the tritium breeding at the specified value of 1.05.

A change of breeding performance from the reference configuration could take conceivably take two forms: An increase or decrease in breeding values with the blanket power remaining constant or an increase or decrease in breeding values accompanied by an increase or decrease in blanket power. Both effects on the total system electricity cost were examined.

The effect on system electricity cost of the varied breeding performance with constant blanket power is shown in Fig. 5.11. From Fig. 5.11, it may be seen that the penalty of reduced breeding is greater than the benefit of comparably increased breeding. For example, decreasing the reference breeding values by a factor of 0.8 increases the breakeven U_3O_8 cost from 145\$/lb to in excess of 200\$/lb. Increasing the reference breeding values by a factor of 1.2 decreases the breakeven U_3O_8 cost from 145\$/lb to 110\$/lb. Similarly, the corresponding effects on system electricity cost are an increase of 2.9 mills/kWhre and a

- decrease of 1.5 mills/kWhre at a U_3O_8 cost of 50$/lb.

This case is for the situation in which a change in breeding does not result in a change of the blanket power. Thus, this case could represent the operating condition discussed in Chapter 3 in which the blanket power remains constant and the fusion power is decreased as the concentration of ^{239}Pu in the blanket decreases. Note that the blanket power swing of an increase of 45% over 4 years of operation would represent an effective blanket coverage factor of 0.7 on Fig. 5.11. Thus, this mode of operation would result in a large increase in system electricity cost due to the reduced breeding and does not appear attractive.

Additionally, this case could represent if additional materials were placed in the blanket which affect breeding but have negligible effects in the neutron energy range above about 1 MeV, which is the energy range in which fast fission occurs. Most of the energy production in the RTFB blanket is due to the fast fission of ^{238}U at BOC and ^{238}U and ^{239}Pu at EOC. It is, however, considered likely that any perturbations that affect the breeding performance will also affect the blanket power. Hence, an additional examination was done in which the breeding performance and blanket power are both varied by the same factors.

The case in which the breeding and blanket power are varied by the same factors is shown in Fig. 5.12. From Fig. 5.11 and Fig. 5.12, it may be seen that the effect on the total system electricity cost is greater when the blanket power varies in addition to the breeding. From Fig. 5.12, the change in the U_3O_8 breakeven cost increases from 145$/lb to 200$/lb as the breeding and blanket power are decreased by a factor of 0.9 and decreases from 145$/lb to 90$/lb as the breeding and blanket thermal power are increased by a factor of 1.2. As in the case in which the breeding alone was varied, larger penalties are seen for lower values of breeding and blanket power than the benefits of correspondingly higher breeding and blanket thermal power.

Fig. 5.11 and Fig. 5.12 can be used to estimate the effect on total system electricity cost and the breakeven U_3O_8 cost of the effective blanket coverage factor. This factor is a combination of the effect on breeding and blanket thermal power of the various penetrations and discontinuities in the blanket. Note that the fraction of the first wall area occupied by penetrations is not the same as the effective blanket coverage factor since the neutrons may still enter the breeding region of the blanket after entering the penetration. Careful design of the blanket around the penetrations can minimize the loss of breeding and thermal power due to the penetrations. However, the determination of the effective blanket coverage factor depends upon a detailed blanket design, along with penetration location information, coupled with detailed three-dimensional neutronic calculations. This detailed evaluation was beyond the scope of the present study. However, the message that can be extracted from Fig. 5.11 and Fig. 5.12 is that the effective blanket coverage factor be allowed to decrease below 1.0 as little as possible. Note also that this statement depends upon the cost of achieving an effective blanket coverage factor, which also depends on a detailed design.

A neutronic evaluation was done in Chapter 3 for a case in which a shield was present and displaced a segment of the inboard side of the blanket and a case in which no shield was present. The shield is required to protect the insulation in the toroidal field coil such that the magnets last essentially the lifetime of the plant. However, the shield displaces a segment of the inboard molten salt and multiplier region, which reduces the breeding and blanket power. If an insulation material could be developed which would not require the shield to survive the life of the plant, the breeding and blanket power level could be increased. Another alternative could be replacement of the toroidal field coils when insulation damages reaches limits. An evaluation was therefore done to determine the effect on the total system electricity cost of removing the shield.

This evaluation is shown in Fig. 5.13. From Fig. 5.13, it is seen that the system electricity cost decreases by 1.5 mills/kWhre if the shield in the RTFB is replaced by blanket. The break even cost of U_3O_8 drops from 145 to 125$/lb. This shift is due to the decreased cost of capacity of the RTFB at the higher power level (a portion of the shield is replaced by the multiplier) and the increased breeding, which results in an increase in the number of client reactors from 9.2 to 10.6.

Note that use of this option would require use of an insulating material in the inboard leg of the toroidal field coil which could withstand higher radiation damage by a factor of 27 than the material assumed in this analysis. Alternatively, the inboard leg of the toroidal field coil would need to be replaced almost yearly.

Additionally, the use of a thicker multiplier region was investigated. The effect on the total system electricity cost of increasing the thickness of the multiplier region from the 11 cm. reference thickness to 16 cm. is shown in Fig. 5.14. From Fig. 5.14, it may be seen that a very small benefit may be gained at U_3O_8 prices less than 15$/lb, but beyond this cost, the lower electricity cost is given by the 11 cm. multiplier. This is due to the slight increase in breeding and power discussed in Chapter 3 (6% and 11%) and the higher cost of purchasing, fabricating and reprocessing the multiplier due to the increased volume.

5.5.6 Financial Parameters

An evaluation of a project such as the RTFB includes, in addition to the cost estimate, assumptions regarding the interest rates, inflation rates and escalation rates in excess of inflation. This section will examine the sensitivities of the system economic evaluation to these parameters.

The effect of inflation on the levelized total electricity cost from the system of the RTFB and its client reactors and the once through PWR is shown in Fig. 5.15. From Fig. 5.15, it may be seen that an increase in the rate of inflation has a much larger effect on the levelized electricity cost than an increase in the cost of U_3O_8 . As the inflation rate increases from 0% to 5% and 10%, the levelized system electricity cost increases by a factor of 1.7 and 2.5, respectively. This contrasts with an increase in electricity cost of a factor of 1.07, for 10% inflation, as the cost of U_3O_8 rises from 0$/lb to 200$/lb. Even for the once through PWR, the effect of inflation rate increases on levelized electricity costs from 0% to 5% and 10% are greater than the effect of increasing the cost of U_3O_8 from 0$/lb to 200$/lb.

It is also seen from Fig. 5.15 that increasing inflation rates do not cause the break even cost of U_3O_8 to shift from the no inflation cost of 150$/lb.

The average present value (APV) of the total system electricity cost is shown in Fig. 5.16. This figure of merit is shown because it is commonly used in fusion breeder economic analyses. Comparing Fig. 5.15 and 5.16, it is seen that the APV electricity costs are lower than the levelized electricity costs with no inflation by a factor of 1.8 for the system and the once through PWR. The relative effects of inflation and U_3O_8 cost are also reversed between Fig. 5.15 and 5.16; for Fig. 5.15, increasing inflation is a more important effect while for Fig. 5.16, increasing uranium cost is a more important effect. This apparent change of the relative importance of these two parameters, inflation and U_3O_8 cost, of has implications for identifying the relative importance of other parameters using the APV electricity cost as a figure of merit. It is noted that the APV electricity cost still gives a breakeven cost of U_3O_8 of 150$/lb, the same as the levelized electricity cost.

Escalation of U_3O_8 prices is next investigated. The escalation rate is

the rate at which U_3O_8 prices increase in excess of inflation. For the initial discussion, inflation is assumed to be zero.

The levelized cost of electricity for U_3O_8 escalation rates of 0%, 5% and 10% and U_3O_8 prices from 0 to 200 \$/lb is shown in Fig. 5.17. From Fig. 5.17, it is seen that the system electricity cost is relatively insensitive to the escalation rate, with a maximum effect of an increase of a factor of 1.15 as escalation changes from 0% to 10% at a U_3O_8 price of 200\$/lb. This contrasts to the once through PWR, for the same increase in escalation and at the same U_3O_8 price, where an increase of a factor of 1.9 is seen. Additionally, the break even cost of U_3O_8 is seen to shift to lower values as the escalation rate increases. The break even cost shifts from 150 \$/lb for an escalation rate of 0% to 75\$/lb for an escalation rate of 5% to 35 \$/lb for an escalation rate of 10%. This occurs because the RTFB-client reactor system electricity cost is relatively insensitive to the cost of uranium, while the once through PWR is much more sensitive to the cost of uranium, particularly when the cost of U_3O_8 is assumed to escalate.

The variation of the APV electricity cost with the escalation rate and U_3O_8 price is shown in Fig. 5.18. Qualitatively, the behavior of the APV is similar to the levelized electricity cost, but the magnitude of the APV electricity cost is lower than the levelized electricity cost by a factor of approximately 1.8.

5.5.7 Summary of Sensitivity Analyses

Several factors related to the system electricity cost were evaluated in this section. This subsection summarizes the sensitivity of the system electricity cost to these parameters.

The breeder fuel cycle length has a large effect on the system electricity cost since lengthening the fuel cycle reduces the cost per kWhre of the fuel cycle costs by distributing the fixed cost of fabricating and reprocessing the multiplier over a longer period of time. The system cost of electricity decreases by a factor of 1.3 as the RTFB fuel cycle is lengthened from 1 year to 4 years.

The RTFB capital cost also has a large effect on the cost of electricity from the system. Increasing the RTFB capital cost by a factor of 2 increases the system electricity cost by a factor of 1.3 and shifts the breakeven U_3O_8 cost beyond 200$/lb. Decreasing the capital cost by a factor of 2 decreases the system electricity cost by a factor 0.85 and shifts the breakeven U_3O_8 cost to 25$/lb.

Increasing the client reactor fuel cycle cost by a factor of 2 results in an increase in the system electricity cost a factor of 2.3 greater than the increase in system electricity cost as the cost of U_3O_8 increases from 0 to 200$/lb. The effect of decreasing the client reactor fuel cycle costs by a factor of 2 is approximately the same change as increasing the U_3O_8 cost from 0 to 200$/lb.

The effective blanket coverage factor also has a large effect on the system electricity cost, particularly for values less than 1. The break even cost of U_3O_8 shifts from 145 to 200$/lb as the effective blanket coverage factor decreases from 1.0 to 0.9.

If an insulating material is developed which would allow deletion of the inboard shield, the power and breeding of the RTFB could be increased. This increase would result in a decrease of the break even cost of U_3O_8 from 145 to 125 $/lb.

Including the effect of inflation in the analysis results in an increased sys-

tem electricity cost as the rate of inflation is increased. The break even cost of U_3O_8 does not shift with inflation. The APV electricity cost indicates that an increase in uranium cost causes a larger increase in system electricity cost than an increase in inflation. The levelized system electricity cost indicates that, for the same range of inflation and U_3O_8 costs, an increase in inflation gives a larger increase in system electricity cost than an increase in U_3O_8 cost. This is also true for the once through PWR electricity cost.

Adding the effect of escalation of U_3O_8 prices results in a decrease in the breakeven cost of U_3O_8 primarily due to the increase of the electricity cost from the once through PWR. The RTFB system is relatively insensitive to the cost of U_3O_8 . The APV system electricity cost behaves similarly to the levelized cost when escalation is included.

5.6 Comparison to Other Fusion Breeders

This section compares the RTFB to two other fusion breeders which have been previously evaluated by other groups. These two fusion breeders, one a tokamak [5.4] and the other a tandem mirror [5.2], are based on fission suppressed blankets and use of superconducting magnets.

In order to evaluate these two machines on the same basis as the RTFB, the COST code was modified to permit direct input of the appropriate data, such as capital cost and net electric power, to the system economic evaluation portion of the code. This subset of the COST code was called MINIC (for Mini COST).

The information for the two superconducting fusion breeders is summarized in Table 5.7. The direct cost was taken from the reference and the same

factors for indirect cost and interest during construction were applied that were used for the RTFB. It is noted that the superconducting fusion breeders have the fuel cycle facilities included in the capital cost shown. Thus, the fuel cycle components in the system evaluation using MINIC are zero.

The comparison between the RTFB, the Fission Suppressed Superconducting Tokamak (FSST) and the Fission Suppressed Superconducting Mirror (FSSM) is shown in Fig. 5.19 through Fig. 5.26. The levelized and APV cost of electricity with no inflation and escalation are shown in Fig. 5.19 and Fig. 5.20. It may be seen that the cost of electricity from the FSST and FSSM systems is not sensitive to the cost of U_3O_8 , since the thorium used is recycled within the system. The small cost of make up fertile material is not considered. The break even costs for the RTFB, FSST and FSSM are 150, 160 and 175 \$/lb U_3O_8 . It is noted that the cost of electricity from the RTFB system is lower than the FSST or FSSM systems over the range of U_3O_8 costs of 0 to 200 \$/lb.

Next, the effect of inflation is considered. The levelized and APV electricity costs for the RTFB, FSST and FSSM are shown in Fig. 21 and Fig. 22 for no escalation and an inflation rate of 5%. The RTFB is seen to have a higher cost relative to the FSST and FSSM than in the case with no inflation. This occurs because the RTFB fuel cycle costs become more important relative to capital costs in the inflated analysis. Since the FSST and FSSM fuel cycle costs are included in the capital costs, this does not affect the two superconducting machines. However, it is seen that the RTFB has a lower system electricity cost than the FSST over a range of U_3O_8 cost from 0 to 135\$/lb and a lower system electricity cost than the FSSM over the range of U_3O_8 cost of 0 to 200 \$/lb. The break even U_3O_8 prices for this analysis for the RTFB, the FSST and the FSSM are 145, 145 and 160 \$/lb. Thus, the RTFB and the FSST are equivalent. The APV cost of electricity gives a slightly lower break even cost than the levelized cost for the FSSM of 155 \$/lb U_3O_8 .

Escalation of U_3O_8 prices will now be considered. The levelized system electricity cost and the APV system electricity cost are shown in Fig. 5.23 and Fig. 5.24 for no inflation and a U_3O_8 escalation rate of 5%. As expected, the break even cost for U_3O_8 shifts to substantially lower costs than the cases with no escalation. The break even cost of U_3O_8 for the RTFB, the FSST and the FSSM is 75, 85, and 90 \$/lb. Note also that the dependence of the RTFB fuel cycle cost on U_3O_8 cost results in the RTFB system electricity cost exceeding the FSST above 125\$/lb and the FSSM above 175\$/lb. It should also be noted, however, that the break even cost with the once through PWR is lowest for the RTFB, which would indicate a preference for the RTFB.

The levelized and APV system electricity costs are shown in Fig. 5.25 and Fig. 5.26 for an inflation rate of 5% and a U_3O_8 escalation rate of 2%. This case is shown to compare to the inflation and escalation rates considered in the evaluation of the FSST and the FSSM. It may be seen that the U_3O_8 break even cost is 115\$/lb for the RTFB and the FSST and 125\$/lb for the FSSM. This may be compared to the break even cost for the FSST evaluation of 41\$/lb U_3O_8 in 1983\$. Using the values from the FSST evaluation to adjust this value to 1990\$ (return on investment=9.1%, inflation=5% and escalation=2%) the break even cost of U_3O_8 is 117\$/lb, which is essentially equal to the break even cost for the analysis method used in the present work.

Thus, the RTFB is essentially equivalent in performance to the FSST and marginally better than the FSSM, based on the break even cost of U_3O_8 compared to the once through PWR. It is also noted that the RTFB performance could be improved somewhat by allowing recycle of the uranium in the multiplier. The effect would be to eliminate the RTFB system electricity cost dependence on U_3O_8 price at the penalty of an increased cost of fabricating the multiplier from recycled uranium. The increased cost of fabricating recycled uranium was not estimated, due to the uncertainties. An indication of the effect

of increased fabrication cost and recycling the uranium can be seen from the earlier sensitivity analysis of increased RTFB fuel cycle costs for 0$/lb U_3O_8 .

An additional figure of merit used in the FSST and FSSM evaluation is the net system benefit. The net system benefit is defined as the integrated present value of the year-by-year difference between the value of electricity from the client reactors and the value of electricity from an equal number of once through PWRs. This figure of merit is shown in Fig. 5.27 through Fig. 5.30 for the cases of no inflation or escalation, 0.05 inflation and no escalation, no inflation and 0.05 escalation and 0.05 inflation and 0.02 escalation, the same cases as considered previously. The net system benefit is seen to give the same breakeven costs, for the corresponding cases, as the average present value of the total system electricity cost.

It should be noted that the mode of operation of the FSST and the FSSM could also be adopted to the RTFB. Both the FSST and the FSSM include in the capital cost a fabrication facility and a reprocessing facility for the thorium metal used in the blanket. The thorium in the blanket is recycled and refabricated after processing to remove the bred fissile material. The capital cost of this additional facility is $330M. which includes beryllium fabrication. The discharge enrichment (0.0143) and the average fissile production (4905 kg/yr) give a required Th processing rate of 343 MT/yr. For the carrying charges (15%/yr) used in the FSST study, this gives a cost of fabricating and reprocessing the Th of 144$/kg. The cost of remanufacturing the Be is also included. This should be compared with the total fabrication, reprocessing and waste disposal (including transportation) cost of 400$/kg used for the RTFB.

Additionally, it is noted that the RTFB fuel form (plates clad in steel) is more conventional than the fuel form in the FSST and FSSM (Th snap rings around Be pebbles).

If the RTFB is operated in a mode in which the fuel cycle facilities are included in the capital cost, similar to the FSST and the FSSM, the total system electricity cost would decrease. This can be evaluated by increasing the RTFB capital cost by a factor of 1.038 and setting fuel cycle costs to zero. The factor of 1.038 applied to the capital cost adds \$114M to the capital cost for fuel cycle facilities. The \$114M is based on the FSST fuel cycle facility costs and the relative throughput of the RTFB and the FSST (86 MT/yr for the RTFB and 343 MT/yr for the FSST). Although the capital cost increases, the total system electricity cost decreases due to the elimination of the fuel cycle charges. Thus, the reference RTFB levelized system electricity cost for inflation of 5% and U_3O_8 escalation of 2% decreases from 88.1 mills/kWhre to 84.7 mills/kWhre. The breakeven cost of U_3O_8 decreases from 115\$/lb to 80\$/lb, as seen from Fig. 5.25.

5.7 Summary

This chapter presents the system economic analysis for the RTFB and its associated system of client reactors. The basis for comparison is the PWR on the once through uranium fuel cycle. The client reactor system is composed of PWRs identical to the once through PWR, but operating on the ^{239}Pu and ^{233}U fuel cycles with recycle.

A system economic evaluation methodology is developed which allows for the time value of money in adjusting the cost of the various fuel cycle transactions to a common point in time, the time of fuel load. General inflation and escalation of U_3O_8 prices are allowed. The cost of the bred fuel within the system is determined and carrying charges are paid on the value of the fissile fuel within the RTFB-client reactor system. Levelized values are calculated. Additionally, for comparison to other fusion breeders, the average present value (APV) and

net system benefit are calculated. The average present value is defined as the average of the year-by-year costs, discounted to the beginning of operation. The net system benefit is defined as the integrated present value of the year-by-year differences in cost of the number of client reactors selling electricity at the total system electricity cost and the same number of once through PWRs selling electricity at the cost determined by the U_3O_8 cost. The breakeven U_3O_8 cost is the cost of U_3O_8 at which the cost of electricity from the once through PWR and the RTFB-client reactor system is equal.

The fuel cycle length of the RTFB was determined to be 4 years. This is the length of time that the multiplier remains in place before removal for reprocessing. The system cost of electricity decreases by a factor of 1.3 as the RTFB fuel cycle length increases from 1 year to 4 years. The concentration of ^{239}Pu after a 4 year exposure is 0.02 a/o, which is the limit imposed in Chapter 3 from criticality considerations.

An increase of a factor of 2 in the RTFB capital cost increases the system electricity cost by a factor of 1.3 and shifts the breakeven U_3O_8 cost to beyond 200$/lb. Also, a decrease in the RTFB capital cost by a factor of 2 results in a decrease in the system electricity cost of a factor of 0.85 and shifts the breakeven U_3O_8 cost to 25$/lb.

The fuel cycle costs of the RTFB are also varied. It is shown that an increase of a factor of 2 in the RTFB fuel cycle costs increases the system electricity cost by 2 mills/kWhre (5%), which is similar to the effect of increasing the cost of U_3O_8 from 0 to 200$/lb. The breakeven U_3O_8 cost is 145$/lb for the reference case.

The fuel cycle costs of the client reactors are shown to have a larger effect on the system electricity cost. Increasing the client reactor fuel cycle costs by a

factor of 2 increases the system electricity cost by 5.4 mills/kWhre (10%). The breakeven cost of U_3O_8 is seen to shift to beyond 200$/lb.

The effect of the breeding performance of the RTFB is also evaluated. The penalty of decreased breeding is shown to be greater than the benefit of increased breeding. Decreasing the breeding by a factor of 0.8 shifts the breakeven U_3O_8 cost from 145$/lb to beyond 200$/lb. Increasing the breeding by a factor of 1.2 shifts the breakeven cost of U_3O_8 from 145$/lb to 110$/lb. These values are for the case in which the breeding changes, but the blanket power remains constant. If the blanket power and breeding are decreased by a factor of 0.9, the breakeven U_3O_8 cost shifts from 145$/lb to 200$/lb. An increase in the breeding and blanket power of a factor of 1.2 shifts the breakeven U_3O_8 cost from 145$/lb to 90$/lb.

The effect of removing the shield required in the RTFB is to shift the breakeven U_3O_8 cost from 145$/lb to 125$/lb. This is due to the increased blanket power and breeding resulting from replacing the shield with multiplier and molten salt. Note that this option would require development of an insulating material which will withstand a radiation dose of 27 times allowable with currently available materials.

Increasing the thickness of the multiplier region from 11 cm. to 16 cm. is seen to result in higher system electricity costs for U_3O_8 costs in excess of 15$/lb due to the higher costs associated with the multiplier.

The effect of financial parameters on the total system electricity cost is also evaluated. Inflation increases the cost of electricity, but does not shift the breakeven U_3O_8 cost. Escalation of U_3O_8 costs also increases the cost of electricity, but has less of an effect than the same inflation rate. However, escalation also shifts the breakeven cost of electricity.

It is also noted that the average present value cost of electricity, a figure of merit commonly used in fusion breeder studies, gives a similar result when escalation alone is considered. However, when inflation alone is considered, the APV cost shows increasing U_3O_8 cost to be more important than inflation while the levelized electricity cost shows inflation to be more important than U_3O_8 cost.

The RTFB is also compared to the FSST and FSSM, a superconducting tokamak and a superconducting tandem mirror fusion breeder using fission-suppressed blankets. The RTFB is shown to give a lower breakeven cost of U_3O_8 (150\$/lb) than the FSST(160\$/lb) and FSSM (175\$/lb) for analyses with no inflation and escalation. When inflation of 5% is considered, the RTFB and the FSST have the same breakeven cost of U_3O_8 (145\$/lb), with the FSSM higher (160\$/lb). Inflation affects the RTFB more than the FSST and the FSSM since the two superconducting machines incorporate the fuel cycle costs into the capital cost.

For 5% escalation of U_3O_8 cost, the breakeven cost for the RTFB (75\$/lb) is also lower than for the FSST (85\$/lb) and the FSSM (90\$/lb). The RTFB system electricity cost is more sensitive to U_3O_8 escalation since the fuel cycle costs depend on the U_3O_8 cost.

For the conditions considered in the FSSM and FSST analysis of 5% inflation and 2% escalation of U_3O_8 prices, the RTFB is essentially equivalent to the FSST and marginally better than the FSSM. The breakeven prices of U_3O_8 for the RTFB, FSST and FSSM are 115, 115 and 125\$/lb for these financial parameters. It is noted that the RTFB cost of electricity could be reduced by assuming the same front end and back end costs as the FSST and FSSM, namely 144\$/kg vs. 400\$/kg for the RTFB. Note that the FSST and FSSM front end cost is for fabricating recycled Th and the RTFB front end cost is for fabricat-

ing unrecycled uranium. Additionally, the RTFB fuel form (plates) is of a more conventional type than the FSSM and FSST (Th snap rings around Be pebbles).

If the RTFB is operated in a mode in which the fuel cycle facilities are included in the capital cost, similar to the FSST and the FSSM, the total system electricity cost would decrease. This can be evaluated by increasing the RTFB capital cost by a factor of 1.038 and setting fuel cycle costs to zero. The factor of 1.038 applied to the capital cost adds \$114M to the capital cost for fuel cycle facilities. The \$114M is based on the FSST fuel cycle facility costs and the relative throughput of the RTFB and the FSST (86 MT/yr for the RTFB and 343 MT/yr for the FSST). Although the capital cost increases, the total system electricity cost decreases due to the elimination of the fuel cycle charges. Thus, the reference RTFB levelized system electricity cost for inflation of 5% and U_3O_8 escalation of 2% decreases from 88.1 mills/kWhre to 84.7 mills/kWhre. The breakeven cost of U_3O_8 decreases from 115\$/lb to 80\$/lb, as seen from Fig. 5.25.

References

[5.1] U.S. Department of Energy, "Nuclear Proliferation and Civilian Nuclear Power: Report of the Nonproliferation Alternative System Assessment Program." DOE-NE-0001, (June 1980).

[5.2] Berwald, D.H., et al.,"Fission-Suppressed Hybrid Reactor - The Fusion Breeder," Lawrence Livermore National Laboratory Report UCID-19638, (December 1982).

[5.3] Waltar, A.E. and Reynolds, A.B., *Fast Breeder Reactors*, Pergamon Press, (1981).

[5.4] Moir, R. W., et al., "Feasibility Study of a Fission-Suppressed Tokamak Fusion Breeder," Lawrence Livermore National Laboratory Report UCID-20154, (December 1984).

TABLE 5.1

Once-Through and Client PWR Fuel Cycle Information

	Once Through	^{233}U Based	^{239}Pu Based
Power (MWe)	1300	1300	1300
Capacity Factor	0.75	0.75	0.75
Fuel Cycle			
Length (yr)	3	3	3
Lead Time (yr)	1	1	1
Lag Time (yr)	1	1	1
Feed (kg/yr)	35096	31920	35075
Discharge (kg/yr)	33200	30195	33180
Make-Up (kg/yr/MWe)	-	0.316	0.395
Separative Work (kg SWU/yr)	153000	-	-
U_3O_8 Purchased (ST/yr)	254	-	-

TABLE 5.2

Once-Through and Client PWR Costs in 1978, 1984 and 1990 Dollars

	Once Through	^{233}U Based	^{239}Pu Based
Costs in 1978$			
Capital ($/kWe)	800	800	800
Operating and Maintenance			
Fixed ($/yr/kWe)	13	13	13
Variable ($/yr/kWe)	1	1	1
Fuel Cycle			
Enrichment Cost ($/kg SWU)	100	-	-
Fabrication Cost ($/kg)	110	570	370
Back End Cost ($/kg)	135	490	450
Costs in 1984$			
Capital ($/kWe)	1245	1245	1245
Operating and Maintenance			
Fixed ($/yr/kWe)	19.02	19.02	19.02
Variable ($/yr/kWe)	1.46	1.46	1.46
Fuel Cycle			
Enrichment Cost ($/kg SWU)	146	-	-
Fabrication Cost ($/kg)	161	834	541
Back End Cost ($/kg)	197	717	658
Costs in 1990$			
Capital ($/kWe)	1624	1624	1624
Operating and Maintenance			
Fixed ($/yr/kWe)	24.80	24.80	24.80
Variable ($/yr/kWe)	1.91	1.91	1.91
Fuel Cycle			
Enrichment Cost ($/kg SWU)	191	-	-
Fabrication Cost ($/kg)	210	1087	706
Back End Cost ($/kg)	258	935	859

TABLE 5.3

RTFB Fuel Cycle Cost Information

Costs in 1978$	
Fabrication Cost ($/kg)	140
Shipping and Waste Disposal Cost ($/kg)	90
Costs in 1982$	
Reprocessing Cost ($/kg)	60
Costs in 1984$	
Fabrication Cost ($/kg)	204
Reprocessing Cost ($/kg)	65
Shipping and Waste Disposal Cost ($/kg)	131
Back End Cost ($/kg)	196
Costs in 1990$	
Fabrication Cost ($/kg)	267
Back End Cost ($/kg)	256

TABLE 5.4

RTFB Performance

Total Direct Cost (1984M$)	2170
Total Capital Cost (1984M$)	3010
Average Gross Electric Power (MWe)	1760
Average Net Electric Power (MWe)	1250
^{233}U Production (kg/yr)	2056
^{239}Pu Production (kg/yr)	1734
Availability	0.75

TABLE 5.5

Financial Information for System Economic Analysis

Fixed Charges	0.05
Fraction Bonds	0.55
Fraction Equity	0.45
Bond Interest	0.025
Equity Interest	0.07
Tax Rate	0.50
Plant Life	30 yr

TABLE 5.6

Once-Through and Client PWR Electricity Costs 50 $/lb U_3O_8. No Inflation and Escalation

	Once Through	^{233}U Based	^{239}Pu Based
Costs in 1990$ (mills/kWhre)			
Capital Costs			
Capital Cost	15.2	15.2	15.2
Fixed Costs	12.4	12.4	12.4
Taxes	4.5	4.5	4.5
Total Capital Cost	32.1	32.1	32.1
Operating and Maintenance	4.0	4.0	4.0
Fuel Cycle Costs			
Front End			
Fuel	3.6	1.0	1.8
Enrichment	4.1	–	–
Fabrication	1.0	4.9	3.5
Total Front End	8.7	5.9	5.3
Back End			
Spent Fuel Disposal	1.0	–	–
Reprocessing	–	3.2	3.2
Total Back End	1.0	3.2	3.2
Fuel Cycle Taxes	1.1	0.8	1.4
Total Fuel Cycle	10.7	10.7	10.7
Total Electricity Cost	46.8	46.8	46.8

TABLE 5.7

Superconducting Fission-Suppressed Tokamak and Tandem Mirror Fusion Breeder Input to MINIC

	Tokamak	Tandem Mirror
Total Direct Cost (1984M$)	3610	4590
Total Capital Cost (1984M$)	5010	6380
Gross Electric Power (MWe)	1667	2226
Net Electric Power (MWe)	1385	1720
Net ^{233}U Production (kg/yr)	5255	6038
Availability	0.75	0.75

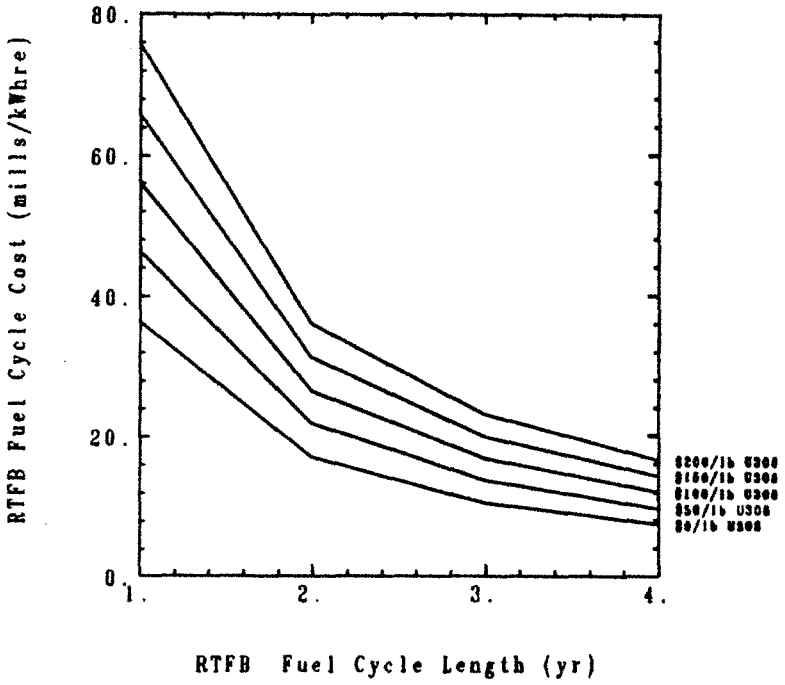

Figure 5.1 RTFB Fuel Cycle Costs for Fuel Cycle Length and U_3O_8 Cost

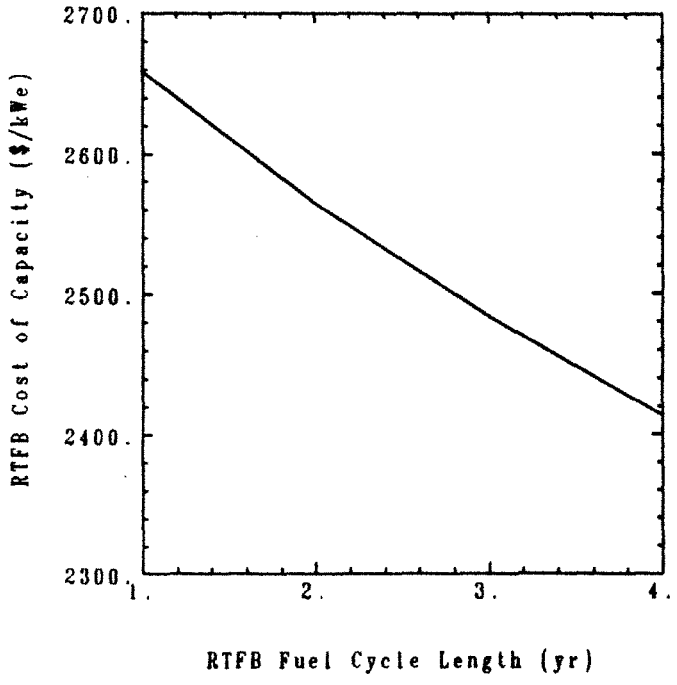

Figure 5.2 RTFB Cost of Capacity for Fuel Cycle Length

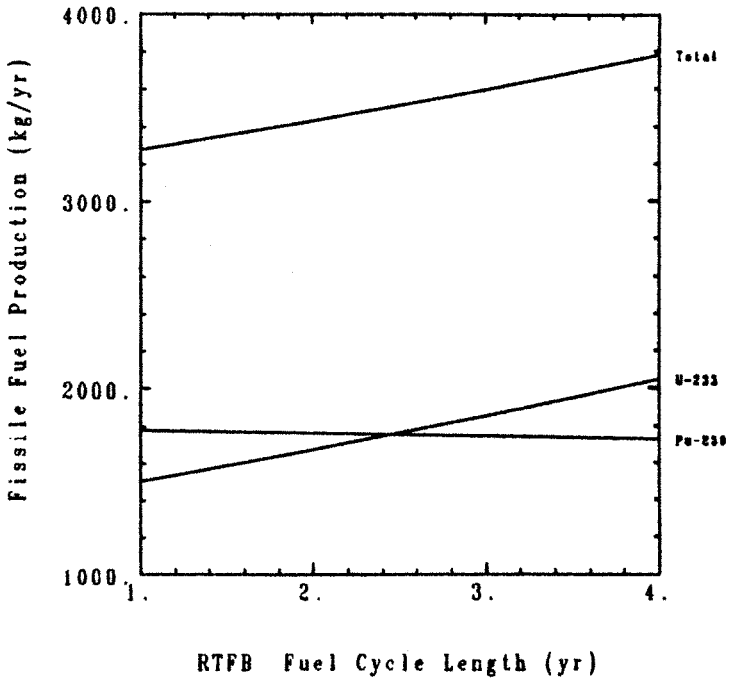

Figure 5.3 RTFB Fissile Fuel Production for Fuel Cycle Length

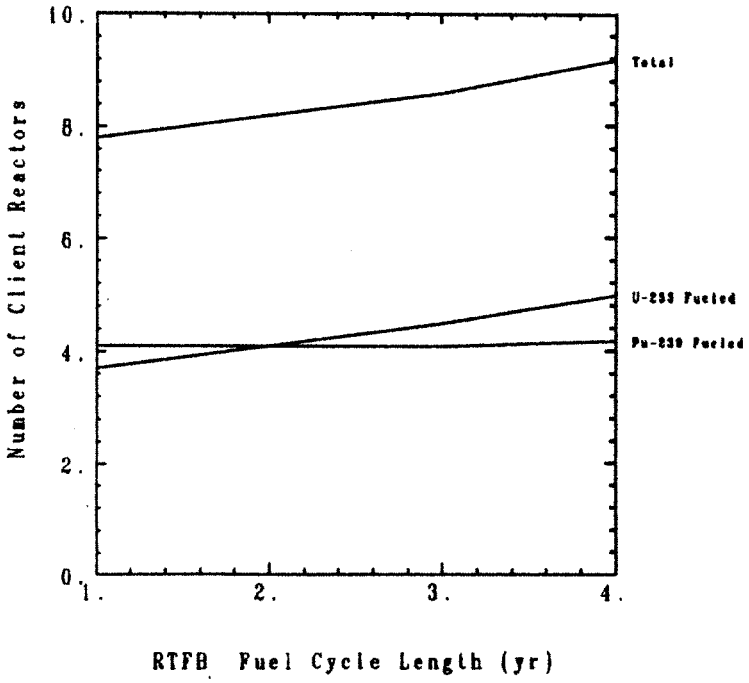

Figure 5.4 Number of Client Reactors Supported for RTFB Fuel Cycle Length

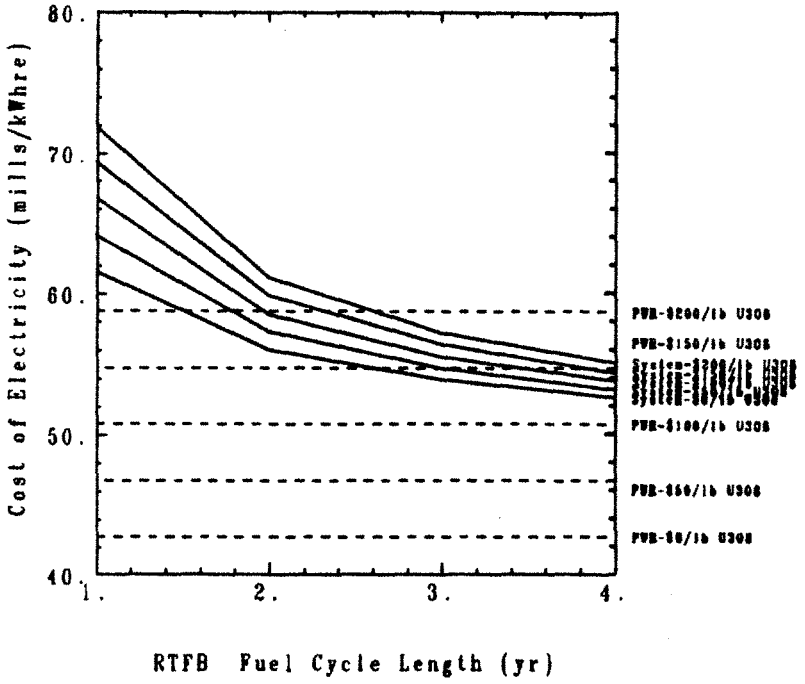

Figure 5.5 Total System Electricity Cost for Fuel Cycle Length and U_3O_8 Cost

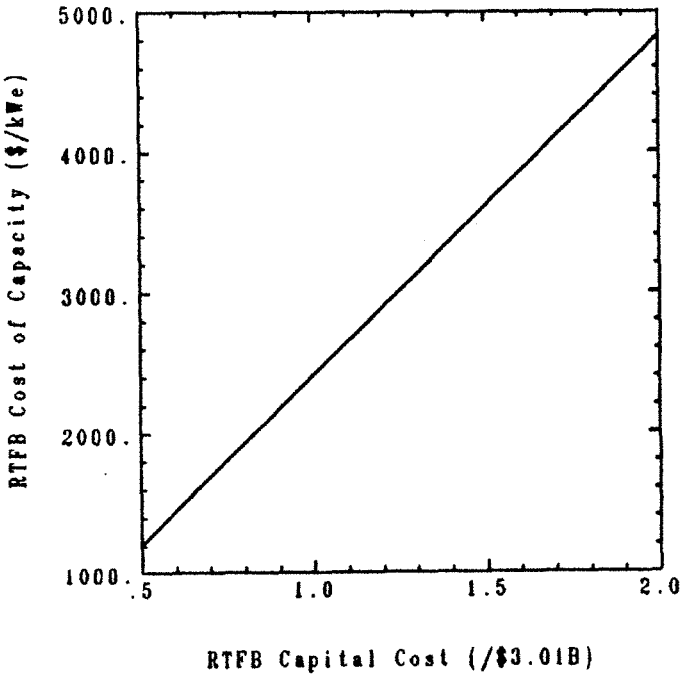

Figure 5.6 RTFB Cost of Capacity for Capital Cost

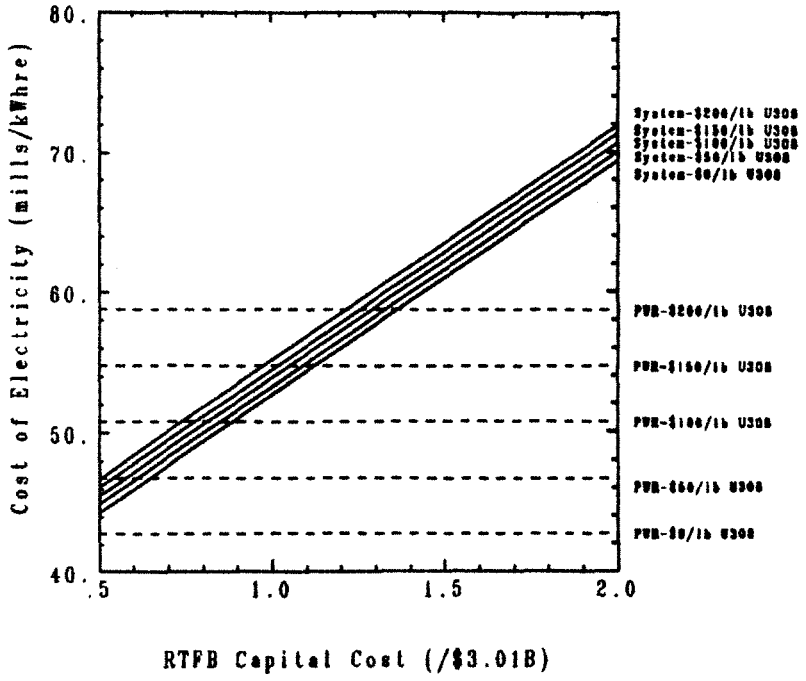

Figure 5.7 Total System Electricity Cost for RTFB Capital Cost and U_3O_8 Cost

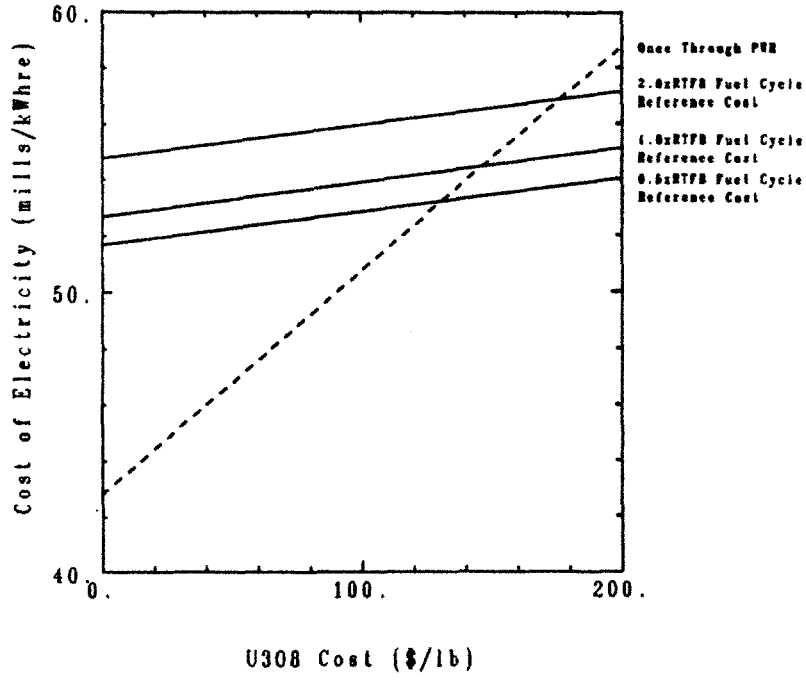

Figure 5.8 Total System Electricity Cost for RTFB Fuel Cycle Cost and U_3O_8 Cost

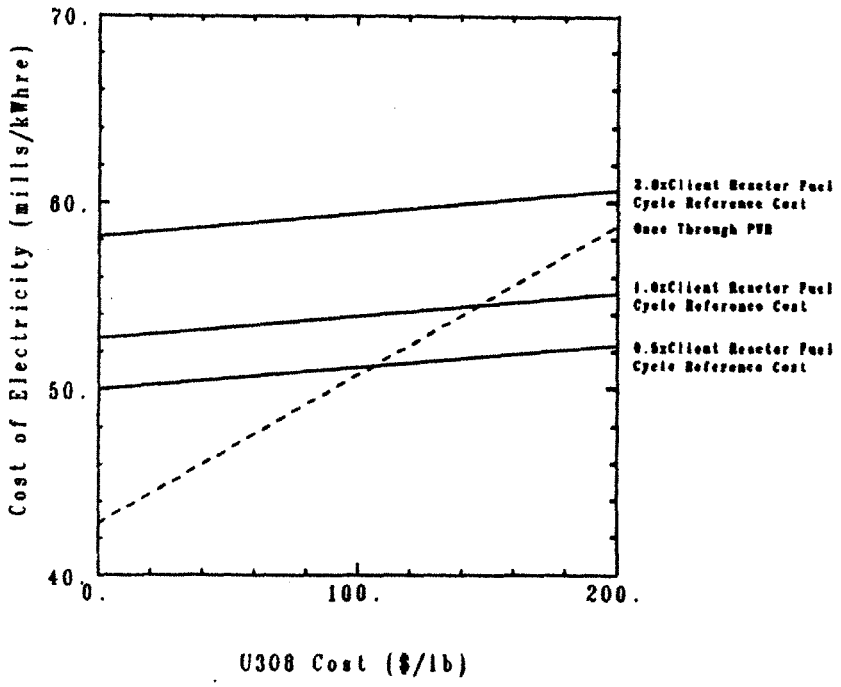

Figure 5.9 Total System Electricity Cost for Client Reactor Fuel Cycle Cost and U_3O_8 Cost

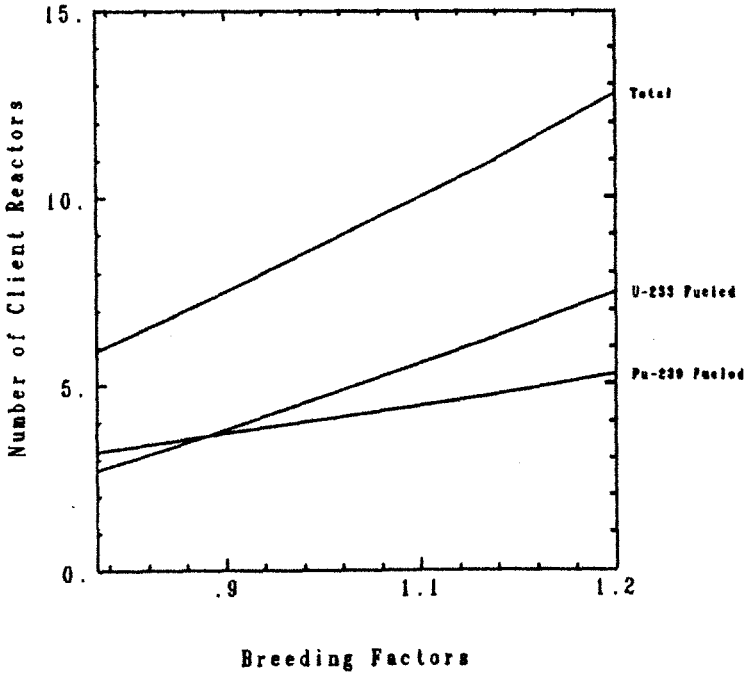

Figure 5.10 Number of Client Reactors Supported for RTFB Breeding

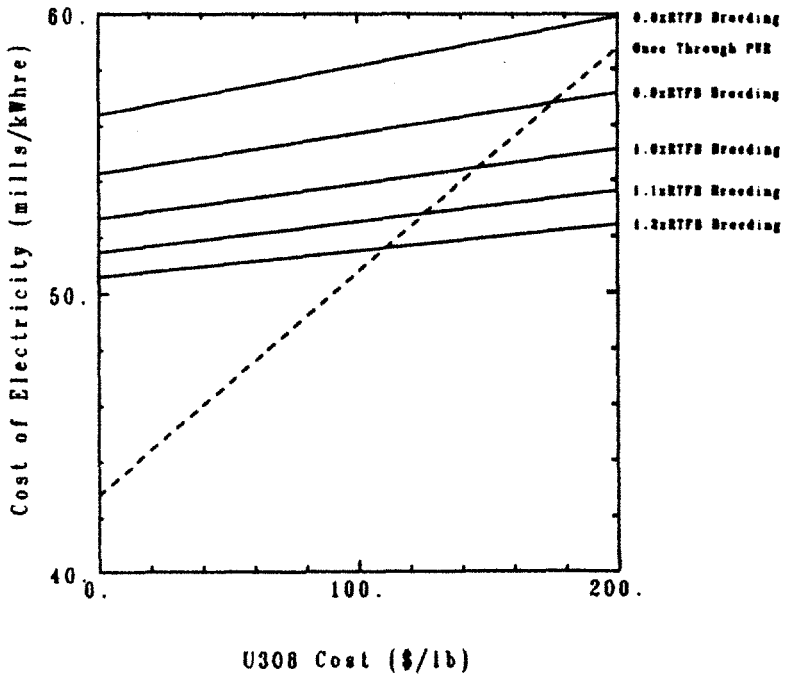

Figure 5.11 Total System Electricity Cost for RTFB Breeding and U_3O_8 Cost – Constant Blanket Power

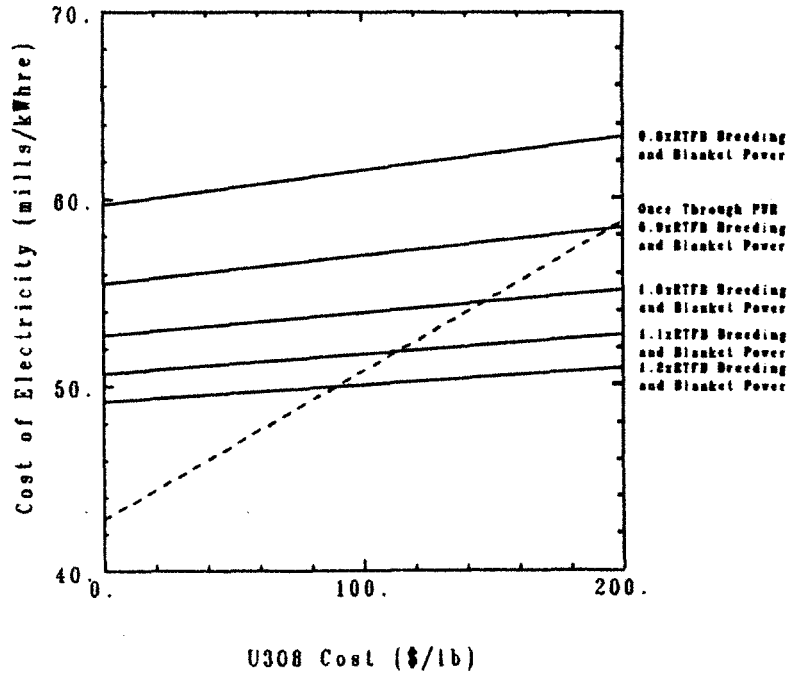

Figure 5.12 Total System Electricity Cost for RTFB Breeding and U_3O_8 Cost – Variable Blanket Power

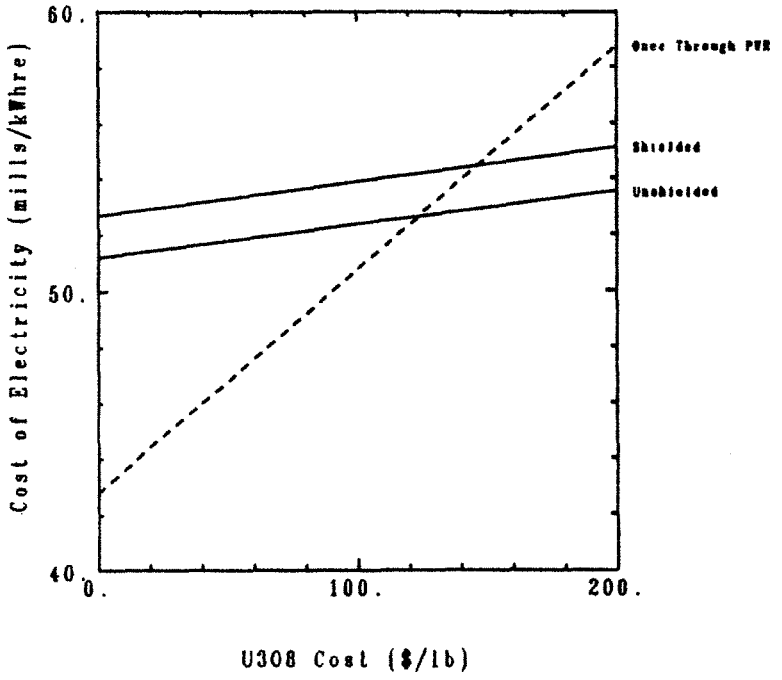

Figure 5.13 Total System Electricity Cost for RTFB With and Without Shielding for U_3O_8 Cost

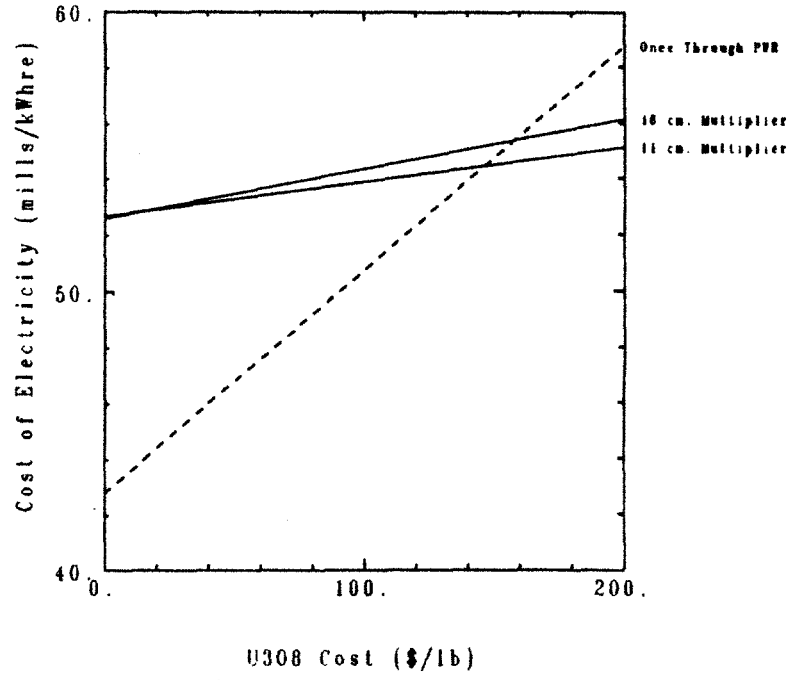

Figure 5.14 Total System Electricity Cost for RTFB With 11 cm and 16 cm Multiplier

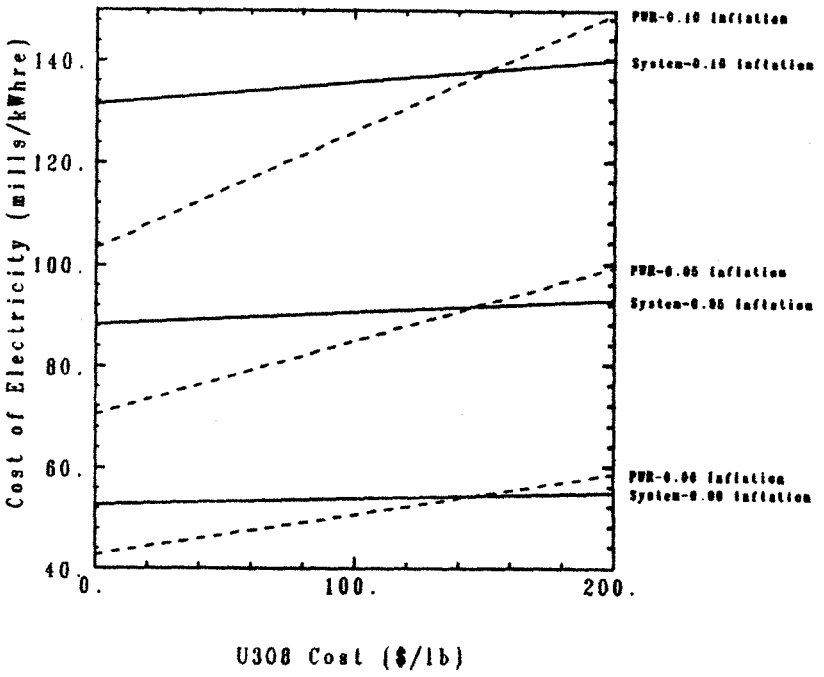

Figure 5.15 Levelized Total System Electricity Cost With Inflation

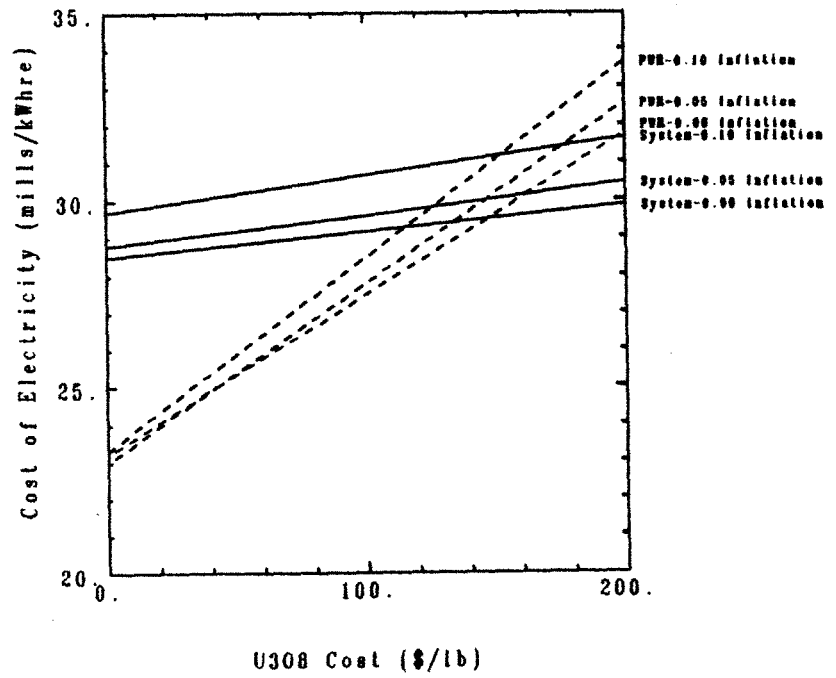

Figure 5.16 Average Present Value Total System Electricity Cost With Inflation

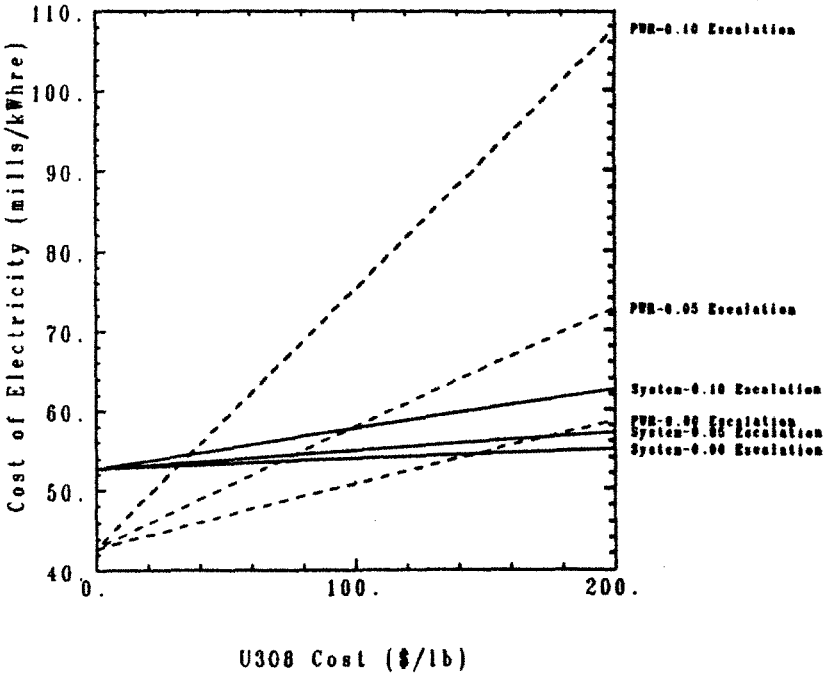

Figure 5.17 Levelized Total System Electricity Cost With U_3O_8 Escalation

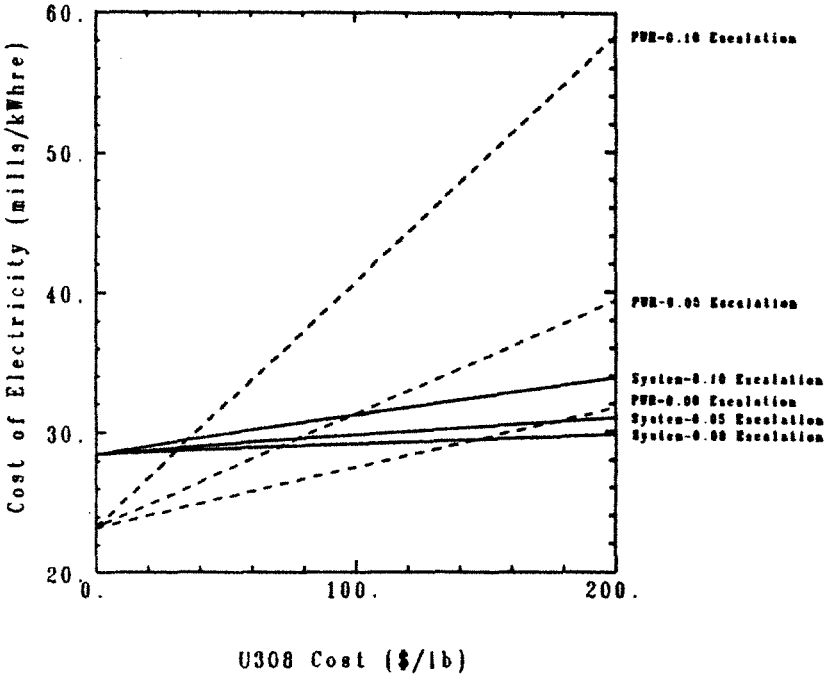

Figure 5.18 Average Present Value Total System Electricity Cost With U_3O_8 Escalation

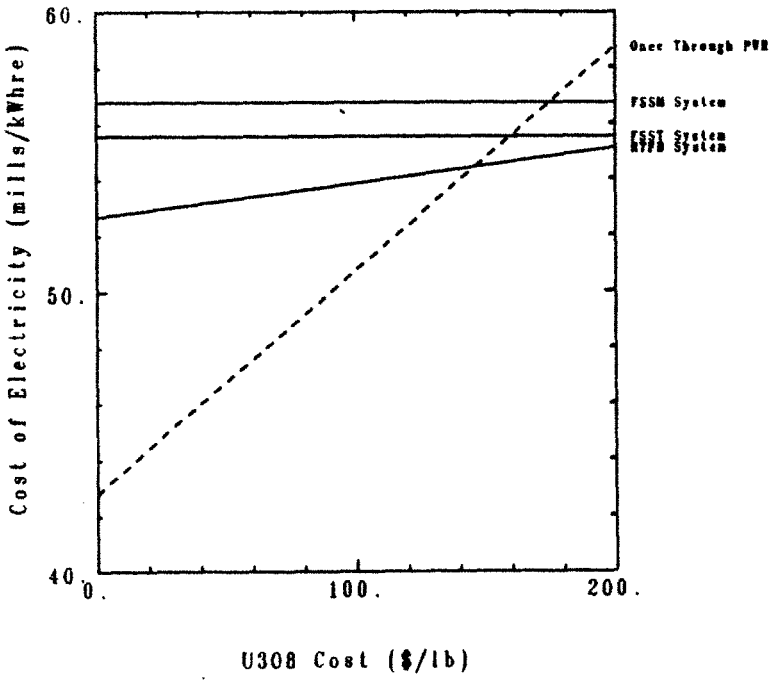

Figure 5.19 Comparison of Levelized Total System Electricity Cost RTFB, FSST and FSSM – No Inflation or U_3O_8 Escalation

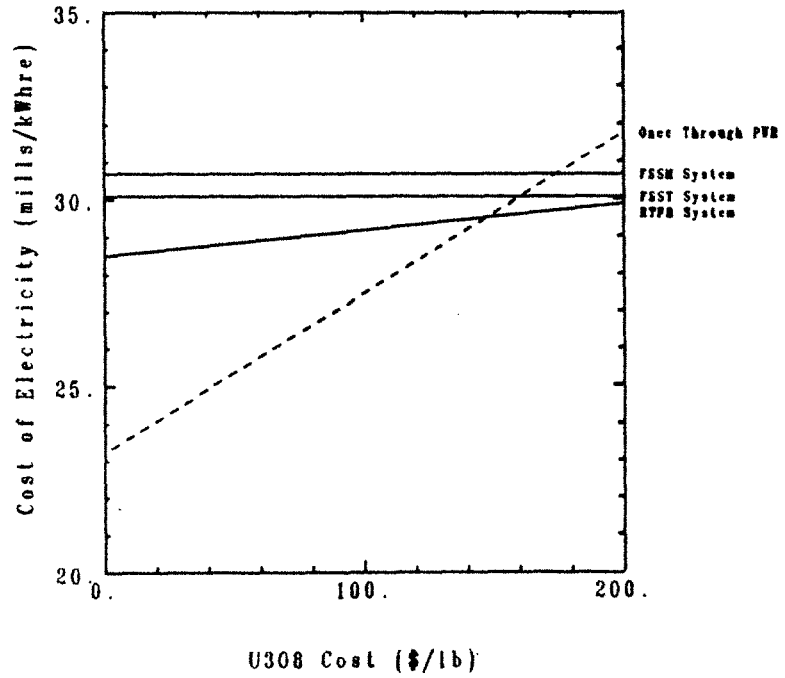

Figure 5.20 Comparison of Average Present Value Total System Electricity Cost RTFB, FSST and FSSM – No Inflation or U_3O_8 Escalation

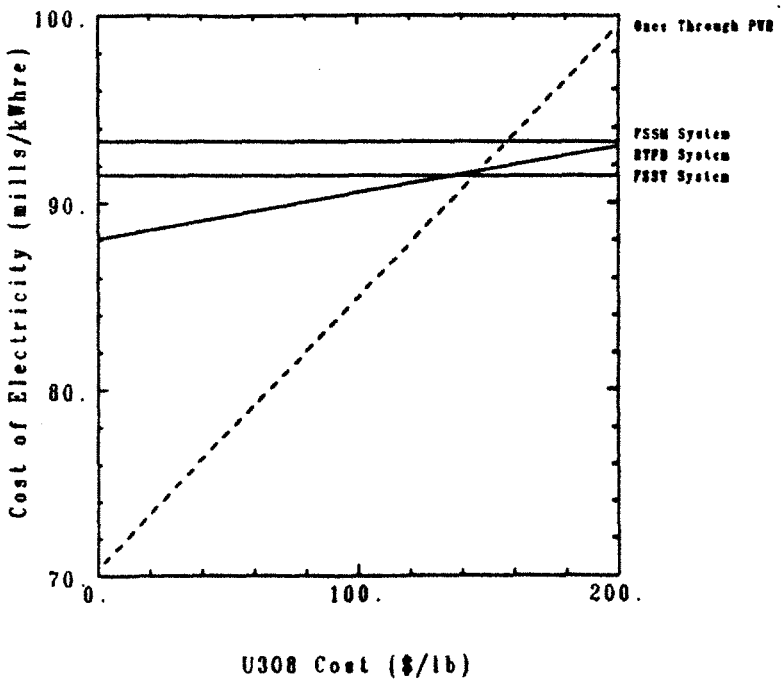

Figure 5.21 Comparison of Levelized Total System Electricity Cost RTFB, FSST and FSSM – Inflation=0.05 – U_3O_8 Escalation=0.00

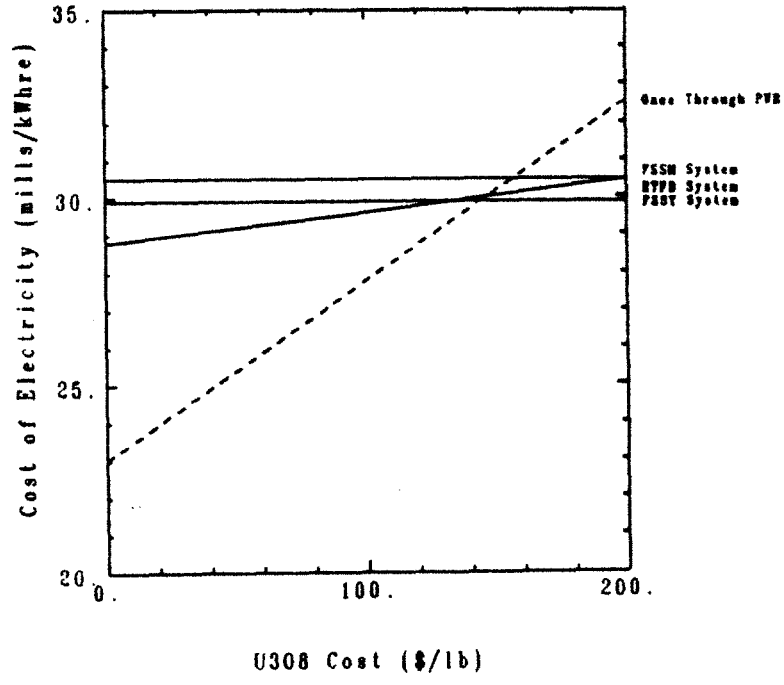

Figure 5.22 Comparison of Average Present Value Total System Electricity Cost RTFB, FSST and FSSM – Inflation=0.05 – U_3O_8 Escalation=0.00

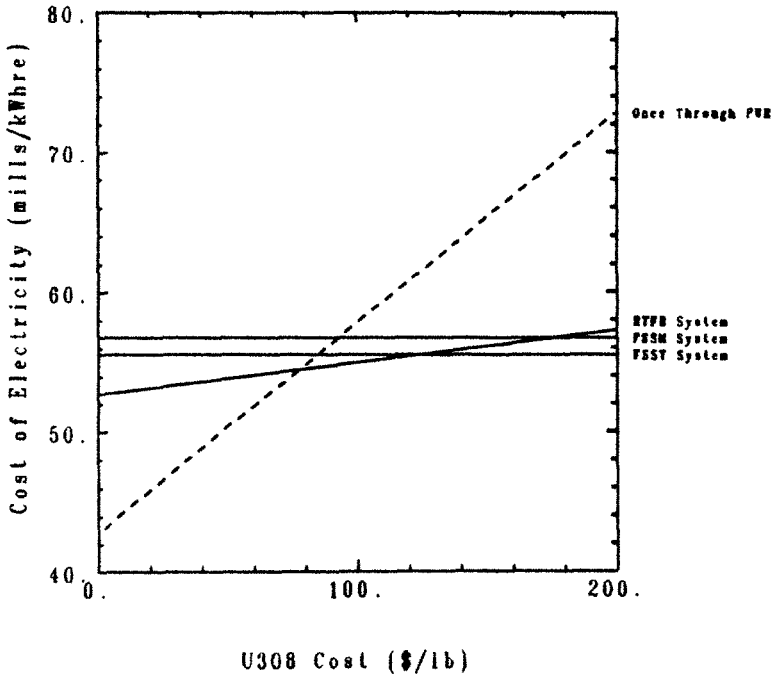

Figure 5.23 Comparison of Levelized Total System Electricity Cost RTFB, FSST and FSSM – Inflation=0.00 – U_3O_8 Escalation=0.05

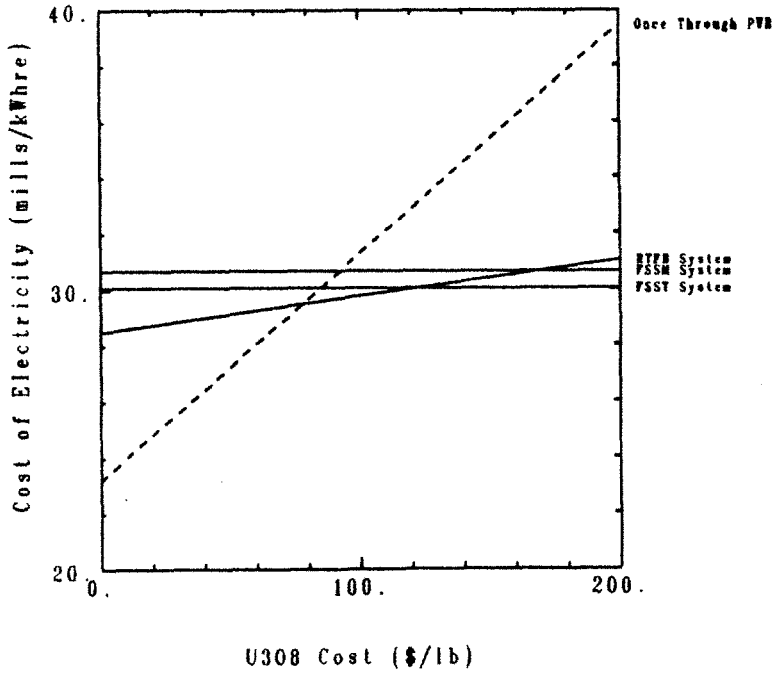

Figure 5.24 Comparison of Average Present Value Total System Electricity Cost RTFB, FSST and FSSM – Inflation=0.00 – U_3O_8 Escalation=0.05

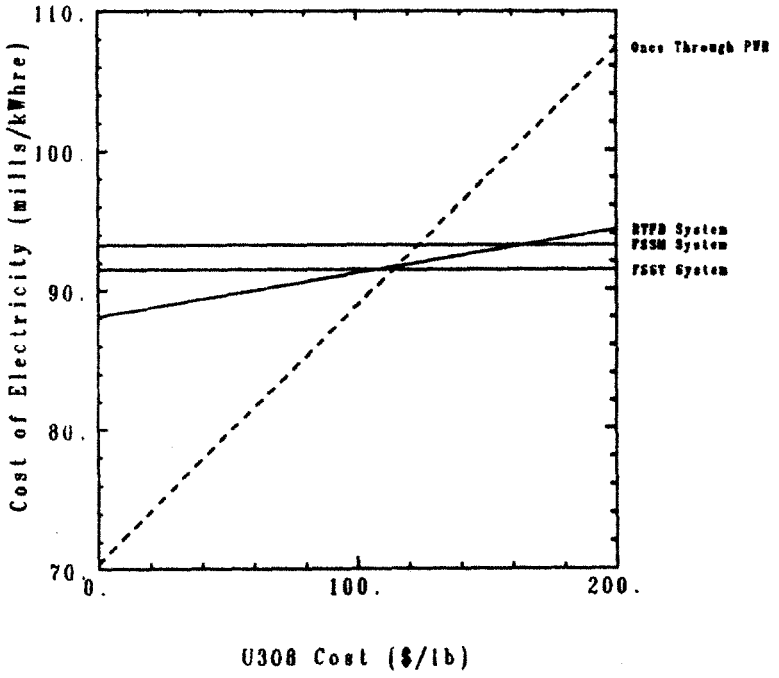

Figure 5.25 Comparison of Levelized Total System Electricity Cost RTFB, FSST and FSSM – Inflation=0.05 – U_3O_8 Escalation=0.02

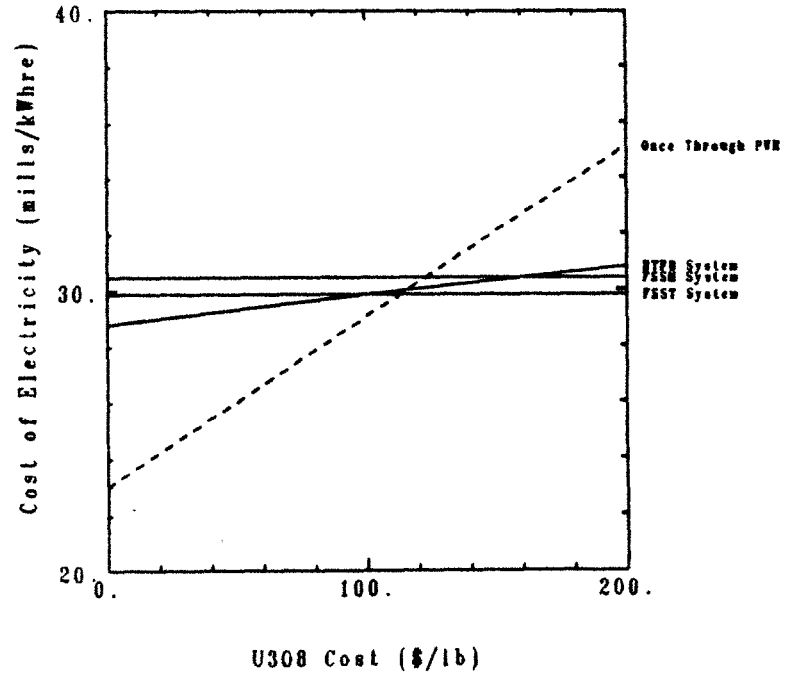

Figure 5.26 Comparison of Average Present Value Total System Electricity Cost RTFB, FSST and FSSM – Inflation=0.05 – U_3O_8 Escalation=0.02

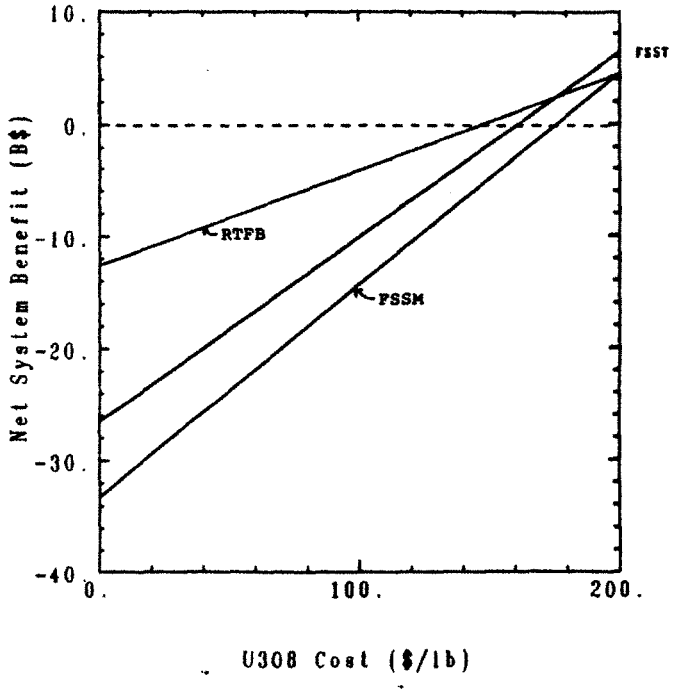

Figure 5.27 Comparison of Net System Benefit RTFB, FSST and FSSM – Inflation=0.00 – U_3O_8 Escalation=0.00

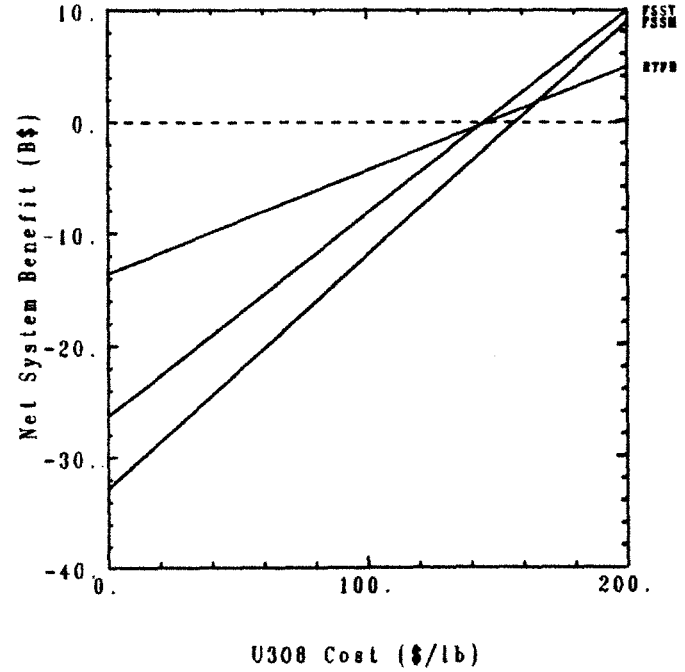

Figure 5.28 Comparison of Net System Benefit RTFB, FSST and FSSM – Inflation=0.05 – U_3O_8 Escalation=0.00

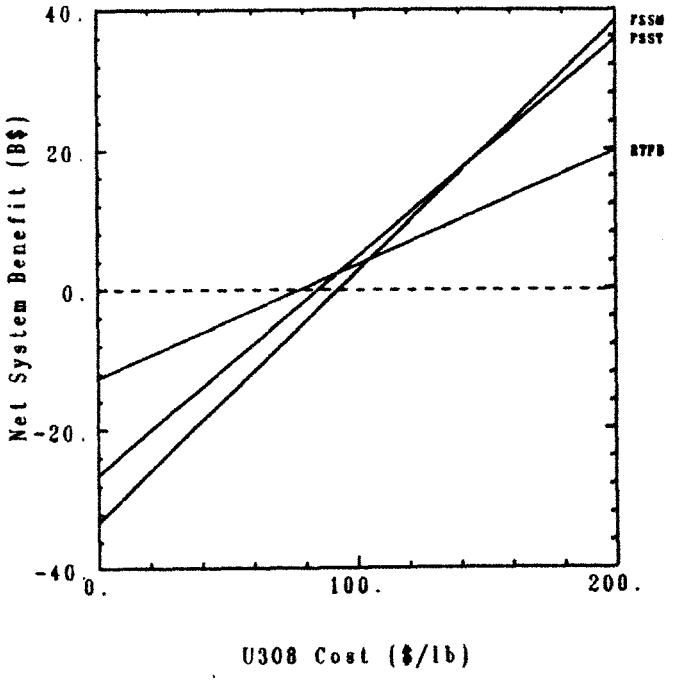

Figure 5.29 Comparison of Net System Benefit
RTFB, FSST and FSSM - Inflation=0.00 - U_3O_8 Escalation=0.05

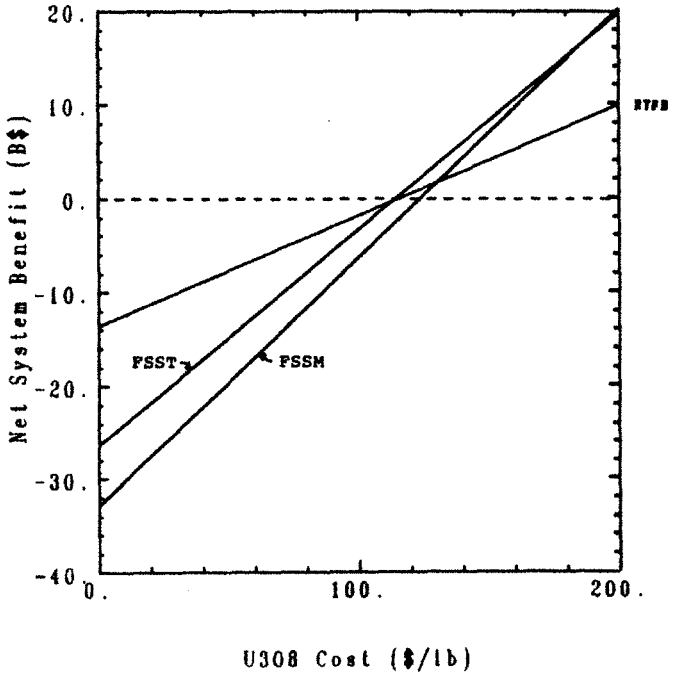

Figure 5.30 Comparison of Net System Benefit
RTFB. FSST and FSSM - Inflation=0.05 - U_3O_8 Escalation=0.02

6. SUMMARY, CONCLUSIONS AND RECOMMENDATIONS

6.1 Introduction

Fusion breeders have been previously investigated as potential applications of superconducting magnet tokamak and tandem mirror reactors by others [6.1-6.8]. Additionally, the Riggatron was considered for fissile fuel production but suffered from poor breeding performance since the blanket was outside the magnets [6.9]. These studies have shown that fissile fuel production can be achieved with fusion machines, but at higher prices than may be currently acceptable. However, if uranium prices rise in the future, these machines could produce fissile fuel which is cost competitive with mined uranium.

The machine considered in this study is the Resistive magnet Tokamak Fusion Breeder (RTFB). The RTFB is a compact tokamak using Bitter plate toroidal field coils. The blanket consists of two zones: the first zone is adjacent to the plasma and contains uranium metal clad in steel and cooled by lithium followed by a thorium bearing molten salt zone. The multiplier region, which contains uranium, multiplies the energy of the fusion neutrons through fissions, as well as breeding ^{239}Pu and tritium from neutrons captures in ^{238}U and Li. The molten salt region breeds ^{233}U and tritium through captures in Th and Li. Energy multiplication is necessary, for the machines considered most extensively in this study, to achieve net electric production. A comparison of the RTFB and STARFIRE is shown in Fig. 6.1.

The ALCATOR A and ALCATOR C experiments at MIT have demonstrated the application of resistive magnets of Bitter-plate construction for toroidal field coils in tokamaks [6.10]. The design studies related to ZEPHYR provided further information on the characteristics of Bitter-plate type magnets

in larger machines [6.11]. The recent series of Long pulse Ignition Test Experiment (LITE) [6.12,13] and Resistive Commercial Tokamak Reactor (RCTR) [6.14-16] studies are investigating the application of Bitter-plate type magnets to ignition test experiments and commercial fusion reactors. Resistive magnets appear to offer the following significant advantages over superconducting magnets:

- More compact – less shielding. Resistive toroidal field coils typically require less shielding than superconducting coils which results in a more compact design.

- Possibility of demountable joints. Resistive magnets offer the possibility of more easily engineered demountable joints than superconducting magnets [6.17].

- More robust design. Resistive magnets do not suffer from the limitations of current density, temperature and magnetic field that are imposed on superconducting magnets, though other limitations exist.

- Less structure required. For Bitter plate type magnet, the magnet is most of the structure required.

- No refrigeration. Cooling of the magnet is by water or helium gas with no cryogenic cooling required.

The conceptual time frame of this study is January 1, 1984 for the beginning of construction of the RTFB and initial commercial operation on January 1, 1990. In this time frame, the PWR on the once-through uranium fuel cycle is selected as the basis for comparison of electricity costs from the RTFB-client reactor system. Similarly, the PWR on the ^{233}U and ^{239}Pu fuel cycles with

recycle is selected as the client reactor system.

Other potential sources of fissile fuel include fast breeder fission reactors, accelerator breeders and uranium from seawater. Due to the lower number of client reactors supported by each FBR, the FBR-client reactor system characteristics would be dominated by the FBR. In contrast, the RTFB would supply make-up fuel to a larger number of client reactors. Thus, the RTFB-client reactor system characteristics would be dominated by the client reactors.

Uranium from seawater is currently projected to have a wide range of costs. The goal for uranium from seawater, and hence, the upper limit for uranium prices considered in the present study, is 200 \$ /lb U_3O_8 [6.18]. Hence, uranium from seawater is be considered to place an upper bound on the price of mined uranium with which the fusion breeder must compete.

6.2 Parametric Analysis

The STRESS code, previously developed by the Reactor Studies Group at the MIT Plasma Fusion Center, uses analytic expressions, scaling rules and fits to more complex analytic techniques to model resistive magnet tokamaks. STRESS was used to parametrically examine potential designs for the RTFB.

Major parametric scans were done varying neutron wall load, blanket envelope and the plasma β scaling parameter. Constraints were placed on the design to take advantage of the unique attributes of the resistive magnet tokamak. The major radius of the plasma was limited to less than 4 m. The neutron wall load was selected to be 2.0 MW/m^2 which gives a fusion power that will keep the total blanket power in the 4000-5000 MWth range. The stress in the throat of the toroidal field coil was fixed at 103 MPa, to insure conservative stress levels

in the throat of the magnet. The thickness of the outboard leg of the toroidal field coil was set at 0.75 m., since costing calculations show this thickness to give the lowest cost of capacity (capital cost per unit of net electrical output. $/kWe).

These constraints resulted in a machine with a major radius of 3.81 m. and a minor radius of 1.3 m. The fusion power is 618 MW and the toroidal field coil power requirement is 260 MWe. The equilibrium field magnet power requirement is 170 MWe. The space envelope for the blanket is 0.35 m. inboard and 0.75 m. outboard and upper and lower. This includes a 0.15 m. allowance for first wall scrape off. The RTFB parameters are summarized in Table 6.1.

6.3 Blanket Analysis

The blanket in the RTFB produces tritium to sustain the plasma and fissile fuel for use in a client reactor system. Additionally, the energy of the fusion neutrons is recovered and multiplied in the blanket. Consequently, the blanket was analyzed for neutronic performance in terms of breeding and energy multiplication. Shielding requirements to limit radiation dose rate to the insulation in the inboard leg of the toroidal field coils were evaluated. Additionally, the heat removal from the blanket was evaluated in terms of the pressure drop in the lithium coolant circuit and the uranium multiplier plate thickness. The size of the residual heat removal system was also determined. A summary of each of these analyses follows.

The blanket, shown in Fig. 6.2, consists of two zones: a multiplier zone adjacent to the plasma and a molten salt zone following the multiplier. The multiplier zone is 11 cm. thick and contains uranium metal clad in steel and cooled by liquid lithium. Fissions in the multiplier zone multiply the energy

of the fusion neutrons. These fissions occur primarily in ^{238}U , but as the concentration of ^{239}Pu increases with blanket life, fissions in ^{239}Pu increase and cause the blanket power to increase. Energy multiplication is necessary to achieve net electric output.

The molten salt zone thickness is 24 cm. inboard and 64 cm. outboard. The molten salt is continuously processed to remove the bred ^{233}U . Thus, the power level in the molten salt does not change due to an increase in concentration of ^{233}U , but does change due to the increased number of fissions in the multiplier.

Nuclear analyses were performed for the RTFB using the one-dimensional discrete ordinates code ONEDANT [6.19] and the three-dimensional Monte Carlo code MCNP [6.20]. The ONEDANT analyses were done to examine the effect of changing the materials in the inboard and outboard regions of the blanket and varying the thickness of the different regions. The ONEDANT calculations for the reference blanket yield a value of total breeding, T+F, of 2.89 and a blanket thermal power of 4986 MWth. Although the tritium breeding parameter is less than one for the reference configuration (T=0.97), it is shown that the value of T can be increased to 1.18 by using natural Li in the molten salt in place of the depleted Li. This increase in tritium breeding comes at the expense of ^{233}U breeding, which decreases. These values of T are for the ONEDANT beginning of cycle (BOC) analyses.

The effect of increasing the thickness of the multiplier region and increasing and decreasing the thickness of the molten salt region on breeding and energy multiplication was also investigated with ONEDANT. It was shown that increasing the multiplier thickness from 11 cm. to 16 cm. increases the total T+F by 6% and the blanket power by 11%. This case will be investigated more completely in the system economic analysis where the change in fissile fuel pro-

duction and blanket power will be considered. The effect on breeding and energy multiplication of increasing and decreasing the outboard molten salt thickness by 10 cm. is small, for example, less than 1% effect on ^{233}U breeding.

Additionally, ONEDANT analyses were done to investigate the effects on blanket power and breeding of the increasing concentration of ^{239}Pu in the multiplier. The limit of ^{239}Pu concentration was established by calculating the infinite medium multiplication factor, k_∞, for the uranium metal with varying concentration of ^{239}Pu . This value was limited to 0.9 to insure that criticality would not be reached, even under accident scenarios. This limit was determined to be 0.02 a/o ^{239}Pu in the uranium metal. The blanket power increases by a factor of 1.45 as the concentration of ^{239}Pu increases from 0.00 a/o to 0.02 a/o. The tritium and ^{233}U production rates increase with blanket lifetime due to the increased fissions as more ^{239}Pu is present in the blanket. Although the production rate of ^{239}Pu from captures in ^{238}U increases with blanket lifetime, the net production rate of ^{239}Pu decreases due to the increased captures in ^{239}Pu .

The dose rate to the magnet insulation on the plasma side of the inboard leg of the toroidal field coil was also calculated with ONEDANT. The dose rate with the reference blanket was shown to give a magnet insulation lifetime of 1.1 years. Hence, a shield must be provided to extend the magnet lifetime. The shield selected to replace the blanket consists of tungsten, steel, titanium hydride, boron carbide and water and gives a magnet insulation lifetime of 26.3 years, which is considered sufficient. These magnet insulation lifetimes are based on an allowable integral dose of 1.4–12 rads [6.21].

MCNP analyses were done for both one-dimensional and three-dimensional models. The one-dimensional results were compared to the ONEDANT calculation for the reference blanket and showed relatively good agreement in breeding.

with a total T+F value from MCNP that is 2% lower than ONEDANT. The three-dimensional MCNP results were used to estimate the BOC values of the breeding parameters and energy multiplication with and without the shield in place. The total breeding from MCNP was 2.4% less than ONEDANT and the blanket power was 11% lower than ONEDANT. for the case without the shield. With the shield in place the BOC breeding values are T=0.85, ^{233}F=0.87, ^{239}F=0.87, T+F=2.59 and the blanket thermal power is 4071 MWth. Reference BOC breeding and blanket power values are shown Table 6.2. The differences between the ONEDANT results and the MCNP results can be attributed to differences in the cross section treatment (multi-group in ONEDANT vs. continuous energy in MCNP) and geometry differences (one-dimensional in ONEDANT vs. three-dimensional in MCNP).

The design of the lithium coolant system as shown in Fig. 6.3 and Fig. 6.4 for the multiplier region was also considered. Pressure drop and pumping power calculations, summarized in Table 6.3, were done considering the MHD induced pressure drops for both uninsulated and insulated ducts of 0.5 cm. thickness. For the uninsulated case, it was shown that a 15 cm. duct half thickness along the magnetic field can give a maximum duct pressure of 2.20 MPa. This duct geometry gives a maximum allowable pressure of 1.98 MPa. However, considering the uncertainties in the pressure drop calculations, this design is considered to be acceptable. For the uninsulated duct, a duct half thickness of 5 cm. gives a maximum pressure drop of 1.35 MPa, which is less than the allowed value of 1.98 MPa. It is also noted that the pumping power for all cases in which the pressure drop is considered acceptable, the pumping power is within a reasonable range (less than 40 MW).

The uranium plate fuel thickness was also evaluated to determine that the multiplier region could be cooled using uranium plates of reasonable thickness. A uranium plate thickness of 1.0 cm. allows maintaining the clad-lithium interface

at less than 550°C and the peak uranium temperature ~300°C below the melting point of uranium metal. Additionally, the size of the residual heat removal system was determined to be 2.5% of the primary coolant system capacity to allow removal of the decay heat in the multiplier region after shutdown.

6.4 Cost Estimate for RTFB

This section discusses the cost estimating methodology and the cost estimate for the RTFB. The cost was estimated by using two methods: system cost scaling and unit costing. In system cost scaling, the cost is estimated by using a previous cost estimate for a similar system and adjusting the cost for the RTFB by an appropriate factor. In unit costing, the cost of the RTFB item or system is estimated by calculating, for example, the capacity or mass (such as, MWth or kg) and multiplying by the unit cost (for example, $/MWth or $/kg). The costs of the various systems are summed to give the cost of each account. The standard accounts for fusion reactor cost estimating have been established to insure uniformity among fusion reactor cost estimates [6.22]. The accounts are assigned contingency allocations and summed to give the total cost of the reactor. A construction time and expenditure pattern are then assumed to give the interest during construction. The interest, along with construction and management charges, is added to the total direct cost to give the total capital cost.

The costs used in the RTFB cost estimate are taken from many sources which estimated costs at different times. Hence, the costs must all be adjusted to the same point in time. The prescribed method for this adjustment is to use indices from the Handy Whitman Index [6.23] or the Department of Commerce Survey of Current Business [6.24]. Most of the cost information was taken from the Non-Proliferation Alternative Systems Assessment Study [6.25], the

Battelle Pacific Northwest Laboratory report "Fusion Reactor Design Studies - Standard Unit Costs and Cost Scaling Rules," [6.26] and the STARFIRE design study [6.27].

The cost estimate for the RTFB is shown in Table 6.4, along with a comparison to STARFIRE, which is the basis for the cost estimate [6.28]. Although the RTFB fusion power is lower than STARFIRE by a factor of 5.8, the input power to the turbine is higher by a factor of 1.45. This is due to the energy multiplication in the RTFB blanket. The recirculating power of the RTFB is a factor of 2.3 higher than in STARFIRE. The net electric output of the RTFB is 1552 MWe at EOC, compared to 1202 MWe for STARFIRE. The average electric output of the RTFB is 1247 MWe.

The RTFB capital cost is 2% less than the STARFIRE capital cost. Although the RTFB nuclear island is more compact than STARFIRE, the reactor plant equipment account is only 14% less expensive than STARFIRE. This is due to the different cooling system of the RTFB, which uses liquid metal and molten salt. STARFIRE uses water cooling, which eliminates the need for an intermediate coolant loop between the primary cooling system and the main steam system. However, the RTFB does not require the massive shield used in STARFIRE to limit nuclear heat deposition in the superconducting magnets.

It should be noted that the limiter cooling system for the RTFB is assumed to be the same as STARFIRE, namely, water cooling. Other options for cooling the limiter are available if water cooling is considered unacceptable from a safety standpoint.

The cost of electricity for the RTFB was estimated, on the same basis as STARFIRE and is shown in Table 6.5. Note that this comparison does not include the fuel cycle costs and the value of the fissile fuel produced by the RTFB.

The comparison is on the same basis as the STARFIRE financial assumptions. On this basis, the cost of electricity from the RTFB is 42.4 mills/kWhre and 44.9 mills/kWhre from STARFIRE. These costs are in 1984$.

The sensitivity of the RTFB cost estimate and cost of electricity to various parameters is also investigated. The cost of electricity is seen to be a minimum for each outboard leg thickness over a range of toroidal field coil unit costs. For the estimated toroidal field coil cost of $30/kg, the cost of electricity is minimum for an outboard leg thickness of 0.75 m.

The effect of the number of turbines and availability on the electricity cost is shown in Fig. 6.5. Increasing the number of turbines increases the cost of electricity from the RTFB. The RTFB reference case uses 2 turbine-generators. Decreasing the capacity factor increases the cost of electricity and increasing the capacity factor decreases the cost of electricity. As an example, the base case capacity factor of 0.75 gives a cost of electricity of 42.4 mills/kWhre; a decreased capacity factor of 0.65 gives a cost of electricity of 49.5 mills/kWhre, an increase of 17%; an increased capacity factor of 0.85 gives a cost of electricity of 37.0 mills/kWhre, a decrease of 13%. Thus, the benefits of an increased capacity factor are not as great as the penalties of a decreased capacity factor.

It is also shown that the RTFB magnet power requirement could rise by a factor of 1.07, from 452 MWe to 500 MWe, and maintain the same cost of electricity as STARFIRE.

The blanket power variation with blanket lifetime is modelled in the COST code by sizing all components based on the EOC power level, which is the highest power, and calculating the cost of all electricity cost components on the basis of the average electric output. The RTFB fuel cycle length is selected to be 4 years, since this length gives the lowest cost of capacity and cost of electricity.

consistent with the limitations on k_{eff} discussed in section 6.3. Thus, the cost of the reference design of the RTFB is \$3.01B in 1984\$.

6.5 System Economic Analysis

This section discusses the system economic analysis for the RTFB and its associated system of client reactors. The basis for comparison is the PWR on the once through uranium fuel cycle. The client reactor system is composed of PWRs identical to the once through PWR, but operating on the ^{239}Pu and ^{233}U fuel cycles with recycle.

A system economic evaluation methodology is developed which allows for the time value of money in adjusting the cost of the various fuel cycle transactions to a common point in time, the time of fuel load. General inflation and escalation of U_3O_8 prices are allowed. The cost of the bred fuel within the system is determined and carrying charges are paid on the value of the fissile fuel within the RTFB-client reactor system. Levelized values are calculated. Additionally, for comparison to other fusion breeders, the average present value (APV) and net system benefit are calculated. The average present value is defined as the average of the year-by-year costs, discounted to the beginning of operation. The net system benefit is defined as the integrated present value of the year-by-year differences in cost of the number of client reactors selling electricity at the total system electricity cost and the same number of once through PWRs selling electricity at the cost determined by the U_3O_8 cost. The breakeven U_3O_8 cost is the cost of U_3O_8 at which the cost of electricity from the once through PWR and the RTFB-client reactor system is equal.

The fuel cycle length of the RTFB was determined to be 4 years. This is the length of time that the multiplier remains in place before removal for

reprocessing. The system cost of electricity decreases by a factor of 1.3 as the RTFB fuel cycle length increases from 1 year to 4 years. The concentration of ^{239}Pu after a 4 year exposure is 0.02 a/o, which is the limit imposed by the neutronic calculations from criticality considerations. The breakeven cost of U_3O_8 for a 4 year fuel cycle length is 145$/lb. Key parameters for the RTFB with a 4 year fuel cycle length are shown in Table 6.6.

An increase of a factor of 2 in the RTFB capital cost increases the system electricity cost by a factor of 1.3 and shifts the breakeven U_3O_8 cost to beyond 200$/lb. Also, a decrease in the RTFB capital cost by a factor of 2 results in a decrease in the system electricity cost of a factor of 0.85 and shifts the breakeven U_3O_8 cost to 25$/lb. This is shown in Fig. 6.6.

The fuel cycle costs of the RTFB are also varied. It is shown that an increase of a factor of 2 in the RTFB fuel cycle costs increases the system electricity cost by 2 mills/kWhre (5%), which is similar to the effect of increasing the cost of U_3O_8 from 0 to 200$/lb. The breakeven U_3O_8 cost is 145$/lb for the reference case.

The effect of the breeding performance of the RTFB is also evaluated. The penalty of decreased breeding is shown to be greater than the benefit of increased breeding. Decreasing the breeding by a factor of 0.8 shifts the breakeven U_3O_8 cost from 145$/lb to beyond 200$/lb. Increasing the breeding by a factor of 1.2 shifts the breakeven cost of U_3O_8 from 145$/lb to 110$/lb. These values are for the case in which the breeding changes, but the blanket power remains constant. If the blanket power and breeding are decreased by a factor of 0.9, the breakeven U_3O_8 cost shifts from 145$/lb to 200$/lb. An increase in the breeding and blanket power of a factor of 1.2 shifts the breakeven U_3O_8 cost from 145$/lb to 90$/lb.

The effect of removing the shield required in the RTFB is to shift the breakeven U_3O_8 cost from 145\$/lb to 125\$/lb. This is due to the increased blanket power and breeding resulting from replacing the shield with multiplier and molten salt. Note that this option would require development of an insulating material which will withstand a radiation dose of 27 times allowable with currently available materials.

Increasing the thickness of the multiplier region from 11 cm. to 16 cm. is seen to result in higher system electricity costs for U_3O_8 costs in excess of 15\$/lb due to the higher costs associated with the multiplier.

The effect of financial parameters on the total system electricity cost is also evaluated. Inflation increases the cost of electricity, but does not shift the breakeven U_3O_8 cost. Escalation of U_3O_8 costs also increases the cost of electricity, but has less of an effect than the same inflation rate. However, escalation also shifts the breakeven cost of electricity.

It is also noted that the average present value cost of electricity, a figure of merit commonly used in fusion breeder studies, gives a similar result when escalation alone is considered. However, when inflation alone is considered, the APV cost shows increasing U_3O_8 cost to be more important than inflation while the levelized electricity cost shows inflation to be more important than U_3O_8 cost.

The RTFB is also compared to the Fission-Suppressed Superconducting Tokamak fusion breeder (FSST) [6.1] and the Fission-Suppressed Superconducting tandem Mirror fusion breeder (FSSM) [6.5]. From Fig. 6.7 and Fig. 6.8, the RTFB is shown to give a lower breakeven cost of U_3O_8 (150\$/lb) than the FSST (160\$/lb) and FSSM (175\$/lb) for analyses with no inflation and escalation. When inflation of 5% is considered, as in Fig. 6.9 and Fig. 6.10, the

RTFB and the FSST have the same breakeven cost of U_3O_8 (145$/lb), with the FSSM higher (160$/lb). Inflation affects the RTFB more than the FSST and the FSSM since the two superconducting machines incorporate the fuel cycle costs into the capital cost.

For 5% escalation of U_3O_8 cost, shown in Fig. 6.11 and 6.12, the breakeven cost for the RTFB (75$/lb) is also lower than for the FSST (85$/lb) and the FSSM (90$/lb). The RTFB system electricity cost is more sensitive to U_3O_8 escalation since the fuel cycle costs depend on the U_3O_8 cost.

For the conditions considered in the FSSM and FSST analysis of 5% inflation and 2% escalation of U_3O_8 prices, the RTFB is essentially equivalent to the FSST and marginally better than the FSSM, as shown in Fig. 6.13 and 6.14. The breakeven prices of U_3O_8 for the RTFB, FSST and FSSM are 115, 115 and 125$/lb for these financial parameters.

The net system benefit, another figure of merit used in the FSSM and FSST analyses is shown in Fig. 6.15-18 for the various financial assumptions considered above. The net system benefit is defined as the integrated present value of the difference between the client reactors selling electricity at the system electricity cost and the same number of PWRs on the once through fuel cycle selling electricity at the cost determined for the once through. A negative value means the fusion breeder-client reactor system would cost more than the once through PWR. A zero net benefit gives the breakeven cost of U_3O_8 . The net system benefit gives the same breakeven cost of U_3O_8 as the average present value for the respective cases.

It is noted that the RTFB cost of electricity could be reduced by assuming the same front end and back end costs as the FSST and FSSM, namely 144$/kg vs. 400$/kg for the RTFB. Note that the FSST and FSSM front end cost is for

fabricating recycled Th and the RTFB front end cost is for fabricating unrecycled uranium. Additionally, the RTFB fuel form (plates) is of a more conventional type than the FSSM and FSST (Th snap rings around Be pebbles).

If the RTFB is operated in a mode in which the fuel cycle facilities are included in the capital cost, similar to the FSST and the FSSM, the total system electricity cost would decrease. This can be evaluated by increasing the RTFB capital cost by a factor of 1.038 and setting fuel cycle costs to zero. The factor of 1.038 applied to the capital cost adds $114M to the capital cost for fuel cycle facilities. The $114M is based on the FSST fuel cycle facility costs [6.1] and the relative throughput of the RTFB and the FSST (86 MT/yr for the RTFB and 343 MT/yr for the FSST). Although the capital cost increases, the total system electricity cost decreases due to the elimination of the fuel cycle charges. Thus, the reference RTFB levelized system electricity cost for inflation of 5% and U_3O_8 escalation of 2% decreases from 88.1 mills/kWhre to 84.7 mills/kWhre. The breakeven cost of U_3O_8 decreases from 115$/lb to 80$/lb, as seen from Fig. 6.13.

6.6 Conclusions

The major conclusions of this study are summarized as follows:

1. The RTFB appears competitive with superconducting magnet tokamaks and tandem mirrors for fissile fuel production. Based on comparisons with superconducting magnet tokamak and tandem mirror fusion breeders, the RTFB appears to give a breakeven cost of U_3O_8 which is equivalent to the tokamak (115$/lb) and marginally lower than the tandem mirror (125$/lb). Due to the potential advantages of resistive magnets over superconducting magnets, the RTFB should be further considered for fissile fuel production.

2. Varying the capital cost of the RTFB has major effect on the breakeven price of U_3O_8 . If the capital cost of the RTFB is decreased by one half, the breakeven cost of U_3O_8 shifts from 145$/lb to 25$/lb. Conversely, if the RTFB capital cost is increased by a factor of 2, the breakeven cost of U_3O_8 shifts to beyond 200$/lb. Hence, the capital cost of the RTFB should be kept as low as possible.

3. If the fuel cycle charges can be incorporated into the capital cost at the same cost ($/kg) as the FSST and the FSSM, the breakeven U_3O_8 cost can be reduced to 80$/lb from 115$/lb. for 5% inflation and 2% escalation.

4. The effective blanket coverage factor is important. This directly affects the breeding and blanket thermal power. A decrease in either the breeding or blanket thermal power has an adverse affect on the system electricity cost. This is due to lower electricity production in the RTFB and the higher costs of the RTFB being "spread out" over fewer client reactors. Thus, the effective blanket coverage factor should be maintained as high as possible.

5. Use of pyroprocessing looks very attractive for the multiplier. If the projected low costs for pyroprocessing of 60$/kg can be achieved, the cost of reprocessing the multiplier region can be kept relatively low. If higher cost of reprocessing the multiplier are realized, the total system electricity cost will rise. Note that higher reprocessing costs will affect the FSSM and FSST to a much greater extent, due to the higher average throughput in the blanket (~340 MT/yr vs. 86 MT/yr for the RTFB).

6. Use of the average present value of the various figures of merit, instead of levelized values, gives an erroneous impression of the cost of the products of the fusion breeder system. The costs appear much lower using the average present value rather than the levelized costs. The average present

value does give the same breakeven U_3O_8 costs as the levelized values. However, when inflation alone is considered, the average present value shows increasing U_3O_8 cost to give higher electricity costs than increasing inflation, while the levelized costs show increasing inflation to give higher electricity costs than increasing U_3O_8 cost.

7. The use of uninsulated ducts for the lithium coolant appears feasible from the standpoint of pressure drops. The larger width of these ducts would require more detailed neutronics analysis to determine the effect on breeding of the increased volume of lithium and structure in the blanket. Additionally, the acceptability of the larger penetrations in the magnet would need to be evaluated.

8. Due to the large fission power in the blanket, a substantial decay heat removal capacity (2.5% of the primary cooling system capability) is necessary. Since the fuel is in the form of fixed plate elements, the fuel must be cooled in place.

6.7 Recommendations for Future Work

In view of the apparent attractiveness of the RTFB for fissile fuel production, relative to the FSST and the FSSM, the following recommendations for future work are offered.

1. The capital cost of the RTFB was shown to have a major impact on the breakeven cost of U_3O_8 . Hence, options for reducing the capital cost of the RTFB should be investigated. Specifically, reducing the cost of the reactor plant equipment account should be investigated, since this account represents 50% of the direct cost. The primary and intermediate coolant

systems are major items in this account which were estimated on a unit cost basis. Incorporation of economies of scale should reduce the cost of these major items.

2. Incorporation of the fuel cycle costs in the RTFB capital cost may reduce the breakeven cost of U_3O_8 by 35$/lb. Hence, incorporating a fabrication and reprocessing plant for the multiplier in the RTFB capital cost should be further investigated. Additionally, recycling of the uranium within the RTFB should be considered.

3. The effect of reprocessing costs on the system economics was shown to be significant for both the RTFB and the client reactors. The estimated cost of the pyrochemical reprocessing should be verified. If this process does appear attractive, pyrochemical processing should also be applied to the client reactor system, with allowances for the additional steps necessary or the differences in the client reactor fuel cycle.

4. The preconceptual design of the RTFB uses lithium and molten salt for both breeding and heat removal. Sodium is used in the intermediate coolant loop. The limiter and magnets are both cooled by water, although other options exist. Hence, the presence of both lithium and water in the nuclear island is a concern. Thus, the requirement and desirability of non-water options for cooling the limiter and magnets should be assessed. Specifically, the question of the minimum allowable proximity of lithium and water systems should be addressed.

5. The shield required to protect the magnet insulation in the inboard leg of the toroidal field coil displaces a section of the multiplier and molten salt region. The resulting decrease in blanket breeding and power causes the system electricity cost to increase. Hence, other options for protecting the

magnet insulation should be investigated, such as increasing the blanket thickness. Additionally, the desirability of replacing the inboard leg of the toroidal field coil periodically should be evaluated. This would involve trading off considerations of magnet design, available insulation options, impact on availability and impact on breeding.

6. This study has specifically considered compact, moderate performance fusion machines. This is one segment of a wide spectrum of possible fusion drivers. Thus, this work should be extended to larger machines of higher fusion performance. Note that higher fusion performance fusion machines may require different blankets to maintain the power within reasonable ranges.

7. Due to the large uncertainty in the pressure drop calculations, more study is needed to determine the degree of uncertainty in the calculations. This is particularly true for the RTFB due to the high power density in the multiplier region.

8. The lithium cooling ducts and molten salt flow duct penetrate the toroidal field coil. The allowable size of these penetrations may be limited by magnet structural considerations. Thus, the maximum penetration size allowable should be determined by detailed structural analysis.

9. The high fission power density in the multiplier region indicates the potential for more severe accident scenarios than for fission suppressed blankets or pure fusion blankets. Thus, the accident sequences should be studied to determine the requirements for emergency cooling systems.

10. The blanket used in this study appears attractive. However, other blanket options should be investigated to determine if better breeding performance

can be achieved.

11. The high value of total breeding obtained with the RTFB indicates that excess tritium could also be produced for use in other fusion reactors. This should be evaluated by determining the value of tritium production vs. fissile production.

12. This study has considered PWRs as client reactors. Advanced converter reactors should also be evaluated, since the lower make up fuel requirements could make these systems more attractive, in terms of a lower system electricity cost. Additionally, the RTFB should be evaluated as a fuel source for providing fuel to some inherently safe reactors, such as the modular HTGR. Although fuel costs are not a driving factor in the consideration of inherently safe designs, the availability of a source of ^{233}U might lower the fuel cycle costs, and thus, make these systems more economically attractive.

13. The RTFB should be compared to fast breeder reactors to determine if lower electricity costs can be obtained with the RTFB. Additionally, the sensitivity of the respective system electricity costs to the uncertainties in the different technologies should be evaluated.

References

[6.1] Moir, R. W., et al., "Feasibility Study of a Fission-Suppressed Tokamak Fusion Breeder," Lawrence Livermore National Laboratory Report UCID-20154, (December 1984).

[6.2] Jassby, D. L., et al., "Fast-Fission Tokamak Breeder Reactors," *Proceedings of the Sixth Topical Meeting on the Technology of Fusion Energy*, San Francisco, CA (1985), to be published in *Fusion Technology*.

[6.3] Westinghouse Electric Corporation. "Conceptual Design of a Commercial Tokamak Hybrid Reactor (CTHR) Final Report." WFPS: TME-80-012, (December 1980).

[6.4] Westinghouse Electric Corporation. "Design Study of a Fusion-Driven Tokamak Hybrid Reactor for Fissile Fuel Production," Electric Power Research Institute Report ER-1083, Volume 1 and 2, (May 1979).

[6.5] Berwald, D.H., et al.,"Fission-Suppressed Hybrid Reactor – The Fusion Breeder," Lawrence Livermore National Laboratory Report UCID-19638, (December 1982).

[6.6] Lee, J.D., et.al., "Feasibility Study of a Fission-Suppressed Tandem-Mirror Hybrid Reactor." Lawrence Livermore National Laboratory Report UCID-19327, (April 1982).

[6.7] Moir, R.W., et.al., "Tandem Mirror Hybrid Reactor Design Study Final Report," Lawrence Livermore National Laboratory Report UCID-18808, (September 1980).

[6.8] Bender, D. J., et al., "Reference Design for the Standard Mirror Hybrid Reactor." Lawrence Livermore National Laboratory Report UCRL-52478, (May 1978).

[6.9] INESCO, Inc., "Presentation to the Riggatron Review Group." U. S. Department of Energy, Germantown, MD (July 16, 1979).

[6.10] Weggel, C., Hamburger, W., Montgomery, B., and Pierce, N., "The Alcator C Magnetic Coil System," in Engineering Problems of Fusion Research (Proc. 7th Symposium, Knoxville, TN, 1977).

[6.11] Williams, J. E. C., et al., "Conceptual Design of a Bitter Magnet Toroidal Field System for the ZEPHYR Ignition Test Reactor." Massachusetts Institute of Technology Plasma Fusion Center Report PFC/RR-81-24, (May 1981).

[6.12] Bromberg, L., Cohn, D. R., Williams, J. E. C., Yang, T. and Jassby, D. L., "Engineering Aspects of LITE (Long Pulse Ignition Test Experiment) Devices," in *Proceedings of the Tenth Symposium on Fusion Engineering*,

Philadelphia, PA. (December 1983).

[6.13] Bromberg, L.,Cohn, D. R., Williams, J. E. C. and Jassby, D. L., "A Long Pulse Ignited Test Experiment (LITE)." *Nuclear Technology/Fusion*, Vol. 4, 1013 (1983).

[6.14] LeClaire, R. J., Potok, R. E., Bromberg, L., Cohn, D. R., Meyer, J. E. and Yang, T. F., "Systems Studies of Commercial Tokamak Reactors with Resistive Magnets." *Proceedings of the Sixth Topical Meeting on the Technology of Fusion Energy*, San Francisco, CA (1985), to be published in *Fusion Technology*.

[6.15] Bromberg, L., " Design Options for Commercial Reactors with Resistive Magnets." *Proceedings of the Sixth Topical Meeting on the Technology of Fusion Energy*, San Francisco, CA (1985), to be published in *Fusion Technology*.

[6.16] Bromberg, L., Cohn, D. R., and Jassby, D. L., "Commercial Tokamak Reactors with Resistive Magnets". *Fusion Technology*, **6** 597 (1984).

[6.17] Yang, T. F., LeClaire, R. J., Bobrov, E. S., Bromberg, L., Cohn, D. R. and Williams, J. E. C., "A Demountable Copper TF Coil System for Ignition Test Experiments and Commercial Reactors." *Proceedings of the Sixth Topical Meeting on the Technology of Fusion Energy*, San Francisco, CA (1985), to be published in *Fusion Technology*.

[6.18] Driscoll, M. J., personal communication, Massachusetts Institute of Technology.

[6.19] O'Dell, R. D., Brinkley, F. W. and Marr D. R., "User's Manual for ONEDANT: A Code Package for One-Dimensional, Diffusion-Accelerated, Neutral Particle Transport," Los Alamos National Laboratory Report LA-9184-M, (February 1982).

[6.20] Los Alamos Monte Carlo Group, "MCNP - A General Monte Carlo Code for Neutron and Photon Transport, Version 2D," Los Alamos National Laboratory Report LA-7396-M, Revised (December 1982).

[6.21] Shmunck, R. E. and Becker, H., "Extension of the Irradiation and Testing

of SPAULRAD-S for Fusion Magnet Application," *Proceedings of the Sixth Topical Meeting on the Technology of Fusion Energy*, San Francisco, CA (1985), to be published in *Fusion Technology*.

[6.22] Schulte, S. C., Willke, T. L., Young, J. R., "Fusion Reactor Design Studies – Standard Accounts for Cost Estimates," Pacific Northwest Laboratory Report PNL-2648, (May 1978).

[6.23] *The Handy Whitman Index of Public Utility Construction Costs*, Whitman, Requardt and Associates, Bulletin No. 119, To January 1, 1984, Baltimore, MD.

[6.24] *Survey of Current Business*, United States Department of Commerce, Bureau of Economic Analysis, Washington, D. C., (July 1984).

[6.25] U.S. Department of Energy, "Nuclear Proliferation and Civilian Nuclear Power: Report of the Nonproliferation Alternative System Assessment Program," DOE-NE-0001, (June 1980).

[6.26] Schulte, S. C., et al., "Fusion Reactor Design Studies – Standard Unit Costs and Cost Scaling Rules," Pacific Northwest Laboratory Report PNL-2987, (September 1979).

[6.27] Baker, C. C., et al., "STARFIRE – A Commercial Tokamak Fusion Power Plant Study," Argonne National Laboratory Report ANL/FPP-80-1, (September 1980).

[6.28] Evans, K., "A Tokamak Reactor Cost Model Based on STARFIRE / WILDCAT Costing," Argonne National Laboratory Report ANL/FPP/TM-168, (March 1983).

TABLE 6.1

Resistive Magnet Tokamak Fusion Breeder Reference Design

Plasma Parameters	
Major Radius of Plasma (m)	3.81
Minor Radius of Plasma (m)	1.30
Aspect Ratio	2.93
$\langle\beta\rangle$	0.055
Plasma Elongation	1.6
Performance × Elongation	3.8
Margin to Ignition × Elongation	2.9
Average Electron Density (m^{-3})	1.0+20
Average Electron Temperature (keV)	20
Plasma Current (amps)	9.3+6
Magnet Field at the Plasma Axis (T)	4.6
Inboard Magnet-Plasma Distance (m)	0.50
Outboard Magnet-Plasma Distance (m)	0.90
Upper and Lower Magnet-Plasma Distance (m)	0.90
Plasma Scrape-Off/First Wall Region (m)	0.15
Volume of Plasma (m^3)	203.36
Fusion Power (MWth)	618
Magnet Parameters	
Toroidal Field Magnet Height (m)	7.17
Toroidal Field Magnet Inner Radius (m)	1.50
Toroidal Field Magnet Outer Radius (m)	6.76
Volume of Toroidal Field Magnet (m^3)	379
Mass of Toroidal Field Magnet (Gg)	3.0
Toroidal Field Magnet Power (MWe)	260
Toroidal Field Magnet Stress (MPa)	103
Ohmic Heating Magnet Inner Radius (m)	0.75
Ohmic Heating Magnet Outer Radius (m)	1.50
Volume of Ohmic Heating Magnet (m^3)	22.05
Mass of Ohmic Heating Magnet (Gg)	0.2
Ohmic Heating Magnet Stress (MPa)	51.9
Ohmic Heating Magnet Power (MWe)	66.9
Equilibrium Field Magnet Power (MWe)	170

TABLE 6.2

Reference BOC Breeding and Energy Deposition With and Without Shield

	With Shield	Without Shield
Breeding		
T	0.85	0.93
^{233}F	0.87	0.94
^{239}F	0.87	0.95
T+F	2.59	2.82
BOC Energy Deposition		
Molten Salt (MWth)	314	341
Multiplier (MWth)	3757	4095
Total (MWth)	4071	4436

TABLE 6.3

Pumping Power and Pressure Drops for Uninsulated and Insulated Ducts

Toroidal Segments	Poloidal Segments	Max. Pumping Power (MW)	Duct Mass (MT)	Maximum Δp (MPa)
$a = 0.15$ m. $t_1 = 0.005$m. $t_2 = 0.0025$m.				
8	10	54.80	22.94	3.09
8	20	48.50	29.78	2.73
8	30	44.62	36.23	2.51
8	40	42.09	42.32	2.37
8	50	40.31	48.06	2.27
8	60	39.01	53.50	2.20
$a = 0.05$ m. $t_1 = 0.00025$m. $t_2 = 0.000125$m.				
8	10	30.57	18.98	1.72
8	20	28.71	21.36	1.62
8	30	27.07	23.60	1.52
8	40	25.77	25.71	1.45
8	50	24.73	27.70	1.39
8	60	23.89	29.57	1.35

TABLE 6.4

RTFB Cost Comparison With STARFIRE (January 1, 1984 M$)

Account	Items	RTFB	STARFIRE
20	Land Acquisition and Relocation	4.01	4.01
21	Structure and Site Facilities	387.50	427.18
22	Reactor Plant Equipment	1075.52	1257.61
23	Turbine Plant Equipment	484.08	328.11
24	Electric Plant Equipment	158.64	145.96
25	Misc. Plant Equipment	55.39	55.39
26	Special Materials	0.30	0.30
90	Total Direct Cost	2165.43	2218.57
91	Construction Facilities, Equipment & Services	216.54	221.86
92	Engineering & Construction Management Services	173.23	177.49
93	Other Costs	108.27	110.93
94	Interest During Construction	347.05	355.57
99	Total Reactor Capital Cost	3010.53	3084.41
	Cost of Capacity($/kWe ave.)	2414	2566
	Cost of Electricity (mills/kWhre)	42.4	44.9

TABLE 6.5

RTFB Cost of Electricity Comparison With STARFIRE

Cost of Electricity by Component (mills/kWhre)	RTFB	STARFIRE
Capital Cost	36.9	39.1
Operation and Maintenance	4.5	3.0
Scheduled Component Replacement	1.1	2.9
Fuel Cost	0.0	0.1
Total Cost of Electricity	42.4	44.9

TABLE 6.6

RTFB Performance

Total Direct Cost (1984M$)	2170
Total Capital Cost (1984M$)	3010
Average Gross Electric Power (MWe)	1760
Average Net Electric Power (MWe)	1250
^{233}U Production (kg/yr)	2056
^{239}Pu Production (kg/yr)	1734
Availability	0.75

TABLE 6.7

Superconducting Fission-Suppressed Tokamak and Tandem Mirror Fusion Breeder Performance

	Tokamak	Tandem Mirror
Total Direct Cost (1984M$)	3610	4590
Total Capital Cost (1984M$)	5010	6380
Gross Electric Power (MWe)	1667	2226
Net Electric Power (MWe)	1385	1720
Net ^{233}U Production (kg/yr)	5255	6038
Availability	0.75	0.75

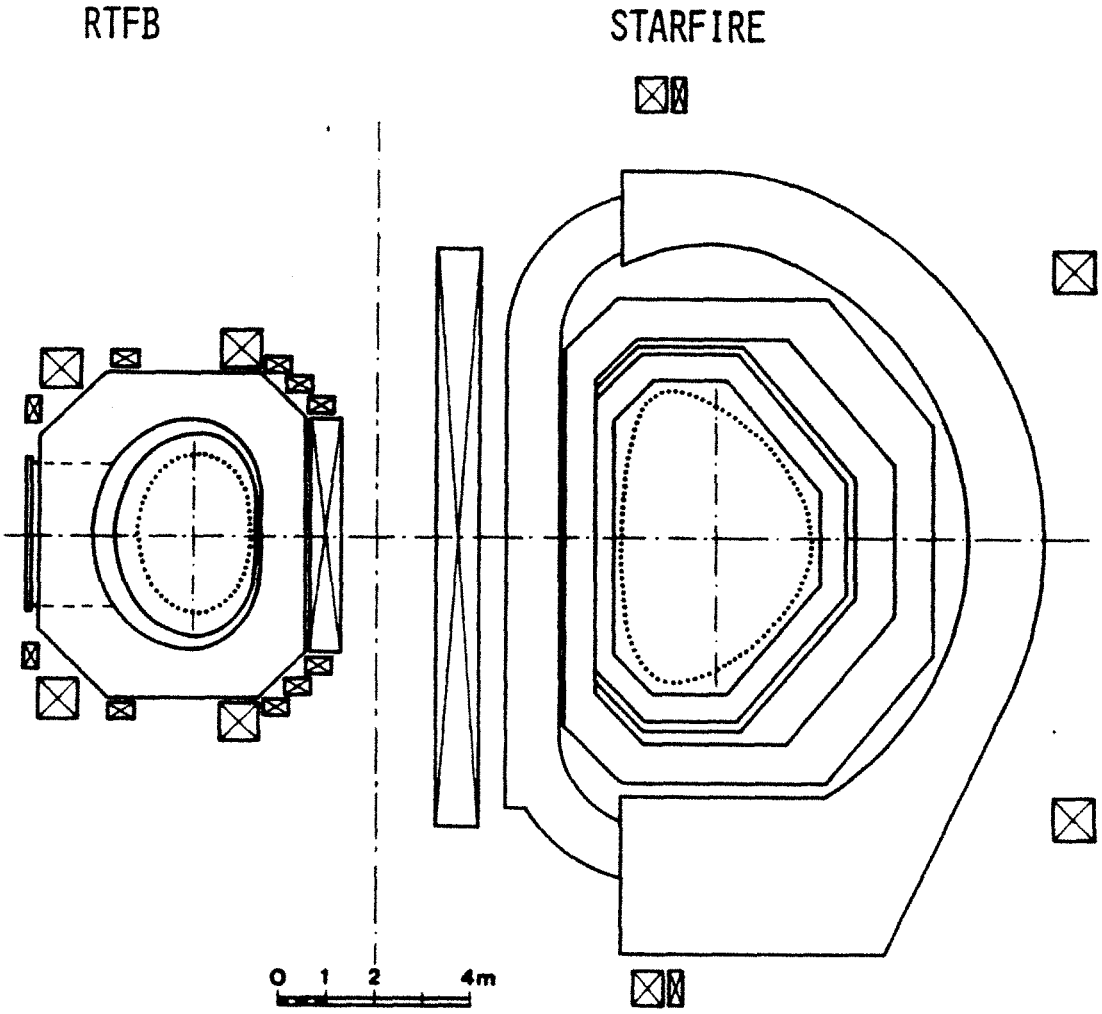

Figure 6.1 Resistive Tokamak Fusion Breeder and STARFIRE Comparison

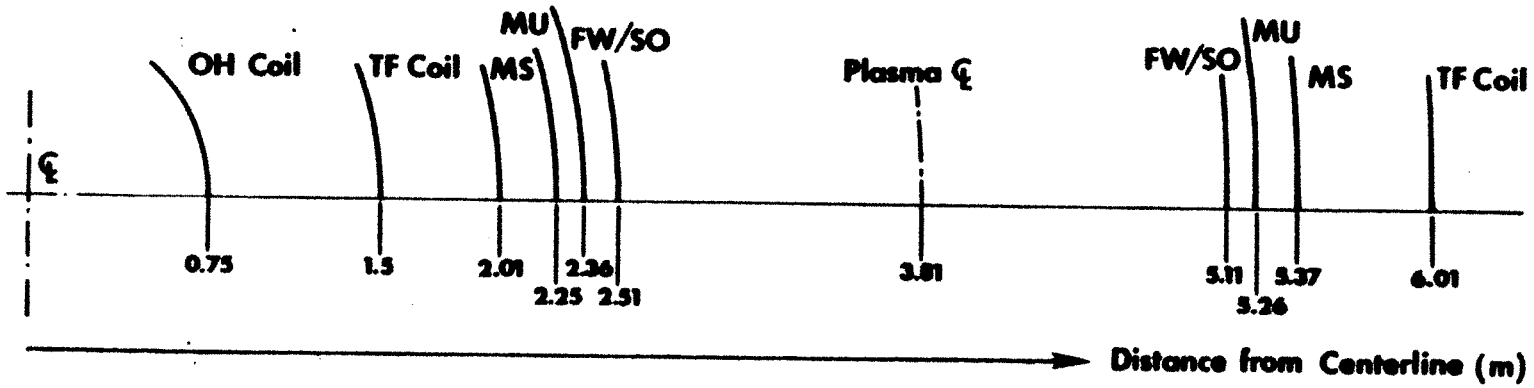

MU=MULTIPLIER
MS=MOLTEN SALT
FW/SO=FIRST WALL/SCRAPE OFF

Figure 6.2 ONEDANT Reference Blanket Model

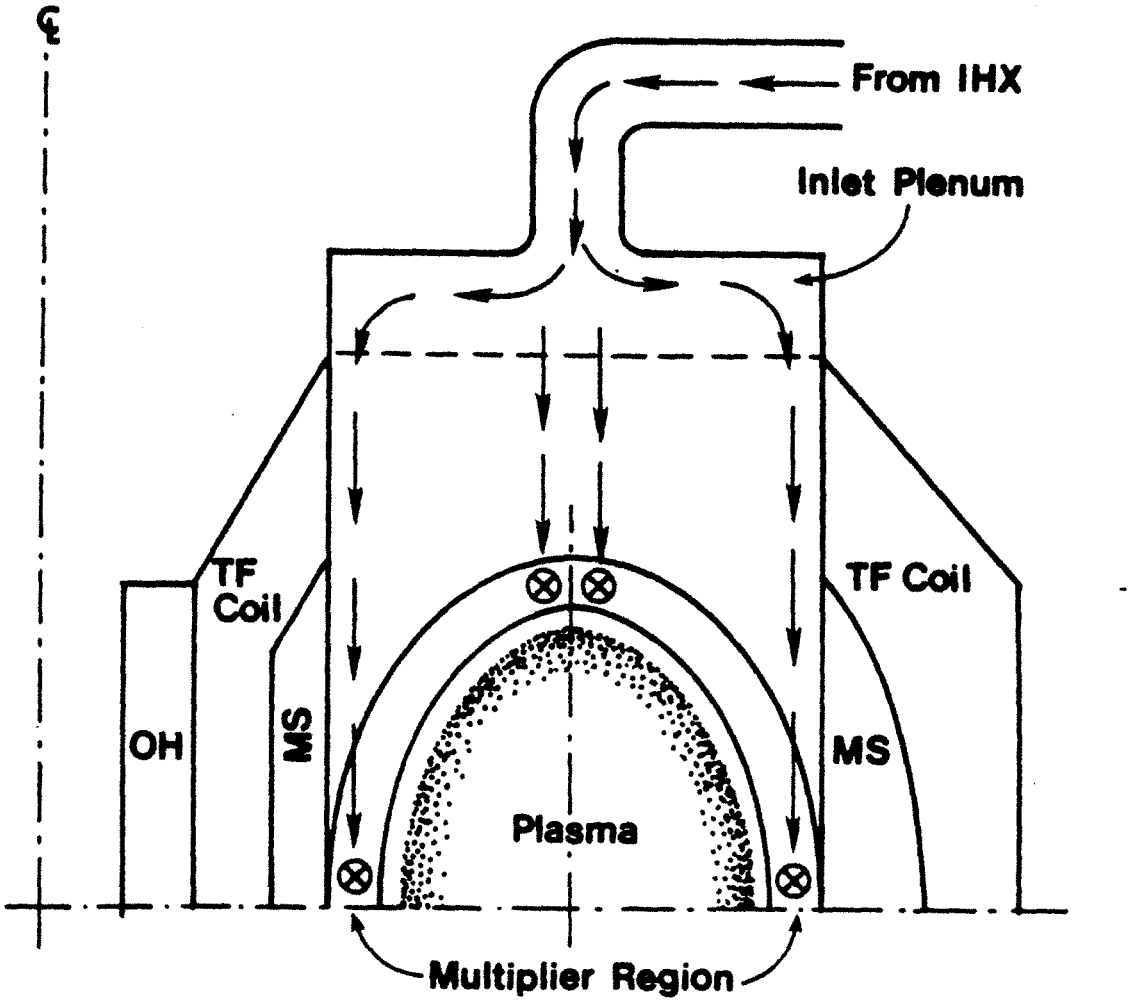

Figure 6.3 Lithium Flow Path - Section View

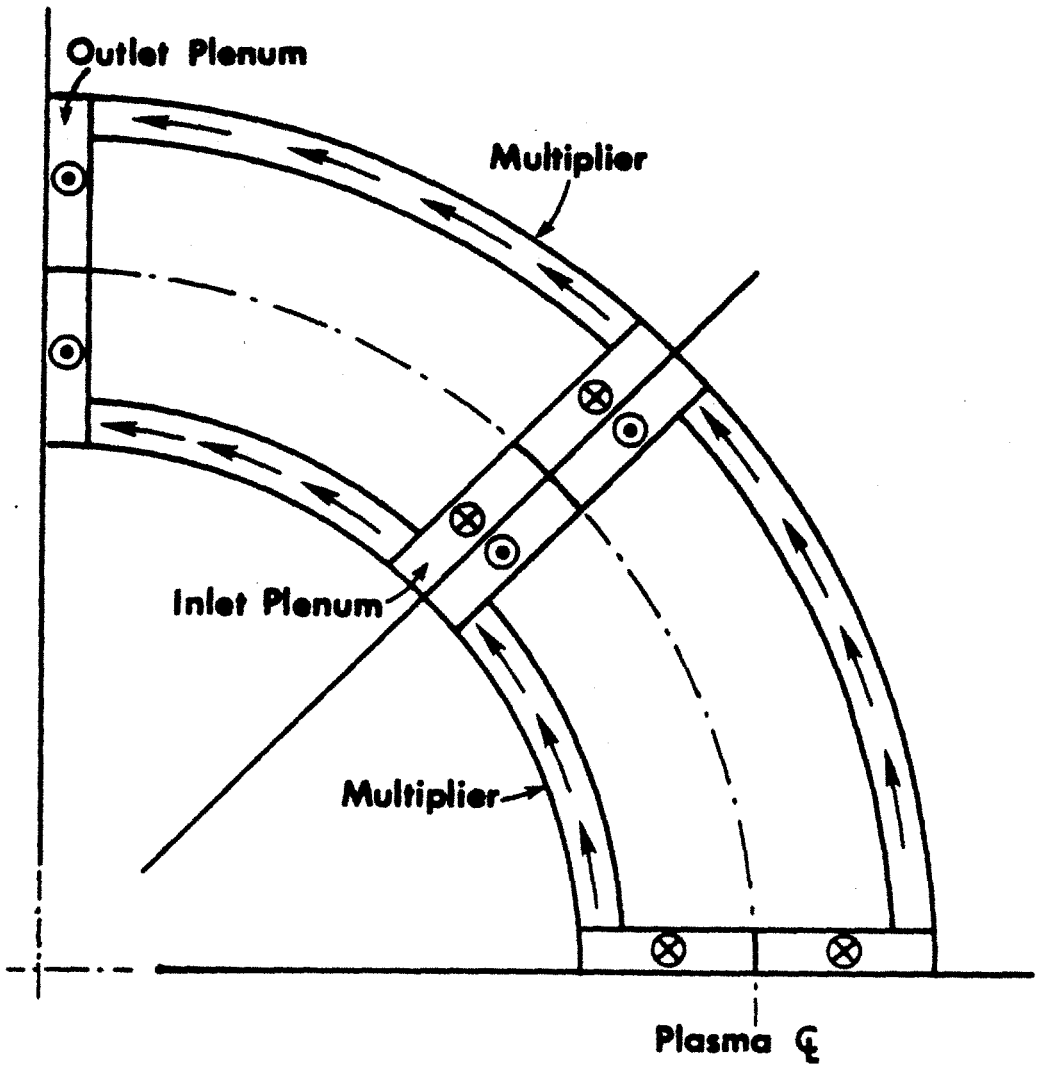

Figure 6.4 Lithium Flow Path - Plan View

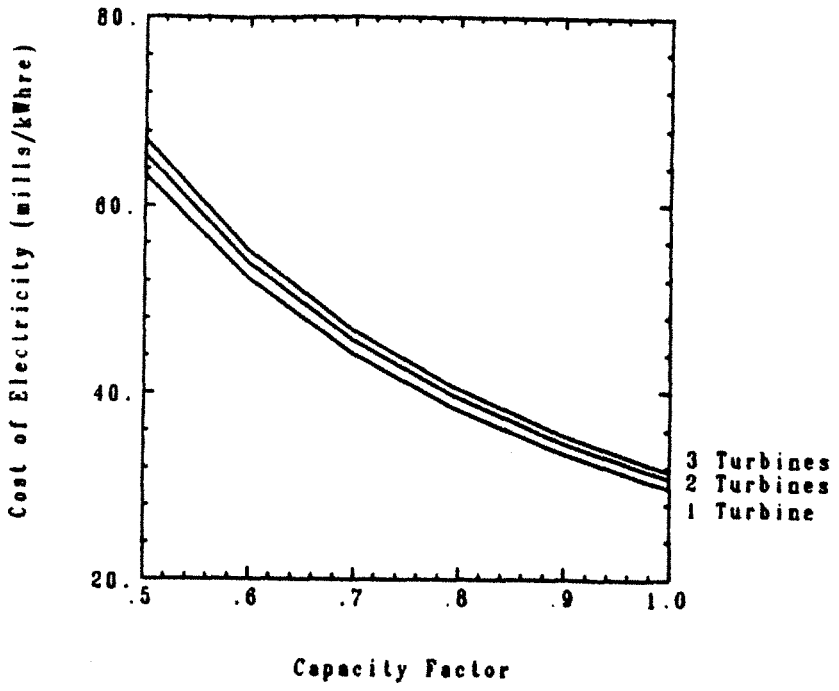

Figure 6.5 Cost of Electricity for Capacity Factor and Number of Turbines

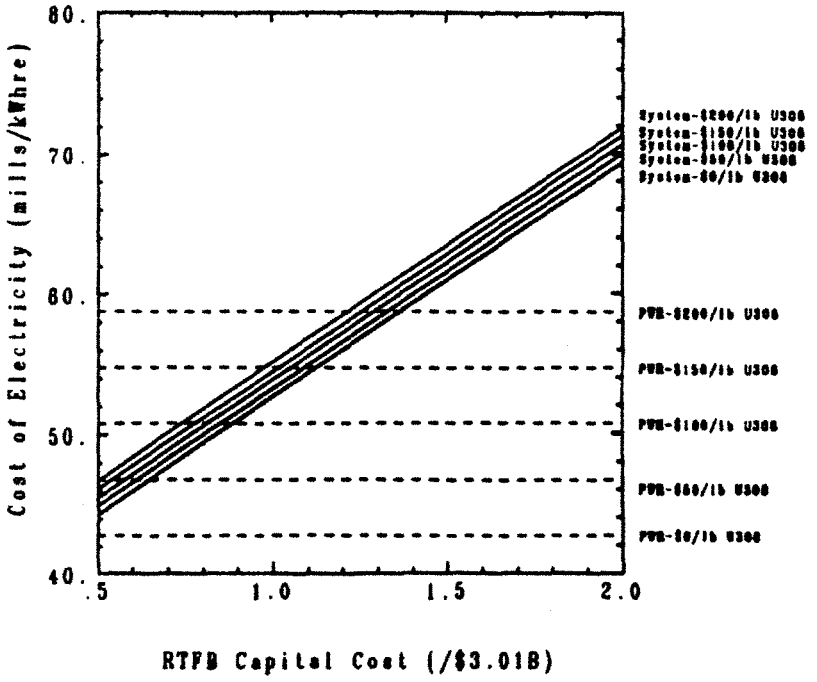

Figure 6.6 Total System Electricity Cost for RTFB Capital Cost and U_3O_8 Cost

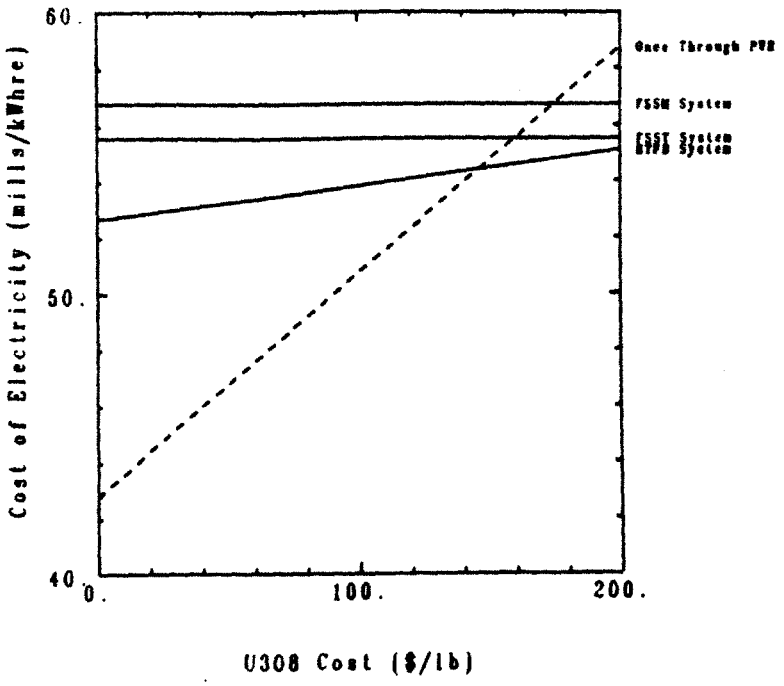

Figure 6.7 Comparison of Levelized Total System Electricity Cost RTFB, FSST and FSSM – No Inflation or U_3O_8 Escalation

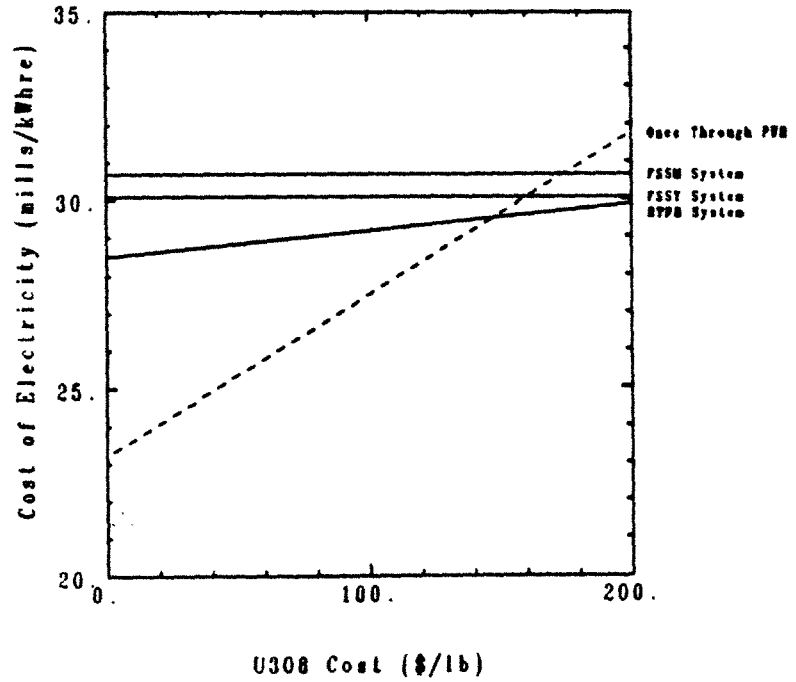

Figure 6.8 Comparison of Average Present Value Total System Electricity Cost RTFB, FSST and FSSM – No Inflation or U_3O_8 Escalation

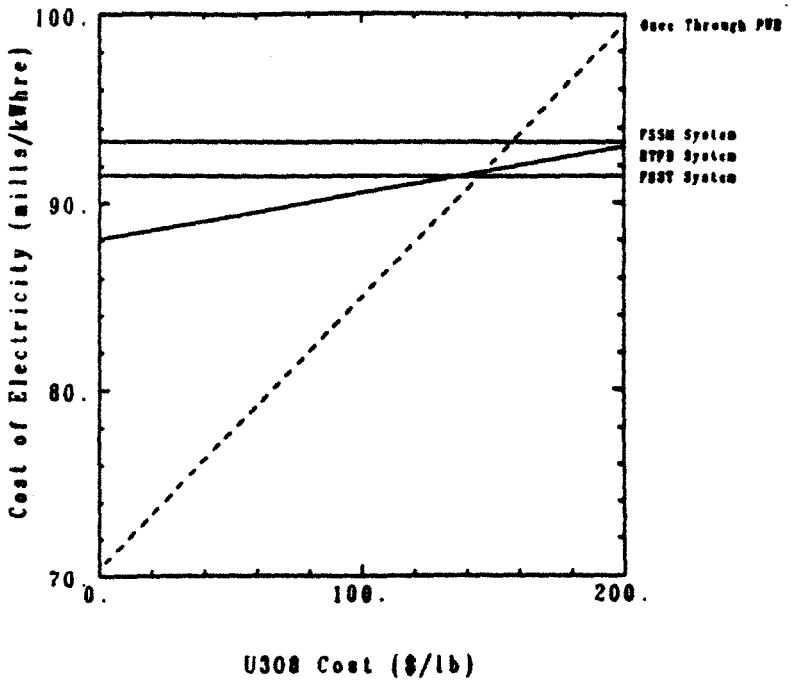

Figure 6.9 Comparison of Levelized Total System Electricity Cost RTFB, FSST and FSSM - Inflation=0.05 - U_3O_8 Escalation=0.00

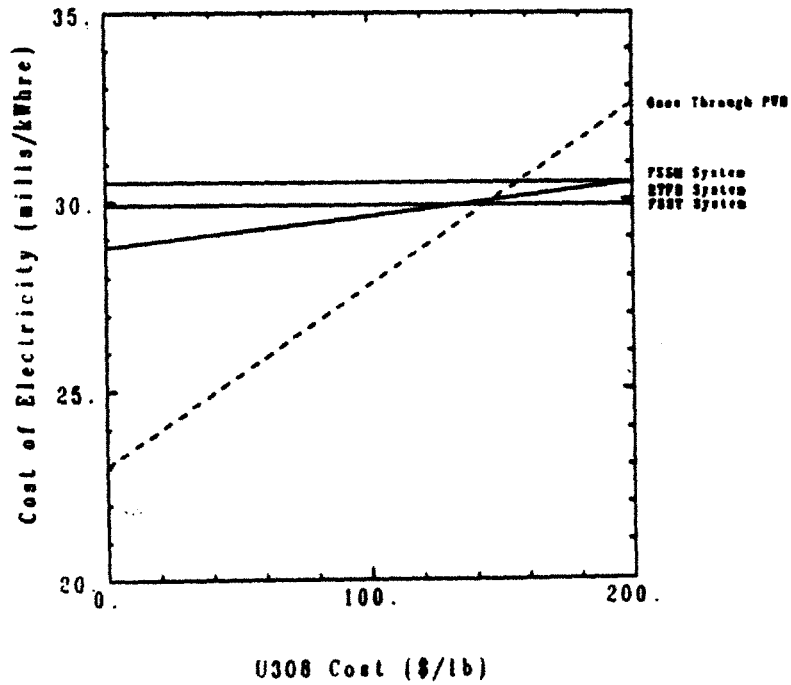

Figure 6.10 Comparison of Average Present Value Total System Electricity Cost RTFB, FSST and FSSM - Inflation=0.05 - U_3O_8 Escalation=0.00

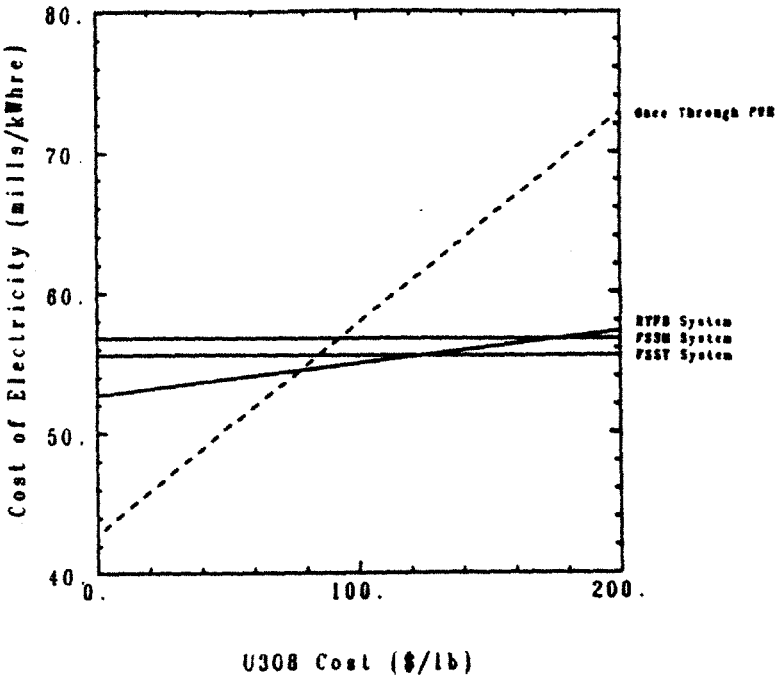

Figure 6.11 Comparison of Levelized Total System Electricity Cost RTFB, FSST and FSSM - Inflation=0.00 - U_3O_8 Escalation=0.05

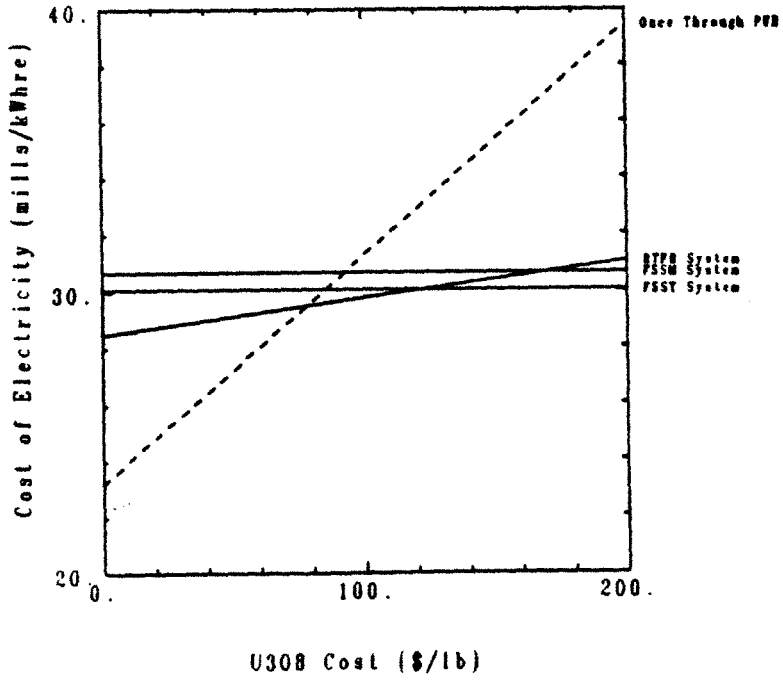

Figure 6.12 Comparison of Average Present Value Total System Electricity Cost RTFB, FSST and FSSM - Inflation=0.00 - U_3O_8 Escalation=0.05

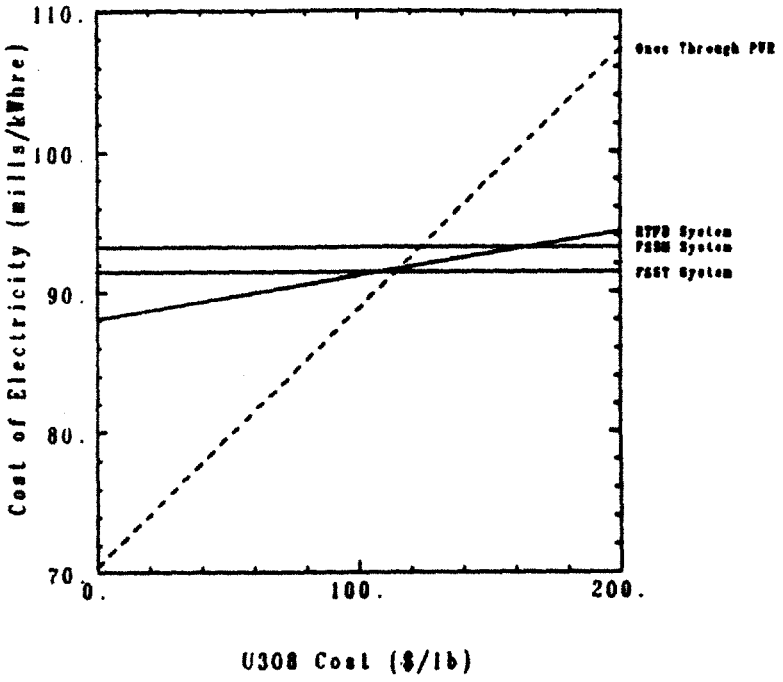

Figure 6.13 Comparison of Levelized Total System Electricity Cost RTFB, FSST and FSSM – Inflation=0.05 – U_3O_8 Escalation=0.02

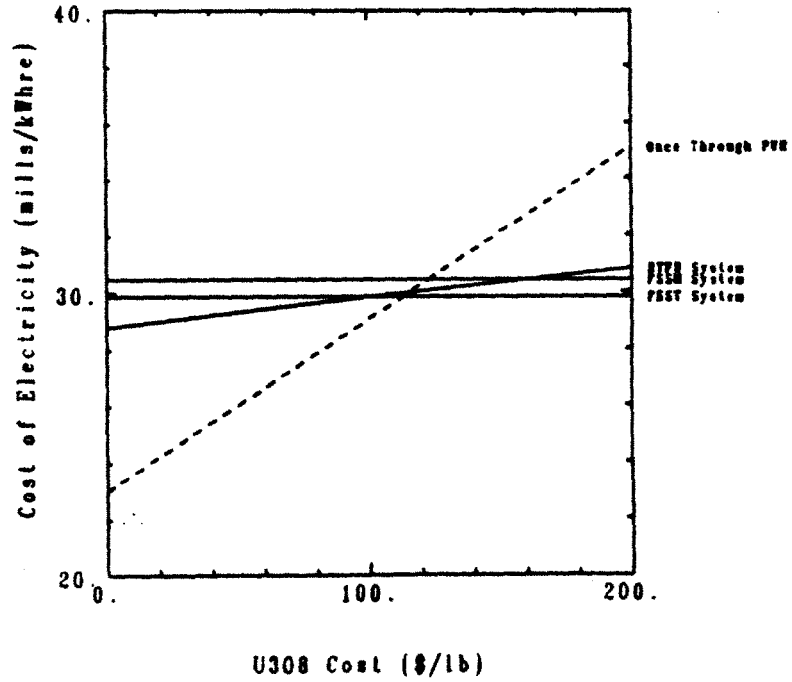

Figure 6.14 Comparison of Average Present Value Total System Electricity Cost RTFB, FSST and FSSM – Inflation=0.05 – U_3O_8 Escalation=0.02

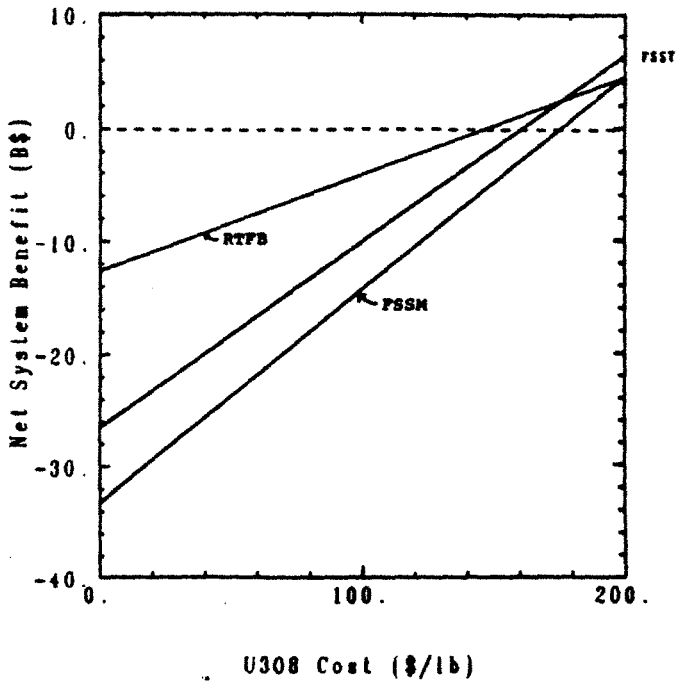

Figure 6.15 Comparison of Net System Benefit RTFB, FSST and FSSM - Inflation=0.00 - U_3O_8 Escalation=0.00

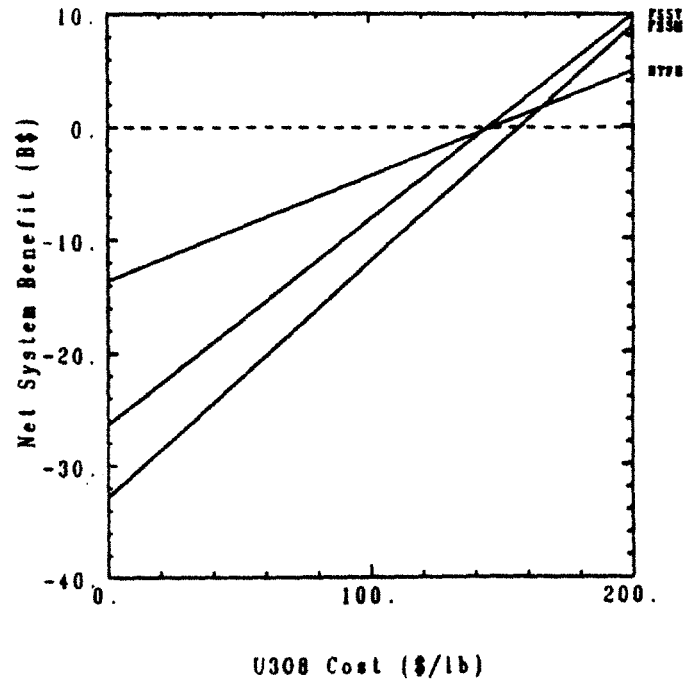

Figure 6.16 Comparison of Net System Benefit RTFB, FSST and FSSM - Inflation=0.05 - U_3O_8 Escalation=0.00

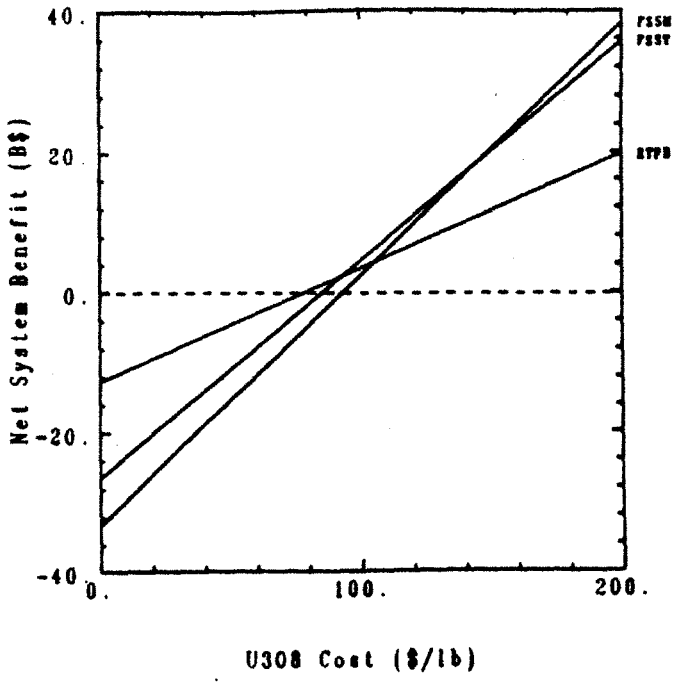

Figure 6.17 Comparison of Net System Benefit
RTFB, FSST and FSSM - Inflation=0.00 - U_3O_8 Escalation=0.05

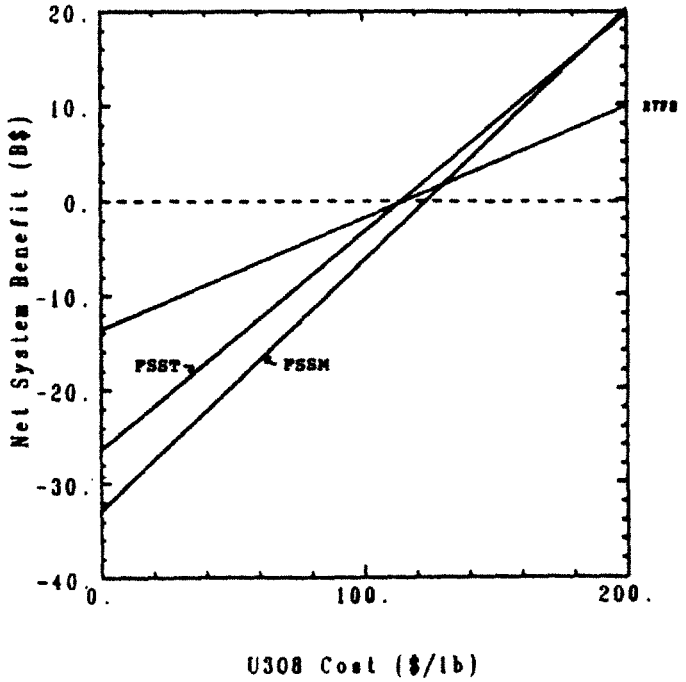

Figure 6.18 Comparison of Net System Benefit
RTFB. FSST and FSSM - Inflation=0.05 - U_3O_8 Escalation=0.02

APPENDIX A. FISSION-SUPPRESSED RESISTIVE MAGNET TOKAMAK

A.1 Introduction

As a supplement to the analysis presented in this thesis, a point analysis was done for a resistive magnet tokamak with a fission-suppressed blanket. This analysis does not represent an optimized design, but an effort to investigate the attractiveness of a resistive magnet tokamak with a fission-suppressed blanket. This machine is called the Fission-Suppressed Resistive magnet Tokamak (FSRT).

A.2 Analysis of the FSRT

The major parameters of the FSRT are summarized in Table A.1. The FSRT fusion power is 5.3 times the fusion power of the RTFB (3260 MW vs. 618 MW) which would allow consideration of a fission-suppressed blanket.

The FSRT was assumed to use the same blanket design used in the Fission-Suppressed Superconducting Tokamak (FSST). The performance of the blanket was assumed to be the same in the FSRT as in the FSST. The performance parameters of the FSRT are summarized in Table A.2. A comparison of the levelized system electricity cost with the machines considered in this thesis is shown in Fig. A.1. From Fig. A.1, it is seen that the FSRT has the same levelized system electricity cost as the fission-suppressed superconducting mirror, which is slightly greater than the RTFB or the FSRT. Thus, the FSRT may be an attractive option for fission-suppressed blanket designs.

TABLE A.1

FSRT Representative Parameters

Plasma Parameters	
Major Radius of Plasma (m)	7.27
Minor Radius of Plasma (m)	2.08
Aspect Ratio	3.50
β	0.060
Plasma Elongation	1.8
Performance × Elongation	8.8
Margin to Ignition × Elongation	6.7
Magnet Field at the Plasma Axis (T)	4.2
Inboard Magnet-Plasma Distance (m)	0.70
Outboard Magnet-Plasma Distance (m)	0.70
Upper and Lower Magnet-Plasma Distance (m)	0.70
Plasma Scrape-Off / First Wall Region (m)	0.15
Fusion Power (MWth)	3260
Magnet Parameters	
Toroidal Field Magnet Height (m)	11.50
Toroidal Field Magnet Inner Radius (m)	2.80
Toroidal Field Magnet Outer Radius (m)	11.35
Mass of Toroidal Field Magnet (Gg)	17.8
Toroidal Field Magnet Power (MWe)	235
Toroidal Field Magnet Stress (MPa)	103
Ohmic Heating Magnet Inner Radius (m)	1.40
Ohmic Heating Magnet Outer Radius (m)	2.80
Volume of Ohmic Heating Magnet (m^3)	138
Mass of Ohmic Heating Magnet (Gg)	1.1
Ohmic Heating Magnet Stress (MPa)	89
Ohmic Heating Magnet Power (MWe)	208
Equilibrium Field Magnet Power (MWe)	282

TABLE A.2

FSRT Economic Analysis

Total Capital Cost (1984M$)	5020
^{233}U Production (kg/yr)	5690
Average Net Electric Output (MWe)	1150
Average Gross Electric Output (MWe)	1820
Levelized System Electricity Cost (mills/kWhre)	93.3

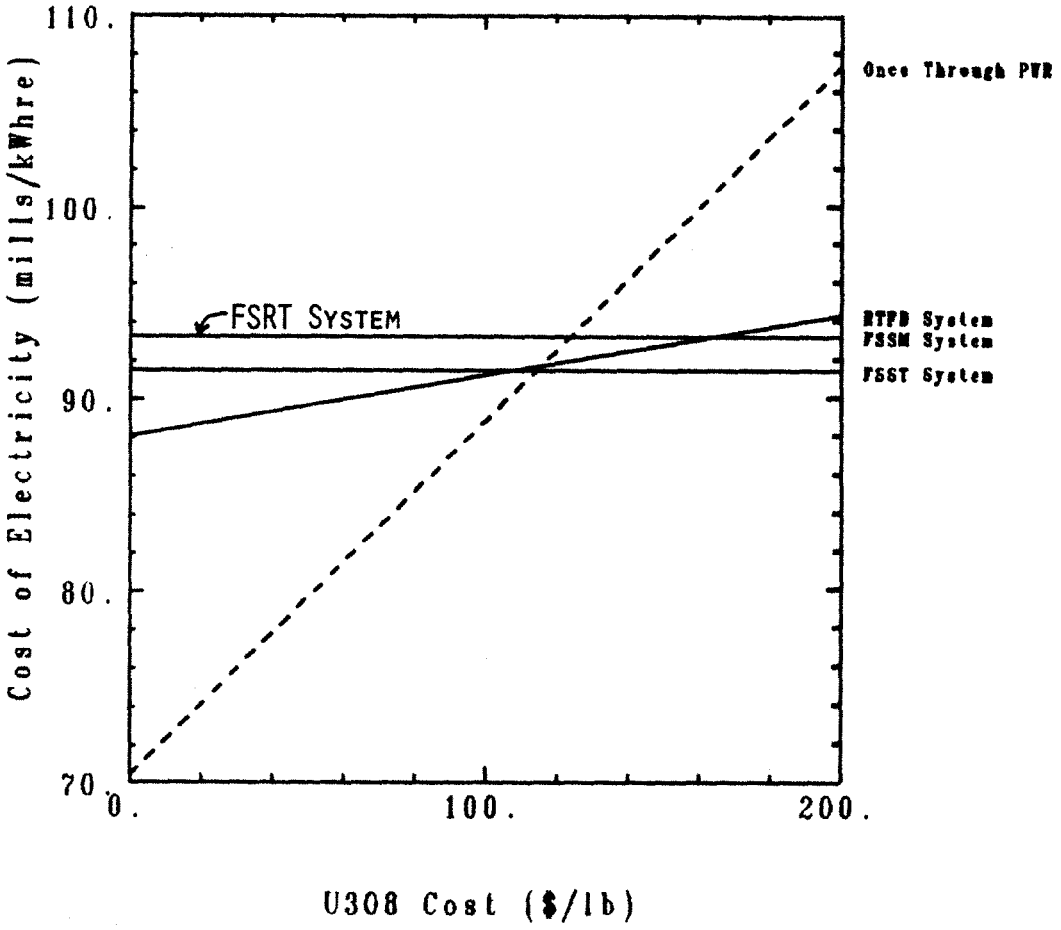

Figure A.1 Comparison of Levelized Total System Electricity Cost Fission-Suppressed Resistive Magnet Tokamak With RTFB, FSST and FSSM - Inflation=0.05 - U_3O_8 Escalation=0.02

APPENDIX B. NUCLEAR ANALYSIS OF THE RESISTIVE MAGNET FUSION BREEDER

B.1 Introduction

This appendix summarizes, in tabular form, the results of the neutronics studies done for the RTFB. These analyses were done with the ONEDANT one-dimensional discrete ordinates transport code and the MCNP three-dimensional Monte Carlo transport code. Sample input for the ONEDANT and MCNP analyses is also given.

B.2 ONEDANT Analyses

A brief description of each of the ONEDANT runs is given in Table B.1. Sample ONEDANT input for the reference case (HPT07) is shown in Table B.2. The results from the breeding calculations are shown in Tables B.3. The insulation damage calculations are shown in Tables B.4 and B.5.

B.3 MCNP Analyses

MCNP analyses were performed to compare to the ONEDANT breeding calculations. These results are shown in Table B.6. Additionally, MCNP three-dimensional analyses were done to estimate the breeding and blanket energy deposition for a more geometrically realistic configuration. Sample input for the three-dimensional MCNP calculation is shown in Table B.7. A schematic of the MCNP poloidal segmentation is shown in Fig. B.1. The results of the three-dimensional calculations are shown in Tables B.8 and B.9.

TABLE B.1

ONEDANT Descriptions

HPT07 Reference case.

HPT08 Inboard molten salt replaced by stainless steel.

HPT09 Inboard molten salt and multiplier replaced by stainless steel.

HPT10 Inboard molten salt and multiplier replaced by lead.

HPT11 Inboard molten salt and multiplier replaced by lead, outboard multiplier thickness increased from 11 cm. to 16 cm.

HPT12 Inboard molten salt and multiplier replaced by lead, outboard multiplier lithium changed to 100% ^{6}Li.

HPT13 Inboard molten salt and multiplier replaced by tungsten.

HPT14 Inboard blanket thickness reduced from 35 cm. to 30 cm.

HPT15 Inboard blanket thickness reduced from 35 cm. to 25 cm.

HPT16 Inboard blanket thickness reduced from 35 cm. to 20 cm.

HPT17 Inboard blanket thickness reduced from 35 cm. to 15 cm.

HPT18 Outboard blanket thickness reduced from 75 cm. to 65 cm.

HPT19 Outboard blanket thickness increased from 75 cm. to 85 cm.

HPT20 Natural Li composition in molten salt.

TABLE B.1 (Continued)

ONEDANT Descriptions

HPT21 Molten salt replaced by TF coil.

HPT22 Inboard blanket replaced by 34 cm. tungsten, 1 cm. stainless steel.

HPT23 Inboard blanket replaced by 24 cm. tungsten, 1 cm. stainless steel, major radius decreases.

HPT24 Inboard blanket replaced by 14 cm. tungsten, 1 cm. stainless steel, major radius decreases.

HPT25 Inboard blanket replaced by 4 cm. tungsten, 1 cm. stainless steel, major radius decreases.

HPT26 HPT22 with composite shield.

HPT27 HPT22 with 0.9 v/o uranium inboard.

HPT28 HPT22 with 0.9 v/o tungsten inboard.

HPT29 HPT22 with 0.9 v/o uranium and 0.1 v/o water inboard.

HPT30 HPT22 with 0.9 v/o tungsten and 0.1 v/o water inboard.

HPT31 Inboard molten salt and multiplier replaced by 17 cm. uranium followed by 17.5 cm. composite shield.

HPT32 HPT07 with 0.01 a/o ^{239}Pu added to multiplier.

TABLE B.1 (Continued)

ONEDANT Descriptions

HPT33 HPT32 with depleted uranium in multiplier.

HPT34 HPT07 with depleted uranium in multiplier.

HPT35 HPT07 with 0.6 theoretical density uranium, added insulation to tf coil.

HPT36 HPT07 with 1.0 theoretical density uranium, added insulation to tf coil.

HPT37 HPT36 with 0.01 a/o ^{239}Pu for k_{eff}.

HPT38 HPT07 with 0.02 a/o ^{239}Pu.

HPT39 HPT33 with 0.01 a/o ^{239}Pu.

HPT40 HPT37 with 0.02 a/o ^{239}Pu for k_{eff}.

TABLE B.2

Sample ONEDANT Input

```
     1
hpt07 - resistive magnet tokamak - reference blanket
igeom=2  ngroup=42 isn=12  niso=24  mt=9
nzone=13  im=19  it=196
maxscm=50000 maxlcm= 250000
/  noexec= 1 1 0
  t
xmesh= 0.0 20.0 75.0 150.0 201.0 201.5 224.0 224.5 235.5 236.0 251.0
  381.0 511.0 526.0 526.5 537.5 538.0 600.5 601.0 751.0
xints= 10 5 20 20  2 15 2 11 2 3 13 13 3 2 11 2 30 2 30
zones= 0 0 1 2 3 4 5 6 7 0 0 0 0 8 9 10 11 12 13
  t
lib=xslib
kwikrd=0
savbxs= 1
maxord=3  ihm=52 iht=10 ifido=1 ititl=1
names= h li6 li7 be b10 b11 c o f na si ti cr mn fe ni cu mo w pb
  th u233 u235 u238
edname= ngam nfis nt n2n n3n nheat gheat
  t
matls=  water  h  6.687e-2  o  3.343e-2  ;
/  new li salt 7/19/83
  lisalt li6 1.852e-4 li7 1.833e-2 be 5.216e-4 th 7.042e-3 f 4.773e-2 ;
  unat u235 3.417e-4 u238 4.773e-2 ;
  udep u235 9.614e-5 u238 4.797e-2 ;
  lithe li6 2.871e-2 li7 1.231e-2 ;
  iron fe 8.490e-2 ;
  ss316 c 1.990e-4 si 1.360e-3 ti 4.980e-5 cr 1.150e-2 mn 1.650e-3
    fe 5.430e-2 ni 1.060e-2 mo 1.290e-3 ;
  copr cu 0.0829 ;
  graf c 1.128e-1
assign=  oh copr 0.95 water 0.05 ;
  itf copr 0.95 water 0.05 ;
  w1 iron 1.0 ;
  ibkt lisalt 1.0 ;
  w2 iron 1.0 ;
  imult unat 0.63 lithe 0.24 ss316 0.13 ;
  w3 iron 1.0 ;
  w4 iron 1.0 ;
  omult unat 0.63 lithe 0.24 ss316 0.13 ;
  w5 iron 1.0 ;
  obkt lisalt 1.0 ;
  w6 iron 1.0 ;
  obtf water 0.05 copr 0.40 ss316 0.55
  t
ievt=-1  isct=3 fluxp=1 sourcp=3
iquad=4 iitl=30 iitm=50 norm=1.0
chi= 8.46734e-5 1.63357e-4 4.65778e-4 2.13636e-3 9.82692e-3 2 63255e-2
     1.32240e-1 1.03080e-1 1.14231e-1 1.13900e-1 1.04230e-1 1.62929e-1
     1.04707e-1 6.05544e-2 3.24279e-2 2.53146e-2 5.79024e-3 1.24759e-3
     2.72354e-4 5.85389e-5 1.29888e-5 1.27421e-6 6.37776e-9 7r 0.0
     f 0.0
source= 0.0 1.0 28r 0.0  f 0.0
sourcx= 90r 0.0 26r 1.0 f 0.0
  t
zned=1
edxs= ngam nfis nt n2n n3n nheat gheat
edisos= h o li6 li7 be f th c si ti cr mn fe ni mo cu u235 u238
edcons= h o li6 li7 be f th c si ti cr mn fe ni mo cu u235 u238
micsum=    li6,li7,be,th,f,0,ngam,0,
```

TABLE B.2 (Continued)

Sample ONEDANT Input

```
 li6,li7,be,th,f,0,nfis,0,
 li6,li7,be,th,f,0,nt,0,
 li6,li7,be,th,f,0,n2n,0,
 c,si,ti,cr,mn,fe,ni,mo,0,ngam,0,
 c,si,ti,cr,mn,fe,ni,mo,0,nt,0,
 c,si,ti,cr,mn,fe,ni,mo,0,n2n,0
t
```

TABLE B.3

ONEDANT Breeding Calculations

Identifier	HPT07	HPT08	HPT09	HPT10	HPT11
Inboard					
^{6}T	0.2593	0.2632	-	-	-
^{7}T	0.0056	0.0023	-	-	-
^{233}F	0.1814	-	-	-	-
^{239}F	0.2966	0.2974	-	-	-
Fissions	0.1417	0.1414	-	-	-
MS Heating	1.92+6	1.48+6	1.77+6	8.00+5	8.09+5
Mult. Heating	3.24+7	3.27+7	2.95+6	1.68+6	1.69+6
Outboard					
^{6}T	0.6831	0.6962	0.6951	0.7729	0.9617
^{7}T	0.0211	0.0211	0.0210	0.0211	0.0151
^{233}F	0.6704	0.6783	0.6621	0.7218	0.5035
^{239}F	0.7697	0.7847	0.8068	0.8901	1.0814
Fissions	0.4506	0.4515	0.4440	0.4584	0.5277
MS Heating	7.08+6	7.12+6	1.77+6	7.40+6	4.61+6
Mult. Heating	1.01+8	1.01+8	2.95+6	1.04+8	1.21+8
Total					
^{6}T	0.9424	0.9594	0.6951	0.7729	0.9617
^{7}T	0.0267	0.0234	0.0210	0.0211	0.0151
$^{6}T + ^{7}T$	0.9691	0.9828	0.7161	0.7940	0.9768
^{233}F	0.8518	0.6783	0.6621	0.7218	0.5035
^{239}F	1.0663	1.0821	0.8068	0.8901	1.0814
$^{233}F + ^{239}F$	1.9181	1.7604	1.4689	1.6119	1.5849
T+F	2.8872	2.7432	2.1850	2.4059	2.5617
Fissions	0.5923	0.5929	0.4440	0.4584	0.5277
MS Heating	9.00+6	8.60+6	8.75+6	8.20+6	5.42+6
Mult. Heating	1.33+8	1.34+8	1.03+8	1.06+8	1.22+8
Total Heating	1.42+8	1.43+8	1.12+8	1.14+8	1.27+8
Thermal Power	4986	5021	3930	4003	4460

TABLE B.3 (Continued)

ONEDANT Breeding Calculations

Identifier	HPT12	HPT13	HPT14	HPT15	HPT16
Inboard					
^{6}T	-	-	0.2561	0.2523	0.2471
^{7}T	-	-	0.0053	0.0048	0.0041
^{233}F	-	-	0.1562	0.1214	0.0766
^{239}F	-	-	0.2940	0.2909	0.2860
Fissions	-	-	0.1402	0.1385	0.1366
MS Heating	7.71+5	1.43-6	1.73+6	1.45+6	1.05+6
Mult. Heating	1.66+6	4.38-6	3.21-7	3.18+7	3.14+7
Outboard					
^{6}T	0.9563	0.6712	0.6853	0.6877	0.6903
^{7}T	0.0133	0.0207	0.0212	0.0213	0.0214
^{233}F	0.6627	0.6442	0.6728	0.6754	0.6781
^{239}F	0.7730	0.7587	0.7723	0.7750	0.7779
Fissions	0.4516	0.4356	0.4518	0.4532	0.4545
MS Heating	7.04+6	6.83+6	7.10+6	7.13+6	7.17+6
Mult. Heating	1.03+8	9.79+7	1.01+8	1.02+8	1.02+8
Total					
^{6}T	0.9563	0.6712	0.9414	0.9400	0.9374
^{7}T	0.0133	0.0207	0.0265	0.0261	0.0255
$^{6}T + ^{7}T$	0.9696	0.6919	0.9679	0.9661	0.9629
^{233}F	0.6627	0.6442	0.8290	0.7968	0.7547
^{239}F	0.7730	0.7587	1.0663	1.0659	1.0639
$^{233}F + ^{239}F$	1.4357	1.4029	1.8953	1.8627	1.8186
T+F	2.4053	2.0948	2.8632	2.8288	2.7815
Fissions	0.4516	0.4356	0.5920	0.5917	0.5911
MS Heating	7.81+6	8.26+6	8.83+6	8.58+6	8.22+6
Mult. Heating	1.05+8	1.02+8	1.33+8	1.34+8	1.33+8
Total Heating	1.13+8	1.10+8	1.42+8	1.43+8	1.41+8
Thermal Power	3970	3860	5005	5040	4951

TABLE B.3 (Continued)

ONEDANT Breeding Calculations

Identifier	HPT17	HPT18	HPT19	HPT20	HPT21
Inboard					
^{6}T	0.2392	0.2593	0.2593	0.3062	0.2470
^{7}T	0.0030	0.0056	0.0056	0.0054	0.0023
^{233}F	0.0259	0.1814	0.1814	0.1486	-
^{239}F	0.2745	0.2966	0.2966	0.2879	0.1865
Fissions	0.1340	0.1417	0.1417	0.1413	0.0877
MS Heating	4.37+5	1.92+6	1.92+6	2.00−6	-
Mult. Heating	3.10+7	3.24+7	3.24+7	3.23+7	2.01+7
Outboard					
^{6}T	0.6938	0.6830	0.6831	0.8490	0.6469
^{7}T	0.0215	0.0211	0.0211	0.0202	0.0077
^{233}F	0.6816	0.6658	0.6720	0.5288	-
^{239}F	0.7814	0.7698	0.7697	0.7460	0.7347
Fissions	0.4559	0.4505	0.4506	0.4496	0.4398
MS Heating	7.20−6	7.04+6	7.09+6	7.22+6	8.04+6
Mult. Heating	1.02+8	1.01+8	1.01+8	1.01+8	1.13+8
Total					
^{6}T	0.9330	0.9423	0.9424	1.1552	0.8939
^{7}T	0.0245	0.0267	0.0267	0.0256	0.0100
$^{6}T - ^{7}T$	0.9575	0.9690	0.9691	1.1808	0.9039
^{233}F	0.7075	0.8472	0.8534	0.6774	-
^{239}F	1.0559	1.0664	1.0663	1.0339	1.0117
$^{233}F - ^{239}F$	1.7634	1.9136	1.9197	1.7113	1.0117
T−F	2.7209	2.8826	2.8888	2.8921	1.9084
Fissions	0.5899	0.5922	0.5923	0.5909	0.5780
MS Heating	7.64−6	8.96−6	9.01+6	9.22−6	-
Mult. Heating	1.33−8	1.33+8	1.33+8	1.34−8	1.32+8
Total Heating	1.41−8	1.42+8	1.42+8	1.42−8	1.32+8
Thermal Power	4970	4990	4990	4990	4640

TABLE B.3 (Continued)

ONEDANT Breeding Calculations

Identifier	HPT32	HPT33	HPT34	HPT35	HPT36
Inboard					
^{6}T	0.2827	0.2744	0.2522	0.2356	0.2592
^{7}T	0.0057	0.0056	0.0055	0.0083	0.0056
^{233}F	0.1992	0.1922	0.1753	0.1914	0.1815
^{239}F	0.3212	0.3145	0.2910	0.1733	0.2967
^{239}Pu abs.	0.0307	0.0300	–	–	–
Fissions	0.1785	0.1621	0.1274	0.0992	0.1417
MS Heating	2.09+6	2.01+6	1.86+6	2.43+6	1.92+6
Mult. Heating	4.00+7	3.67+7	2.96+7	2.27+7	3.24+7
Outboard					
^{6}T	0.7399	0.7199	0.6658	0.6174	0.6831
^{7}T	0.0214	0.0212	0.0210	0.0321	0.0211
^{233}F	0.7279	0.7053	0.6506	0.7203	0.6704
^{239}F	0.8286	0.8131	0.7567	0.4456	0.7697
^{239}Pu abs.	0.0821	0.0800	–	–	–
Fissions	0.5472	0.5046	0.4132	0.3170	0.4506
MS Heating	7.57−6	7.35−6	6.89−6	9.13+6	7.08+6
Mult. Heating	1.21−8	1.12−8	9.36−7	7.08+7	1.01+8
Total					
^{6}T	1.0226	0.9943	0.9180	0.8530	0.9423
^{7}T	0.0271	0.0268	0.0265	0.0404	0.0267
$^{6}T - ^{7}T$	1.0497	1.0211	0.9445	0.8934	0.9690
^{233}F	0.9271	0.8975	0.8259	0.9117	0.8519
^{239}F	1.1498	1.1276	1.0477	0.6189	1.0664
^{239}Pu abs.	0.1128	0.1100	–	–	–
$^{239}F_{net}$	1.0370	1.0176	1.0477	0.6189	1.0664
$^{233}F - ^{239}F_{net}$	1.9641	1.9151	1.8736	1.5306	1.9183
T−F	2.9867	2.9362	2.8181	2.4240	2.8873
Fissions	0.7257	0.6667	0.5406	0.4162	0.5923
MS Heating	9.66−6	9.36+6	8.75−6	1.16−7	9.00+6
Mult. Heating	1.61+8	1.49+8	1.23+8	9.35−7	1.33+8
Total Heating	1.71+8	1.58+8	1.32+8	1.05+8	1.42+8
Thermal Power	6030	5570	4640	3700	4990

TABLE B.4

ONEDANT Insulation Damage Calculation
Energy Deposition in Insulation
Plasma Side, Inboard Leg of TF Coil
Varying Tungsten Thickness

Identifier	HPT22	HPT23	HPT24	HPT25
Neutron*	1.45	6.76	29.4	119.4
Gamma	1.07	4.07	13.4	40.3
Total	2.52	10.8	42.8	159.7

*eV/sec/cm^3 per source n/sec/cm

TABLE B.5

Energy Deposition in Insulation
Plasma Side, Inboard Leg of TF Coil

Identifier	Neutron*	Gamma*	Total*
HPT22	1.45	1.07	2.52
HPT26	0.35	0.18	0.53
HPT27	11.62	4.29	15.91
HPT28	2.46	1.71	4.17
HPT29	2.54	1.10	3.64
HPT30	0.43	0.27	0.70

*eV/sec/cm^3 per source n/sec/cm

TABLE B.6

MCNP One-Dimensional Breeding Calculations

Identifier	HP101A	HP102A	HP103A
Inboard MS			
^{6}T	0.0318(0.0280)	0.0073(0.0572)	0.0119(0.0441)
^{7}T	0.0236(0.0330)	0.0002(0.3283)	0.0029(0.0958)
^{233}F	0.4474(0.0180)	0.1020(0.0367)	0.1759(0.0303)
Fissions	0.0133	0.0008	0.0009
Inboard Mult.			
^{6}T	0.4331(0.0143)	0.1719(0.0210)	0.2493(0.0183)
^{7}T	0.0072(0.0112)	0.0002(0.1004)	0.0019(0.0353)
^{239}F	0.4809(0.0145)	0.1918(0.0212)	0.2837(0.0185)
Fissions	0.4314	0.0393	0.1336
Outboard MS			
^{6}T	0.0181(0.0311)	0.0502(0.0209)	0.0407(0.0221)
^{7}T	0.0010(0.1795)	0.0272(0.0352)	0.0134(0.0510)
^{233}F	0.2992(0.0247)	0.7991(0.0144)	0.6649(0.0167)
Fissions	0.0012	0.0154	0.0075
Outboard Mult.			
^{6}T	0.3845(0.0168)	0.6458(0.0133)	0.6446(0.0126)
^{7}T	0.0005(0.0637)	0.0077(0.0116)	0.0069(0.0157)
^{239}F	0.4394(0.0169)	0.7256(0.0133)	0.7248(0.0120)
Fissions	0.0890	0.4861	0.4281
Total			
^{6}T	0.8657	0.8752	0.9465
^{7}T	0.0323	0.0353	0.0251
$^{6}T + ^{7}T$	0.8980	0.9105	0.9716
^{233}F	0.7466	0.9011	0.8408
^{239}F	0.9203	0.9174	1.0085
$^{233}F + ^{239}F$	1.6669	1.8185	1.8493
T+F	2.5649	2.7290	2.8290
Fissions	0.5349	0.5416	0.5701

TABLE B.7

Sample MCNP Input

```
*file name=hp309a
mcnp 3-d model - 14.1 mev uniform source
c       cell cards
     1  0  -1  +15
     2  0  +1  -2  +15
     3  1 -7.98  +2  -3  +15
     4  2 -13.11  +3  -4  +15
     5  1 -7.98  +4  -5  +15
     6  3 -4.44  +5  -6  +11  +15
     7  1 -7.98  +6  -7  +10  +15
     8  0  -8  -14  +15
     9  4 -8.56  +8  -9  -14  +15
    10  4 -8.56  +9  -10  -14  +15
    11  4 -8.56  +7  +11  -12  -14
    12  5 -7.96  +7  +12  -13  -14  +15
    13  1 -7.98  -6  +10  -11  +15
    14  4 -8.56  +7  +10  -11  -14
    15  0  +14  -13
    16  0  +13  +15
    17  0  -15

c       surface cards
     1  tz 0.0 0.0 0.0 381.0 208.0 130.0
     2  tz 0.0 0.0 0.0 381.0 223.0 145.0
     3  tz 0.0 0.0 0.0 381.0 223.5 145.5
     4  tz 0.0 0.0 0.0 381.0 234.5 156.5
     5  tz 0.0 0.0 0.0 381.0 235.0 157.0
     6  tz 0.0 0.0 0.0 381.0 297.5 219.5
     7  tz 0.0 0.0 0.0 381.0 298.0 220.0
     8  cz 75.0
     9  cz 150.0
    10  cz 201.0
    11  cz 201.5
    12  cz 381.0
    13  cz 751.0
    14  pz 400.0
   *15  pz 0.0
c       the following surfaces are for segmenting poloidally
    20  z  0.0  381.0   70.5998  503.2824   78.3751  516.7498
    21  z  0.0  381.0  152.7871  469.2117  166.7521  477.2744
    22  z  0.0  381.0  152.7871  292.7883  166.7521  284.7256
    23  z  0.0  381.0   70.5998  258.7176   78.3751  245.2504
    24  cz 380.9

    in  1 1 1 1 1 1 1 1 1 1 1 1 1 0 0 0
  src4  0.0 0.0 0.0 1 1 250.9 511.1 208.1 0.0 0.0 1.0
    si  14.1 14.1
    sp  0 1
c        void
    e0  1.0e-5 0.01 1.0 10.0 14.0 15.0
  drxs  1001 8016 14000 22000 24000 25055 26000 28000 29000 42000
print
    c0  0.0 1.0 t
    f1  2
   fs1  -23 -22  -24  -21 -20 t
   fc1  poloidal variation of first wall current - inboard to outboard
    f2  2
   fs2  -23 -22  -24  -21 -20 t
   fc2  poloidal variation of first wall flux - inboard to outboard
    f4  4
```

TABLE B.7 (Continued)

Sample MCNP Input

```
   fs4  -23 -22  -24  -21 -20 t
   fc4  poloidal variation of breeding in multiplier region
        inboard to outboard - f-239 t-6 t-7
   fm4  ( 3.007e-2 6 (102))  ( 6.890e-3 7 (205))  ( 2.954e-3 8 (205))
   f24  6
  fs24  -23 -22  -24  -21 -20 t
  fc24  poloidal variation of breeding in molten salt region
        inboard to outboard - t-6 t-7 f-233
  fm24  ( 1.852e-4 9 (205))  ( 1.833e-2 10 (205))  ( 7.042e-3 11 (102))
   sd4  ( 1 1 1 1 1 1 1 1 )
  sd24  ( 1 1 1 1 1 1 1 1 )
c       material cards
c       ss316
    m1  6012 1.990e-4 14000 1.360e-3 22000 4.980e-5 24000 1.150e-2
        25055 1.650e-3 26000 5.430e-2 28000 1.060e-2 42000 1.290e-3
c       multiplier region - 0.63 u, 0.24 lithe, 0.13 ss316
    m2  92235 2.153e-4 92238 3.007e-2 3006 6.890e-3 3007 2.954e-3
        6012 2.587e-5 14000 1.768e-4 22000 6.474e-6 24000 1.495e-3
        25055 2.145e-4 26000 7.059e-3 28000 1.378e-3 42000 1.677e-4
c       molten salt
    m3  3006 1.852e-4 3007 1.833e-2 4009 5.216e-4 9019 4.733e-2
        90232 7.042e-3
c       inboard tf/oh mixture
    m4  29000 8.066e-2 1001 3.344e-3 8016 1.672e-3
c       outboard tf mixture
    m5  26000 4.670e-2 29000 3.396e-2 1001 3.344e-3 8016 1.672e-3
c       the following materials are for edits
c       edits for multiplier region
    m6  92238 3.007e-2
    m7  3006 6.890e-3
    m8  3007 2.954e-3
c       edits for molten salt region
    m9  3006 1.852e-4
   m10  3007 1.833e-2
   m11  90232 7.042e-3
   nps  5000
*mcnp inp=hp309a outp=hp309ao
*netout hp309ao
*allout fr80 hp309ao box m18 jim doyle hp309ao
*filem write .hp309a alwith. +mcnp runtp hp309a
```

TABLE B.8

MCNP Three-Dimensional Breeding Calculations
HP309A

Sector	1	2	3	4	5	6	Total
Multiplier							
^{6}T	0.0736	0.0915	0.1341	0.1899	0.1888	0.1665	0.8444
^{7}T	0.0007	0.0009	0.0013	0.0019	0.0020	0.0018	0.0088
^{239}F	0.0820	0.1039	0.1523	0.2127	0.2137	0.1879	0.9525
Fissions							0.5485
MS							
^{6}T	0.0042	0.0061	0.0082	0.0133	0.0139	0.0122	0.0578
^{7}T	0.0017	0.0021	0.0027	0.0044	0.0052	0.0045	0.0205
^{233}F	0.0629	0.1012	0.1420	0.2099	0.2198	0.1992	0.9350
Fissions							0.0130
Total							
^{6}T	0.0778	0.0976	0.1423	0.2032	0.2027	0.1787	0.9022
^{7}T	0.0024	0.0030	0.0040	0.0063	0.0072	0.0063	0.0293
$^{6}T + {}^{7}T$	0.0802	0.1006	0.1463	0.2095	0.2099	0.1850	0.9315
^{233}F	0.0629	0.1012	0.1420	0.2099	0.2198	0.1992	0.9350
^{239}F	0.0820	0.1039	0.1523	0.2127	0.2137	0.1879	0.9525
$^{233}F - {}^{239}F$	0.1449	0.2051	0.2943	0.4226	0.4335	0.3871	1.8875
T+F	0.2251	0.3057	0.4406	0.6321	0.6434	0.5721	2.8190
Fissions							0.5615

TABLE B.9

MCNP Three-Dimensional Blanket Power Calculation
Includes Shield Region (MeV/fusion n)
HP310

	Multiplier	Molten Salt	Total
Entire Blanket			
Neutron	103.1(0.0095)	3.94(0.0265)	107.1(0.0093)
Gamma	13.6(0.0119)	5.77(0.0153)	19.4(0.0106)
Fission	101.0(0.0098)	2.07(0.0301)	103.0(0.0096)
Total	116.7	9.71	126.5
Blanket Power (MW/th)	4092	340	4436
Shield Region			
Volume	2.65	6.76	9.41
Neutron	8.45(0.0472)	0.32(0.1011)	8.76(0.0470)
Gamma	1.11(0.0427)	0.42(0.0586)	1.53(0.0402)
Fission	8.26(0.0484)	0.17(0.1131)	8.43(0.0483)
Total	9.56	0.74	10.29
Blanket Power (MW/th)	3757	314	4071

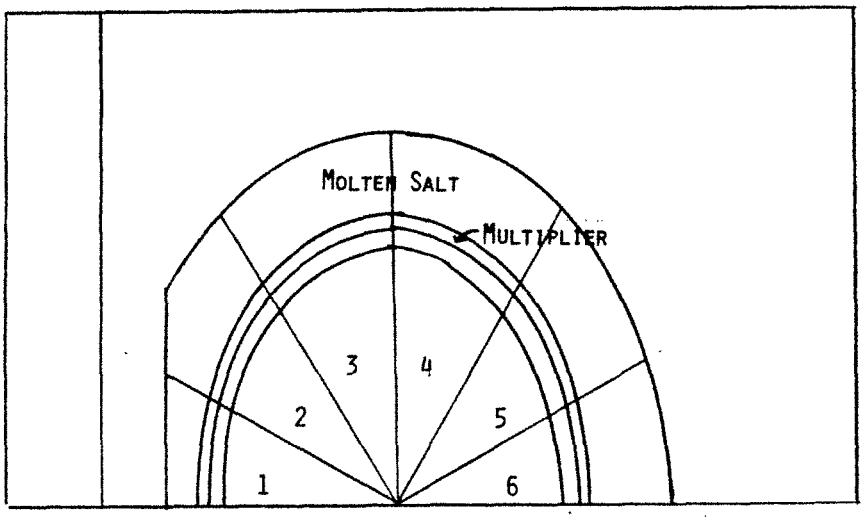

Figure B.1 MCNP Three-Dimensional Model Showing Poloidal Segmentation

APPENDIX C. PUMPING POWER AND PRESSURE DROP ANALYSIS

This appendix summarizes the pumping power and pressure drop calculations done for the uninsulated and insulated ducts. The calculation results for the uninsulated ducts are shown in Tables C.1 – C.3. The results of the calculations for the insulated ducts are shown in Tables C.4 – C.6.

TABLE C.1

Pumping Power and Pressure Drops
a = 0.05 m.
t_1= 0.005 m.
t_2= 0.0025 m.

Toroidal Segments	Poloidal Segments	Pumping Power (MW)	Max. Pumping Power (MW)	Duct Mass (MT)	Max. Δp (MPa)
2	10	736.65	1389.57	4.52	78.27
2	20	643.27	1227.65	5.09	69.15
2	30	574.02	1094.25	5.63	61.63
2	40	520.77	989.75	6.13	55.75
2	50	478.55	906.36	6.61	51.05
2	60	444.24	838.42	7.07	47.22
4	10	363.07	689.10	9.04	38.81
4	20	316.38	608.10	10.18	34.25
4	30	281.75	541.39	11.25	30.49
4	40	255.13	489.13	12.27	27.55
4	50	234.02	447.44	13.23	25.20
4	60	216.86	413.46	14.13	23.29
8	10	179.45	342.30	18.08	19.28
8	20	156.10	301.77	20.36	17.00
8	30	138.79	268.42	22.51	15.12
8	40	125.48	242.29	24.54	13.65
8	50	114.92	221.44	26.45	12.47
8	60	106.34	204.45	28.26	11.52

TABLE C.2

Pumping Power and Pressure Drops
a = 0.10 m.
t_1= 0.005 m.
t_2= 0.0025 m.

Toroidal Segments	Poloidal Segments	Pumping Power (MW)	Max. Pumping Power (MW)	Duct Mass (MT)	Max. Δp (MPa)
2	10	240.55	412.49	5.13	23.23
2	20	209.99	358.38	6.27	20.19
2	30	190.84	321.44	7.34	18.11
2	40	177.73	295.75	8.36	16.66
2	50	168.20	276.95	9.31	15.60
2	60	160.96	262.62	10.22	14.79
4	10	113.64	199.08	10.25	11.21
4	20	98.37	171.96	12.54	9.69
4	30	88.79	153.48	14.69	8.65
4	40	82.24	140.63	16.71	7.92
4	50	77.47	131.23	18.63	7.39
4	60	73.85	124.07	20.44	6.99
8	10	54.19	96.70	20.51	5.45
8	20	46.55	83.12	25.07	4.68
8	30	41.76	73.87	29.37	4.16
8	40	38.49	67.44	33.43	3.80
8	50	36.10	62.74	37.26	3.53
8	60	34.29	59.16	40.88	3.33

TABLE C.3

Pumping Power and Pressure Drops
a = 0.15 m.
t_1 = 0.005 m.
t_2 = 0.0025 m.

Toroidal Segments	Poloidal Segments	Pumping Power (MW)	Max. Pumping Power (MW)	Duct Mass (MT)	Max. Δp (MPa)
2	10	160.51	248.64	5.73	14.00
2	20	146.11	223.66	7.45	12.60
2	30	138.01	208.18	9.06	11.73
2	40	132.82	198.08	10.58	11.16
2	50	129.21	191.00	12.02	10.76
2	60	126.56	185.78	13.38	10.46
4	10	72.66	116.12	11.47	6.54
4	20	65.47	103.56	14.89	5.83
4	30	61.41	95.81	18.12	5.40
4	40	58.82	90.75	21.16	5.11
4	50	57.02	87.21	24.03	4.91
4	60	55.69	84.60	26.75	4.77
8	10	33.32	54.80	22.94	3.09
8	20	29.72	48.50	29.78	2.73
8	30	27.69	44.62	36.23	2.51
8	40	26.40	42.09	42.32	2.37
8	50	25.50	40.31	48.06	2.27
8	60	24.83	39.01	53.50	2.20

TABLE C.4

Pumping Power and Pressure Drops
a = 0.05 m.
t_1= 0.00025 m.
t_2= 0.000125 m.

Toroidal Segments	Poloidal Segments	Pumping Power (MW)	Max. Pumping Power (MW)	Duct Mass (MT)	Max. Δp (MPa)
2	10	96.01	142.68	4.74	8.04
2	20	91.34	135.38	5.34	7.63
2	30	87.88	128.86	5.90	7.26
2	40	85.21	123.69	6.43	6.97
2	50	83.10	119.55	6.92	6.73
2	60	81.38	116.17	7.39	6.54
4	10	42.74	65.66	9.49	3.70
4	20	40.41	61.96	10.68	3.49
4	30	38.68	58.69	11.80	3.31
4	40	37.35	56.10	12.86	3.16
4	50	36.29	54.03	13.85	3.04
4	60	35.43	52.34	14.79	2.95
8	10	19.29	30.57	18.98	1.72
8	20	18.12	28.71	21.36	1.62
8	30	17.25	27.07	23.60	1.52
8	40	16.59	25.77	25.71	1.45
8	50	16.06	24.73	27.70	1.39
8	60	15.63	23.89	29.57	1.35

TABLE C.5

Pumping Power and Pressure Drops
a = 0.10 m.
t_1 = 0.00025 m.
t_2 = 0.000125 m.

Toroidal Segments	Poloidal Segments	Pumping Power (MW)	Max. Pumping Power (MW)	Duct Mass (MT)	Max. Δp (MPa)
2	10	80.69	101.37	5.38	5.71
2	20	79.17	99.48	6.57	5.60
2	30	78.21	97.78	7.69	5.51
2	40	77.55	96.55	8.75	5.44
2	50	77.08	95.64	9.74	5.39
2	60	76.71	94.94	10.68	5.35
4	10	33.72	43.53	10.76	2.45
4	20	32.96	42.52	13.15	2.39
4	30	32.48	41.66	15.39	2.35
4	40	32.15	41.04	17.50	2.31
4	50	31.91	40.58	19.48	2.29
4	60	31.73	40.23	21.36	2.27
8	10	14.23	18.92	21.52	1.07
8	20	13.85	18.39	26.30	1.04
8	30	13.61	17.96	30.78	1.01
8	40	13.44	17.65	34.99	0.99
8	50	13.32	17.42	38.96	0.98
8	60	13.23	17.24	42.71	0.97

TABLE C.6

Pumping Power and Pressure Drops
a = 0.15 m.
t_1= 0.00025 m.
t_2= 0.000125 m.

Toroidal Segments	Poloidal Segments	Pumping Power (MW)	Max. Pumping Power (MW)	Duct Mass (MT)	Max. Δp (MPa)
2	10	84.16	100.05	6.02	5.64
2	20	83.45	99.65	7.81	5.61
2	30	83.04	99.04	9.49	5.58
2	40	82.78	98.59	11.07	5.55
2	50	82.60	98.26	12.56	5.53
2	60	82.47	98.01	13.96	5.52
4	10	34.49	41.83	12.04	2.36
4	20	34.13	41.55	15.61	2.34
4	30	33.93	41.23	18.98	2.32
4	40	33.80	41.01	22.14	2.31
4	50	33.71	40.84	25.12	2.30
4	60	33.64	40.72	27.93	2.29
8	10	14.23	17.66	24.07	0.99
8	20	14.05	17.49	31.23	0.99
8	30	13.95	17.33	37.95	0.98
8	40	13.89	17.21	44.27	0.97
8	50	13.84	17.13	50.23	0.96
8	60	13.81	17.07	55.86	0.96